KU Leuven
Biomedical Sciences Group
Faculty of Medicine
Department of Neurosciences
Laboratory of Neurobiology

The role and therapeutic potential of EGLN2/PHD1 in amyotrophic lateral sclerosis

Christine Germeys

Jury:

Promotor: Prof. dr. Ludo Van Den Bosch
Co-promotor: Dr. Tijs Vandoorne

Jury members:
Prof. dr. Joris De Wit
Prof. dr. Sandrine Da Cruz
Prof. dr. Séverine Boillée
Prof. dr. Rickie Patani

Dissertation presented in partial fulfilment of the requirements for the degree of Doctor in Biomedical Sciences.

November 2024

“If you are curious, you'll find the puzzles around you.

If you are determined, you will solve them”

Ernő Rubik

Acknowledgments

When I started my PhD five years ago, I did not know what to expect. Now, looking back, I can tell that it exceeded anything I could have imagined. It has been a true adventure, full of highs and lows, however one that I genuinely enjoyed. This journey was made all the more special because I had the privilege of sharing it with the most wonderful mentors, colleagues, friends and family. Their support and guidance shaped this unique experience, and I would like to express my heartfelt gratitude to each of them.

Prof. Ludo Van Den Bosch, **Ludo**, ik herinner mij jouw lessen neurobiologie in mijn derde bachelor nog levendig. Vooral de delen over ALS, waar jij natuurlijk extra enthousiast les over gaf, intrigeerde me. Daar is voor mij dan ook echt het zaadje gepland om mij meer te verdiepen in die vreselijke ziekte. Ik was dan ook heel enthousiast dat ik mijn master thesis en later ook mijn PhD in jouw labo mocht doen. Een doctoraat mogen doen in het LVDB labo is echt een cadeau. Naast de (oneindige) wetenschappelijk mogelijkheden, ben je er ook in geslaagd om een super aangename sfeer te creëren waardoor ik er mij er onmiddellijk thuis voelde. Dankjewel om mij de mogelijkheid de geven om een doctoraat te doen in deze geweldig inspirerende omgeving, om mij te introduceren in het ALS onderzoek, om mij mee te nemen naar conferenties (waarvan de Packard meeting toch echt een hoogtepunt was!), om te geloven in mij en om mij de ruimte te geven om zelfstandig te groeien als wetenschapper.

Tijs, ik prijs mezelf gelukkig dat jij niet alleen mij supervisor wou zijn tijdens mijn master thesis maar dat je na jouw PhD ook nog een gaatje in je drukke agenda wist te vinden om mij te begeleiden tijdens mijn doctoraat. Ondanks je eigen bloeiende carrière, wist je altijd tijd te maken voor onze meetings, om even te bellen als ik ergens vast mee zat en om mij bij te staan met wetenschappelijk advies en de wijze levenslessen van bompa Tijs (zoals jij ze zelf graag noemt 😊). Ik ben je enorm dankbaar dat je niet alleen mijn wetenschappelijke basis hebt gelegd maar me hebt gemotiveerd om tot het uiterste te gaan en uit mijn comfortzone te stappen. Dat heeft niet alleen mijn doctoraat, maar ook mijn persoonlijke groei enorm verrijkt. Jouw gedrevenheid en passie voor alles wat je doet zijn een voorbeeld voor mij. Dankjewel om die passie met mij te delen. Ik weet dat jij nog prachtige dingen gaat bereiken in je carrière en ik wens je het allerbeste in zowel je professionele als privéleven, samen met je gezin.

Prof. Philip Van Damme, heel erg bedankt voor al je waardevolle feedback en de kritische vragen die je steeds stelde tijdens mijn laboseminaries.

To all the members of the examining board, I would like to express my gratitude for the time and effort that they have invested in reading my thesis and providing valuable feedback. **Prof. De Wit**, **Prof. Da Cruz**, thank you for your guidance and feedback through my thesis. I really appreciated our scientific discussion during my yearly evaluations. **Prof. Boillée**, **Prof. Patani**, it is a real honor to have you both in my examining committee. Thank you for the time you devoted to reviewing my thesis and for traveling to Belgium to attend my public defence.

ALS liga, jullie oneindige inzet is van onschatbare waarde voor ALS patiënten en hun geliefden en voor het onderzoek naar ALS. Dankjewel daarvoor!

During my PhD, I had the privilege to work with some world-leading experts that made it possible to apply state-of-the-art techniques in this thesis. Thank you, **Dr. Suresh Poovathingal** and **Dr. Kris Davie**,

Dr. Stefaan Derveaux, **Dr. Rekin's Janky** and the rest of **Nucleomics core** team, **Prof. Ghesquière, Dr. Camila Takeno Cologna** and the **Metabolomics core**, **Dr. Nicolas Peredo** and the **Bioimaging core** and **Dr. Arefe Nami**, for all your valuable input and support during this PhD.

My PhD experience was shaped by the incredible colleagues I could share it with. Therefore, I would like to thank them one by one.

Adrià, I know that behind the 'grumpy' facade you put up, is an incredibly kind and caring person. I realized this through all the help and support you offered me, from the start of my master's thesis to the end of my PhD which I appreciate enormously, thank you! I wish you, **Laura R** (thank you for the career advice!) and Arnau all the best! **Adriana**, your passion and dedication to ALS research are truly inspiring. I have no doubt they'll lead to an outstanding PhD. Thank you for your kindness, wishing you all the best! Than the Italian gang! All jokes aside, I was so happy that every one of you joined the lab! **Alessio**, your drive and interest in science are admirable. Even when you were the only one working on CMT, you went out of your way to connect, collaborate and offer help, thank you for that! I have no doubt you'll complete your PhD brilliantly and go on to achieve even greater things. Good luck! **Benedetta**, from the moment you joined the lab, I was impressed by you. You have a sharp scientific mind, clear goals and an incredible drive, all while being compassionate and supportive to those around you. With your mindset, I am sure you will get far and I am more than happy that I will be able to support you on the way. **Matilde**, with the amount of minions Jimmy had, impressing him is not that easy anymore but you did it! And with your organization skills and work ethic, I completely understand why. I was happy to be your office neighbor and to answer all of your quick questions 😊 Thank you for all your advice on my posters and graphical abstract in return. I wish you all the best! **Marcello**, I am impressed by your determination to pursue a PhD in fundamental research as a medical doctor. However, with your bright mind and persistence, I have no doubt that you will be successful. Thank you for your help with CellProfiler analysis and good luck with your PhD! **Amber,** het is fijn om te zien hoe gedreven je bent. Heel veel succes met je master thesis! **Begga**, bedankt om mij in mijn eerste jaar op te leiden toen ik nog niet eens wist hoe een muis vast te houden en al de hulp in de jaren erna! **Dufie**, dankjewel om je passie voor muziek met mij te delen! Jij maakte elk feestje, karaokeavond, optreden of festival tot een echt feest. Ik weet zeker dat je het in je hebt om je doctoraat op een geweldige manier af te ronden! You go girl! **Elena**, I really appreciate all the help with the organization of my PhD. Nothing I asked for, was too much. Thank you! **Fouke**, het is mooi om te zien hoe jij alles wat je doet met volle overgave doet, inclusief het combineren van je werk in het ziekenhuis en je onderzoek, wat al een prestatie is op zich. Dankjewel voor al je enthousiasme en om mij met jouw onderzoek een inkijk te geven in klinische kant van het ALS onderzoek. **Frederik,** Fredje, onze 2000 baby lol. Ik ben blij dat je uiteindelijk toch de beslissing hebt gemaakt om een doctoraat te starten want met jouw interesse in het onderzoek, zag ik niet in waarom niet. Heel veel succes, je gaat het super doen! **Geethika,** I admire how you combine your bioinformatic skills with your biological background and are therefore always able to translate between the two worlds! Thank you for all your help with the (single-nuclei) RNAseq analysis. **Jimmy**, wat had ik toch zonder jou gedaan tijdens mijn doctoraat… Jij en je post-itjes hebben er in ieder geval voor gezorgd dat ik geen enkel deadline kon missen 😊 Daarnaast is het nog eens volledig jouw verdienste dat mijn planten mijn doctoraat overleefd hebben. En dit zijn nog maar twee voorbeelden van hoe je mij hebt geholpen tijdens mijn doctoraat. Dankjewel om altijd klaar te staan om wie dan ook met wat dan ook te helpen in het labo. Het labo mag heel dankbaar zijn dat jij wil blijven om je wijsheid nog iets langer te delen mijn de nieuwe garde. Ik wens je het allerbeste toe samen met Sam en Milo! **Joke**, wat ben ik blij dat ik jou beter heb

leren kennen in de laatste jaren van mijn doctoraat. Jij bent naast een indrukwekkende onderzoekster, ook nog eens zo een lieve en behulpzame collega. Ik apprecieerde onze gesprekken en jouw advies enorm. Dankjewel! **Jonas**, wie had er gedacht dat er in jou zo een musical talent verscholen zat. Ik in ieder gevalt niet maar na onze karaokeavond ben ik ervan overtuigd dat, moest je genoeg hebben van je doctoraat (wat ik trouwens niet verwacht want je doet het geweldig), er altijd nog een carrière op je wacht in de theaterwereld. Veel succes met welk pad je ook kiest 😊 **Joris** en **Jozefien**, jullie zijn beide een geweldige toevoeging aan het labo en het was fijn om te zien hoe snel jullie beide integreerden. Veel succes met de postdoc en het doctoraat! **Kristel**, onze iPSC-expert, wat heb ik veel bij geleerd van jou! Jouw kennis, je passie voor de wetenschap en de precisie waarmee je aan onderzoek doet zijn indrukwekkend en een voorbeeld voor mij. Dankjewel voor al je hulp tijdens mijn doctoraat en de aangename uurtjes achter de flow die we samen hebben gedeeld. **Lenja**, ik heb genoten van de frisse wind vol enthousiasme die met jouw komst is meegekomen. Je bent ondertussen al een tijdje bezig met je doctoraat, maar je doet het nog steeds met dezelfde gedrevenheid, wat fijn is om te zien! Dankjewel voor de hulp met de zebravis experimenten en nog veel succes met je doctoraat! **Lieselotte** en **Louise**, jullie zijn beiden een waardevolle aanvulling voor het labo. Louise, dank je wel dat je altijd even vraagt hoe het met me gaat wanneer we elkaar tegenkomen. Lieselotte, het is leuk om te zien hoe gedreven je bent. Veel succes nog allebei met jullie doctoraat! **Lisha**, thank you for always bringing a smile to my face whenever we crossed paths in the lab. I genuinely enjoyed all our times at the flow together and I will never forget how you managed to get into the Gordon meeting (in your sandals). Your persistence and hard work are inspiring and I know they'll pay off soon. You are almost there! **Maria**, your dedication to bridging your medical expertise with bioinformatics is more than impressive. Thank you for your help with the single-cell experiment and good luck with the remainder of your PhD! **Melissa**, de dag dat jij je doctoraat afrondt en het labo verlaat, weet ik niet wat er met het labo gebeurd. Wat jij naast al jouw werk voor je PhD nog voor het labo doet is indrukwekkend. Bedankt voor alle leuke momenten samen en om zelfs 's avonds terug naar het labo te gaan om mijn confocal uit te zetten. **Nicole**, jij bent van onschatbare waarde voor het labo. Ik kan waarschijnlijk niet eens volledig opsommen waarmee je me allemaal hebt geholpen tijdens mijn doctoraat. Ontzettend bedankt voor al je hulp en steun, voor de geweldige activiteiten die je organiseerde met het ecoteam en voor jouw nuchtere blik die ons labo soms zo hard nodig had. **Nikita**, ik vond het erg gezellig toen je mijn buur werd in ON&4. Ondanks dat ik je in het nieuwe labo iets minder zie, tovert het horen van jouw aanstekelijke lach in de gangen nog altijd een glimlach op mijn gezicht. Bedankt daarvoor! Ik wens je het allerbeste toe met je gezin! **Paraskevi**, thank you for always taking a moment to check in with me whenever we crossed paths in the lab. I'm happy for you on completing your PhD and I wish you all the best in whatever comes next! **Pegah**, ik heb erg genoten van onze trip naar Baltimore voor de Packard meeting en ons aansluitend tripje naar Washington. Dankjewel voor al je steun tijdens mijn doctoraat! Ik wens je het allerbeste met je nieuwe positie in Brussel! **Raheem**, hoe jij er jouw levensdoel van hebt gemaakt om de mensen uit je geboorteland te helpen, is meer dan bewonderenswaardig! Dankjewel om daarnaast ook nog eens zo'n vriendelijke en behulpzame collega te zijn. Ik wens je het allerbeste toe! **Silke**, samen door de 'valley of shit' schept toch echt wel een band! Ik was zo blij dat jij hetzelfde pad bewandelde en dat ik, vooral in het laatste jaar, zo vaak kon ventileren tegen jou. Dankjewel om mijn klankbord te zijn, om zelfs op de moeilijkste momenten je enthousiaste, optimistische zelf te blijven en mee te manifesten (op zen West-Vlaams) voor een goede afloop van ons doctoraat. Naast the lows, hebben we ook zeker de highs gedeeld! Onze trip naar Zwitserland, met DonDon, Jimmy's verbrande hoofd, onze niet-verbrande ruggen en onze tocht tussen de koeien en prikkeldraad, blijft toch een van mijn favoriete herinneringen aan mijn

doctoraat. Dankjewel daarvoor! Ik ben super trots op ons beide dat we, met nog geen maand tussen, ons doctoraat allebei kunnen afronden! We did it! **Thibault**, thank you for all your help with the mice and for forwarding all the interesting metabolism articles. I wish you all the best! **Val**, you are a great scientist! I really appreciated al our chats and your advice on my (zebrafish) experiments. Wishing you all the best in your professional and family life! **Wendy S**, dankjewel om zo'n lieve en betrokken collega te zijn! Ik waardeerde onze gesprekjes in de gang enorm. **Wendy V**, ik mag van geluk spreken dat ik jouw hulp heb gekregen tijdens het laatste jaar van mijn doctoraat. Met jouw eindeloze technische skills nam je moeiteloos een deel van mijn experimentele last over, wat tijdens de meest stressvolle periode als een geschenk voelde. Je nam zoveel gewicht van mijn schouders, en dat niet alleen, je was ook nog eens een ontzettend empathische en lieve collega. Dankjewel voor alles!

In addition to the current lab members, I would like to acknowledge and thank those who were part of the lab at the beginning or throughout my PhD journey but have since moved on.

Annet, dankjewel om zo vaak de gesprekken tijdens de middagpauzes op te starten met de vragen op je theezakjes en om je zo in te zetten voor het ecoteam. Je was een ontzettend lieve college! **Arun**, in addition to being an outstanding scientist, you were also a wonderful colleague, always ready to help everyone. I still remember how proudly you shared the news of becoming a father. Wishing you and your lovely family all the best! **Caroline**, ondanks dat onze tijd in het lab maar kort overlapte, wist je een blijvende indruk op me te maken, niet alleen als geweldige wetenschapster, maar ook als een ontzettend behulpzaam persoon. Vooral tegen het einde, toen ik zocht naar mijn volgende stappen, was jij er met waardevol carrièreadvies waarvoor ik je enorm dankbaar ben. **Christine M**, dankjewel dat je altijd al mijn technische vragen kon beantwoorden. Zelfs toen je niet meer in ons lab werkte, hielp je me nog met advies en ontbrekende compounds. **Donya** and **Joni**, the most iconic duo our lab has ever known. I must admit that, as a young master student, I was a bit intimidated by the two of you at first. However I quickly learned that behind all that intense energy, there were two impressive women with strong values and clear goals from who I could learn a lot. I believe the best advice you gave me was that a PhD is a marathon and not a sprint, which I repeated to myself a lot during my PhD. Wishing you both all the very best! **Elisabeth,** ik ben heel blij dat ik de kans heb gekregen om tijdens je postdoc meer met jou te kunnen samenwerken. Dankjewel voor al je hulp en voor al de duidelijke protocollen die ik met veel plezier gebruikt heb tijdens mijn PhD. **Elke**, vanaf het begin van mijn master thesis heb ik het indrukwekkend gevonden met welke gedrevenheid en enthousiasme jij je doctoraat aanpakte. Daarnaast was je ook gewoon een geweldig lieve en behulpzame collega. Ondanks dat ik onze lunch en koffiepauzes gemist heb in de laatste jaren van mijn PhD, ben ik heel blij voor jou dat je zo gelukkig bent in je nieuwe job en wens ik jou en Johan het allerbeste toe! **Eveline**, ik ben blij dat ik jou tijdens ENCALS beter heb leren kennen. Dankjewel dat ik erbij mocht zijn op jouw top trouwfeest! Ik wens je het allerbeste met Wouter en hopelijk kunnen we binnenkort nog eens bijpraten. **Kara**, het was leuk om je te zien groeien van een student in ons labo naar de verantwoordelijke van de zebravisfaciliteit, wat geen gemakkelijke job was en die je, naast al je lopende experimenten, meer dan goed vervulde. Dankjewel voor al je hulp met de zebravisexperimenten, ik vond het zalig om met jou samen te werken! Ik wens je het allerbeste met je nieuwe job en in je nieuwe appartement! **Katarina**, thank you for introducing me to the fascinating world of astrocytes! I was truly impressed by how you managed your project so meticulously while still finding time to help so many of us in the lab, including me. Thank you for being such an inspiring example and to show me how you can be a great scientist while maintaining a healthy work-life balance. **Laura F**, from the moment I started my master thesis in the lab, you were such a sweet and supporting colleague! I was so happy we could catch up again

during the Gordon conference last year. I wish you all the best! **Lien,** na te hebben meegemaakt wat jij allemaal deed voor het labo tijdens mijn master thesis, was ik even bang dat het labo zou instorten na jouw vertrek. Gelukkig was er **Annelies** die de zware taak om jou te vervangen perfect vervuld heeft. Lien en Annelies, dankjewel dat jullie altijd klaar stonden voor al mijn vragen! **Margot**, dankjewel voor je enthousiasme, je aanstekelijke lach en om mij te helpen met de muizencoupes. Ik wens je veel succes met je nieuwe studie en alles wat erna mag komen! **Mathias**, 1/3 van mr. Friday, confocal expert, top wetenschapper en sinds kort ook nog eens papa, zoveel verschillende rollen en allemaal volbracht met evenveel overgave! Daarlangs stond je ook nog eens klaar met waardevolle hulp en feedback. Dankjewel daarvoor! **Matthieu**, ik moet toegeven dat toen jij vertrok er toch wel een lichte paniek uitbrak bij mij, aangezien je me nu niet meer kon helpen bij de analyse van het single-cel experiment. Het is uiteindelijk toch goed gekomen maar enorm bedankt om voor een lange tijd altijd klaar te staan om je expertise te delen waar nodig. **Nuray,** de dag dat jij in het labo kwam, was het moment dat er een nieuwe energie het labo binnenkwam. Dankjewel voor al je zotte ideeën en voor je eindeloze hulp tijdens mijn doctoraat! **Rob**, thank you for lighting up so many of the lunch breaks. In addition to being a great story teller, you are an even more remarkable scientist! Keep pushing forward CMT research. I truly believe that, with people like you, a treatment is within reach! **Stijn**, vanaf het begin heb jij me enorm welkom laten voelen in het labo en zorgde je altijd voor een fijne sfeer. Dankjewel voor je hulp en expertise met de muizen. Ik vond het heel spijtig toen jij en Annet het labo verlieten maar ben blij dat we toch nog geregeld kunnen bijpraten. **Tom**, I believe you are one of the smartest people I've ever met, paired with incredible kindness and a great sense of humor. Thank you for all the valuable input you provided on my project! **Wenting**, it was great catching up at the iMND meeting! Thank you for the tremendous effort you put into establishing the iPSC work in the lab. Wishing you all the best as you set up your own research group! **Yvonne**, thank you for bringing a pop of color to the lab, not only with your hair but also with your cheerful personality. I really enjoyed all the great chats we shared!

Finally, a special thanks to the 'gürlz' (aka FWO's Fantastic Five)! **Miri**, **Ayşe**, **Blanca** and **Dorien**, thank you for our meet-ups where we could openly vent about the highs and lows of our PhD journeys. And thank you Dorien for bringing in the perspective of life after the PhD. I look forward to celebrating all our defences soon!

Daarnaast wil ik ook graag de mensen bedanken die niet op een wetenschappelijke manier, maar door hun persoonlijk steun, een minstens even belangrijke bijdrage hebben geleverd aan deze thesis.

Ondanks dat ik moet toegeven dat mijn sociaal leven soms toch wel de dupe werd van dit doctoraat, ben ik daardoor des te dankbaar om zo'n geweldige vrienden in mijn leven te hebben. Lieve vrienden van **De Vriendschapsband**, ik prijs mezelf zo gelukkig dat deze vriendschapsband ontstaan in het middelbaar, nog altijd standhoudt. Door onze uiteenlopende achtergronden, vind ik het heerlijk om onze avonden te vullen met het delen van al onze uiteenlopende verhalen of om gewoon herinneringen op te halen naar onze middelbareschooltijd toen alles uiteindelijk toch wel iets gemakkelijk was (al waren we daar toen nog niet overtuigd van). Dankjewel om altijd klaar te staan en om regelmatig mijn gedachten te hebben verzet. Ik ben zo trots op wat wel al allemaal bereikt hebben en nog trotser dat we het nog steeds met elkaar kunnen delen! Dan lieve vrienden van de **Familie Helsen**! Wie had gedacht dat er bij een vriend, zo een toffe vriendengroep kwam. Dankjewel om altijd te vragen hoe het ging en al minstens één week per jaar in de Ardennen of Frankrijk mijn gedachten te verzetten. Jullie zijn een voor een toppers! Ten slotte, **Anaïs**, na 25 jaar vriendschap weet ik wel

zeker dat, wat er ook is, jij altijd maar 1 telefoontje weg bent. Ondanks dat ik niet altijd de beste ben in contact houden, is deze vriendschap zo waardevol voor mij! Dat ik nu ook nog eens meter mag worden van jou en **Kevin**'s dochtertje is het grootste cadeau dat jullie me hadden kunnen geven. Dankjewel voor jullie vertrouwen en jullie oneindige steun!

Lieve familie en schoonfamilie, dankjewel voor al jullie steun! **Heidi** en **Frans**, dankjewel om mij met open armen te hebben ontvangen, om regelmatig klaar te staan met lekker eten of hulp met ons huis en om ook begrip te hebben als ik er eens niet bij kon zijn. Aan mijn ouders, dankjewel voor alle kansen die ik gekregen heb. **Papa**, hoewel ik misschien niet al je communicatieve vaardigheden heb meegekregen, ben ik toch vaak dankbaar geweest voor de Germeys-genen wanneer ik een presentatie moest geven die goed verliep. Dank je wel dat jij en **Claudia** er altijd voor me zijn, dat jullie geïnteresseerd zijn, dat jullie me eraan herinneren dat ik af en toe best wat minder hard mag werken en voor jullie onvoorwaardelijke steun. **Mama**, jouw onvoorwaardelijke steun, hulp en vermogen om dingen te relativeren hebben me het zelfvertrouwen gegeven om deze uitdaging aan te gaan. Dankjewel voor alles, om altijd klaar te staan, om te helpen waar je maar kan en om zo'n inspirerend voorbeeld te zijn. Ik hoop dat ik in mijn toekomstige carrière, net als jij, alle uitdagingen kan aangaan terwijl ik trouw blijf aan mezelf. Dan last but not least, lieve **Niels**, dankjewel om dit avontuur met mij te zijn aangegaan. Het is zeker niet altijd makkelijk geweest voor ons beide maar jouw oneindige positivisme, motivatie, steun en liefde, hebben ervoor gezorgd dat ik kon doorzetten! Dankjewel om altijd voor mij klaar te staan met een luisterend oor, een knuffel, lekker eten of een dosis relativisme en er mij aan te helpen herinneren dat er meer was in het leven dan mijn doctoraat. Je successen zijn maar zoveel waard als de mensen waarmee je ze kan delen en wat heb ik geluk dat dit met jou kan delen. Ik weet niet wat de volgende avonturen nog gaan brengen, maar wat ik wel weet is dat ik ze enkel met jou wil aangaan. Want samen met ons twee kunnen wij de wereld aan!

Dankjewel, Thank you,

Christine

Table of Contents

Acknowledgments i

List of abbreviations xi

CHAPTER 1 INTRODUCTION 3

1.1 Amyotrophic lateral sclerosis – a heterogeneous neurodegenerative disease 3

1.1.1 ALS clinical picture – phenotypic variability 3

1.1.2 ALS etiology – multifactorial with genotypic variability 5

1.2 Modeling ALS – not one model answers all questions 8

1.2.1 Cellular models 8

1.2.2 Small animal models 9

1.2.3 Rodents 10

1.2.4 Patient-derived induced pluripotent stem cells (iPSCs) 12

1.3 ALS pathology – an interplay between cell-autonomous and non-cell-autonomous mechanisms 14

1.3.1 Motor neurons 14

1.3.2 Microglia 19

1.3.3 Oligodendrocytes 20

1.3.4 Astrocytes 21

1.4 A new era of ALS drug discovery 27

1.5 EGLN2/PHD1, a promising target for ALS? 28

CHAPTER 2 AIMS OF THE STUDY 33

CHAPTER 3 MATERIALS & METHODS 37

3.1 Ethical approval 37

3.2 Zebrafish micro-injections and follow-up 37

3.2.1 DNA constructs and AMO 37

3.2.2 Motor axonopathy analysis 37

3.3 Mice breeding and follow-up 38

3.3.1 Disease onset and survival 38

3.3.2 Behavioral testing 39

3.3.3 Motor neuron counts 39

3.4 iPSC lines, differentiation and treatments 39

3.4.1 Generation and quality control of EGLN2 knock-out iPSCs 40

3.4.2 Astrocyte differentiation 42

3.4.3 Motor neuron differentiation 43

3.5 Immunofluorescence 43

3.5.1 Mice 43

3.5.2 iPSC-derived astrocytes 44
3.6 Quantitative real-time polymerase chain reaction (qRT-PCR) and reverse transcription PCR (RT-PCR) 44
3.6.1 Mice 44
3.6.2 Zebrafish 44
3.7 Western blot (WB) analysis 45
3.8 Single-nuclei RNA sequencing (snRNA-seq) of mice lumbar spinal cord 45
3.8.1 Single nuclei extraction. 45
3.8.2 10x Genomics data processing 46
3.8.3 Gene ontology (GO) analysis and gene set enrichment analysis (GSEA). 47
3.9 RNAScope in situ hybridization 47
3.10 Live-cell calcium imaging 48
3.11 Radioactive flux experiments 48
3.12 Tetramethylrhodamine methyl ester perchlorate (TMRM) analysis 49
3.13 RNA sequencing (RNA-seq) analysis of iPSC-derived astrocytes 49
3.13.1 RNA extraction and quality control 49
3.13.2 RNA-seq 50
3.14 Neurite outgrowth 51
3.15 Statistic analysis 51
CHAPTER 4 RESULTS 57
4.1 Targeting Egln2 rescues the motor axonopathy in ALS zebrafish 57
4.1.1 Downregulation of *egln2* in zebrafish using an AMO 57
4.1.2 *Egln2* downregulation rescues the motor axonopathy in SOD1-ALS zebrafish 58
4.1.3 *Egln2* downregulation rescues the motor axonopathy in C9ORF72-ALS zebrafish 58
4.1.4 Concluding Remarks 60
4.2 Targeting EGLN2 mitigates the ALS phenotype in SOD1-ALS but not FUS-ALS mice 60
4.2.1 Generation of ALS mice with an *Egln2* deletion 60
4.2.2 Deletion of *Egln2* increases the survival and protects the motor neurons of $SOD1^{G93A}$ mice 61
4.2.3 Deletion of *Egln2* does not affect the ALS phenotype in $FUS^{+/+}$ mice 63
4.2.4 Concluding remarks 64
4.3 SnRNA-seq reveals the cell-specific effect of *Egln2* deletion on the spinal cord of $SOD1^{G93A}$ mice 64
4.3.1 SnRNA-seq transcriptionally profiles neuronal and non-neuronal nuclei in $SOD1^{G93A}$ spinal cord 64
4.3.2 *Egln2* deletion induces transcriptomic changes in neuronal and non-neuronal cells from $SOD1^{G93A}$ spinal cord 68

4.3.3 *Egln2* deletion downregulates the STING-induced interferon response in SOD1^{G93A} astrocytes 71
4.3.4 Concluding remarks 72
4.4 Targeting EGLN2 mitigates ALS phenotypes in patient-derived astrocytes 74
4.4.1 *SOD1^{A4V}*-ALS patient-derived iPSCs differentiate into mature astrocytes 74
4.4.2 Metabolic profiling of *SOD1^{A4V}*-ALS patient-derived astrocytes 75
4.4.3 Transcriptomic profiling of *SOD1^{A4V}*-ALS patient-derived astrocytes 78
4.4.4 Generation of *SOD1^{A4V}*-ALS patient-derived astrocytes with an *EGLN2* deletion 80
4.4.5 Deletion of *EGLN2* normalizes the interferon response in *SOD1^{A4V}*-ALS patient-derived astrocytes 83
4.4.6 Deletion of *Egln2* in SOD1^{A4V} astrocytes does not affect motor neurite outgrowth via CAM treatment 88
4.4.7 Concluding remarks 88
CHAPTER 5 GENERAL CONCLUSION AND DISCUSSION 93
5.1 EGLN2 downregulation offers motor neuron protection in multiple *in vivo* ALS models 93
5.2 SnRNA-seq as tool to investigate ALS targets 94
5.3 EGLN2 and metabolic dysfunction in ALS at single-cell resolution 95
5.4 EGLN2 and interferon signaling in ALS at single-cell resolution 96
5.5 Limitations of the study 97
5.6 Future directions and therapeutic implications 98
5.7 General conclusion 100
5.8 Graphical abstract 101
Summary 103
Samenvatting 105
Scientific acknowledgments 109
Personal contributions 109
Conflicts of interest 110
References 111
Supplementary figures and tables 138
Curriculum vitae 145

List of abbreviations

91S	91 sense C9ORF72 hexanucleotide repeats
a.u.	arbitrary units
A4A	$SOD1^{A4A}$
A4V	$SOD1^{A4V}$
ADM	astrocyte differentiation medium
ADP	adenosine diphosphate
AICAR	5-aminoimidazole-4-carboxamide-1-β-d-ribofuranoside
ALS	amyotrophic lateral sclerosis
AMM	astrocyte maturation medium
AMO	antisense oligonucleotide morpholino
AMPA	α-amino-3-hydroxy-5-methyl-4-isoxazolepropionic acid
AMPK	AMP-activated protein kinase
APC	astrocyte progenitor cell
AQP4	odorant binding protein ASP4
Array-CGH	array-comparative genomic hybridization
ASO	antisense oligonucleotide
ATP	adenosine triphosphate
ATXN1/2	ataxin 1/2
BBB	blood-brain-barrier
BDNF	brain-derived neurotrophic factor
Bp	base-pair
BSA	bovine serum albumin
C. elegans	Caenorhabditis elegans
C9ORF72	chromosome 9 open reading frame 72
CAM	conditioned astrocyte medium
CCNF	cyclin F
CFD	Cutting Frequency Determination
cGAMP	2’3’-cyclic guanosine monophosphate–adenosine monophosphate
cGAS	cyclic GMP-AMP synthase
CHMP2B	charged multivesicular body protein 2B
Chr	chromosome
CME	Centrum Menselijke Erfelijkheid
CNTF	ciliary neurotrophic factor
CRISPR	clustered regularly interspaced palindromic repeats
ctrl	control
Cu	copper
Cx43	connexin 43
DAPI	4’,6-diamidino-2-phenylindole
DCTN1	dynactin subunit 1
DEG	differentially expressed gene
DIV	days in vitro
DMEM	Dulbecco's modified eagle medium
DMSO	dimethyl sulfoxide
DNA	deoxyribonucleic acid
DPR	dipeptide repeats

DR6	death receptor 6
dsDNA	double-stranded DNA
E2I2	exon 2 intron 2 splice-junction
EB	embryoid body
EEAT2	excitatory amino acid transporter 2
EGLN1-3	egl-9 family hypoxia-inducible factor 1-3
EMA	European Medicines Agency
ExpB	experimental block
FBS	fetal bovine serum
FCCP	carbonyl cyanide 4-(trifluoromethoxy)phenylhydrazone
FDA	US Food and Drug Administration
FDR	false discovery rate
Fe^{2+}	ferrous iron
FISH	fluorescent in situ hybridization
FOXO3A	forkhead box O3A
FPKM	fragments per kilobase million
FTD	frontotemporal dementia
FUS	fused in sarcoma
GABA	gamma aminobutyric acid
GAPDH	glyceraldehyde 3-phosphate dehydrogenase
GDNF	glial cell line-derived neurotrophic factor
GFAP	glial fibrillary acidic protein
GFP	green fluorescent protein
GLM	generalized linear model
GluR2	glutamate receptor 2
GO	gene ontology
gRNA	guide RNA
GSEA	gene set enrichment
GSIB4	isolectin GS-IB4
HEK	human embryonic kidney cells
HIFα	hypoxia-inducible factor alpha
Hpf	hours post fertilization
HRP	horseradish peroxidase
IFN	interferon
IGF1	insulin- like growth factor 1
IKKβ	IκB kinase
Il	interleukin
IPSC	induced pluripotent stem cell
IRF3	interferon regulatory factor 3
ISG	interferon-stimulated genes
JAK/STAT	janus kinase/signal transducer and activator of transcription
kDa	kilodalton
KIF5A	kinesin family member 5A
LPS	lipopolysaccharides
MAV	mitochondrial antiviral-signaling protein
MCT1	monocarboxylate transporter 1
MCT1/4	monocarboxylate transporter 1/4
MHC1	major histocompatibility complex 1

MMP9	matrix metalloproteinase-9
N	biological replicate
n	technical replicate
NANOG	homeobox transcription factor NANOG
Nefh	neurofilament heavy
Nefl	neurofilament light
Nefm	neurofilament medium
NEK1	NIMA related kinase 1
NFκB	nuclear factor kappa-light chain-enhancer of activated B cells
NI	non-injected
NIM	neuronal induction medium
NLRP3	NLR family pyrin domain containing 3
NLS	nuclear localization signal
NMJ	neuromuscular junction
NMM	neuronal maturation medium
NO	nitric oxide
NPC	neural progenitor cell
OCT4	octamer-binding transcription factor 4
OPTN	optineurin
OT	off-target
PBS	phosphate buffered saline
PET	positron emission tomography
PFA	paraformaldehyde
PFKFB3	6-phosphofructo-2-kinase/fructose-2,6-biphosphatase 3
PGC1α	proliferator-activated receptor gamma coactivator 1 alpha
PHD1-3	prolyl hydroxylase domain enzymes 1-3
PLO	poly-L-ornithine hydrochloride
polyP	polyphosphate
Prnp	prion protein
Prph	peripherin
qRT-PCR	quantitative real-time polymerase chain reaction
RA	retinoic acid
RAN	repeat-associated non-AUG
RNA	ribonucleic acid
RNA-seq	RNA sequencing
RNP	ribonucleoprotein
ROCKi	rho-associated kinase inhibitor
ROS	reactive oxygen species
RRM	RNA-recognition motifs
RT-PCR	reverse transcription polymerase chain reaction
SEM	standard error of the mean
SAG	smoothened agonist
sALS	sporadic ALS
SCD-1	stearoyl-CoA desaturase 1
SETX	senataxin
sgRNA	single guide RNA
SNP	single nucleotide polymorphism
snRNA-seq	single-nuclei RNA sequencing

SOD1	superoxide dismutase 1
SOX2	sex determining region Y-box 2
SOX9	transcription factor SOX-9
SPAST	spastin
SQSTM1	sequestosome 1
SSEA4	stage-specific embryonic antigen-4
STING	stimulator of interferon genes
STMN2	stathmin-2
SV2	synaptic vesicle glycoprotein 2
SYP	synaptophysin
TARDBP	TAR DNA binding protein
TBK1	TANK binding kinase 1
TCA	tricarboxylic acid
TIC	TNFα, IL-1α and C1q
TIGAR	TP53-inducible glycolysis and apoptosis regulator
TMRM	tetramethylrhodamine methyl ester perchlorate
TNFα	tumor necrosis factor alpha
TOMM20	translocase of outer mitochondrial membrane 20
TRPA1	transient receptor potential cation channel member A1
Tspo	translocator protein
TUBA4A	alpha-tubulin 4A
Ubb	ubiquitin b
UBQLN2	ubiquilin 2
Uchl1	ubiquitination markers ubiquitin c-terminal hydrolase l1
UMAP	uniform manifold approximation and projection
UNC13A	unc-13 homolog A
US	United States
VAPB	VAMP associated protein B
VCP	valosin containing protein
VEGF	vascular endothelial growth factor
VEH	vehicle
VIM	vimentin
WB	western blot
WT	wildtype
WTA	whole transcriptome analysis
Zn	zinc

CHAPTER 1 INTRODUCTION

Parts of this chapter appeared in:

Germeys, C. (2019) Using iPSCs to investigate the effect of HDAC inhibition on human FUS-ALS motor neurons. [Master dissertation, KU Leuven].

Germeys, C., Vandoorne, T., Bercier, V., and Van Den Bosch, L. (2019). Existing and Emerging Metabolomic Tools for ALS Research. Genes (Basel) *10*. 10.3390/genes10121011.

Germeys, C.*, Vandoorne, T.*, Davie, K., Poovathingal, S., Heeren, K., Vermeire, W., Nami, F., Moisse, M., Quaegebeur, A., Sierksma, A., et al. (2024). Targeting EGLN2/PHD1 protects motor neurons and normalizes the astrocytic interferon response. Cell Rep *43*, 114719. 10.1016/j.celrep.2024.114719
*These authors contributed equally

CHAPTER 1 INTRODUCTION

1.1 Amyotrophic lateral sclerosis – a heterogeneous neurodegenerative disease

Amyotrophic lateral sclerosis (ALS), also known as Lou Gehrig's disease in the United States (US), is a fatal neurodegenerative disorder characterized by progressive degeneration of upper motor neurons in the motor cortex and lower motor neurons in the brainstem and the spinal cord (Figure 1.1). ALS is part of a group of motor neuron disorders with other members being primary lateral sclerosis, progressive muscular atrophy, progressive bulbar palsy, and pseudobulbar palsy[1]. ALS, described by Jean-Martin Charcot in 1869, is the most common motor neuron disease in adults with an incidence of approximately 2 cases per 100,000 and a prevalence of 6 per 100,000[2]. While often perceived as a rare disorder, the estimated cumulative lifetime risk is 1 in 472 for women and 1 in 350 for men at the age of 70[3,4]. Moreover, a global increase of 69% is estimated from 2015 to 2040 explained by the ageing of the population[5]. Nevertheless, a cure for this devastating disorder is still absent. The difficulty in finding a cure for ALS lays in the complexity and the heterogeneity of the disorder. Indeed, ALS shows a large phenotypic and genotypic variability, further discussed below.

1.1.1 ALS clinical picture – phenotypic variability

The clinical picture of ALS varies between ALS patients and a high degree of heterogeneity is observed in different aspects of the disease.

First, while ALS typically starts around the age of 60, disease onset has been described at almost every age including cases of juvenile ALS[6].

Second, the site of initial symptoms differs between patients[6,7] (Figure 1.1). Limb-onset is found in 70% of the ALS patients, presenting a combination of upper and lower motor neuron signs in the limbs. Bulbar onset is described in 25% of the patients and is characterized by initial speech and swallowing difficulties followed by limb weakening in later stages of the disease. Finally, in a few cases (3-5%) respiratory onset is observed. These ALS patients suffer from orthopnea or dyspnea and mild or even absent spinal or bulbar signs. Loss of upper motor neurons is typically characterized by spasticity and muscle stiffness while lower motor neuron degeneration results in excessive electrical irritability, leading to muscle fasciculations.

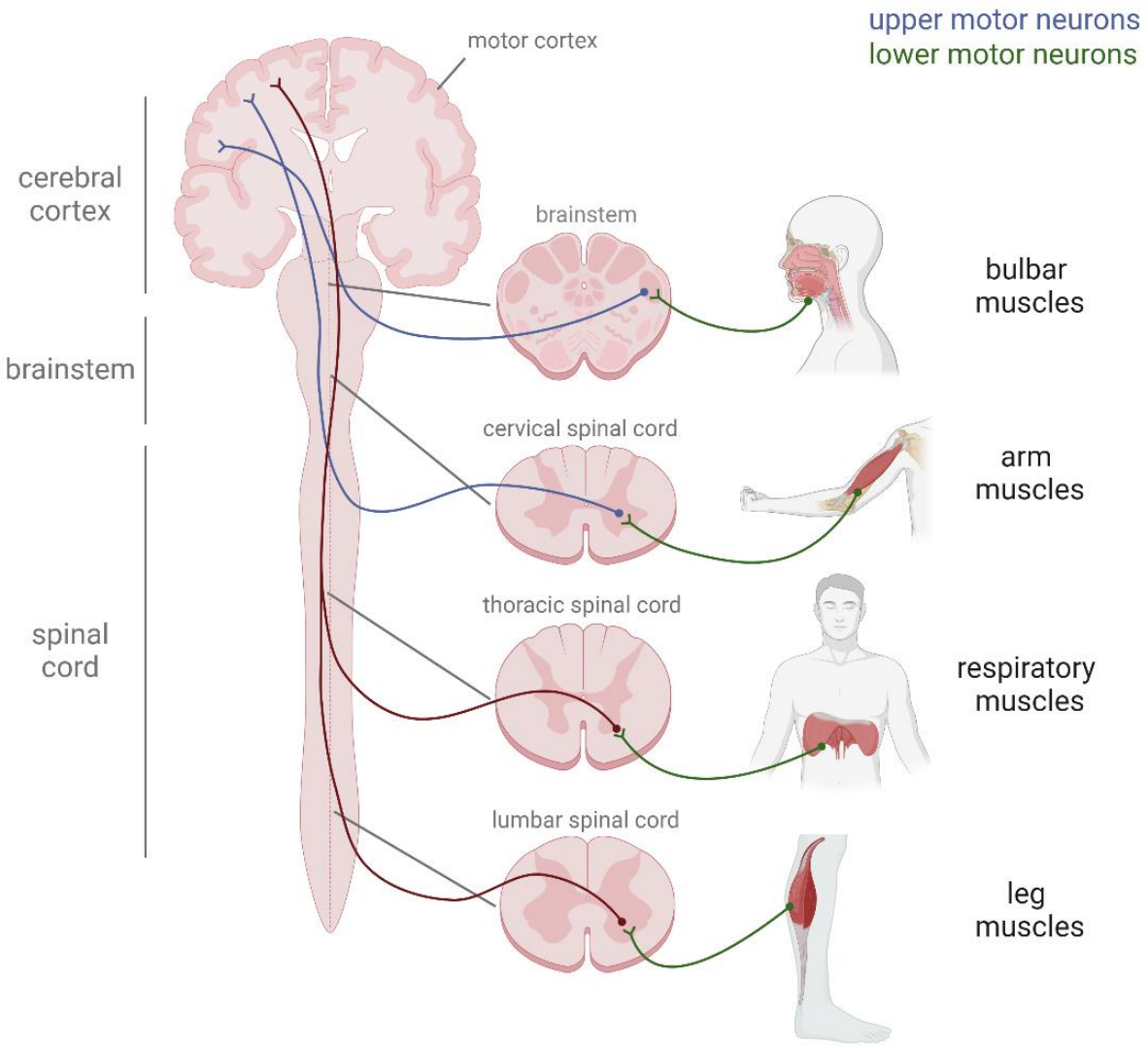


Figure 1.1 Motor neuron degeneration in ALS. ALS impacts the corticospinal motor neurons (upper motor neurons) that originate from the motor cortex projecting to the brainstem and the spinal cord and the bulbar or spinal motor neurons (lower motor neuron) that project to the skeletal muscles. Motor neuron degeneration of the specific motor neurons leads to muscle wasting in the bulbar region, the trunk and the upper and lower limbs. Figure adapted from Taylor *et al*.[13] with BioRender.com.

Third, ALS patients can also present various degrees of non-motor neuron involvement, including cognitive and behavioral symptoms. The presence of cognitive impairment, and overlap between genetic and mechanistic aspects, led to the idea that ALS is part of a disease spectrum with frontotemporal dementia (FTD) at the other end[8]. FTD is a neurodegenerative disorder affecting the frontal and temporal lobes of the brain leading to personality and behavioral changes and language impairments[9]. Similar to ALS, where 50% of the patients present cognitive and behavioral symptoms, 15% of FTD patients also show motor neuron symptoms[10,11]. These findings gave rise to the idea of a

disease spectrum with pure ALS on one side, pure FTD on the other side and patients presenting an overlap of symptoms from both disorders in the middle.

Finally, the degeneration of both upper and lower motor neurons will result in wasting of the respiratory muscles, which leads to early death of the patient. Life expectancy of ALS patients has been shown to be variable[12]. However, patients typically pass away within three to five years after diagnosis[2].

The progressive nature and poor prognosis of ALS underlines the need for adequate therapeutic strategies. In an effort to find a cure for ALS, research has focused on the cause of the disease. However also here, a large degree of variability has been described.

1.1.2 ALS etiology – multifactorial with genotypic variability

ALS is a multifactorial disease. The minority of ALS patients (10%) have a familial form (fALS) while 90% of the cases are considered as sporadic (sALS), lacking a familial history[14] (Figure 1.2). However, even in seemingly sporadic cases the genetic burden can range from 17 to 28%[15]. Heritability estimates based on twin studies, GWAS datasets and population registers range from 38% to 78%, indicating additional causes for ALS including suggested environmental factors[14]. Currently, there are two hypotheses to explain the interaction between genetic and environmental factors. The gene-time-environment hypothesis suggests that ALS is a result from the interaction of a genetic basis with environmental exposures during ageing. The multistep hypothesis on the other hand states that several hits[16,17], which can be genetic or environmental, are required to trigger ALS, even for penetrant ALS mutations. Studies focusing on ALS genetics have led to the identification of more than 150 genes involved in ALS pathophysiology (http://alsod.iop.kcl.ac.uk/). The most commonly affected genes, in chronological order of their discovery, are superoxide dismutase 1 (*SOD1*), TAR DNA binding protein (*TARDBP*), fused in sarcoma (*FUS*) or chromosome 9 open reading frame 72 (*C9ORF72*), altogether accounting for more than half of fALS cases (Figure 1.2)[13].

1.1.3.1 SOD1

The genetic era of discovery for ALS began in 1993 with the finding that mutations in *SOD1* can cause the disease[18]. *SOD1* consisting of 153 amino acids, encodes for the ubiquitously expressed copper/zinc (Cu/Zn) superoxide dismutase 1 (32 kilodalton [kDa]) which is a dimer that catalyzes the conversion of superoxide radicals to hydrogen peroxide, playing a crucial role in the cellular antioxidant defense mechanisms[19]. More than 200 mutations spread all over *SOD1* are associated with ALS accounting for approximately 12% of the fALS cases and 1-2% of sALS cases[14]. Since many variants retain partial or full

dismutase activity, it is suggested that the pathological mechanism is the result of one or more toxic properties of SOD1 mutants and not from reduced dismutase activity[20]. Moreover, some ALS-related SOD1 mutants are not able to fold properly resulting in ubiquitinated cytoplasmic inclusions possibly contributing to the toxicity in ALS[21].

1.1.3.2 TARDBP

In 2006, mutations in *TARDBP*, encoding DNA/RNA binding protein TDP-43, were reported as a cause of ALS[22]. TDP-43 consists of two RNA-recognition motifs (RRM), a C-terminal glycine-rich domain and a nuclear localization domain and plays a role in RNA splicing and transcription[23]. While mutations in *TARDBP* only occur in 4% of fALS and 1% of sALS patients[14], 95% percent of all ALS patients show TDP-43-positive inclusions which are the result of its mislocalization from the nucleus to the cytoplasm where it can form aggregates[24]. Moreover, these TDP-43-containing inclusions are not only a pathological hallmark of ALS, but also occur in 50% of FTD patients[25] and other neurodegenerative disorder such as Alzheimer's disease, Parkinson disease, Huntington disease and more[26].

1.1.3.3 FUS

A year after the discovery of ALS-linked mutations in *TARDBP*, also mutations in *FUS* were found to be present in 3% of fALS and 0.3% of sALS patients[27,28]. Similar to *TARDBP*, *FUS* encodes a multifunctional DNA/RNA-binding protein that consists of one RRM domain and multiple glycine/arginine-rich domains and it is primarily localized in the nucleus where it plays a role in transcription, RNA splicing, RNA transport and translation. Notably, mutations are mainly clustered at the C-terminal region of the protein, containing the nuclear localization signal (NLS), which could explain the increased cytoplasmic distribution of the mutant FUS protein resulting in cytoplasmic FUS accumulations.

1.1.3.4 C9ORF72

The next breakthrough was the discovery of a hexanucleotide (GGGGCC-) repeat expansion in *C9ORF72* which is the most frequent genetic cause of ALS in the Western world[29,30] with 40% of fALS and 7% of sALS patients carrying G4C2 repeat expansions[14]. While healthy individuals harbor 2 to 30 repeats, patients can carry 100 up to 1000 repeats[31]. The repeat expansion in *C9ORF72* leads to nuclear RNA foci, repeat-associated non-AUG (RAN) translated dipeptide repeat proteins (DPRs), alternatively spliced *C9ORF72* transcript and lower expression of *C9ORF72*[32]. These processes are all hypothesized to contribute to ALS etiology but it remains unknown which one is leading or whether they interact. *C9ORF72* repeats are not only the most frequent genetic cause in ALS, but also in FTD patients accounting for 25-30%[33,34].

1.1.3.5 Other genes

While the previously discussed genes account for the mutation in half of the fALS patients, genetic discoveries have led to a continuously growing number of genes linked to ALS. Examples of such genes that lead to ALS when mutated in a minority of fALS patients are cyclin F (*CCNF*; 4% of fALS)[35], NIMA related kinase 1 (*NEK1*; 2% of fALS)[36,37], valosin containing protein (*VCP*; 1% of fALS)[38], sequestosome 1 (*SQSTM1*; 1% of fALS)[39], optineurin (*OPTN*; <1% of fALS)[40], TANK binding kinase 1 (*TBK1*; <1% of fALS)[41] and many more[14]. Other genes might not directly cause the disease in a monogenetic way but in line with ALS being a multifactorial disorder increase the susceptibility of the disease. Examples of these are a variant of unc-13 homolog A (*UNC13A*) or repeats in ataxin 1 and 2 (*ATXN1* and *ATXN2*), all increasing the risk to get ALS[42-44].

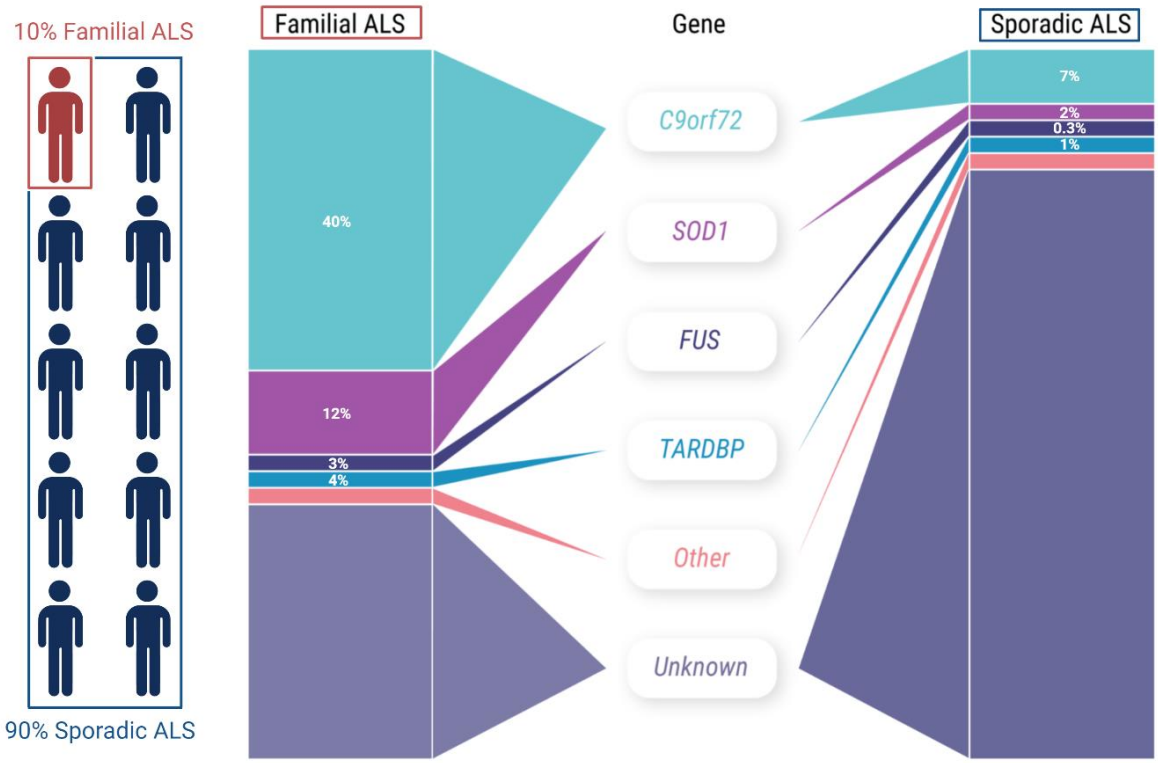


Figure 1.2 Genetic epidemiology of fALS and sALS. 10% of ALS cases are familial (fALS, in red) showing familial history and a clear monogenetic cause, while 90% of the patients have a sporadic form (sALS, in blue) with no clear familial history. However, the genetic burden has reported to range from 17 to 28% in sporadic cases. This figure shows the most commonly affected genes in fALS and sALS being *C9ORF72*, *SOD1*, *FUS* and *TARDBP*. Figure adapted from Roggenbuck *et al.*[45] with BioRender.com.

1.1.3.6 Environmental factors

In addition to the genetic risk factors, environmental factors can also contribute to the multifactorial risk for ALS. Evidence for a role of environmental factors in ALS etiology can be found in the incomplete heritability and spatial clusters of ALS[46]. However, research on the origin of these environmental factors is not evident. Nevertheless, studies, often based on environmental assessments, questionnaires and biofluid analysis, have been performed in an attempt to identify potential environmental factors. These have suggested a link between ALS and several factors including pesticides, several occupational exposures such as military service, agriculture, manufacturing and painting, physical activity, head trauma, air pollution, the microbiome, micronutrient intake, smoking and alcohol intake[46]. However causal evidence for any of these is still lacking

A better understanding of the disease etiology, contributes to a better understanding of the disease pathology which is crucial to find a cure for ALS. Especially, the discovery of the different genetic mutations has been instrumental in developing preclinical models essential for studying the disease pathology of both fALS and sALS, which are clinically indistinguishable. The following paragraph provides an overview of the available models that have advanced our understanding of the underlying disease mechanisms.

1.2 Modeling ALS – not one model answers all questions

Numerous models have been created to study different forms of ALS, all with their own advantages and disadvantages (Figure 1.3). Here, the most widely used models together with their strengths and weaknesses will be discussed together with examples of how they contributed to our current knowledge about ALS.

1.2.1 Cellular models

Simple cell models can be useful to unravel the biological function of ALS-associated proteins or for compound screening. Immortalized human cell lines such as HeLa, human embryonic kidney (HEK)-293 and U2OS cells or neuroblastoma lines such as SH-SY5Y are commonly used tools in neurodegeneration research. An example of their value in ALS research, is the discovery of the role of low-complexity domains in ALS proteins (e.g. FUS) in stress granule formation[47]. However, a limitation of these cell models is that they have widespread and unstable genotypic abnormalities and lack a truly neuronal profile. Next to these simple human cell lines, primary motor neuron or glial cell cultures derived from ALS rat or mouse models can be used to study motor neuron vulnerability to for example C9ORF72 RAN translation-induced DPRs[48] or glial-induced toxicity[49]. While useful, these cell lines are non-human

and are not able to completely capture the *in vivo* complexity of ALS which makes direct translation of findings in these cell lines to humans challenging.

1.2.2 Small animal models

Various small animals are used in research to model the effect(s) of diverse genetic causes of ALS. The advantages of these small models are that they are: (1) generated quickly; (2) cheap to maintain and (3) amenable to genetic or compound screening. They can also be used to model interactions between different genetic causes and modifiers[50].

1.2.2.1 Caenorhabditis elegans

A small animal model used to study genetic pathways is the nematode *Caenorhabditis elegans* (*C. elegans*)[50]. *C. elegans* has a short life cycle, is easy to manipulate genetically and has a simple but well characterized nervous system. Its genome consists for 75% of human homologues with 42% of them comprising disease-causing genes. Moreover, the transparency of the organism offers the possibility to follow green fluorescent protein (GFP)-labeled proteins over time *in vivo*. The available ALS *C. elegans* models carry the main ALS-associated genetic mutations, namely *SOD1*, *C9ORF72*, *TARDBP* and *FUS*, leading to different pathological hallmarks of ALS. As an example, it was shown in a FUS *C. elegans* model that the low-complexity domains of FUS drives phase separation and the formation of aggregates[51].

1.2.2.2 Drosophila melanogaster

The most widely used small animal model is *Drosophila melanogaster* because 75% of human disease genes have a fly ortholog and striking structural similarities exist between human and fly genes[32]. Moreover, it has a rapid life cycle, sophisticated nervous system and a high number of (genetic) tools and assays that are available to study its nervous system. Numerous fly models overexpressing mutant human transgenes such as *TARDBP*, *FUS*, *C9ORF72* and many more exist, all showing cellular toxicity[52-55]. As such, the C9ORF72 fly model led to the finding that neurodegeneration in C9ORF72-ALS can be mediated by arginine-rich DPRs[56].

1.2.2.3 Danio rerio

Zebrafish (*Danio rerio*) offer a valuable tool for ALS research because of the 70% homology between the human and zebrafish genome and because 80% of disease relevant genes have at least one zebrafish ortholog[32]. Moreover, it is a vertebrate that is translucent, has a fast reproduction rate,

shows high protein homology with human proteins and can be easily genetically manipulated, enabling rapid screening. A commonly used method in zebrafish is the injection of RNA or antisense oligonucleotide morpholinos (AMOs) to generate overexpression or knockdown models. In addition, clustered regularly interspaced palindromic repeats (CRISPR)-Cas9-mediated gene editing to create stable transgenic zebrafish has been established[57]. Zebrafish models have led to the observation that mutant SOD1 leads to gain-of-function-dependent neuronal toxicity[58] and that mutations in *TARDBP*, *FUS* and *C9ORF72* lead to a combination of gain- and loss-of-function effects[59-62].

As discussed above, these small animal models have proven their use, especially in genetic and compound screening. However, despite the genetic overlap, there are still significant differences between these animal models and ALS patients that should be considered, especially regarding their size and the complexity of their nervous system. Therefore, they are particularly suited as hypothesis-generating platforms leading to potential therapeutic targets which can be validated in rodents or patient-derived models.

1.2.3 Rodents

Rodent models have been the golden standard in ALS research for a long time. Although the field is moving towards alternatives, especially with the introduction of patient-derived induced pluripotent stem cells (iPSCs), mouse models still play an important role in ALS research.

The first available model, and still the most commonly used one, is the SOD1^{G93A} mouse, overexpressing the human mutant *SOD1^{G93A}* gene (18-25 times)[63]. These mice closely model the disease as seen in patients with adult-onset motor neuron degeneration leading to motor defects, paralysis and premature death. Moreover, this model shows several of the main hallmarks of the disease in patients such as protein misfolding and aggregation, metabolic and mitochondrial abnormalities, neuroinflammation marked by astrogliosis and microgliosis and many more[64]. As a result, this mouse model has played a major role in the current knowledge on the pathology of ALS and contributed to a number of breakthroughs in the field including the non-cell-autonomous nature of ALS[65-67].

In addition to the SOD1^{G93A} mouse model, also SOD1^{G37R}, SOD1^{G85R} and SOD1^{G86R} mice have been generated which differ in onset and other clinical aspects but all display neuroinflammation, mitochondrial defects and other pathological hallmarks, however all lacking the TDP-43 proteinopathy present in 95% of ALS patients[68-70].

With the discovery of more disease-causing mutations in other proteins, mouse models for the most prevalent ones have been generated including mice expressing mutant or wildtype *TARDBP* and *FUS*[71].

Indeed, next to the models based on the expression of ALS-linked mutations found in *TARDBP* and *FUS* the overexpression of the wild-type human transgene itself also results in an ALS-like phenotype, as they model the ALS-linked mislocalization of TDP-43 and FUS protein. For example, mice expressing human wild-type FUS driven by a prion protein (Prnp) gene promoter show a severe ALS phenotype with progressive motor neuron degeneration, hind-limb paralysis and premature death around 12 weeks of age[72]. In addition, deletion of *TARDBP*[73], but not *FUS,* also results in ALS-like symptoms in mice[74,75].

Finally, C9ORF72 mouse models have been generated modelling the *C9ORF72* hexanucleotide repeat expansion leading to C9ORF72 ALS hallmarks, such as RNA foci and RAN-induced DPRs or mice with loss of *C9ORF72* showing an immune phenotype[71]. However, these models lack a clear ALS pathology with no motor phenotype or motor neuron degeneration. More recently, also mouse models expressing DPRs have been generated[76,77], showing clinical and pathological hallmarks of ALS, however still failing to show the typical ALS phenotype observed in patients and other mouse models.

In addition to these mouse models, also rats modeling SOD1-, TDP-43-, FUS- and C9ORF72-ALS have been used in ALS research[71]. These have the advantage that they are bigger in size compared to mice making some handling or *in vivo* treatment procedures easier. However, with the increased size of these animals, the costs of housing and care of these models also increases.

A disadvantage of a number of these beforementioned rodent models is that they are based on the overexpression of a human transgene, where the overexpression itself can already cause several disease-related defects. This especially raised concerns in SOD1^{G93A} and C9ORF72 mouse models where spontaneously copy number loss has been reported affecting the disease phenotype[78]. Knock-in models that bare mutations in endogenous mouse genes could provide a solution for the dosage issue of the overexpression-based models[80]. Moreover, humanized knock-in models, in which the mouse locus is replaced with the human orthologous sequence, express physiological levels of human splice isoforms[81].

While it is crucial to look for therapeutic strategies that are beneficial *in vivo*, it remains important to also understand their mechanism of action and investigate if acting on this mechanism is relevant for patients. This can be done by investigating patient and *postmortem* data but also by using models that are patient-derived which was made possible by the generation of iPSCs.

1.2.4 Patient-derived induced pluripotent stem cells (iPSCs)

The ability to generate iPSCs from human somatic cells by transfection with the Yamanaka factors[82] created new opportunities to model ALS starting from patient material. iPSCs are marked by their self-renewal and pluripotent character making it possible to differentiate them in all possible somatic cell types. Differentiation can be facilitated by small molecules[83] or via the use of overexpressed or inducible transcription factors[84]. This allows for the first time to study the central and peripheral nervous cells of patients over the disease course. Moreover, gene editing techniques, such as CRISPR-Cas9, can be used to correct the disease causing-mutations in iPSCs creating isogenic controls. Alternatively, also the opposite is possible where starting from one control line, ALS-linked mutations can be inserted in the same genetic background[85]. These isogenic controls make it possible to study the causal effect of disease-causing point mutations. Furthermore, in addition to modelling the ALS cases that are familial, iPSCs also finally made it possible to model the larger sALS population. As a result, iPSC-derived (motor) neurons and glial cells are currently widely used in the field to study ALS pathology and possible new therapeutic strategies.

iPSCs from numerous patients carrying the most prevalent genetic defects but also more rare variants of the disease together with sALS lines have been generated. The Answer ALS initiative alone already generated over 1000 iPSC lines from control and ALS patients[86]. Investigation of these cell lines have led to the discovery of pathways that contribute to the (spinal) motor neuron vulnerability in fALS and sALS including axonal transport defects, protein mislocalization, hyper-/hypoexcitability, neurofilament misregulation and many more[87]. Moreover, iPSC-derived cells offer a valuable tool to study the cell-type specific pathways involved in ALS.

While iPSCs have a number of advantages compared to other models, they also have their limitations. A disadvantage of this newly risen model is the lack of standardized differentiation protocols. As a result, iPSC-derived motor neurons with the same mutations give rise to contradictory findings. As an example, both hyper- and hypoexcitability have been reported in motor neurons carrying *SOD1* mutations[88,89] which could be explained by the use of different differentiation protocols leading for example to differences in the interneuron and glial content in the motor neuron cultures or differences in the timing of the electrophysiological measurement in relation to the cell cycle exit. Furthermore, iPSC-derived cells are often still in an immature stage of development and lack *in vivo* complexity. However, a solution for the latter can be provided by more complex 2D and 3D co-culture systems with multiple iPSC-derived cell types that are becoming increasingly better at modelling the *in vivo* situation[90]. In addition to a better understanding of the disease, these could also be used for therapy

screening. However, extra attention should still be paid to the numbers of the different cell types in the model and if they represent the *in vivo* ratios as seen in human central nervous system.

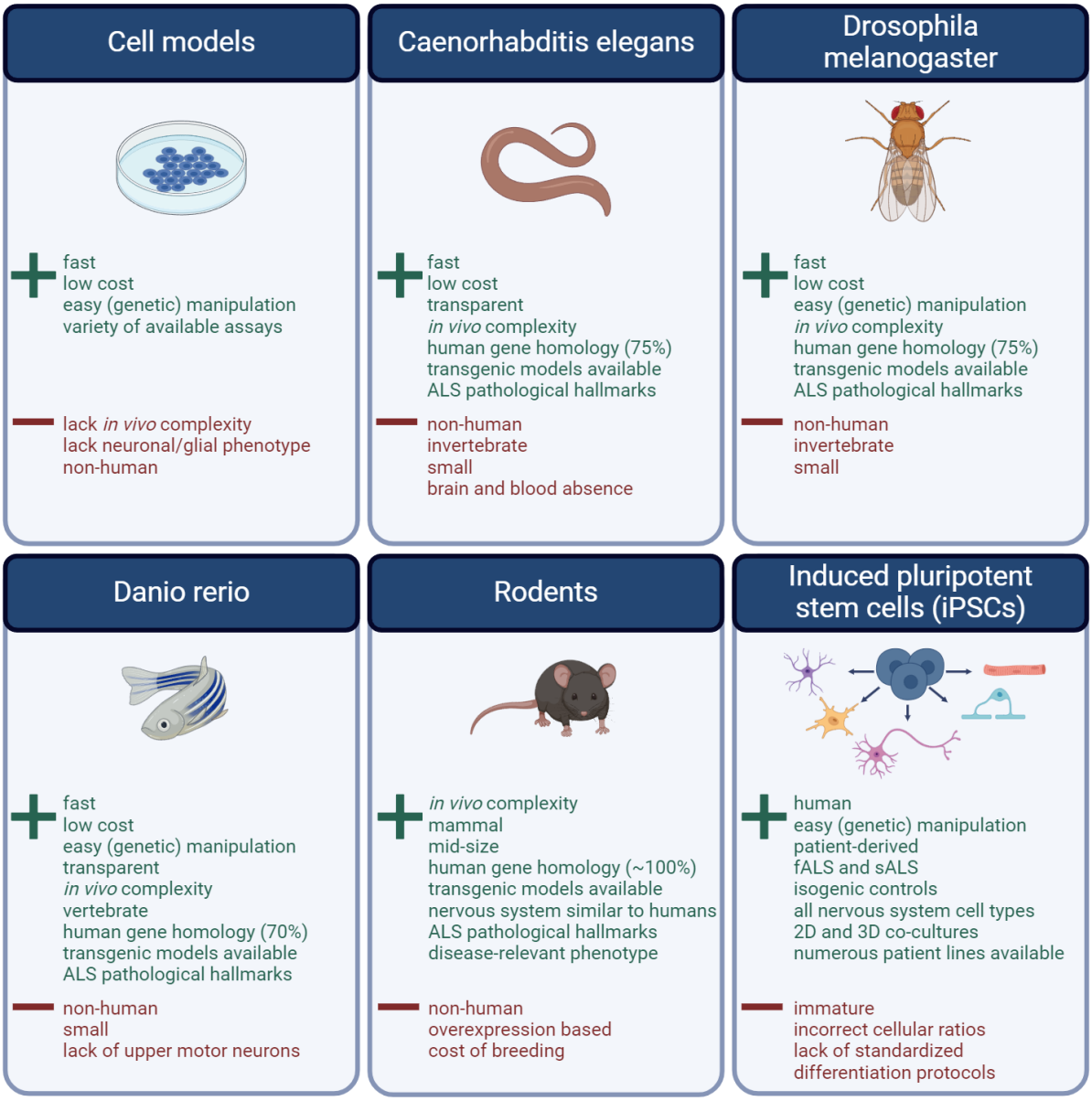


Figure 1.3. Overview of the widely used ALS models with their strengths and weaknesses. Model systems are crucial to unravel the disease mechanism of ALS. In this figure the most widely used models in ALS research, namely cellular models, *Caenorhabditis elegans*, *Drosophila melanogaster*, *Danio rerio*, rodents and induced pluripotent stem cells (iPSCs), are displayed together with their strengths (in green) and weaknesses (in red). Figure made with BioRender.com.

As demonstrated in this paragraph, no model is perfect and they all have their own strengths that are useful for ALS research. Instead of trying to find a perfect model for ALS, using a combination of different optimized models for different research questions might bring us further in understanding the complex pathology of ALS. Indeed, while numerous pathways have been linked to the disease, we do not fully understand the mechanism(s) leading to the disease yet. Pathways that have been identified and linked to ALS in multiple studies are listed in the next paragraph.

1.3 ALS pathology – an interplay between cell-autonomous and non-cell-autonomous mechanisms

For a long time, motor neurons were the main focus when studying the pathological mechanisms of ALS. However, based on the initial studies in SOD1 mice that showed that silencing mutant SOD1 expression in microglia, oligodendrocytes or astrocytes affects early and/or late disease progression[65-67], we know that also the surrounding cells play a crucial role in the disease pathology. Motor neurons are highly specialized cells with particular needs. To meet these needs, they require the support from their surroundings. In the following paragraph, we will discuss the motor neuron-autonomous mechanisms and introduce the most studied cell types, with a focus on glial cells, in relation to their effect on motor neurons in health and disease (Figure 1.4).

1.3.1 Motor neurons

Motor neurons are large, excitable and polarized cells of which the axon length can reach up to one meter leading to specific needs related to transport, energy demand and RNA/protein homeostasis making them especially vulnerable. Indeed, multiple pathways have been found to be dysfunctional in ALS motor neurons leading to their degeneration. Here we will briefly discuss some of the most reported ones.

1.3.1.1 DNA damage

Starting at the DNA level, DNA damage and a dysfunctional DNA repair response have been linked to ALS. DNA is highly exposed to endogenous and exogenous damaging agents. Therefore, a functional DNA repair system is crucial to maintain healthy and functional cells, especially during ageing when different stressors such as oxidative stress are accumulating. Moreover, post-mitotic motor neurons with their high oxygen consumption are especially vulnerable to oxidative DNA damage[91]. Different ALS-linked genes of which the encoded proteins play a crucial role in the DNA repair system such as *TARBP*, *FUS*, senataxin (*SETX*)[92], *VCP*[35], *CCNF*[35] and *NEK1*[36,37] have been found to be mutated in ALS, pointing towards a dysfunctional DNA repair system[93]. Moreover, DNA damage can be recognized by

the DNA sensor cyclic guanosine monophosphate-adenosine monophosphate synthase (cGAS), leading to 2'3'-cyclic GMP-AMP (cGAMP) synthesis and activation of the stimulator of interferon genes (STING)[94]. CGAS/STING signaling subsequently activates the downstream interferon response which is upregulated in motor neurons from ALS patients and models[95]. In addition to DNA damage, also endoplasmic reticulum stress[96], loss of *C9ORF72*[97], DPRs[98], cytoplasmic double-stranded DNA (dsDNA)[99] and TDP-43-mediated cytosolic mitochondrial DNA[100] have reported to induce cGAS/STING signaling in ALS. Finally, also pathways that have been linked to ALS such as excitotoxicity, mitochondrial dysfunction and neuroinflammation can lead to increased DNA damage.

1.3.1.2 Disturbed RNA metabolism

Next to DNA repair, both TDP-43 and FUS also play a role in RNA metabolism. Indeed, TDP-43 and FUS are heterogeneous nuclear ribonucleoproteins, regulating RNA metabolism at various stages of the RNA life cycle. Therefore, disturbances in the function of TDP-43 and FUS have the potential to impact RNA metabolism on a broad scale.

To start, proteins together with RNA can assemble in membranelles organelles, called granules, during cellular stress[101]. These granules are formed by phase separation, a process that is mediated by the low complexity sequence domains in TDP-43 and FUS. ALS-linked mutations can alter the dynamics of these granules leading to the formation of pathological amyloid-like fibrils deposited in the cell bodies and neuropil[47]. Besides TDP-43 and FUS, also *C9ORF72* hexanucleotide repeat expansions seem to play a role in phase separation as C9ORF72 itself as well as arginine-rich DPRS can affect granule formation and dynamics[102,103]. Moreover, disturbed phase separation leads to loss of the normal functioning of key RNA-binding proteins[104].

Next, both TDP-43 and FUS redistribute from the nucleus to the cytoplasm. This has several implications including disturbed dynamic cytoplasmic RNA granules and defects in nucleocytoplasmic trafficking among several others. Moreover, because TDP-43 regulates alternative splicing, nuclear loss and cytoplasmic overexpression of this protein results in decreased levels of correctly spliced protein-encoding mRNAs[105], including the missplicing of stathmin-2 (*STMN2*)[106,107] and *UNC13A*[108,109] leading to motor neuron degeneration. Also loss of nuclear FUS results in the dysregulation of, a different set, of mRNAs[110]. In addition, not only TDP-43 and FUS play a role in the mRNA redistribution but also VCP seems to play a role as inhibition of VCP partially restored mRNA as well as protein localization[111].

Finally, both TDP-43 and FUS are known to be part of the macromolecular complexes generating small non-coding RNAs (microRNAs) that function in RNA silencing. Since microRNAs play a role in the maintenance of neuromuscular junctions, motor neurons may be especially sensitive to changes in the

microRNA metabolism[112]. Evidence of a disturbed microRNA metabolism was provided by the finding that microRNAs were downregulated in motor neurons from sALS patients[113].

1.3.1.3 Impaired proteostasis

Also, protein homeostasis is proposed to be dysregulated in ALS at different levels. Evidence is provided by the presence of ubiquitinated protein aggregates with TDP-43 as major component[25]. Moreover, also FUS and SOD1 aggregates are found within motor neurons and glial cells of ALS patients[114]. The presence of these aggregates suggests a disturbed protein homeostasis. Motor neurons, with their long axons and polarized morphology, are susceptible to age-induced disturbances of proteostasis. Especially because of their post-mitotic character, cell division cannot dilute the pathological protein aggregates[115]. Moreover, disruption of the ubiquitin-proteasome system and autophagy, being the two major protein clearance pathways, are suggested to play a role in ALS[116,117]. The many disease-causing mutations in genes involved in protein degradation, including ubiquilin 2 (*UBQLN2*), *SQSTM1*[39], *OPTN*[40], *VCP*[38], charged multivesicular body protein 2B (*CHMP2B*)[118] and VAMP associated protein B (*VAPB*)[119] support this hypothesis.

1.3.1.4 Impaired axonal transport and local translation

Due to the long length of motor neuron axons, axonal transport of organelles such as mitochondria and lysosomes but also proteins, RNA and lipids is crucial to maintain healthy motor neurons. Disorganization of this crucial process has been associated with ALS. Genes encoding proteins playing a role in cytoskeletal dynamics and axonal transport such as dynactin subunit 1 (*DCTN1*), kinesin family member 5A (*KIF5A*), spastin (*SPAST*) and alpha-tubulin 4A (*TUBA4A*) are linked to ALS[120,121]. Moreover, mutant *SOD1* mice have been reported to slow down both anterograde and retrograde transport months before disease onset[122]. Disrupted axonal transport of mitochondria was also shown to be present in SOD1-[123], FUS-[124], TDP-43-[125] and C9ORF72-ALS[126] patient-derived motor neurons. In addition, kinesin hyperphosphorylation was shown to contribute to this mitochondrial transport in FUS-ALS[127]. Furthermore, neurons need to transport all of the necessary components for translation to enable gene expression at the synapse. The spatial distribution of mRNAs depends on proper microtubule-dependent transport which is regulated by several RNA-binding proteins associated with ALS, including TDP-43 and FUS[128]. Moreover, it has been shown that axons display a distinct transcriptome when compared to the soma with differentially expressed mRNAs related to oxidative energy production and ribogenesis and that this pattern is affected by ALS resulting in many dysregulated transcripts[129]. Motor neuron homeostasis also requires local translation at the level of the axon to allow rapid changes in the distal motor axon, explaining the axonal enrichment in

ribogenesis-related transcripts. Moreover, this process is known to be affected in ALS[130], further contributing to the reduced axonal health in ALS. In addition, the axonal enrichment in mRNA related to oxidative energy production can be explained by the high energetic need to maintain axonal homeostasis, further explained in the next paragraph.

1.3.1.5 Mitochondrial dysfunction and metabolic defects

Axonal transport is indeed a highly energy demanding process because the molecular motors driving axonal transport require one adenosine triphosphate (ATP) molecule, resulting from on-board glycolysis[131], for every 8 nm displacement of their cargo[132,133]. In addition, also action potential propagation and synaptic homeostasis are energy-consuming processes[134,135]. Altogether, these processes result in the high need of motor neurons for energy and explain their vulnerability to metabolic defects. The metabolic vulnerability of motor neurons in ALS is further underlined by the initial degeneration of fast-fatigable motor neurons, which require higher peak needs of ATP compared to the slow motor neurons which are less prone to neurodegeneration[136]. While glucose is the main energy substrate in the central nervous system[137], it is still unclear to which extent glucose is processed by other cells before it is used by neurons to meet their energy demand[138]. *In vitro* and *ex vivo* studies have shown that neurons oxidize other non-glucose substrates such as glutamate[138-140]. Additionally, neurons are also able to process ketone bodies to maintain energetic homeostasis[141-143]. As opposed to glia, neurons are suggested to be primarily oxidative, meaning that glycolysis is followed by the full oxidation of glucose or of its metabolites by the tricarboxylic acid (TCA) cycle and the electron transport chain taking place in the mitochondria[144,145]. Due to their metabolic vulnerability, motor neuron degeneration could be the result of a dysregulated energy metabolism. This is supported by clinical and preclinical evidence. Both fALS and sALS patients exhibit decreased weight and fat depots, which could be the result of a combined decrease in energy uptake, e.g. to a loss in appetite, and an increase in energy expenditure[146-149]. While dysbalanced energy homeostasis is an early event in ALS rodent models[150-153], it remains to be determined whether this is a primary or secondary event in ALS patients[154]. In addition to the systemic metabolism, changes have also been observed at different levels of cellular energy metabolism.

First, cellular energy homeostasis appears to be impaired in ALS. The activity of AMP-activated protein kinase (AMPK) was shown to be elevated in motor neurons of ALS patients[155]. This kinase is an important player in cellular energy homeostasis as it acts as a cellular energy sensor. Active AMPK results in an increase in catabolic and a decrease in anabolic pathways[123]. Moreover, 5-aminoimidazole-4-carboxamide-1-β-d-ribofuranoside (AICAR)-mediated activation of AMPK in NSC34

(motor) neuron-like cells resulted in cytoplasmic TDP-43 mislocalization, linking energy depletion to TDP-43 pathology[155].

Second, mitochondrial dysfunction is known to be an ALS hallmark. These organelles play a crucial role in cellular homeostasis due to their role in energy supply, as they are the site where oxidative phosphorylation takes place and due to their involvement in calcium homeostasis and apoptosis[156]. Mitochondrial dysfunction has been studied extensively after the discovery of *SOD1* mutation in ALS[18]. Subsequently, mitochondrial changes have been reported in ALS patients and in SOD1-ALS mice and iPSC-derived models but also in TDP-43, FUS and C9ORF72 models[69,123,124,153,155,157-164]. The latter indicates that mitochondrial dysfunction could represent a general hallmark of ALS, rather than being attributed to mutations in *SOD1*.

Third, there is evidence pointing towards a defective carbohydrate metabolism in ALS. Studies using [18F]-2-fluoro-2-deoxy-D-glucose positron emission tomography (PET) reported that cortical glucose uptake is reduced in ALS patients, while local glucose uptake seems to be increased in both the cervical and dorsal spinal cord[165-167]. Furthermore, cortical hypometabolism is suggested to be an early diagnostic event that can be linked to the severity of the disease[165,168]. Similarly, *in vivo* imaging in mutant $SOD1^{G93A}$ mice indicates that glucose uptake in the spinal cord is increased presymptomatically but declines as the disease progresses[169]. Microarray analysis and proteomics studies also provided evidence for a disturbed carbohydrate metabolism in ALS. Indeed, several studies explored the downregulation of glycolysis components in ALS patients, including the key enzymes phosphoglucomutase 2 like 1 and phosphoglycerate kinase[152,170]. Consistently, 6-phosphofructo-2-kinase/fructose-2,6-biphosphatase 3 (PFKFB3) mRNA was found to be reduced in the *postmortem* cortex of ALS patients[171].

Finally, lipid metabolism is also suggested to be affected in ALS. Dysregulated lipid metabolism has been mainly attributed to skeletal muscle tissues that increase their lipid-based energy metabolism early in the course of the disease[172]. Nevertheless, research focusing on the role of lipid metabolism in motor neuron toxicity has been instigated by the observation that increased levels of lipid-derived oxidative pathway intermediates could contribute to neuronal oxidative stress[173-176]. As glucose metabolism seems to be downregulated, it is hypothesized that other energy substrates are used to meet the energy demand in motor neurons. In support of this, lipid catabolism is found to be increased in ALS mice and ketone bodies are elevated in the cerebrospinal fluid of ALS patients[177-180]. Moreover, proliferator-activated receptor gamma coactivator 1 alpha (*PGC1α*) and stearoyl-CoA desaturase 1 (*SCD-1*), both involved in fatty acid metabolism, are reported to be downregulated in ALS mouse models and ALS patients[181-185]. Furthermore, metabolic changes have recently been suggested to result

from changes in the microbiome. The gut-microbiome is a major source of low-molecular-mass metabolites that are able to modulate metabolic, transcriptional and epigenetic processes upon crossing the blood-brain-barrier (BBB)[186]. Evidence for the involvement of a disturbed microbiome in ALS is provided by several studies that reported a dysbiotic microbiome and an increased gut permeability in ALS mouse models and ALS patients[187-190].

While metabolic dysfunction has been extensively linked to ALS, we found that the energy metabolism seems to be normal in patient-derived motor neurons despite the observation of other phenotypes in these cells[138]. This supports the notion that other cell types may be involved in the observed metabolic disturbances in ALS and demonstrates the importance of investigating the role of non-neuronal cells in ALS.

1.3.2 Microglia

Microglia are the resident macrophages of the central nervous system. Their main role is to defend the central nervous system against intruders. During their resting state microglia will scan their environment searching for any disturbances of which the presence will lead to microglial activation resulting in transcriptomic, morphological and functional changes[191-193]. For a long time, microglial activation was classified as neurotoxic M1 or neuroprotective M2 activation[194-196]. However, we now know that this is too simplified and that microglial activation is a spectrum that depends on several factors including the location, type of disturbance and age[192-194]. In addition to their protective function, they also support neurons by secreting soluble factors, regulating synapses and clearing dead cells and misfolded proteins, making them crucial for neuronal homeostasis[197].

In ALS patients, increased microglial activation has been described and linked to neuronal and axonal loss as well as a more rapid disease progression[198-203]. In addition, also in SOD1-[64,204,205], TDP-43-[206], FUS-[72,207] and C9ORF72-ALS[76,77] mouse models, microgliosis has been reported. In some SOD1-ALS mice this was observed well before disease-onset[64,204,205]. While expression of mutant *SOD1*^{G93A} in microglia was not sufficient to induce motor neuron degeneration in mice[208], wild-type microglia or selective silencing of mutant *SOD1* in microglia did offer protection as it delayed disease progression[65,208].

Altogether these data demonstrate how microglia and their activation affect the severity of ALS by loss-of-support or gain-of-toxic events. In addition to the microglia, also peripheral immune cells can modify the disease course of ALS via infiltration or via the axons of spinal motor neurons that project outside the central nervous system and are surrounded by peripheral immune cells[209].

1.3.2.1 Neuroinflammation

The gain-of-toxic events are mostly linked to increased activation of microglia leading to neuroinflammation. Mutant SOD1^{G93A} microglia showed higher expression of protective M2 and lower expression of neurotoxic M1 at disease onset compared to the microglia towards the end of the disease. Moreover, when isolated these early SOD1^{G93A} microglia were neuroprotective in co-culture with motor neurons while the end stage microglia were neurotoxic[210]. Both an increased secretion of anti-inflammatory cytokines such as interleukin- (IL-)10[211] and pro-inflammatory factors such as reactive oxygen species, nitric oxide (NO), tumor necrosis factor α (TNFα) and IL-1β have been reported by mutant SOD1[208,212-214] and TDP-43[215,216] microglia resulting in motor neuron toxicity in co-cultures. In addition, reduced expression of *C9ORF72* increased the expression of microglial activation genes with increased levels of pro-inflammatory cytokines Il-1β and Il-6 as a result[217,218]. Moreover, human C9ORF72 iPSC-derived microglia also showed increased expression and release of pro-inflammatory mediators such as matrix metalloproteinase-9 (MMP9), Il-1β, IL-6, NLR family pyrin domain containing 3 (NLRP3) and nuclear factor kappa-light chain-enhancer of activated B cells (NFκB) activation but only after stimulation with lipopolysaccharides (LPS)[219-221]. Finally, targeted gene modulation of peripheral myeloid cells reduced microglial activation resulting in increased survival of SOD1-ALS mice, suggesting an important role of the peripheral immune cells in the microglia-linked neuroinflammation[222]. Altogether, these data propose a potential early neuroprotective effect of microglia in ALS, especially reported in SOD1 models, that converses to a more detrimental state throughout the disease, likely due to activating stimuli resulting from neuronal damage, disease proteins or cytokines.

1.3.2.2 Reduced motor neuron support

In addition to the increased reactivity and secreted pro-inflammatory factors, also a reduced secretion of neuroprotective factors such as insulin- like growth factor 1 (IGF1) have been reported to contribute to motor neuron toxicity mediated by mutant SOD1 microglia[208,212-214]. However, contrary to the widespread neuroinflammation in ALS patients and models, support for this hypothesis only comes from SOD1-ALS models and should be further investigated in other models.

1.3.3 Oligodendrocytes

Other glial cells that are crucial for neuronal and axonal homeostasis are oligodendrocytes. Their main role is to produce myelin to form a myelin sheath that surrounds and insulates the axon to ensure proper signal conduction[223]. In addition, these cells support the neurons metabolically by the production of lactate after glycolysis which is shuttled to the neurons via the monocarboxylate transporter 1 (MCT1) channel where it can be metabolized further by oxidative phosphorylation[223,224].

Oligodendrocyte pathology is present in *postmortem* material from ALS patients[225-227], suggesting a role for these cells in the disease progression. In accordance, degeneration and loss of oligodendrocytes, due to incomplete differentiation, was observed in SOD1^{G93A} spinal cord before disease onset[67,228]. Moreover, removal of mutant SOD1 from oligodendrocyte progenitors in SOD1^{G37R} mice delayed disease onset, premature death and microglial and astrocytic activation, further demonstrating their role in ALS[67]. Indeed, primary SOD1^{G93A} oligodendrocyte progenitors or fALS and sALS patient iPSC-derived oligodendrocytes induce motor neuron toxicity when co-cultured with healthy motor neurons[229].

1.3.3.1 Loss of metabolic support

The oligodendrocyte-induced toxicity could be explained by a reduced metabolic support as both expression of MCT1 as well as lactate production itself were shown to be downregulated in oligodendrocytes from ALS mice, zebrafish and patients[228-231]. In agreement, the observed toxicity was completely rescued when lactate was added to SOD1^{G93A} oligodendrocyte-conditioned medium[229]. However, in co-culture set-up lactate addition did not completely rescue the induced motor neuron toxicity, suggesting an additional contact-dependent mechanism[229]. In agreement, defects in oligodendrocyte progenitor cell lipid metabolism were recently reported [232].

These data demonstrate the presence of oligodendrocyte-mediated motor neuron toxicity early in the disease and connect this toxicity to an incomplete maturation and disturbed lipid metabolism of oligodendrocyte progenitors and loss of the metabolic support of motor neuron via lactate provision.

1.3.4 Astrocytes

Astrocytes also play a crucial role in maintaining a healthy and functional central nervous system. Astrocytes are in close cross-talk with microglia and support adult motor neurons at different levels.

First, astrocytes play a central role in the molecular homeostasis and plasticity of neuronal synapses. Astrocytes modulate synapses by ensheathment to form tripartite synapses[233]. This close connection with neuronal synapses ensures removal of neurotransmitters such as glutamate or gamma aminobutyric acid (GABA) to prevent their accumulation[234] and regulates synapse dynamics by cytokine secretion[235-237]. Moreover, together with the microglia they regulate synaptic pruning[235,236], a process crucial for learning and memory. In addition, they control ion homeostasis at the synapse by buffering the excess amount of K^+ which builds up in the extracellular space during neuronal transmission[237,238]. Furthermore, next to regulating ion and neurotransmitter homeostasis, they also regulate pH and water transport[239].

Second, astrocytes offer structural support and are in close connection with the BBB[239]. The BBB is crucial in protecting the central nervous system from outside intruders. However, interaction between blood vessels and neurons through the blood-barrier is still required to receive nutrients and remove waste products which is facilitated by astrocytes that are in contact with both[239].

Third, astrocytes metabolically support neurons to meet their high energetic need similar to the oligodendrocytes. Astrocytes depend mainly on glycolysis for their ATP production which results in pyruvate that can be converted to lactate which is shuttled to the neurons via the MCT4 channel[240]. Moreover, they are also able to shuttle lactate directly from the blood stream to the neurons via their interaction with the BBB[241]. The high rate of oxidative energy metabolism in neurons results in the build-up of oxidative stress within these cells. However, they have minimal support systems against the oxidative stress that is generated during this process and therefore also depend on the high antioxidant potential of astrocytes for their defense against oxidative stress[242]. Moreover, reactive oxygen species (ROS)-induced lipids, are shuttled from neurons to astrocytes where they can form lipid droplets or can be metabolized in the ketogenic or fatty acid oxidation pathway[154]. In addition, astrocytes are the sole processors of brain glycogen which is the main energy reserve of the brain, released with neuronal activity[243].

Finally, astrocytes also play a role in the defense mechanism of the central nervous system. Any disturbances in the central nervous system such as injury, disease or infection result in the activation of astrocytes, accompanied by transcriptomic changes[244,245]. Analogous to the M1 and M2 microglia, astrocyte activation has also been classified as neurotoxic A1 or neuroprotective A2. However also in the case of astrocytes, this binary division has been shown to be oversimplified. Reactive astrocytes typically become hypertrophic and together with the microglia initiate an immune response through cytokine and interleukin secretion[246]. However, the reactive state of astrocytes can differ based on the stimuli and can be dynamic[247].

Astrocyte-specific deletion of mutant *SOD1* or *TARDBP* resulted in a delay in disease onset[248,249] or in a slower disease progression[66]. Also *in vitro* astrocytes were shown to contribute to motor neuron degeneration as various forms of mutant *SOD1*, *FUS* or *C9ORF72* hexanucleotide expansion in astrocytes induced motor neuron toxicity[49,250-255] and knock-down of mutant *SOD1* decreased mutant motor neuron death[253]. However, in contrast to the latter, Yamanaka *et al.* revealed that selective silencing of mutant $SOD1^{G37R}$ slowed disease progression of these mutant SOD1 mice by modulating the activation of microglia, which are not present in the in vitro model described by Haidet-Phillips *et al*[253]. Finally, while mutant *SOD1*, *FUS* or *C9ORF72* astrocytes[49,250-255] were toxic to motor neurons *in vitro*, the expression of mutant TDP-43 in astrocytes did not affect survival in motor neurons in

murine[256] or iPSC-derived[257] co-culture models. However, the addition of control iPSC-derived astrocytes to motor neurons with TDP-43 aggregates did offer protection[258]. Given these contrasting results in different *in vitro* and *in vivo* ALS models, further research is necessary to elucidate the role of astrocytes in ALS and their interaction with microglia. Given their versatile role in supporting the neurons, disturbances in several pathways contribute to the degeneration of motor neurons in ALS.

1.3.4.1 Neuroinflammation

In *postmortem* ALS tissue, astrocyte reactivity is present. Indeed, astrogliosis, defined as an increased number of astrocytes and abnormal reactivity, is a hallmark of ALS[253,255,259,260] and the extend of astrocyte reactivity correlates with disease progression[253,259,260]. As discussed above, the neuroinflammation present in ALS patient and ALS models is marked by microglial and astroglial activation. Microglia are known to induce a reactive astrocyte state that induces neurotoxicity by the release of IL-1α, TNFα and complement component C1q[261]. Knocking-out these factors in $SOD1^{G93A}$ mice reduced the number of reactive astrocytes and delayed motor neuron loss and disease progression resulting in increased survival[260]. This pro-inflammatory interaction between microglia and astrocytes is reciprocal as was shown by transplantation of $SOD1^{G93A}$ astrocytes in the spinal cord of wild-type rats that led to microglial activation[262] or the delay in microglial activation by deleting mutant SOD1 in astrocytes[66,248]. Inflammatory genes resulting in the expression and release of pro-inflammatory cytokines, chemokines and components of the complement cascade are upregulated in fALS and sALS astrocytes[251-253,263,264]. Also, overexpression of wild-type FUS in astrocytes resulted in an inflammatory response leading to microglial activation and motor neuron toxicity[265]. Moreover, astrocyte-mediated downregulation of major histocompatibility complex 1 (MHC1) on motor neurons, rendered these motor neurons more vulnerable to astrocyte-induced cell death[266]. In addition, the NFκβ pathway is upregulated in astrocytes[253,267] and astrocytic NFκβ activation in $SOD1^{G93A}$ mice induced microglial proliferation and leukocyte infiltration[268]. Nevertheless, inhibition of the NFκβ pathway in astrocytes did not mitigate the ALS phenotype in mutant SOD1 mice[269,270], while inhibition in microglia did offer motor neuron protection and extended survival[270]. Moreover, it was reported that microglial activation preceded disease onset in $SOD1^{G93A}$ mice while increased astrocytic glial fibrillary acidic protein (GFAP) expression is reported later in the disease progression indicating reactivity appeared later[271]. Hence, in ALS, microglia appear to contribute to disease pathology primarily through their inflammatory response, while astrocytes seem to play a role in pathogenesis through a variety of mechanisms.

1.3.4.2 Excitotoxicity

Another ALS pathological mechanism that is based on the involvement of astrocytes is that of increased excitotoxicity. Glutamate propagates signals at synapses by activating ionotropic glutamate receptors present on the postsynaptic neuron. Excitotoxicity results from overstimulation of glutamate receptors due to an increased concentration of glutamate or increased sensitivity for glutamate stimulation. This overstimulation causes an influx of natrium and calcium ions and/or a generation of free radicals resulting in neuronal death. To maintain a healthy glutamate balance, glutamate is removed from the synaptic cleft by the astrocytic glutamate transporter excitatory amino acid transporter 2 (EAAT2)[234]. The hypothesis that excitotoxicity leads to motor neuron death in ALS emerged after studies reported increased glutamate levels in cerebrospinal fluids of sALS patients, reduced glutamate transport and reduced astrocytic EAAT2 expression[272-276]. Astrocytes can protect motor neurons from excitotoxicity by inducing upregulation of neuronal glutamate receptor 2 (GluR2) subunit of α-amino-3-hydroxy-5-methyl-4-isoxazolepropionic acid (AMPA) receptors which reduces their calcium permeability, providing protection. However, ALS-linked mutations in *SOD1* abolished their ability to regulate GluR2, making motor neurons more vulnerable to AMPA receptor-mediated excitotoxicity[277]. In addition, more recently increased expression of connexin 43 (Cx43) was found in fALS and sALS models and patients[278,279]. Cx43 gap junction and hemichannels mediate calcium wave propagation and facilitate ion, metabolite, miRNA and second messenger diffusion messengers[280]. Therefore, their upregulation results in calcium hyperactivity causing motor neuron excitotoxicity and cell death[278,279].

1.3.4.3 Metabolic dysfunction

In addition to their support of neuronal glutamate and ion homeostasis, astrocytes also support motor neurons metabolically. However, numerous studies reported a defective astrocyte metabolism which affects their ability to metabolically support motor neurons.

In astrocytes from SOD1^{G93A} mice a defective mitochondrial respiratory function was reported with decreased oxygen consumption, lack of adenosine diphosphate (ADP)-dependent respiratory control and decreased membrane potential linked to nitro oxidative damage and superoxide radical formation leading to motor neuron toxicity[281]. Moreover, increased levels of oxidative stress were reported in SOD1-ALS patient iPSC-derived astrocytes[282]. Moreover, motor neuron death after treatment with conditioned astrocyte medium (CAM) from *TDP-43*^{A315T} primary astrocytes was linked to nitro oxidative stress[283]. Also reduced levels of the antioxidant factor glutathione were reported in primary astrocytes from *TDP-43*^{Q331K} expressing mice[284]. This reduction in antioxidant factors was further confirmed in

C9ORF72-ALS iPSC-derived astrocytes in which increased levels of oxidative stress were linked to a reduced release of antioxidant factors[285]. In addition, in iAstrocytes differentiated from C9ORF72 and sALS patient fibroblasts, a reduction in metabolic flexibility was reported in starvation conditions with defects in adenosine, fructose and glycogen metabolism[286]. This defect in adenosine metabolism was attributed to low levels of adenosine deaminase, which was found to contribute to neuron toxicity[287].

Next to the reduced release of antioxidant factors, ALS astrocytes were also suggested to fail in their metabolic support due to a reduction in lactate provision, similar to the lactate shuttle hypothesis in oligodendrocytes. This hypothesis was based on SOD1 model and ALS patient material in which a decrease in the astrocytic lactate levels, linked to impaired glycolysis due to nicotinamide adenine dinucleotide (NAD^+) downregulation, and defects in the lactate efflux reporter were reported[288,289]. In addition, a dysregulated metabolism was also reported in primary rat astrocytes with TDP-43 inclusion together with impaired provision of lactate[290].

1.3.4.3 Reduced motor neuron support

In addition to reduced levels of secreted lactate and antioxidants, the loss-of-support by astrocytes in ALS is further exaggerated by a decreased release of neurotrophic factors. Primary astrocytes from mutant TDP-43 rats revealed a downregulation of neurotrophic genes[291]. Moreover, extracellular vesicles of C9ORF72-ALS astrocytes are abnormal with lower secreted levels of miR-494-3p which is linked to motor neuron maintenance and survival[292]. Besides the reduced loss-of function due to reduced secretion of neurotrophic factors, SOD1-ALS iPSC-derived astrocytes also show reduced levels of Kir4.1 expression which is required in the K^+ ion homeostasis[293].

1.3.4.3 Increased motor neuron toxicity

From the moment it was found that medium from ALS astrocytes is toxic to motor neurons, the search for the identification of secreted toxic factors started[49,251,283]. Toxic factors related to an increased astrocytic inflammatory response such as TNFα, IL-6, IL-8, IL-1β and lipocalin 2[294] or increased metabolic and oxidative stress such as NO, ROS and prostaglandins have been found to be increasingly released from ALS astrocytes[49,251,252,295-300]. Moreover, in addition to increased reactivity and dysfunctional metabolism, other astrocyte pathways have been reported to be dysfunctional in ALS leading to motor neuron toxicity. Abnormal extracellular vesicles do not only lead to a loss-of-motor neuron support, but can also be toxic[292]. Moreover, astrocyte-induced dysfunction of motor neuron autophagy has been reported in multiple studies[287,301,302]. In addition, excessive inorganic polyphosphate (polyP), a gliotransmitter regulating neuronal excitability through ion channel modulation, was found to be released from ALS astrocytes and could induce motor neuron toxicity in

culture[298]. Finally, recent use of a bioinformatic prediction model suggested that SOD1^{G93A} astrocytes cause motor neuron death through amyloid precursor protein fragment release and activation of death receptor 6 (DR6) on motor neurons, which was experimentally validated[303].

Altogether, these data point towards a clear role of astrocytes in the pathology of ALS. Given the wide variety of astrocyte roles in the nervous system and the amount of evidence supporting different disease-related dysfunction in multiple pathways, the involvement of astrocytes in ALS seems to be the result from a combination of loss-of-support and gain-off-toxic effects which is confirmed by transcriptomic analyses of various fALS and sALS, human and murine astrocytes[255,263].

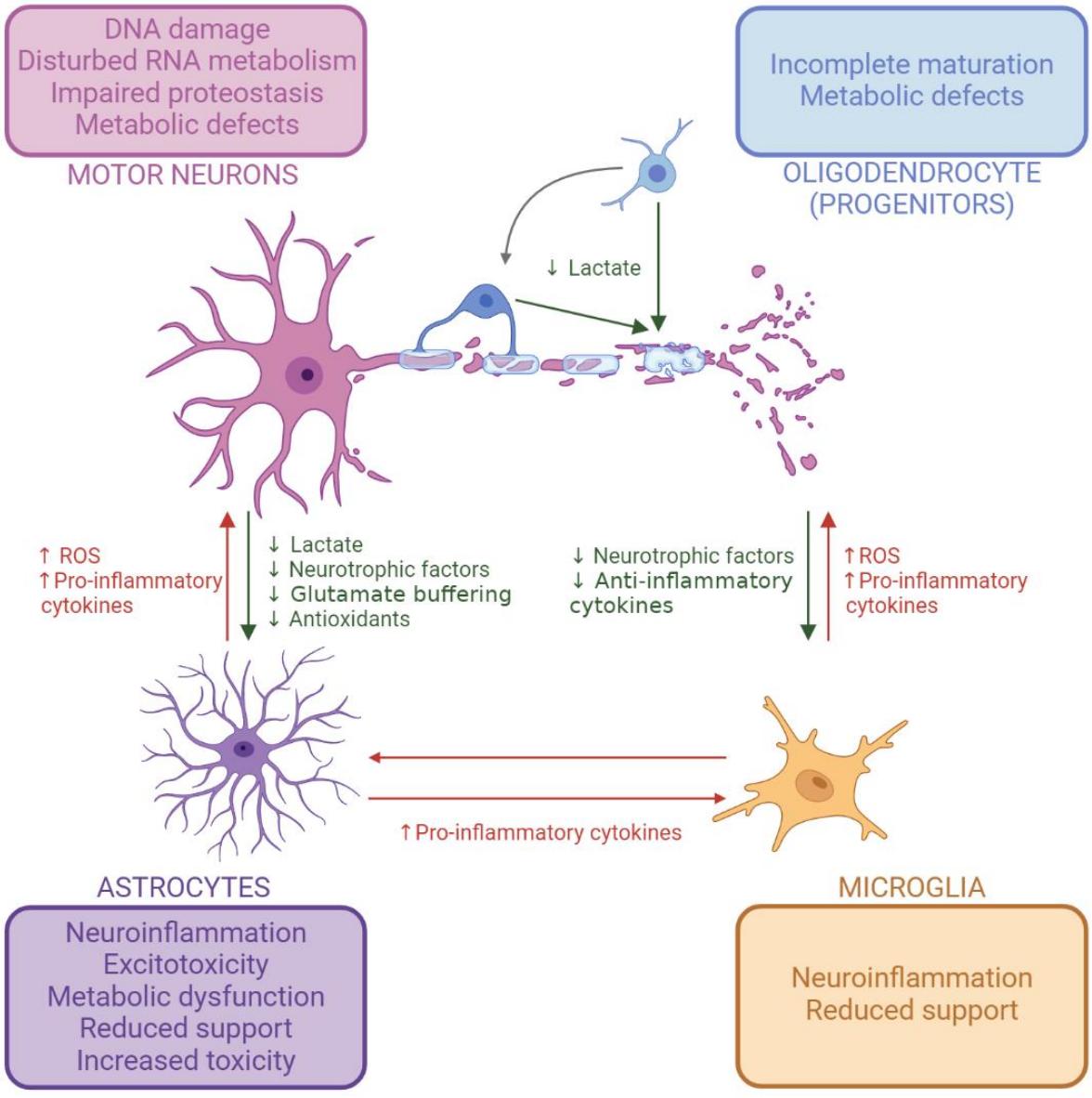


Figure 1.4 Interplay between motor neuron-autonomous and non-cell-autonomous-mechanisms in ALS pathology. Both motor neuron and glial pathways are linked to ALS pathology. In motor neurons, disturbed DNA, RNA and protein homeostasis as well as metabolic defects are reported numerous times. Metabolic defects are also found in oligodendrocytes and astrocytes leading to reduced metabolic support contributing to the metabolic defects in motor neurons. Astrocytes also contribute to motor neuron degeneration via cell-autonomous defects leading to excitotoxicity, reduced neuronal support, increased neuronal toxicity and neuroinflammation. The increased neuroinflammation is in close interaction with the microglia that also show reduced support in addition to the increased neuroinflammation. Finally, oligodendrocyte progenitors also contribute to reduced axonal support by incomplete maturation. Figure adapted from Vahsen et al.[304] with BioRender.com.

The continuously growing amount of evidence showing the involvement of different non-neuronal cells in ALS pathology, reveals their undeniable role in ALS pathology. Therefore, they should not be ignored in our ongoing search for ALS therapeutic strategies.

1.4 A new era of ALS drug discovery

While our knowledge about the disease and its pathology is growing, ALS remains an incurable disease. Nevertheless, optimism is justified as over the last decade significant advances were made in preclinical models, in our knowledge about the pathology and in clinical readouts[305]. These advances resulted this year in a second disease-modifying drug approved by both the US Food and Drug Administration (FDA) and European Medicines Agency (EMA), more than 25 year after the first available therapy[306].

Riluzole, the first and for a long time the only available drug approved by the FDA and EMA, acts on excitotoxicity by blocking glutaminergic neurotransmission, prolonging the survival of patients[307]. After Riluzole, Edaravone[308], a free radical scavenger, and AMX0035[309], mitigating mitochondrial dysfunction and endoplasmic reticulum stress, followed in the US. However, both drugs are not approved by EMA most likely because Edaravone is proven to be beneficial in only a subset of patients and because the effect of both Edaravone and AMX0035, which showed no impact in phase 3 clinical trial, on survival is still unclear.

A new era of drug discovery was initiated with antisense oligonucleotides (ASOs). These single-stranded, chemically modified oligonucleotides can bind specifically to intracellular mRNAs by base pairing, modifying their gene expression at translational level[310]. This year Tofersen, an ASO against *SOD1*, that successfully decreases the expression of SOD1 and the levels of neurofilament in cerebrospinal fluid of patients[306] was approved by the FDA and EMA. Furthermore, multiple other clinical trials against other genetic forms of ALS are ongoing[311]. However, not all of these were positive

as the clinical trials for ASOs against the sense C9ORF72 hexanucleotide repeat expansion were stopped after neurofilament levels increased in cerebrospinal fluid of ALS patients[312]. Further research on the reason why these were unsuccessful is performed. While initial research only focused on genetics forms of ALS, other therapeutically interesting targets, based on ALS pathology, can be targeted with ASOs. As an example, ASOs preventing *STMN2* and *UNC13A* cryptic exon splicing are being investigated[311].

With this new opportunity, the search for the pathological mechanisms and new therapeutic targets is even more than ever crucial.

1.5 EGLN2/PHD1, a promising target for ALS?

The egl-9 family hypoxia-inducible factor (EGLN) enzymes EGLN1, 2 and 3, also known as prolyl hydroxylase domain containing enzymes (PHD) PHD2, 1 and 3 respectively, could form promising new therapeutic targets for ALS. The EGLN enzymes are oxygen sensors and master regulators of the response to hypoxia[313]. Next to oxygen, also α-ketoglutarate, ferrous iron (Fe^{2+}) and ascorbic acid are required co-factors, while other tricarboxylic acid cycle intermediates inhibit EGLN activity[314-316]. As a result, EGLNs also function as metabolic sensors and can respond accordingly via a range of cell- and context-specific targets [317]. Hence they play a central role in several signaling pathways, cell cycle regulation, cellular energy metabolism and transcription[318].

The canonical target of the EGLN enzymes is hypoxia-inducible factor α (HIFα)[319,320]. During normoxia, EGLN enzymes target HIFα for proteasomal degradation through hydroxylation. Under hypoxic conditions, EGLN enzymes lose their ability to hydroxylate HIF, which leads to HIF stabilization and the transcription of HIF targets that play a role in a variety of pathways, including cellular metabolism[321]. Interestingly, genetic ablation of the *EGLN2*, but not *EGLN1* or *EGLN3*, has shown to protect skeletal muscle[322] and hepatocytes[323] against oxidative stress via the activation of a HIF transcriptomic response. Moreover, downregulation of EGLN2 protected cortical neurons against oxidative stress in models for stroke through metabolic rewiring independent from HIF[324]. As discussed before, both increased oxidative stress and metabolic dysfunction are present in ALS. Interestingly, compounds that provide protection against hypoxic stress, via the induction of a HIF1α transcriptional response, increased the survival of ALS mice[325,326]. Moreover, also HIF-induced transcription of vascular endothelial growth factor (VEGF) has been shown to be involved in motor neuron survival[327] and delivery of VEGF *in vivo* and *in vitro* provides protection against motor neuron degeneration[328,329].

While HIFα is the canonical target of EGLN2, numerous HIF-independent and even hydroxylation-independent targets have been described[317,318], such as TP53-inducible glycolysis and apoptosis

regulator (TIGAR) which resulted in the cortical neuron protection upon EGLN2 inhibition[324]. An overview of all targets is provided in Table 1.1. The once that are relevant for (motor) neuron degeneration will be discussed in more detail in line with the context of this thesis.

The ion channel transient receptor potential cation channel member A1 (TRPA1) has been shown to be involved in astrocyte reactivity and has been reported to promote the activation of proinflammatory cytokines in Alzheimer's disease and migraine[330]. In addition, also IκB kinase (IKKβ) is a well-known HIF-independent target of EGLN2[331]. As a result, EGLN2 regulates, via IKKβ, the activity of the NFκB pathway, playing a central role in the cellular inflammatory response[324,331,332]. Moreover, EGLN2 was shown to bind to the C-terminal transmembrane domain of mitochondrial antiviral-signaling proteins (MAVs) in zebrafish, hereby promoting their aggregation and enhancing antiviral responses leading to interferon induction. As discussed before, neuroinflammation characterized by microglial and astroglial activation is a key hallmark of ALS. Increased neuroinflammation is marked by increased NFκB activation in astrocytes and microglia from ALS patients and models[269,270]. In addition, an increased interferon response has also been observed in immune, neuronal and glial cells from ALS models and ALS patients[96-100].

Finally, also the transcription factor activity of forkhead box O3A (FOXO3A), PGC1α, which are regulated by EGLN2, have been linked to motor neuron degeneration in ALS[333-335].

Altogether, these context- and cell-dependent targets of EGLN2, make it a unique target that plays a central role in multiple cell-autonomous and non-cell autonomous mechanisms that are involved in ALS pathology.

TARGET	ABBREVIATION	INTERACTION	EFFECT	REFERENCE
Hypoxia inducible factor-α	HIFα	Hydroxylation	HIFα degradation	Semenza *et al.*[336]
Inhibitor of kappaB kinase β	IKKβ	Hydroxylation (?)	Negative (?) regulation of canonical NFκB pathway	Cummins *et al.*[331]
Large subunit of RNA polymerase II	RBP1	Hydroxylation	Activation of RBP1	Mikhaylova *et al.*[337]
Cerebellar degeneration-related protein 2	CDR2	Binding	Enhanced repression of HIF	Balamurugan *et al.*[338]
Transient receptor potential cation channel, member A1	TRPA1	Hydroxylation	Negative regulation of ion channel activity	Takahashi *et al.*[339]
Activating transcription factor 4	ATF4	Binding	Negative regulation of transcription factor activity	Hiwatashi *et al.*[340]
Sprouty homolog 2	SPRY2	Hydroxylation	Negative regulation of Spry2-mediated inhibition of FGF-induced ERK1/2 activation	Anderson *et al.*[341]
Centrosomal protein 192	Cep192	Hydroxylation	Cep192 proteosomal degradation regulating cell-cycle progression	Moser *et al.*[342]
Forkhead box O3A	FOXO3A	Hydroxylation	Negative regulation of transcription factor activity	Zheng *et al.*[343]
Tumor protein P53	P53	Hydroxylation	P53 activation	Deschoemaeker *et al.*[344]
Peroxisome proliferator-activated receptor gamma coactivator 1 α and Nuclear respiratory factor 1	PGC1α and NRF1	Binding	Positive regulation of transcription factor activity	Zhang *et al.*[345]
TP53-inducible glycolysis and apoptosis regulator	TIGAR	?	Negative regulation of transcription factor activity	Quaegebeur *et al.*[324]
adenylsuccinate lyase	ADSL	Hydroxylation	Activation of ADSL required in purine synthesis	Zurlo *et al.*[346]
leucyl tRNA synthetase	LRS	Binding	Promotion of mTORC1 activity	D'Hulst *et al.*[347]
Dual specificity tyrosine phosphorylation regulated kinase 1A and B	DYRK1A and B	Hydroxylation	DYRK1 activation leading to HIF2α degradation	Lee *et al.*[348]
Mitochondrial antiviral-signaling protein	MAV	Binding	Activation of antiviral responses	Yu *et al.*[349]

Table 1.1 Intracellular hydroxylation-dependent and -independent targets of EGLN2/PHD1.

CHAPTER 2 AIMS OF THE STUDY

CHAPTER 2 AIMS OF THE STUDY

ALS is a complex disorder in which a combination of **cell-autonomous and non-cell-autonomous mechanisms** result in progressive and currently irreversible motor neuron degeneration that leads to paralysis and death of the patient within three to five years after diagnosis. Despite the poor prognosis, **no treatment is available** for ALS. With a **cumulative life-time risk of 1 in 400** to get ALS, there is a high need of new therapeutic strategies. Therefore, we should develop targeted strategies based on our increased molecular understanding of the disease pathology. **EGLN2** formed a promising target because it plays a central role in the oxidative stress response, energy metabolism and neuroinflammation, three key hallmarks of ALS pathology. Therefore, the overarching aim of this thesis was to explore the **role and therapeutic potential of EGLN2**, using **various models and cell-specific tools**.

More specifically, the four main sub-objectives of this thesis were:

I. **To explore whether downregulation of Egln2 could mitigate the motor axonopathy in a C9ORF72 and SOD1 zebrafish model for ALS.** Zebrafish offer a valuable tool to screen for ALS modifiers. Our lab previously established a C9ORF72 and SOD1 zebrafish model that both display a robust motor neuron phenotype. Using and AMO against *egln2*, we aimed to investigate whether downregulation of Egln2 had a beneficial effect on the motor axon abnormalities in these ALS models.

II. **To investigate whether genetic deletion of *Egln2* mitigated the ALS phenotype in SOD1- and FUS-ALS mice.** Mice overexpressing human mutant SOD1 ($SOD1^{G93A}$) and human wildtype FUS ($FUS^{+/+}$) both present an ALS phenotype with motor neuron degeneration, paralysis and premature death. We aimed to investigate whether genetically targeting *Egln2* would be beneficial for these mice and would mitigate their ALS symptoms.

III. **To identify cell-specific pathways affected by *Egln2* deletion in ALS mice.** Using single-nuclei RNA sequencing (snRNA-seq), we aimed to study the cell-specific effects of *Egln2* deletion and to identify the contribution of motor neuron-autonomous and non-autonomous mechanisms to the EGLN2-mediated motor neuron protection.

IV. **To confirm the cell-specific pathways affected by *Egln2* deletion in patient-derived cells.** After identification of the cell-specific pathways that were linked to the beneficial effects of *Egln2* deletion, we aimed to confirm the observed pathways in patient cells using SOD1-ALS patient-derived iPSCs.

CHAPTER 3 MATERIALS & METHODS

Parts of this chapter appeared in:

Germeys, C.*, Vandoorne, T.*, Davie, K., Poovathingal, S., Heeren, K., Vermeire, W., Nami, F., Moisse, M., Quaegebeur, A., Sierksma, A., et al. (2024). Targeting EGLN2/PHD1 protects motor neurons and normalizes the astrocytic interferon response. Cell Rep *43*, 114719. 10.1016/j.celrep.2024.114719
*These authors contributed equally

CHAPTER 3 MATERIALS & METHODS

3.1 Ethical approval

All zebrafish (P112/2021) and mouse (P020/2020) experiments were approved by the Ethic Committee of the KU Leuven. All patient-derived iPSC experiments (S50354) were approved by the Ethical Committee of UZ Leuven.

3.2 Zebrafish micro-injections and follow-up

Zebrafish (AB strain, RRID: ZFIN_ZDB-GENO-960809-7) embryos were kept in a 28°C incubator. Micro-injection of 1000 ng/µl *SOD1*^{WT} and *SOD1*^{G93A} RNA or 181 ng/µl 91 (91S) *C9ORF72* hexanucleotide repeats and *GFP* RNA, as specified before[32,350], and 0.1 mM *egln2* AMO was done in 1–2 cell stage zebrafish oocytes. Motor axons were assessed with an SV2 staining at 30 hpf. The sexual differentiation of zebrafish occurs later on so gender is not relevant.

3.2.1 DNA constructs and AMO

Human cDNA of *SOD1*^{WT} and *SOD1*^{G93A} in the pCLneo vector were kindly provided by R.H. Brown Jr (UMass Chan Medical School, Worcester, US). SOD1 was cloned in the pBCM vector behind a T3 promoter and linearized using Asp718 restriction enzyme (ER0901, Thermo Scientific, Waltham, US). Plasmids containing 91 (91S) *C9ORF72* hexanucleotide repeats under a T7 promotor were obtained and adapted as described previously[56,351]. The GFP control plasmid construct (PS100010, Origene, Rockville, USA) was digested with AgeI restriction enzyme (ER1461, Thermo Scientific). RNA was transcribed from DNA using mMESSAGE mMACHINE™ T3 Transcription Kit (AM1348, Invitrogen, Waltham, US) or mMESSAGE mMACHINE™ T7 ULTRA Transcription Kit (AM1345, Invitrogen) and purified using the MEGAclear™ Transcription Clean-Up Kit (AM1908, Invitrogen). AMOs were designed and obtained from Gene Tools (Philomath, US): control AMO (sequence: CCTCTTACCTCAGTTACAATTTAT) and *egln2* E2I2 AMO (sequence: TATACATCGCCTCTCACTCACCT).

3.2.2 Motor axonopathy analysis

Zebrafish were collected at 30 hpf and fixed overnight with 4% PFA at 4°C. Fixation was followed by permeabilization with acetone for 1 h at -20°C, blocking with 1% bovine serum albumin (BSA), 1% dimethyl sulfoxide (DMSO) phosphate buffered saline (PBS) for 1 h at RT and immunostaining with primary mouse anti-synaptic vesicle glycoprotein 2 (SV2) (Table 3.1) in 1%DMSO/PBS for 3 h at RT. Embryos were incubated overnight at 4°C with secondary Alexa Fluor 555 anti-mouse antibody (Table

3.1) in 1% DMSO/PBS. Stained zebrafish embryos were analyzed with fluorescence microscopy (Leica DM 3000 LED microscope, 20x objective, DMK 33UX250 USB3.0 monochrome industrial camera, The Imaging Source, Wetzlar, Germany) using LUCIA software version 4.60 (Laboratory Imaging). Fish were scored on axonal length and abnormal branching of ventral root projections using a standardized method. Axonal length was measured from the 8th up to the 12th axon on one side in 15 fish per condition in each experiment. Abnormal branching was scored from the 8th up to the 17th axon on both sides. Branching was considered abnormal when at least two out of 20 axons were branched at or above the ventral edge of the notochord.

3.3 Mice breeding and follow-up

SOD1^{G93A} mice overexpressing human mutant *SOD1* (glycine to alanine substitution at codon 93) (stock number: 002726, RRID: IMSR_JAX:002726) and FUS$^{+/-}$ breeding mice overexpressing wild-type human FUS on one allele (stock number: 017916, RRID: IMSR_JAX:017916) were purchased from The Jackson Laboratory (Maine, United States of America (US)). For experiments, FUS$^{+/+}$ mice were used that overexpress wild-type human FUS on both alleles. Both strains were maintained on a C57BL/6 background. *Egln2*$^{-/-}$ mice were generated previously[352] and backcrossed for seven generations to obtain a pure C57BL/6 background. *Egln2*$^{-/-}$ mice were intercrossed with *SOD1*^{G93A} and FUS$^{+/-}$ mice to generate *SOD1*^{G93A}*/Egln2*$^{-/-}$, *SOD1*^{G93A}*/Egln2*$^{+/-}$, *FUS*$^{+/+}$*/Egln2*$^{-/-}$ and *FUS*$^{+/+}$*/Egln2*$^{+/-}$ mice and investigated together with their *SOD1*^{G93A}*/Egln2*$^{+/+}$ littermate and *FUS*$^{+/+}$*/Egln2*$^{+/+}$ controls respectively. Mice were housed at the KU Leuven animal facilities with a 12 h light-dark cycle at a temperature of 20°C. For the SOD1^{G93A} mice, standard rodent chow and water was provided *ad libitum*. For the FUS$^{+/+}$ mice crushed standard rodent chow mixed with water was provided ad libitum from the age of 28 days. Mice were followed-up over their lifespan and additional analyses such as motor neuron count, NMJ quantification and snRNA-seq were performed at P110. For all experiments, littermate controls and both male and female mice were used.

3.3.1 Disease onset and survival

Disease onset was determined by bodyweight and rotarod performance. Disease onset was considered as the last time point at which the mouse maintained 90% of its peak body weight or at the last time point at which the latency to fall on the rotarod (Ugo Basile, Gemonio, Italy) was longer than 150 s at a constant speed of 15 rpm. Survival was determined by the loss of righting reflex within 20 s. This time point was considered as humane endpoint, whereupon the mouse was sacrificed.

3.3.2 Behavioral testing

Motor performances in *FUS*$^{+/+}$*/Egln2*$^{-/-}$, *FUS*$^{+/+}$*/Egln2*$^{+/-}$ and mice *FUS*$^{+/+}$*/Egln2*$^{+/+}$ were measured three times a week starting at 28 days of age. Muscle force was measured using a Grip Strength Meter (Columbus Instruments, Columbus, US) with a triangular bar as a probe to measure the grip strength in the forepaws. An average of three trials per animal was determined. To assess both fore- and hindlimb muscular strength, the hanging wire test was performed. Mice were placed on a wire cage lid which was inverted and the latency to fall was recorded to a maximum of 60 s.

3.3.3 Motor neuron counts

Mice were anesthetized using 10% Dolethal (Vétoquinol, Lure, France) and transcardially perfused with 1X PBS (806552, Sigma-Aldrich, Saint-Louis, US) followed by perfusion with 4% paraformaldehyde (PFA). Lumbar spinal cords were harvested, post-fixed with 4% PFA overnight at 4°C and dehydrated for 48 h in a 30% sucrose solution at 4°C. Following embedding in Optimal Cutting Temperature (O.C.T.) (00411243, VWR, Radnor, US) compound mounting medium for cryometry the samples were stored at -80°C until further processing. 20 micron cryosections were obtained and every tenth section was stained with 2X thionin solution to visualize the motor neuron cell bodies in the ventral horn. Briefly, cryosections were fixed for 1 min in 100% ethanol in a cryochamber and subsequently washed for 15 s in distilled water, stained with 2X thionin during 45 s, washed twice in distilled water and dehydrated in 70%, 90% and 100% ethanol for 30 s each. Histological sections were cleared with Histoclear solution for 1 min and mounted using PerTex (00801, Histolab, Västra Frölunda, Sweden). A minimum of ten spinal cord sections for each mouse were analyzed. Images were taken using the Zeiss Imager M1 microscope (Carl Zeiss Inc., Oberkochen, Germany). Neuron size and number was quantified using ImageJ (RRID: SCR_003070) and were normalized to the ventral horn size of the respective section and multiplied by the ventral horn size of a non-transgenic mouse (300,000 μm^2).

3.4 iPSC lines, differentiation and treatments

iPSCs from a female ALS patient carrying a *SOD1*^{A4V} and its isogenic control (*SOD1*^{A4A}) were generated previously by Kiskinis *et al.*[123] and kindly provided by prof. K. Eggan (Harvard University, Cambridge, US). iPSCs were cultured on Geltrex (A1413201, Gibco, Waltham, US) in Complete Essential 8 medium (A1517001, Gibco) with 1% penicillin/streptomycin (15070063, Gibco) in a humidified 5% CO_2 incubator at 37°C. A CRISPR-Cas9 mediated knock-out of *EGLN2* was generated in *SOD1*^{A4V} iPSCs as explained in detail in the method section.

3.4.1 Generation and quality control of EGLN2 knock-out iPSCs

3.4.1.1 Generation of EGLN2 knock-out iPSCs with CRISPR-Cas9

To perform electroporation, iPSCs were incubated at 37°C for at least 1 h in mTESR1 medium (85850, Stemcell technologies, Vancouver, Canada) containing 10 µM Y-27632 rho-associated kinase inhibitor (ROCKi) (SCM075, Gibco). Next, the colonies were dissociated to single cells by incubation with accutase (A6964, Sigma-Aldrich) at 37°C for 15-20 min. Approximately 1.2 x 10^5 cells were resuspended in 100 µl optimum and mixed with ribonucleoprotein (RNP) form of CRISPR-Cas9 system composed of Cas9 protein (1081058, Alt-R™ S.p. Cas9 Nuclease V3, IDT, Newark, US) and a single guide RNA (sgRNA; Alt-R™ CRISPR-Cas9 sgRNA, IDT) with the following sequence: ACGAAGACCCTGGTAACTGA. After nucleofection using the Nepagene electroporator with the following settings; poring pulse (voltage 125v, pulse length 5 msec, pulse interval 50 msec, number of pulses 2, decay rate of 10%, and polarity set at +) and transfer pulse (voltage 20 v, pulse length 50 msec, pulse interval 50 msec, number of pulses 5, decay rate of 40%, and polarity set at+/-), cells were immediately collected in mTESR1 containing ROCKi, re-plated on plates coated with BD™ Matrigel (356234, BD, Franklin Lakes, US) and placed in the incubator. The day after, medium was switched to E8 Flex supplemented with 10 µM ROCKi. After 10-15 days single colonies were picked using a colony picker tool (Fine Science Tools, Heidelberg, Germany) under a microscope placed in a class I biological safety cabinet. Colonies were genotyped via sequencing the target region using Q5 2x mastermix (M0492S, New England BioLabs, Ipswich, US). Amplicons were purified using PureLink PCR Purification Kit (K310001, Invitrogen) prior to Sanger sequencing (Europhins Genomics, Ebersberg, Germany). Sanger sequencing results were analyzed using SnapGene (RRID: SCR_015052) version 6.1.1 software and Synthego ICE tool (RRID: SCR_024508). Quality control including off-target analysis, immunofluorescence, embryoid body (EB) formation scorecard analysis, single nucleotide polymorphism (SNP) profiling and array-comparative genomic hybridization (array-CGH) were performed as described below.

3.4.1.2 Off-target analysis

Prediction of off-target sites was performed by using CRISPOR tool (http://crispor.tefor.net/, RRID: SCR_015935). Five predicted off target sites with the highest Cutting Frequency Determination (CFD) scores were selected[353]. Off target regions were PCR amplified and subjected to Sanger sequencing. Sanger sequencing results were analyzed using SnapGene version 6.1.1 software and Synthego ICE tool.

3.4.1.3 Immunofluorescence analysis of pluripotent markers

Cells were fixed with 4% PFA for 10 min, washed with PBS and permeabilized with 0.1% Triton-X in PBS, followed by 30 min blocking with 5% goat serum in PBS (Dako, Glostrup, Denmark). Cells were stained overnight at 4°C with primary antibodies (Table 3.1) and washed three times for 5 min with 0.1% Triton-X in PBS. Next, cells were incubated for 60 min at room temperature with the appropriate secondary antibodies (Table 3.1), washed three times and stained with Hoechst 33342 (14533, Sigma-Aldrich, 1:2000 dilution). Coverslips were mounted using Prolong Gold antifade reagent (P36930, Invitrogen) on superfrost microscope slides (10457673, ThermoFisher Scientific). Images were taken using the Axioimager Z.1 fluorescence microscope (Carl Zeiss Inc.).

3.4.1.4 EB formation and Scorecard analysis

To make EBs, iPSCs were washed with PBS and incubated 1 minute with EDTA. Cells were harvested and counted. Approximately one million cells were resuspended in 1mL Essential 6 medium (A1516401, Gibco) and 10µL RevitaCell supplement (A2644501, Gibco), transferred to one well of Ultra-Low Attachment 24-well plates (CLS3471, Corning, New York, US) and maintained for 7 days with half medium changes every other day. The rest of the cells were frozen as dry pellet as Day 0 control. EBs were collected after 7 days for RNA isolation using GenElute™ Total RNA Purification Kit (RNB100, Sigma-Aldrich) and cDNA synthesis using SuperScript™ III First-Strand Synthesis System kit (18080051, Invitrogen). cDNA samples were mixed with water and TaqMan Gene Expression Master Mix (4369016, Applied Biosystems, Waltham, US) and loaded to a TaqMan hPSC Scorecard® 384-well plate (A15870, Applied Biosystems). Results were analyzed with the hPSC Scorecard® analysis software.

3.4.1.5 SNP profiling

SNP profiling was performed using TaqMan® SNP Genotyping Assay (Life Technologies, Carlsbad, US) customized for genotyping SNPs in each sample. Custom made TaqMan® SNP Genotyping Assay (384-well plate) was loaded using 2.5 µl 2x TaqMan™ GTXpress™ Master Mix mixed with 2.5 µl genomic DNA (4ng/µl) per well. Results were analyzed by TaqMan Genotyper Software (Life Technologies).

3.4.1.6 Array-CGH

Genomic DNA samples were extracted using PureLink Genomic DNA kit (Invitrogen). Array-CGH was performed in UZ Leuven, Centrum Menselijke Erfelijkheid (CME). Results were analyzed using CytoSure interpret software.

3.4.2 Astrocyte differentiation

iPSCs were differentiated in mature astrocytes as described previously[300]. In short, iPSCs were dissociated with collagenase type IV (10780004, Gibco) and cultured in Corning ultra-low attachment plates with neuronal induction medium (NIM) consisting of Complete Essential 8 medium with 1% penicillin/streptomycin supplemented with 0.1 µM LDN-193189 (04–0074-02, Stemgent, Beltsville, US) and 10 µM SB431542 (1614, Tocris, Bristol, UK) for the first week to support neuronal induction to form EBs. NIM was changed on day 1, 2 and 4. On day 7, EBs were plated on Geltrex-coated plates in neuronal maturation medium (NMM) consisting of 50% Dulbecco's modified eagle medium (DMEM)/F12 (11330032, Gibco) and 50% Neurobasal medium (21103049, Gibco) with 1% L-glutamine (25030–024, Thermo Scientific), 1% penicillin/streptomycin, 1% N-2 supplement (17502–048, Gibco) and 2% B-27™ without vitamin A (12587–010, Gibco) supplemented with 10 ng/ml recombinant murine fibroblast growth factor (FGF)-2 (450–33, PeproTech, Cranbury UK), 10 ng/ml recombinant human epidermal growth factor (EGF) (CYT-217, ProSpec, Rehivit, Israel), 0.1 µM LDN-193189 and 10 µM SB431542 to allow neural rosette formation and induce neural progenitor cell (NPC) expansion. NMM was changed every other day and NPCs were passaged using accutase when 100% confluency was reached. On day 16, neuronal NMM was switched to astrocyte differentiation medium (ADM) consisting of 90% Neurobasal medium, 1% penicillin/streptomycin, 1% N-2 supplement, 1% non-essential amino acids (11140050, Gibco) and 0.8 µM ascorbic acid (A4403, Sigma-Aldrich) supplemented with 10 ng/ml FGF-2, 200 ng/ml recombinant human IGF1 (100–11, Peprotech), 10 ng/ml human Activin A (PHC9564, Gibco) and 10 ng/ml recombinant human Heregulinβ1 (100–03, Peprotech). ADM was changed every other day until day 25 to convert NPCs to astrocyte progenitor cells (APCs). On day 25 (d25/d+0), a glial switch occurred to commence the astrocyte maturation, which took an additional 4 weeks. APCs were plated on Geltrex-coated plates for expansion and maturation in astrocyte maturation medium (AMM) consisting of 50% DMEM/F12, 50% Neurobasal medium, 1% non-essential amino acids, 1% N-2 supplement, 1% L-glutamine, 1% penicillin/streptomycin, 2% fetal bovine serum (FBS) (10270106, Gibco), 0.8 µM ascorbic acid, and 1% sodium pyruvate (11360–070,Gibco) supplemented with 200 ng/ml IGF-1, 10 ng/ml Activin A and 10 ng/ml Heregulinβ1 which was changed every other day. Astrocytes were used for experiments starting from 28 days of differentiation (d+28). Before transcriptomic analysis cells were treated for 24h with 3ng/ml IL-1α (200-LA-010, Bio-techne, Minneapolis, US), 30 ng/ml TNFα (210-TA-020, Bio-techne) and 400 ng/ml C1q (204876, Sigma-Aldrich) in AMM medium without FBS. Conditioned astrocyte medium (CAM) and control astrocyte medium (AMM) without FBS were collected from d+28 onwards after 48h incubation for the metabolic flux experiment and 24h for the neurite outgrowth experiment. CAM was centrifuged for 2 min at 100 rcf to remove cellular debris and stored at -80 °C.

3.4.3 Motor neuron differentiation

Motor neuron differentiation was performed as established in the lab[124]. To start, iPSC clones were treated with collagenase type IV (17104-019, Life technology) to form small clusters followed by resuspension in Essential 8 Flex medium. During the first two days, medium was changed every day with neuronal basic medium consisting of Dulbecco's Modified Eagle Medium (DMEM) F12 (31330--038, Gibco) plus Neurobasal medium (21103-049, Gibco) with N2 and B27 supplement without vitamin A supplemented with 40 µM SB431542 (1614, Tocris Bioscience), 0.2 µM LDN-193189 (04-0074-02, Stemgent), 3 µM CHIR99021 (4423, Tocris Bioscience), and 5 µM Y-27632 (688001, Merck Millipore). From day 3 on, medium was changed every other day and supplemented with 0.1 µM retinoic acid (RA; R2625, Sigma) and 500 nM smoothened agonist (SAG; 566660, Merck Millipore). From day 8 on, brain-derived neurotrophic factor (BDNF; 10 ng/ml, 450-02B, Peprotech) and glial cell line-derived neurotrophic factor (GDNF; 10 ng/ml, 450-10B, Peprotech) were added. DAPT (10 µM, 2634, Tocris Bioscience) was added on day 9. Floating clusters were dissociated into single cells for plating on day 10 by using 0.05% trypsin (25300062, Gibco). Motor neuron progenitors were subsequently plated on poly-L-ornithine hydrochloride (PLO) (100 µg/ml, P2533, Sigma) and laminin (20 µg/ml, L2020, Sigma) coated 12- or 96-well plates at 150000 or 7500 cells per well respectively. From day 17 on, the cells were switched to motor neuron maturation medium supplemented with BDNF, GDNF, and ciliary neurotrophic factor (CNTF; each 10 ng/ml, 450-13B, Peprotech) to keep long term cultures. Media was changed every other day. For the metabolic flux tracing experiments, motor neurons were treated with 50% CAM from $SOD1^{A4A}$ or $SOD1^{A4V}$ astrocytes or AMM from d23 till d30 when the radioactive tracer experiments were performed. For the neurite outgrowth analysis, motor neurons were treated with 50% CAM $SOD1^{A4A}$ or $SOD1^{A4V}$ astrocytes or AMM from d23 till d37.

3.5 Immunofluorescence

3.5.1 Mice

Mice were anesthetized using 10% Dolethal and transcardially perfused with PBS followed by perfusion with 4% PFA. Lumbar spinal cords were harvested from P110 mice, post-fixed with 4% PFA overnight at 4°C and dehydrated over 48 h in a 30% sucrose solution at 4°C. Following embedding in O.C.T. compound mounting medium samples were stored at -80°C until further processing. Gastrocnemius muscles were harvested from P110 mice, snap-frozen in liquid-nitrogen cooled isopentane, embedded in O.C.T and stored at -80°C until further processing. 20 micron longitudinal (gastrocnemius muscle) or transversal (lumbar spinal cord) sections were obtained and processed for immunostaining. In brief, sections were blocked for 1 h in

10% normal donkey serum (D9663, Sigma-Aldrich), PBS-T (PBS + 0,1% Triton X-100) and incubated subsequently for 1 h at room temperature with the required antibodies (Table 3.1) dissolved in PBS-T supplemented with 10% normal donkey serum. Images were taken with a Leica TCS SP8 confocal laser scanning microscope (Leica Microsystems Heidelberg GmbH, Manheim, Germany) or a Zeiss Axio Scan 7 microscope ((Carl Zeiss Inc.) and analyzed with ImageJ or CellProfiler Image Analysis Software (RRID: SCR_007358)[354].

3.5.2 iPSC-derived astrocytes

iPSC-derived astrocytes were fixed at d+41 with 4% PFA. After fixation, cells were blocked for 1 h in 5% normal donkey serum (D9663, Sigma-Aldrich), PBS-T (PBS + 0,1% Triton X-100) and incubated subsequently for 1 h at room temperature with the required antibodies (Table 3.1) dissolved in PBS-T supplemented with 2% normal donkey serum. Images were taken with a Leica TCS SP8 confocal laser scanning microscope and analyzed with ImageJ.

3.6 Quantitative real-time polymerase chain reaction (qRT-PCR) and reverse transcription PCR (RT-PCR)

3.6.1 Mice

Mice were anesthetized using 10% Dolethal and transcardially perfused using 1X PBS. Tissues were harvested and immediately stored at -80°C until further processing. Total RNA was extracted using TriPure (11667157001, Roche, Basel, Switzerland) and isopropanol purification. cDNA was synthesized using the Superscript™ III First-strand Synthesis Mastermix kit. qRT-PCR reactions were performed on 4uL 1.25 ng/ul cDNA using SYBR green Universal PCR master mix (4309155, Invitrogen) and DNA primers (Table 3.2 and 3.3). Samples were run in triplicate in a 96-well plate and thermal cycling was performed on a StepOne-Plus RT-PCR system (Applied Biosystems) using a standard amplification protocol. Data were analyzed using the delta delta Ct method. Glyceraldehyde 3-phosphate dehydrogenase (*Gapdh*) was used as housekeeping.

3.6.2 Zebrafish

Zebrafish were collected at 30 hpf on dry ice and stored at − 80°C. Total RNA was extracted using the RNeasy kit (74104, Qiagen, Hilden, Germany) and cDNA was synthesized using the Superscript™ III First-strand Synthesis Mastermix kit. RT-PCR was performed using DreamTaq Green PCR Master Mix (K1081, ThermoFisher Scientific) and DNA primers (Table 3.2). RT-PCR products were analyzed on a 1% agarose gel and visualized using MIDORI Green staining (Nippon Genetics, Düren, Germany). qRT-PCR reactions were performed on 4uL 1.25 ng/ul cDNA using SYBR green Universal PCR master mix and

DNA primers (Table 3.2). Samples were run in triplicate in a 96-well plate and thermal cycling was performed on a StepOne-Plus RT-PCR system (Applied Biosystems) using a standard amplification protocol. Data were analyzed using the delta delta Ct method. *Gapdh* and *Elp1* were used as housekeeping.

3.7 Western blot (WB) analysis

P110 mice were anesthetized using 10% Dolethal and transcardially perfused using 1X PBS. Tissues were harvested and immediately stored at -80°C until further processing. Protein was extracted in RIPA buffer (50mM Tris-HCl (pH7.5), 150 mM NaCl, 1% NP-40, 0.5% Na-deoxycholic acid, 0.5% SDS) supplemented with Complete EDTA-free protease inhibitor cocktail (11873580001, Roche). Lumbar spinal cord tissues were homogenized using Lysing Matrix D beads (116913050-CF, MP Biomedicals, Solon, US) and a MagNa Lyser oscillator (Roche) at 6500 rpm for 30 s, three times with 1 min intervals on ice. Next, the samples were centrifuged at 14,000 rpm for 20 min and supernatant was collected. Protein concentrations were determined using the micro BCA kit (23235, Pierce Biotechnology, Rockford, US). 30 µg sample together with reducing sample buffer (15492859, ThermoFisher Scientific) was heated for 10 min at 95 °C. After separation on an SDS–polyacrylamide electrophoresis gel (12%, 90 V), samples were transferred to a polyvinylidene difluoride (PVDF) membrane (IPVH00010, Millipore, Massachusetts, US) by a semi-dry transfer apparatus (Bio-Rad, Hercules, US). Membranes were blocked with 5% milk TBS-T (10mM Tris-HCl (pH 7.5), 150mM NaCl and 1% Tween-20) for 1 h at RT and subsequently incubated with primary antibodies (Table 3.1) overnight at 4°C. Finally, the membranes were incubated with the appropriate secondary antibody conjugated with horseradish peroxidase (HRP) (1/5000; Agilent Technologies (Dako)) for 1 h at RT and protein bands were visualized using enhanced chemiluminescence (ECL substrate, 32106, ThermoFisher Scientific) and an ImageQuant LAS 4000 Biomolecular Imager (GE Healthcare, Illinois, US). Band intensities were quantified using ImageJ.

3.8 Single-nuclei RNA sequencing (snRNA-seq) of mice lumbar spinal cord

3.8.1 Single nuclei extraction.

To extract nuclei from frozen mouse lumbar spinal cords, we used a slightly modified version of the protocol described previously by Swiech et al[355]. In brief, lumbar spinal cords from three P110 littermate pairs (six samples in total) were dissected and frozen immediately in precooled RNAse-free eppendorfs. Tissue was stored at -80°C until nuclei were extracted. At the day of nuclei extraction, frozen tissues were left in homogenization buffer (320 mM sucrose, 5 mM $CaCl_2$, 3 mM Mg Acetate, 10 mM Tris pH8, 0.1 mM EDTA, 0.1% Igepal/NP-40, 0.1 mM PMSF, 1 mM β-mercaptoethanol in H_2O)

for 5 min on ice to prevent nuclei from breaking. Next, tissue was homogenized by 100 gentle manual strokes using a dounce homogenizer (Sigma-Aldrich). Subsequently, a 1:1 volume of gradient medium (5 mM $CaCl_2$, 3 mM Mg Acetate, 10 mM Tris pH 8, 0.1 mM PMSF, 1 mM β-mercaptoethanol, 50% Optiprep, in water) was layered on top of the homogenized sample before ultracentrifugation (7,700 rpm for 30 min at 4°C using a SW41Ti rotor). Subsequently, the nuclei-containing pellet was resuspended in 150 µl resuspension buffer (BSA 1%, nuclease free water 340 mM, RNasin Plus 0.2 U/ µL in 1X PBS). Number and quality of purified nuclei was controlled using a LUNA-FL Dual fluorescence cell counter (Logos Biosystems, Anyang-si, South Korea).

After single nuclei preparation, samples were immediately processed for the single nuclei whole transcriptome analysis (WTA). SnRNA-seq analysis was performed using 10X genomics 3' WTA suite, according to the manufacturer recommendation. In brief, single nuclei were encapsulated in droplets for lysis and subsequent reverse transcription of polyadenylated mRNA species. After the first cDNA amplification, the library was subjected to Trueseq based library preparation to incorporate the Illumina sequencing adaptors and indices. The final library obtained at the end of the snRNA-seq workflow was sequenced on either of the Illumina Hiseq 4000 or Illumina NovaSeq6000 platforms as per the sequencing specification mentioned in the 10X scRNAseq workflow. Each lane was pooled with multiple 10X libraries which were indexed separately.

3.8.2 10x Genomics data processing

Fastq files from 10x experiments were mapped to the mouse genome (mm10-2020-A, provided by 10x genomics) using cellranger count (RRID: SCR_023221) v5.0.2, the includeIntrons option was enabled. Filtered count matrices were loaded into Scanpy (RRID: SCR_018139) v1.8.1 and nuclei with more than 15% reads associated to mitochondrial genes or less than 250 genes expressed were filtered out, next Scrublet (RRID: SCR_018098) v0.2.2 was used to remove doublets with thresholds being determined automatically. All nuclei were combined into a single dataset for further processing, nuclei were then normalized to a total of 10000 counts and log transformed. Highly variable genes were detected using default parameters and the counts were finally scaled to unit variance with a zero mean and values greater than ten were clipped. A principal component analysis was performed, and harmony batch correction (performed via vsn-pipelines v0.25.0 [https://doi.org/10.5281/zenodo.3703108]) was used to integrate data between experiments, the number of components to use for subsequent analyses (uniform manifold approximation and projection [UMAP], tSNE and Leiden clustering) was determined using the pcacv functionality of vsn-pipelines (57 PCs). Leiden clustering was performed at various resolution (0.4 -> 8.0) and marker genes were calculated using standard Scanpy functions. A combined clustering level was created by using the leiden resolution0.8 clusters as a base, and re-annotating cells

from cluster 64 at resolution 4.0 as a new, final cluster. Clusters were annotated to known cell types using publicly available single-cell data[145,356-366] and confirmed by evaluating the expression of known cell type markers in our clusters using the online tool Scope[367] (RRID: SCR_017454). Differential gene expression was performed by first creating pseudobulk samples (summed counts) from each group of interest separated by initial sample of origin, and subsequently performing a DESeq2[368] (RRID: SCR_015687) differential analysis between genotypes, per cluster including the Experiment of origin as a covariate.

3.8.3 Gene ontology (GO) analysis and gene set enrichment analysis (GSEA).

GO enrichment of DEGs were performed using the PANTHER (RRID: SCR_004869) v14.1 GO biological process complete[369]. Only DEGs with $0.5 \leq \log10(FC) \leq -0.5$ and $p<0.05$ were included. GSEA analysis was performed using WebGestalt (RRID:SCR_006786) 2024[370] on the ranked gene sets. Mitochondrially encoded genes, that could be present due to the use of a gentle lysis buffer during nuclei extraction, were excluded from both analyses.

3.9 RNAScope in situ hybridization

RNAscope was performed as previously described by Rué *et al.* [371]. Mice were anesthetized using 10% Dolethal at P110 and transcardially perfused with 1X PBS followed by perfusion with 4% PFA. Lumbar spinal cords were harvested, post-fixed with 4% PFA overnight at 4°C and dehydrated for 48 h in a 30% sucrose solution at 4°C. Following embedding in O.C.T. compound mounting medium for cryometry the samples were stored at -80°C until further processing. 20 micron cryosections, obtained using a CryoStar NX70 Cryostat, were mounted on Superfrost Plus slides. To improve attachment of the spinal cord slices on the slides, slices were post-fixed for 30 min with cold 4% PFA at 4°C, rinsed with PBS and dehydrated in 70%, 90% and 100% ethanol for 5 min each and baked for 30 min at 60°C. RNAscope *in situ* hybridization was performed as indicated by the manufacturer with the RNAscope Multiplex Fluorescent Reagent Kit v2 (Advanced Cell Diagnostics, San Francisco, US). In brief, slides underwent an antigen retrieval step of 5 min at 98-104°C with a Braun Multiquick FS-3000 Steamer (Braun, Kronberg, Germany). Followed by a Protease III incubation step of 30 min at 40°C in a HybEZ™ Oven (Advanced Cell Diagnostics, Newark, US). RNAscope probes against Stathmin-2 (Stmn2, 1:125; RNAscope Probe Mm-Stmn2-C2; Advanced Cell Diagnostics) and Synaptophysin (Syp; 1:150; RNAscope Probe - Mm-Syp-C3; Advanced Cell Diagnostics) were used. Signal amplification was performed as stated in the manufacturer's instructions with TSA Plus Cyanine 3 (NEL744001KT, Perkin Elmer, Waltham, US, diluted 1:500) and TSA Plus Fluorescein (NEL741001KT, Perkin Elmer, diluted 1:750). Nuclear counterstain was performed with Hoechst 33342 (5 µg/ml) and slides were finally mounted with ProLong Gold antifade reagent. Images of the ventral horns were obtained with a Leica TCS SP8

confocal laser scanning microscope with an HC PL APO CS2 20x/0.75 dry lens and a pinhole of 0.5 Airy Units.

3.10 Live-cell calcium imaging

IPSC-derived astrocytes were plated in a 24-well plate at 100,000 cells per well at d+30. At d+35 cells were incubated with 5 µM Fluo-4 AM (F14201, Thermofisher Scientific) for 25min to visualize calcium. Spontaneous Fluo-4 fluorescence was recorded over 60 s with a 10X objective using a Nikon A1R TiE confocal microscope equipped with a Plan Apo 10X objective lens. NIS-elements was used to determine the min and max Fluo-4 AM fluorescence intensity and the difference between these two was calculated. A cell was considered active if the difference between the max and min intensity was larger than 10.

3.11 Radioactive flux experiments

Metabolic fluxes were measured using radiolabeled glucose, lactate, palmitate and glutamine as described before[138]. In short, cells were incubated for 6 h with D-[5-3H]-glucose (NET531001MC, Perkin Elmer), [9,10-3H(N)]-palmitate (NET043001MC, Perkin Elmer), D-[6-14C]-glucose (NEC045X050UC, American Radiolabelled Chemicals), L-[14C(U)]-lactate (NEC599050UC, Perkin Elmer) or L-[14C(U)]-glutamine (NEC451050UC, Perkin Elmer) or for 2 h with 2- [14C(U)]-deoxy-D-glucose (NEC720A050UC, Perkin Elmer). Metabolic fluxes were measured by the release of $^{14}CO_2$ for D-[6-14C]-glucose, L-[14C(U)]-lactate and L-[14C(U)]-glutamine oxidation, $^{3}H_2O$ for glycolysis of D-[5-3H]-glucose and [9,10-3H(N)]-palmitate oxidation or in the cell lysate for the uptake of 2-[14C(U)]-deoxy-D-glucose. Radioactivity was determined by liquid scintillation counting.

Glycolysis. Cells were incubated for 6 h in AMM medium with 5mM glucose and 2mM lactate and without FBS (5Glu2Lac AMM) containing 0.89 µCi D-[5- 3H]-glucose (15.2 Ci/mmol; NET531001MC, Perkin Elmer) per mmol cold glucose. Glycolytic flux was measured by the rate of $^{3}H_2O$ production from D-[5-3H]-glucose. After 6 h incubation, the culture medium was transferred into glass vials sealed with rubber stoppers. $^{3}H_2O$ was captured in hanging wells containing a H_2O-soaked Whatman paper over a period of 48 h at 37 °C.

Fatty acid oxidation. Cells were incubated for 6 h in 5Glu2Lac AMM supplemented with 100 µM unlabeled palmitate and 50 µM carnitine (Sigma-Aldrich) and containing 77.99 µCi [9,10-3H(N)]-palmitate (53.7 Ci/mmol; Perkin Elmer) per mmol cold palmitate. $^{3}H_2O$ recovery was performed as described for glycolysis.

Glucose oxidation. Cells were incubated for 6 h in 5Glu2Lac AMM containing 0.61 µCi D-[6-14C]-glucose (55 mCi/mmol; American Radiolabelled Chemicals) per mmol cold glucose, after which metabolic

reactions were stopped by the addition of perchloric acid. Glucose oxidation was measured by the rate of $^{14}CO_2$ production. Briefly, after adding perchloric acid, wells were covered with 1× hyamine hydroxide-soaked Whatman papers and the released $^{14}CO_2$ was captured into the papers overnight at room temperature.

Glutamine oxidation. Cells were incubated for 6 h in 5Glu2Lac AMM containing 0.94 µCi L-[14C(U)]-glutamine (267 mCi/mmol; Perkin Elmer) per mmol cold glutamine. $^{14}CO_2$ recovery was performed as described for glucose oxidation.

Lactate oxidation: Cells were incubated for 6 h in 5Glu2Lac AMM containing 2.45 µCi L-[14C(U)]-lactate (154.8 mCi/mmol; Perkin Elmer) per mmol cold lactate. $^{14}CO_2$ recovery was performed as described for glucose oxidation.

2-deoxyglucose uptake. Cells were incubated for 2 h in 5Glu2Lac AMM containing 0.56 µCi 2-[14C(U)]-deoxy-D-glucose (264 mCi/mmol; Perkin Elmer) per mmol cold glucose. Uptake was stopped by addition of 50mM glucose in icecold PBS (stop solution). After two subsequent washes with stop solution, cells were lysed with 0.1 N NaOH.

For all experiments, radioactivity was determined by liquid scintillation counting.

3.12 Tetramethylrhodamine methyl ester perchlorate (TMRM) analysis

The mitochondrial membrane potential was measured using tetramethylrhodamine methyl ester perchlorate (TMRM, T668, Invitrogen). Astrocytes were treated with 30 nM TMRM in 0.5% DMSO (D2650, Sigma-Aldrich) for 1.5 h in phenol red free AMM medium, co-loaded with 50 nM Hoechst 33342 at 37°C and 5% CO2. 2.5 µM oligomycin A (4110, Tocris, Bristol, UK) or 2.5 µM carbonyl cyanide 4-(trifluoromethoxy)phenylhydrazone (FCCP, C2920, Sigma-Aldrich) were co-loaded as positive or negative control, respectively. TMRM fluorescence was recorded at 37°C and 5% CO_2 using the Operetta CLS equipped with a 40X water emersion objective lens and analyzed (as TMRM intensity per cell, averaged per well and normalized to WT baseline TMRM intensity) with the Harmony high-content analysis software (RRID:SCR_023543).

3.13 RNA sequencing (RNA-seq) analysis of iPSC-derived astrocytes

3.13.1 RNA extraction and quality control

iPSC-derived astrocytes were collected at d+41 with accutase and total RNA was extracted using the RNeasy kit. RNA concentration and purity were determined spectrophotometrically using the Nanodrop ND-8000 (Nanodrop Technologies, Wilmington, US) and RNA integrity and concentration were assessed using a Fragment Analyzer SS-RNA kit (Agilent, Santa Clara, US).

3.13.2 RNA-seq

Library preparation. Per sample, 250 ng of total RNA was used as input. Using the Illumina Stranded mRNA Sample Prep Kit (protocol version: # 1000000124518 v02 (April 2021)) poly-A containing mRNA molecules were purified from the total RNA input using poly-dT oligo-attached magnetic beads. The purified mRNA was fragmented and in a reverse transcription reaction using random primers and Actinomycin D, RNA was converted into first strand cDNA and subsequently converted into double-stranded cDNA in a second strand cDNA synthesis reaction using dUTP to achieve strand specificity. The cDNA fragments were extended with a single 'A' base to the 3' ends of the blunt-ended cDNA fragments after which pre-index anchors were ligated preparing the fragments for dual indexing. Anchor-ligated fragments were then purified using magnetic beads. Finally, enrichment PCR was carried out to enrich those DNA fragments that have anchor-ligated DNA fragments and to add indexes and primer sequences for cluster generation.

Sequencing. Purified dual-indexed sequence-libraries of each sample were equimolarly pooled and sequenced on Element Biosciences AVITI (2x75 Cloudbreak kit, single-end reads 100 (101-10-10-0)) at the VIB Nucleomics Core (https://nucleomicscore.sites.vib.be/en). Using this approach, an average reading depth of 36 million reads per sample was obtained.

Preprocessing. Low quality ends and adapter sequences were trimmed off from the Illumina reads with FastX (RRID: SCR_005534) 0.0.14 [http://hannonlab.cshl.edu/fastx_toolkit/index.html] and Cutadapt (RRID: SCR_011841) 3.2[372]. Subsequently, small reads (length < 35 bp), polyA-reads (more than 90 % of the bases equal A), ambiguous reads (containing N), low-quality reads (more than 50 % of the bases < Q25) and artifact reads (all but three bases in the read equal one base type) were filtered using using FastX 0.0.14 and ShortRead (RRID: SCR_006813) 1.58.0[373]. With Bowtie2 (RRID: SCR_016368) 2.4.5 we identified and removed reads that align to phix_illumina[374].

Mapping. The preprocessed reads were aligned with STAR aligner (RRID: SCR_004463) v2.5.2b to the reference genome of Homo sapiens (GRCh38.88)[375]. Default STAR aligner parameter settings were used, except for '--outSAMprimaryFlag OneBestScore --twopassMode Basic --alignIntronMin 50 --alignIntronMax 500000 --outSAMtype BAM SortedByCoordinate'. Using Samtools (RRID: SCR_002105) 1.15.1, reads with a mapping quality smaller than 20 were removed from the alignments[376].

Counting .The number of reads in the alignments that overlap with gene features were counted with featureCounts (RRID: SCR_002105) 1.5.3[377]. Following parameters were chosen: -Q 0 -s 2 -t exon -g gene_id. We removed genes for which all samples had less than 1 count-per-million. Raw counts were

further corrected within samples for GC-content and between samples using full quantile normalization, as implemented in the EDASeq (RRID: SCR_006751) 2.32 package from Bioconductor[378].

Differential gene expression. With the EdgeR (RRID:SCR_012802) 3.42.4 package of Bioconductor, a negative binomial generalized linear model (GLM) was fitted against the normalized counts[379]. We did not use the normalized counts directly, but worked with offsets. Differential expression was tested for with a GLM likelihood ratio test, also implemented in the EdgeR package. The resulting p-values were corrected for multiple testing with Benjamini-Hochberg to control the false discovery rate[380].

3.14 Neurite outgrowth

Motor neurons, plated at 7500 cells per well in 96-well plate, were cultured in an Incucyte SX5 (Sartorius, Göttingen, Germany) at 37°C and 5% CO_2 equipped with a 10x objective lens. A brightfield image was taken each day from differentiation day 11 till day 35. Neurite length was quantified using the Inucyte Neurotrack analysis software (RRID:SCR_025411).

3.15 Statistic analysis

Statistical analysis was performed with Graphpad Prism (RRID:SCR_002798). The data represent mean ± SEM with individual values shown. For each experiment, the normal distribution of the data was tested. All statistical analyses performed and the definition and numbers of experimental blocks (ExpB), biological replicate (N) and technical replicate (n) are stated in the figure legend.

Antibody	Host	Source	Identifier	RRID	Dilution
SV2	Mouse	Developmental Studies Hybridoma Bank	AB2315387	AB_2315387	1:200
Neurofilament-L	Rabbit	Cell Signaling	C28E10	AB_823575	1:125
AF555 α-Bungarotoxin	N/A	Invitrogen	B35451	AB_2617152	1:1000
AF647 Isolectin IB4	N/A	Life technologies	I32450		
GFAP	Mouse	Sigma	G3893	AB_477010	1:500
STING	Rabbit	Cell Signaling	13647S	AB_2732796	1:100
Oct4	Rabbit	Santa Cruz	Sc-9081	AB_2167703	1:100
TRA-1-60 (IgM)	Mouse	Cell Signaling	4746S	AB_2119059	1:200
Sox2	Rabbit	Abcam	AB97959	AB_2341193	1:500
SSEA4	Mouse	Santa Cruz	sc-21704	AB_628289	1:200
Nanog	Rabbit	Thermo Scientific	PA1-097	AB_2539867	1:300
SOD1	Rabbit	Enzo	ADI-SOD-100	AB_2039583	1:1000
Calnexin	Rabbit	Enzo	ADI-SPA-860F	AB_11178981	1:1000
VIM	Rabbit	Abcam	Ab92547	AB_10562134	1:1000
AQP4	Mouse	Abcam	Ab9512	AB_307299	1:200
SOX9	Goat	R&D Systems	AF3075	AB_2194160	1:400
TOMM20	Rabbit	Abcam	Ab186735	AB_2889972	1:1000
GAPDH	Mouse	Invitrogen	AM4300	AB_437392	1:1000
TRA-1-81(IgM)		Cell Signaling	4745	AB_2119060	1:200
AF488 anti-Rabbit	Goat	Invitrogen	A11034	AB_2576217	1:500
AF555 anti-Mouse (IgM)	Goat	Invitrogen	A21426	AB_2535847	1:500
AF555 anti-Mouse (IgG)	Goat	Invitrogen	A21424	AB_141780	1:500
AF488 anti-Rabbit	Donkey	Invitrogen	A21206	AB_2535792	1:500
AF555 anti-Mouse (IgG)	Donkey	Invitrogen	A31570	AB_2536180	1:500

Table 3.1. List of primary and secondary antibodies.

Target	Forward primer	Reverse primer
Mouse *Egln1*	5’ GAAGGCGAACCTGTACCCC 3’	5’TTCATGGACGGCACGATGTA 3’
Mouse *Egln2*	5’ AATCAGAACTGGGACGTTAAGGT 3’	5’AGAGTGGCTCGATGTTGGCTA 3’
Mouse *Egln3*	5’ CTGGGCAAATACTACGTCAAGG 3’	5’GACCATCACCGTTGGGGTT 3’
Mouse *Gapdh*	5’ GGAGCGAGATCCCTCCAAAAT 3’	5’GGCTGTTGTCATACTTCTCATGG 3’
Zebrafish *egln2*	5’ TCGGCCATAGTAGGATGAGTAG 3’	5’CACACACACACACACACTTTAC 3’
Zebrafish *egln1a*	5’ GGTAGGTGCAGGATCTCATTT 3’	5’TATAATCGGTGGCCAGCTTC 3’
Zebrafish *egln1b*	5’ TACAGGCTCTGACACCAAAC 3’	5’CCACCATTGCTTTCGTTCTTC 3’
Zebrafish *egln3*	5’ CGAGGTCAAAGGCAATGGT 3’	5’AGACGGGCTTGTGTGTTTAG 3’
Zebrafish *vegfaa*	5’ TGTAAAGGCTGCCCACATAC 3’	5’TTCGAGCGCCTCATCATTAC 3’
Zebrafish *gapdh*	5’ CAAACGAGGACACAACCAAATC 3’	5’CCACCCTTAATGTGAGCAGAA 3’
Zebrafish *elp1*	5’ ATCTACAAATGCGGTGGAAT 3’	5’ATACCAGCCTCAAACTCACC 3’

Table 3.2. List of DNA primers used for RT-PCR and qRT-PCR.

Target	Assay ID	Ref Seq	Assay configuration
Mouse *Glut1*	Mm.PT.58.7590689	NM_011400	Std, DNA primer
Mouse *Vegfa*	Mm.PT.58.14200306	NM_001025257	Std, DNA primer
Mouse *Epo*	Mm.PT.58.32438537	NM_007942	Std, DNA primer
Mouse *Pdk1*	Mm.PT.58.10680444	NM_172665	Std, DNA primer
Mouse *Redd1*	Mm.PT.58.43159110.g	NM_029083	Std, DNA primer
Mouse *Ldha*	Mm.PT.58.29860774	NM_001136069	Std, DNA primer
Mouse *Lat1*	Mm.PT.58.10563809	NM_011404	Std, DNA primer

Table S3.3. List of IDT primer assays for qRT-PCR.

CHAPTER 4 RESULTS

Parts of this chapter appeared in:

Germeys, C.*, Vandoorne, T.*, Davie, K., Poovathingal, S., Heeren, K., Vermeire, W., Nami, F., Moisse, M., Quaegebeur, A., Sierksma, A., et al. (2024). Targeting EGLN2/PHD1 protects motor neurons and normalizes the astrocytic interferon response. Cell Rep *43*, 114719. 10.1016/j.celrep.2024.114719
*These authors contributed equally

CHAPTER 4 RESULTS

4.1 Targeting Egln2 rescues the motor axonopathy in ALS zebrafish

4.1.1 Downregulation of *egln2* in zebrafish using an AMO

To explore if targeting EGLN2 could be beneficial for ALS, we used two different zebrafish models for ALS. To downregulate *egln2* in these zebrafish, we designed an AMO that targets the exon 2 intron 2 (E2I2) splice-junction of *egln2* (Figure 4.1A), as exon 2 encodes the catalytic domain of the protein. Next, we determined the highest non-toxic dose that did not affect the development of the zebrafish by injection with a range of concentrations (0.025 mM – 0.5 mM) and subsequent assessment of morphology in zebrafish 30 hpf (Figure 4.1B). Injection with the highest non-toxic dose, which was 0.1 mM, of the *egln2* AMO resulted in the removal of exon 2 as determined by RT-PCR (Figure 4.1C), without affecting the mRNA levels of *egln1a*, *b* and *egln3* (Figure 4.2A-C).

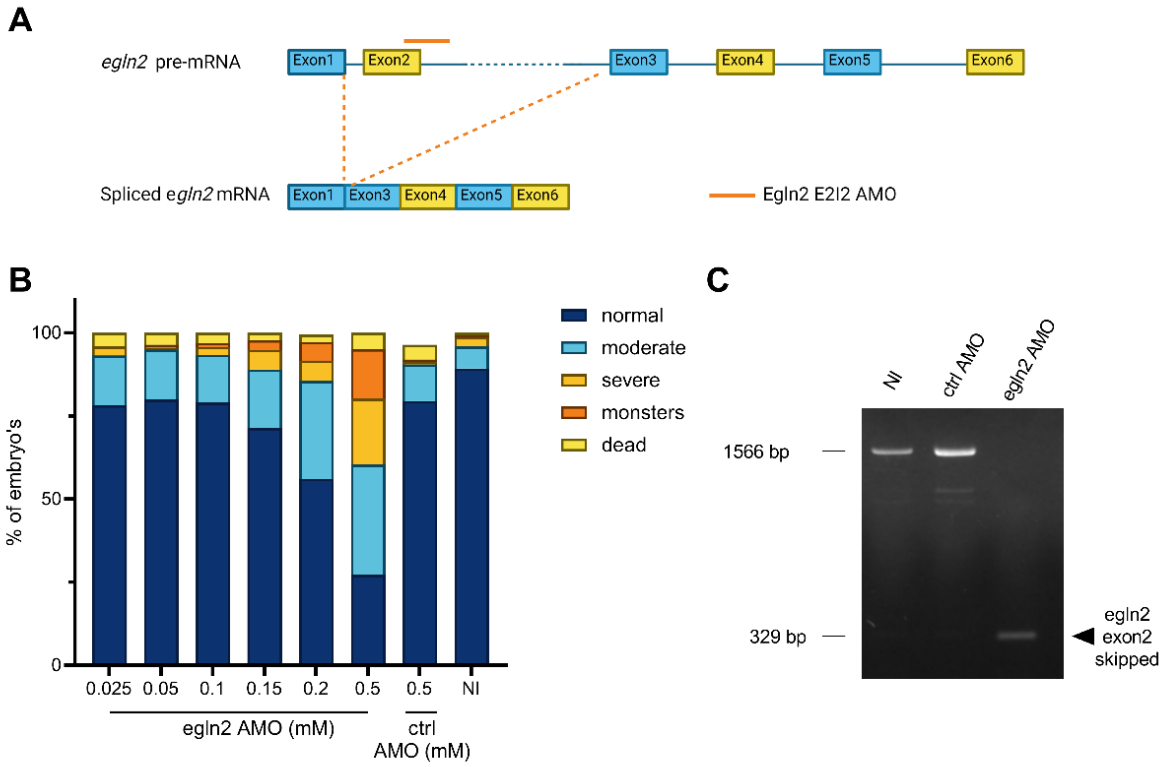


Figure 4.1 *Egln2* AMO induces splice-defect in zebrafish. A, Schematic representation of the splice-block AMO that targets the exon 2-intron 2 (E2I2) splice junction in zebrafish *egln2* pre-mRNA resulting in the removal of exon2. **B**, Morphological assessment of 30 hpf zebrafish embryo's after injection with different concentrations of egln2 morpholino ranging from 0.025 mM to 0.5 mM. ExpB ≥ 3 with N = 41-120 zebrafish. **C**, Validation of the AMO-induced splice-defect using RT-PCR. Wild-type *egln2* cDNA in 30 hpf non-injected (NI) and control (ctrl) AMO or alternative splice product induced by 0.1 mM E2I2 splice-blocking AMO, indicated by the arrowhead.

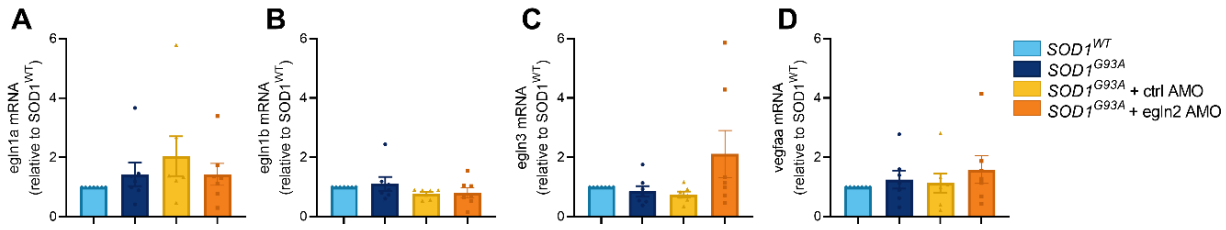


Figure 4.2. *Egln2* downregulation in SOD1^{G93A} zebrafish does not affect *egln2*, *egln3* and *vegfa* expression. A-D, mRNA levels in whole zebrafish at 30 hpf of **A**, *egln1a,* **B**, *egln1b*, **C**, *egln3* and **D**, *vegfaa* normalized to *gapdh* and *elp1* and relative to the levels in *SOD1^{WT}* zebrafish measured using qRT-PCR. Data represent mean ± SEM with individual values shown (ExpB ≥ 7 with N = 15-20 zebrafish per group). Statistical analyses were performed by a Kruskal-Wallis test. No statistical differences nor trends were observed.

4.1.2 *Egln2* downregulation rescues the motor axonopathy in SOD1-ALS zebrafish

After determination of the non-toxic and effective dose of *egln2* AMO, we investigated if downregulation of *egln2* could rescue the motor axonopathy observed in SOD1-ALS zebrafish. These SOD1-ALS zebrafish, in which human mutant *SOD1^{G93A}* RNA (SOD1^{G93A}) was injected, present a motor axonopathy with a decreased axonal length and an increased percentage of abnormally branched axons compared to the zebrafish injected with human *SOD1* wildtype (SOD1^{WT}) RNA (Figure 4.3B-D). Co-injection with the *egln2* AMO and *SOD1^{G93A}* RNA (Figure 4.3A) almost completely rescued the motor axon abnormalities increasing the axonal length and decreasing the abnormal branching of the motor axons (Figure 4.3B-D). Lemmens *et al.* previously demonstrated that upregulation of Vegf could rescue the motor axonopathy induced by mutant *SOD1^{350}*. However, the *egln2* AMO did not affect the expression of *vegfaa* (Figure 4.2D) in SOD1^{G93A} zebrafish as determined by qRT-PCR, suggesting that the motor neuron protective effect is independent from this Hif target.

4.1.3 *Egln2* downregulation rescues the motor axonopathy in C9ORF72-ALS zebrafish

To investigate whether downregulation of *egln2* was also beneficial in another model for ALS, we used the C9ORF72-ALS zebrafish. In these zebrafish 91 copies of the *C9ORF72* hexanucleotide repeats in the sense direction (91S) were injected resulting in a motor axonopathy, similar to that in SOD1-ALS zebrafish, with reduced axonal length and reduced abnormal branching (Figure 4.3E-F). Downregulation of *egln2* in this model using the E2I2 AMO, again rescued the motor axonopathy with increased axonal length and a trend towards decreased abnormal branching (Figure 4.3E-F).

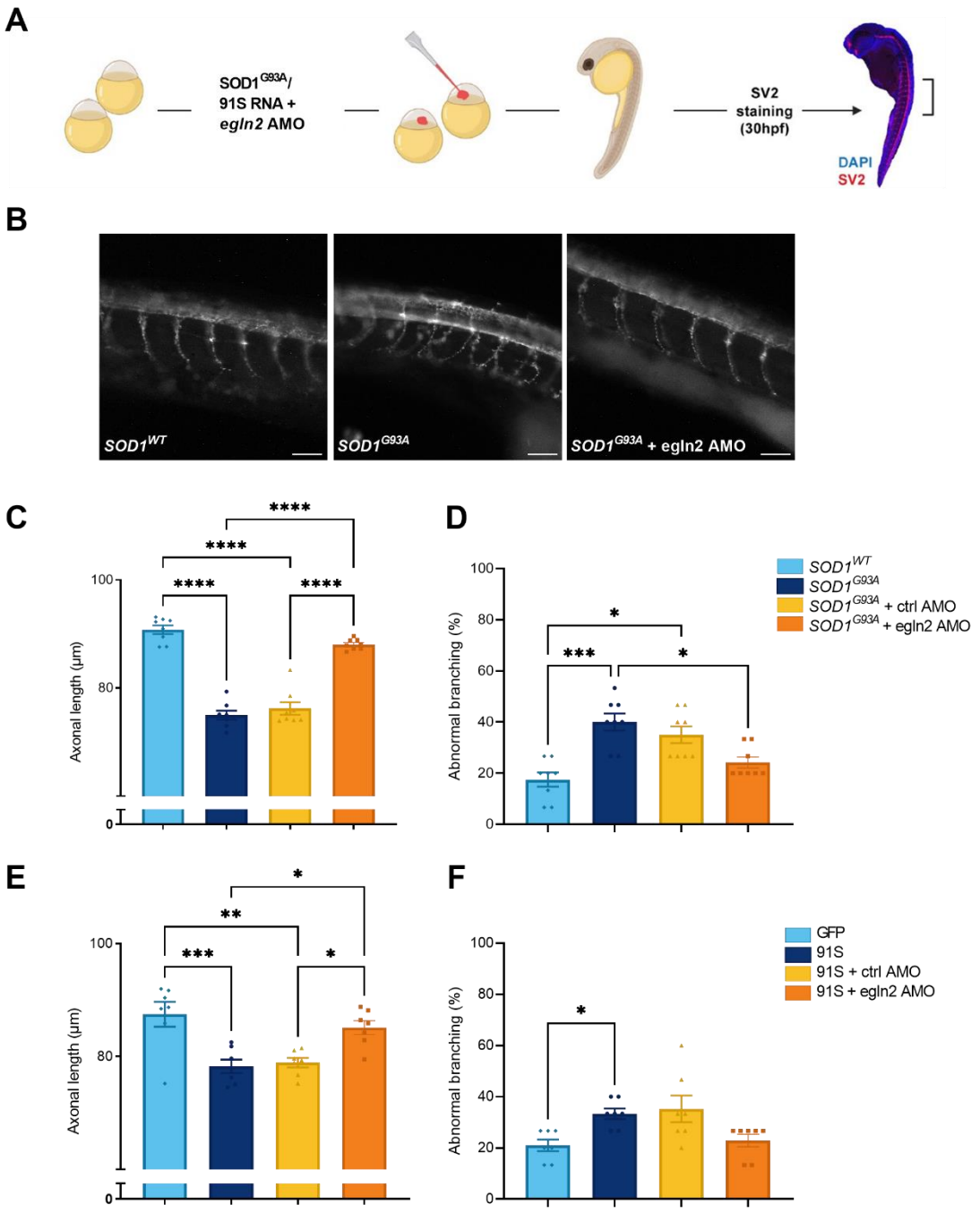


Figure 4.3. *Egln2* downregulation rescues motor axonopathy in SOD1- and C9ORF72-ALS zebrafish. A, Graphical representation of experimental set-up. Adapted from Braems *et al.*[32]. **B**, Representative images of synaptic vesicle glycoprotein 2a (Sv2) staining at 30 hpf in zebrafish injected with *SOD1*^{WT} RNA, *SOD1*^{G93A} RNA and *SOD1*^{G93A} RNA with *egln2* AMO. Scalebar, 50µm. Quantification of the axonal length in **C** and the percentage of abnormally branched axons in **D** in zebrafish injected with *SOD1*^{WT} RNA, *SOD1*^{G93A} RNA and *SOD1*^{G93A} RNA with a control (ctrl) or *egln2* AMO. Quantification of the axonal length in **E** and the percentage of abnormally branched axons in **F** in zebrafish injected with *GFP* RNA (GFP), 91 copies of *C9ORF72* hexanucleotide repeat RNA in the sense direction (91S) and 91S with a control (ctrl) or *egln2* AMO. Data represent mean ± SEM with individual values shown (ExpB = 7-8, each with 15 N = zebrafish per group). Statistical analyses were performed in **C** and **E** by a one-way ANOVA with Sidak's multiple comparison test or in **D** and **F** with the Kruskal-Wallis test with Dunn's multiple comparison test (*p<0.05, **p<0.01, ***p<0.0001).

4.1.4 Concluding Remarks

In conclusion, these zebrafish experiments revealed that downregulation of *egln2* using an oligonucleotide-based approach mitigated the motor axonopathy in both a SOD1 and a C9ORF72 models for ALS. Moreover, at least in the SOD1-ALS zebrafish, this effect was independent from an effect on the Hif target, Vegf. Together these data show that inhibition of Egln2 mitigates the ALS phenotype in zebrafish by acting on one or more mechanism that are involved in the motor neuron toxicity mediated by mutant SOD1 and *C9ORF72* RNA toxicity.

4.2 Targeting EGLN2 mitigates the ALS phenotype in SOD1-ALS but not FUS-ALS mice

4.2.1 Generation of ALS mice with an *Egln2* deletion

Next, we aimed to study whether targeting EGLN2 also protected motor neurons in a more complex model for ALS. To investigate this, we used two different mouse models for ALS, the SOD1^{G93A} mouse model that overexpresses human mutant *SOD1^{G93A}* and the FUS$^{+/+}$ mouse model that overexpresses human wildtype *FUS*, both displaying an ALS phenotype[72,381]. To target EGLN2 in both these mouse models, we crossed them with a previously generated mouse model with a whole-body deletion of *Egln2*[322]. *Egln2* mRNA expression in the spinal cord was reduced by 55% in *SOD1^{G93A}/Egln2$^{+/-}$* compared to *SOD1^{G93A}/Egln2$^{+/+}$* mice and was not detectable in *SOD1^{G93A}/Egln2$^{-/-}$* mice (Figure 4.4A). Moreover, deletion of *Egln2* did not cause any compensatory upregulation of *Egln1* or *Egln3* at the mRNA level (Figure 4.4B-C), nor did it affect human SOD1 expression in the spinal cord of SOD1^{G93A} mice (Figure 4.4D).

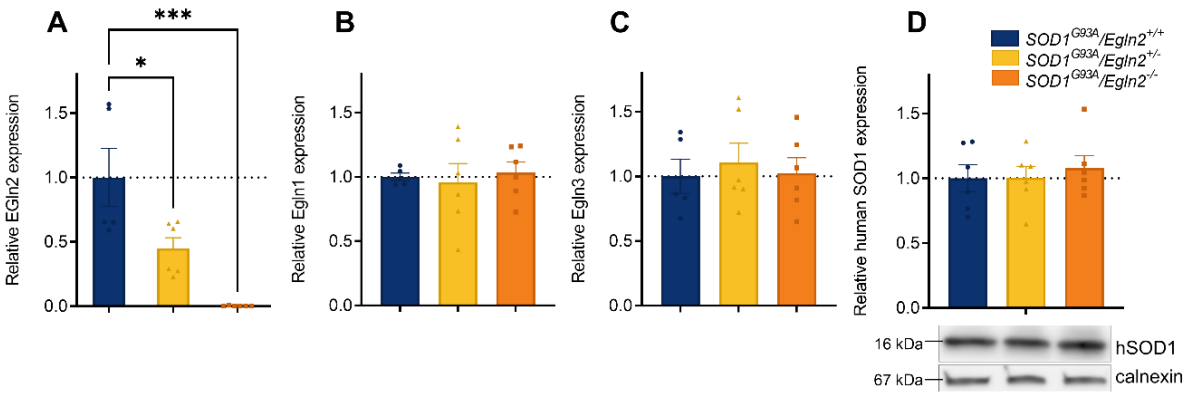


Figure 4.4. *Egln2* deletion in SOD1^{G93A} mice does not affect *Egln1*, *Egln3* and human SOD1 expression. A-C, Relative mRNA levels in the spinal cord of **A**, *Egln2,* **B**, *Egln1* and **C**, *Egln3* normalized to *Gapdh*. **D**, Relative protein levels of human SOD1 in the spinal cord normalized to Calnexin. Data represent mean ± SEM with individual values shown (N ≥ 5 mice per group). Statistical analyses were performed in **A-D** by a One-way ANOVA with Dunnett's multiple comparison test (*p<0.05, ***p<0.001).

4.2.2 Deletion of *Egln2* increases the survival and protects the motor neurons of SOD1^{G93A} mice

To investigate whether targeting EGLN2 could be beneficial in murine ALS models, we started to explore the effect of *Egln2* deletion in SOD1^{G93A} mice. Age at disease onset, defined by a reduction in body weight of 10% and reduced rotarod performance, was not altered by deletion of *Egln2* (Figure 4.5A-B). However, homozygous, but not heterozygous, deletion of *Egln2* significantly prolonged the mean survival of SOD1^{G93A} mice from 147 ± 2 days for *SOD1^{G93A}/Egln2$^{+/+}$* mice to 157 ± 3 days for *SOD1^{G93A}/Egln2$^{-/-}$* mice (Figure 4.5C). As a result, disease duration, defined as the number of days between disease onset and the humane endpoint, increased with 44% in *SOD1^{G93A}/Egln2$^{-/-}$* mice (Figure 4.5D).

To investigate whether the observed survival benefit was linked to a mitigation of motor neuron degeneration, we quantified the neurons in the ventral horn of early symptomatic mice at 110 days of age (P110). The number of remaining neurons in the ventral horn of *SOD1^{G93A}/Egln2$^{-/-}$* mice was higher compared to *SOD1^{G93A}/Egln2$^{+/+}$* mice (Figure 4.5E-F). This neuroprotective effect was more pronounced for large motor neurons (>400 µm^2: +63%) compared to smaller neurons (250-400 µm^2: +44%, 150-200 µm^2: +47%, 200-250 µm^2: +48%) (Figure 4.5E-F). To investigate whether loss of EGLN2 also protected neuromuscular junction (NMJ) innervation, we quantified this in the gastrocnemius muscle at P110. Innervation of the NMJs in the gastrocnemius muscle was better preserved in *SOD1^{G93A}/Egln2$^{-/-}$* mice compared to *SOD1^{G93A}/Egln2$^{+/+}$* mice (Figure 4.5G). Together, this showed that loss of EGLN2 mitigated motor neuron degeneration in early symptomatic SOD1^{G93A} mice. In addition, this was observed in the absence of changes in blood vessel density or an effect on the expression level of HIF target genes in lumbar spinal cord tissue (Figure 4.6), suggesting that the motor neuron protective effect of *Egln2* deletion in SOD1^{G93A} mice, in line with the zebrafish data, was independent from these HIF targets.

Overall, these data indicate that knocking out *Egln2* has a positive effect on the ALS phenotype of SOD1^{G93A} mice, slowing down the disease progression, increasing motor neuron survival and increasing muscle innervation.

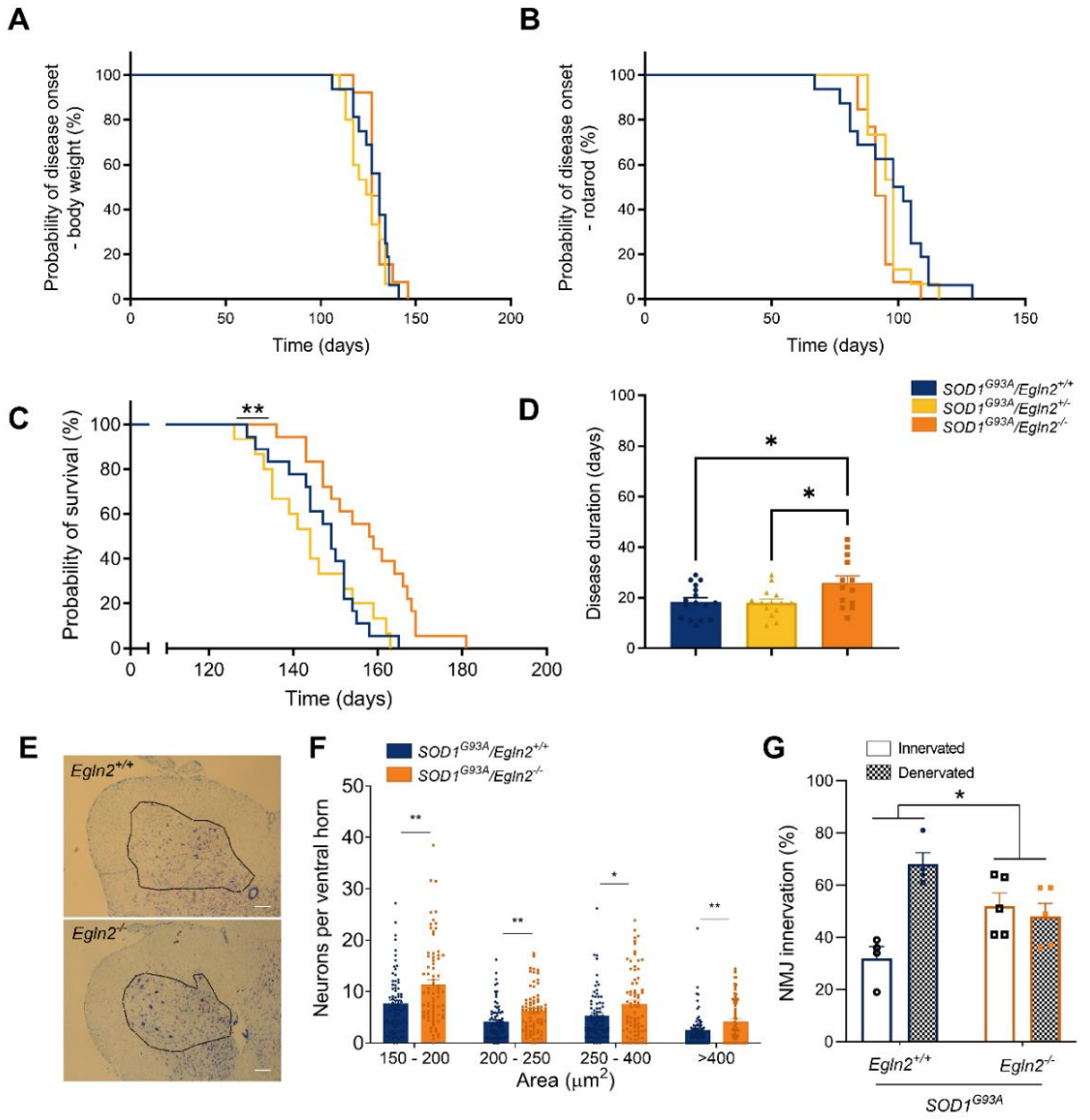


Figure 4.5. *Egln2* deletion prolongs survival and mitigates motor neuron degeneration in SOD1^{G93A} mice. A, Probability of disease onset assessed by a body weight reduction of 10%. *SOD1^{G93A}/Egln2$^{+/+}$* N=16, *SOD1^{G93A}/Egln2$^{+/-}$* N=15, *SOD1^{G93A}/Egln2$^{-/-}$* N=13. **B**, Probability of disease onset assessed by a reduction of the performance time on the rotarod below 150s. *SOD1^{G93A}/Egln2$^{+/+}$* N=16, *SOD1^{G93A}/Egln2$^{+/-}$* N=15, *SOD1^{G93A}/Egln2$^{-/-}$* N=13. **C**, Probability of survival; humane endpoint defined as loss of righting reflex within 20 s. *SOD1^{G93A}/Egln2$^{+/+}$* N=18, SOD1^{G93A}/*Egln2$^{+/-}$* N=15, *SOD1^{G93A}/Egln2$^{-/-}$* N=18. **D**, Disease duration defined as days between disease onset and humane endpoint. *SOD1^{G93A}/Egln2$^{+/+}$* N=16, *SOD1^{G93A}/Egln2$^{+/-}$* N=15, *SOD1^{G93A}/Egln2$^{-/-}$* N=13. **E**, Representative thionin staining of neurons in the lumbar spinal cord of *SOD1^{G93A}/Egln2$^{+/+}$* and *SOD1^{G93A}/Egln2$^{-/-}$* mice at P110. Ventral horn indicated in black. Scale bar, 150 µm. **F**, Quantification of number of neurons in the ventral horn of *SOD1^{G93A}/Egln2$^{+/+}$* and *SOD1^{G93A}/Egln2$^{-/-}$* mice normalized to 300,000 µm^2 of ventral horn and categorized per size. **G**, Innervated and denervated neuromuscular junctions (NMJs) in *SOD1^{G93A}/Egln2$^{+/+}$* and *SOD1^{G93A}/Egln2$^{-/-}$* mice at P110. Data represent mean ± SEM with individual values shown (N ≥ 4 mice per group). Statistical analyses were performed in **A**-**C** by Log-rank Mantel-Cox, in **D** by a one-way ANOVA with Tukey's multiple comparison, in **F** Two-way ANOVA with Sidak's multiple comparison test and in **G** by an Unpaired T-test (*p<0.05, **p<0.01).

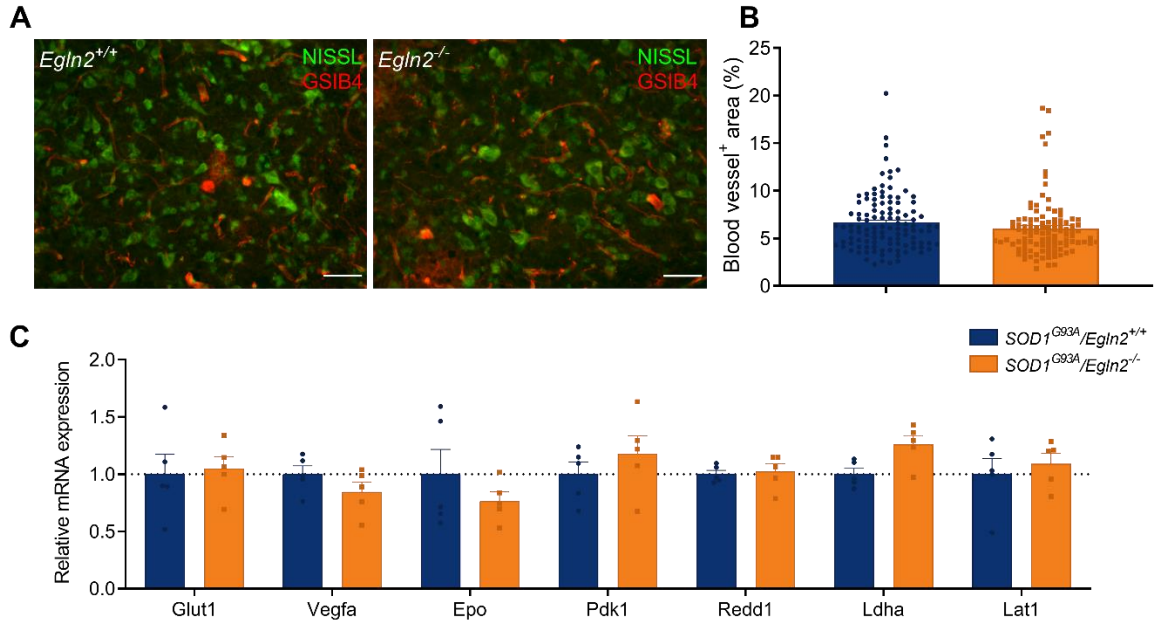


Figure 4.6. *Egln2* deletion does not alter blood vessel density and expression of HIF targets in the spinal cord of SOD1^{G93A} mice. A, Nissl (NISSL, green) and isolectin GS-IB4 (GSIB4, red) staining in lumbar spinal cord of *SOD1^{G93A}/Egln2$^{+/+}$* and *SOD1^{G93A}/Egln2$^{-/-}$* mice marking vasculature in spinal cord tissue at P110. Scale bar, 50 µm. **B**, Quantification blood vessel-positive area. **C**, QRT-PCR on lumbar spinal cord of *SOD1^{G93A}/Egln2$^{+/+}$* and *SOD1^{G93A}/Egln2$^{-/-}$* mice at P110 to evaluate mRNA levels of different HIF targets normalized to *Gapdh*. Data represent mean ± SEM with individual values shown (N ≥ 3 mice per group). Statistical analyses were performed in **B** by an Unpaired t-test and in **C** by Two-way ANOVA with Tukey's multiple comparison test.

4.2.3 Deletion of *Egln2* does not affect the ALS phenotype in FUS$^{+/+}$ mice

Next, we aimed to investigate whether deletion of *Egln2* could also be beneficial in FUS$^{+/+}$ mice. Therefore, we followed *FUS$^{+/+}$/Egln2$^{+/+}$*, *FUS$^{+/+}$/Egln2$^{+/-}$* and *FUS$^{+/+}$/Egln2$^{-/-}$* along the disease course to evaluate whether *Egln2* deletion improved disease. This revealed that deletion of *Egln2* did not affect survival (Figure 4.7A), nor did it affect motor function as measured by grip strength (Figure 4.7B) and performance on the hanging wire test (Figure 4.7C).

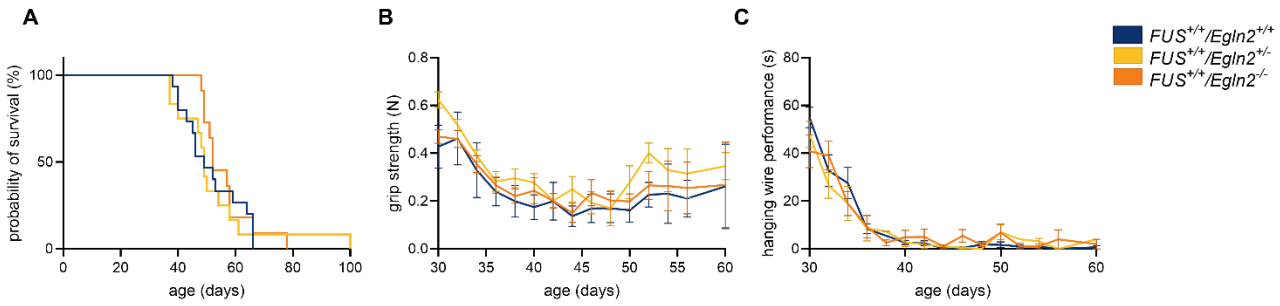


Figure 4.7. Deletion of *Egln2* does not affect ALS phenotype in FUS$^{+/+}$ mice. A, Probability of survival; humane endpoint defined as loss of righting reflex within 20 s. **B**, Grip strength in forelimbs; average measurement of 3 trials. **C**, Latency to fall during hanging wire test. Data represent mean ± SEM with individual values shown. *FUS*$^{+/+}$*/Egln2*$^{+/+}$ N=15, *FUS*$^{+/+}$*/Egln2*$^{+/-}$ N=12, *FUS*$^{+/+}$*/Egln2*$^{-/-}$ N=11. Statistical analyses were performed in **A** by Log-rank Mantel-Cox and in **B-C** by a Mixed-effects analysis.

4.2.4 Concluding remarks

Here we demonstrated that deletion of *Egln2* mitigated the ALS phenotype in SOD1^{G93A} mice but not FUS$^{+/+}$ mice. These findings suggest that the deletion of *Egln2* interferes with a mechanism that is mainly relevant for SOD1-ALS but not FUS-ALS. Though it could also be explained by the model itself as the FUS$^{+/+}$ mice shows a very severe phenotype with early onset[72]. The SOD1^{G93A} mouse model remains the most widely used model for ALS research because it replicates the age-dependent and progressive motor neuron degeneration as seen in ALS patients[381]. Therefore, we aimed to study the mechanisms responsible for the beneficial effects of loss of EGLN2 in SOD1^{G93A} mice.

4.3 SnRNA-seq reveals the cell-specific effect of *Egln2* deletion on the spinal cord of SOD1^{G93A} mice

4.3.1 SnRNA-seq transcriptionally profiles neuronal and non-neuronal nuclei in SOD1^{G93A} spinal cord

To gain insight into the cell-specific pathways underlying the beneficial effect of *Egln2* downregulation, we performed snRNA-seq on the lumbar spinal cord of P110 *SOD1*^{G93A}*/Egln2*$^{+/+}$ and *SOD1*^{G93A}*/Egln2*$^{-/-}$ mice. We transcriptionally profiled a total of 42,278 nuclei (quality control; Table S4.1) and identified 35 distinct nuclei clusters accounting for the different neuronal and non-neuronal cell types present in murine spinal cord (Figure 4.8A), annotated by comparison of their cluster markers with publicly available single-cell data[145,356-366]. This strategy enabled us to annotate the vast majority of clusters to known cell types including myelinating oligodendrocytes, oligodendrocyte progenitor cells, committed

oligodendrocyte progenitors, astrocytes, Schwann cells, microglia, macrophages, endothelial cells, vascular cells, pericytes and multiple neuronal clusters (Figure 4.8A). By evaluating the expression of known cell type markers in our clusters using the online tool Scope[367], we confirmed the annotation results of our mapping approach (Figure 4.8B-G).

Next, we focused on the different neuronal sub-clusters and annotated them as excitatory or inhibitory neurons based on expression of known neurotransmitter-related genes and publicly available single-cell data on different neuronal subtypes (Figure 4.8A)[145,356-363]. Cluster 35 (in purple) was identified as the motor neuron cluster as this cluster specifically expressed known motor neuron markers including cholinergic markers such as vesicular acetylcholine transporter (*Slc18a3*) and sodium/choline cotransporter (*Slc5a7*) but also neurofilament light (*Nefl*), medium (*Nefm*), and heavy chain (*Nefh*), the ubiquitination markers ubiquitin c-terminal hydrolase l1 (*Uchl1*) and ubiquitin b (*Ubb*), peripherin (*Prph*), and *Stmn2*[106,107,382]. *Stmn2* was confirmed to colocalize specifically with large synaptophysin-positive neurons in the ventral horn of the lumbar spinal cord using RNAscope *in situ* hybridization[106,107] (Figure 4.9B-C).

All clusters, including the motor neuron cluster, contained nuclei of all six samples (Figure 4.10), which allowed us to study the effect of *Egln2* deletion on the cluster-specific gene expression.

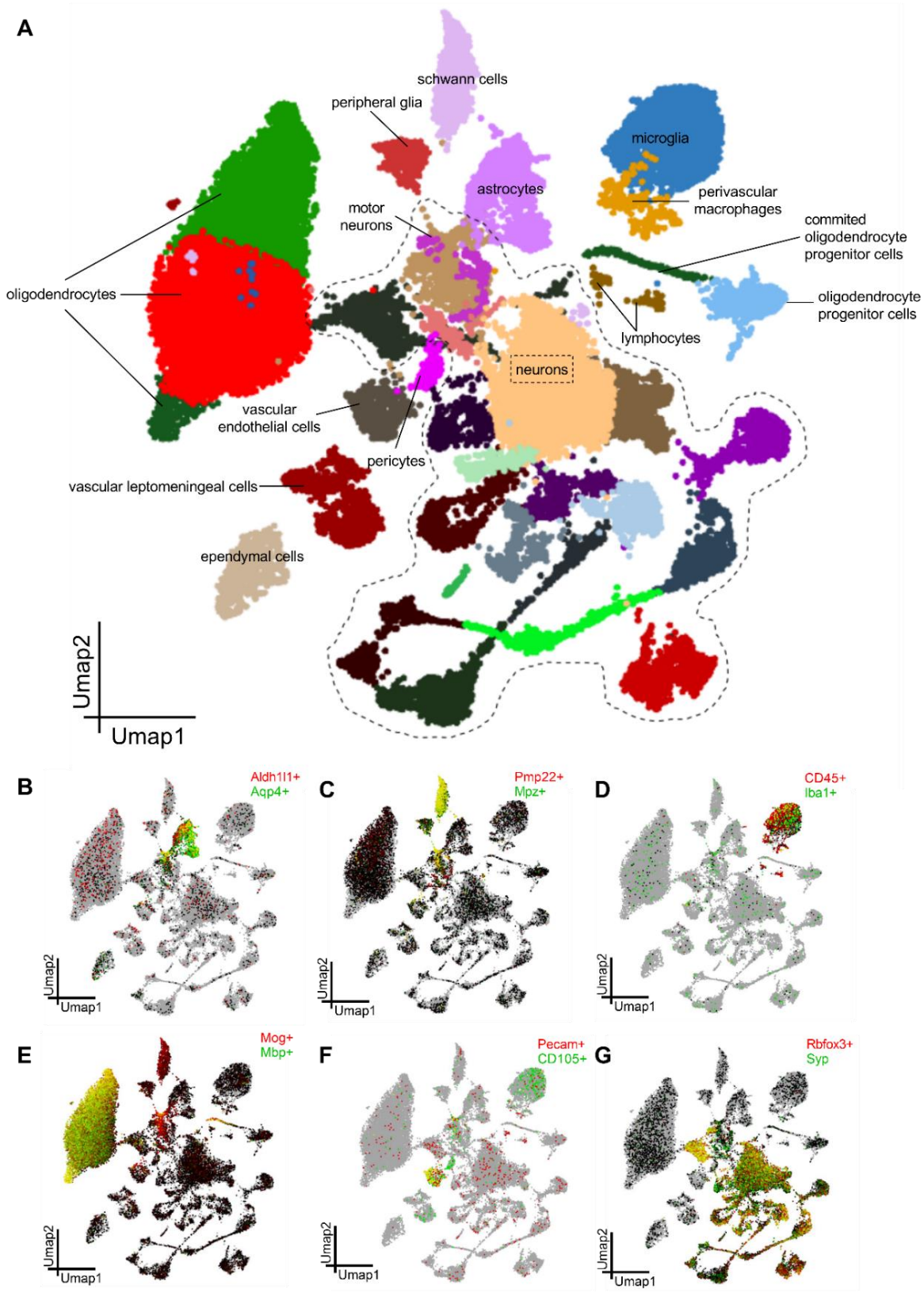


Figure 4.8. Single-nuclei transcriptomics reveals neuronal and non-neuronal cell clusters in SOD1^{G93A} spinal cord. A, UMAP plot visualizing 42,278 nuclei isolated from the lumbar spinal cord of P110 *SOD1^{G93A}/Egln2$^{+/+}$ and SOD1^{G93A}/Egln2$^{-/-}$* mice (N = 3 mice per group). Annotation of different clusters based on publicly available transcriptomics data. **B-G**, Individual nuclei colored by expression for classical markers for **B**, astrocytes; **C**, Schwann cells; **D**, microglia; **E**, myelinating oligodendrocytes; **F**, endothelial cells; **G**, neurons using SCope.

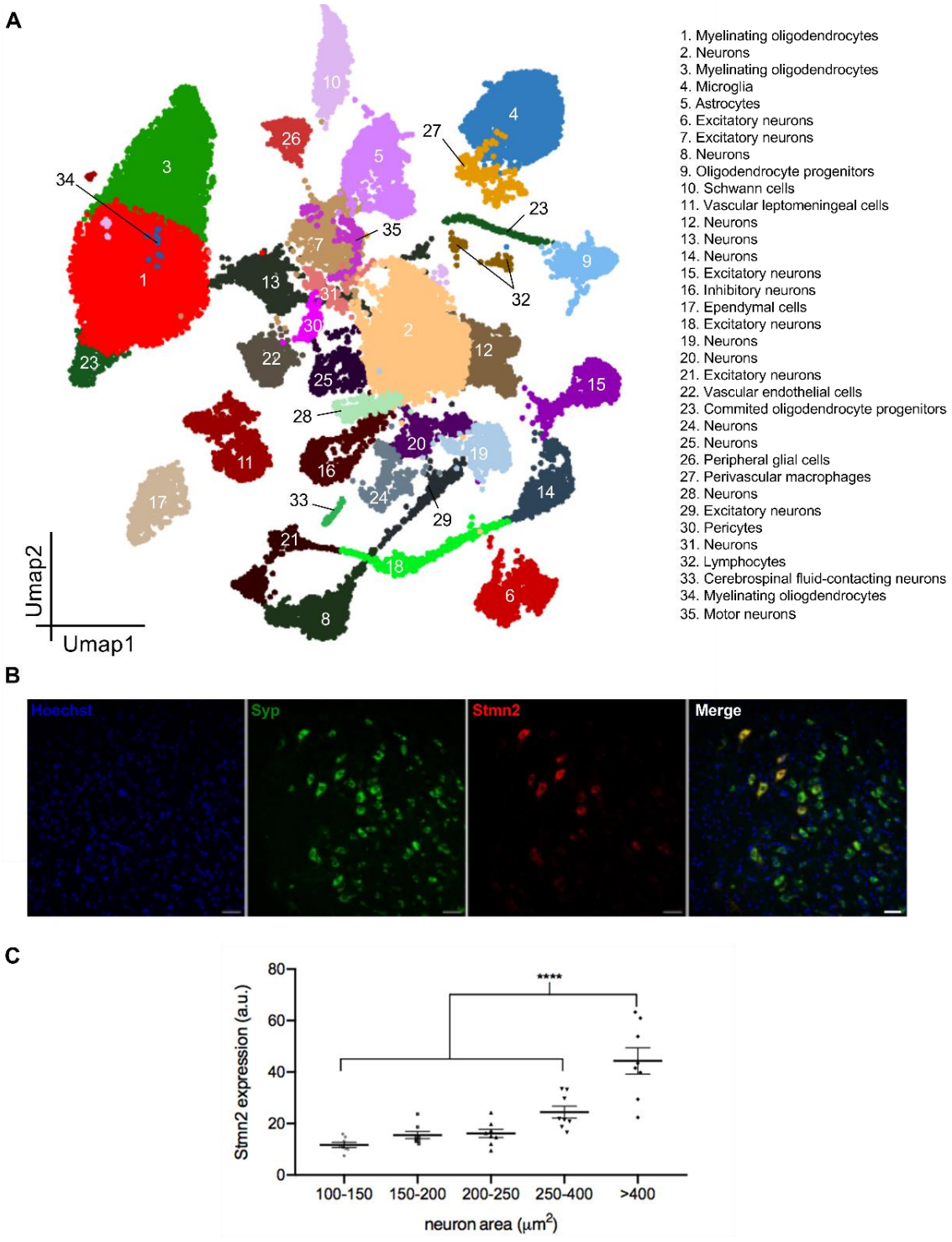


Figure 4.9. SnRNA-seq reveals neuronal cell clusters in SOD1^{G93A} spinal cord, including motor neurons. A, UMAP plot visualizing 42,278 nuclei isolated from the lumbar spinal cord of P110 *SOD1^{G93A}/Egln2$^{+/+}$* and *SOD1^{G93A}/Egln2$^{-/-}$* mice (N = 3 mice per group). Annotation of different clusters based on publicly available transcriptomics data. **B**, Representative images of pan-neuronal marker synaptophysin (*Syp*, green) and stathmin-2 (*Stmn2*, red) fluorescent in situ hybridization (FISH) using RNAscope with nuclear marker Hoechst (blue) staining in the ventral spinal cord of SOD1^{G93A} mice at P110. Scale bar, 50 µm. **C**, Quantification of *Stmn2* fluorescence arbitrary units (a.u.) normalized to 300,000 µm^2 of ventral horn and categorized per size. Data represent mean ± SEM with individual values shown (N ≥ 8 mice). Statistical analyses were performed in **C** by One-way ANOVA with Dunnett's multiple comparison test (****p<0.0001).

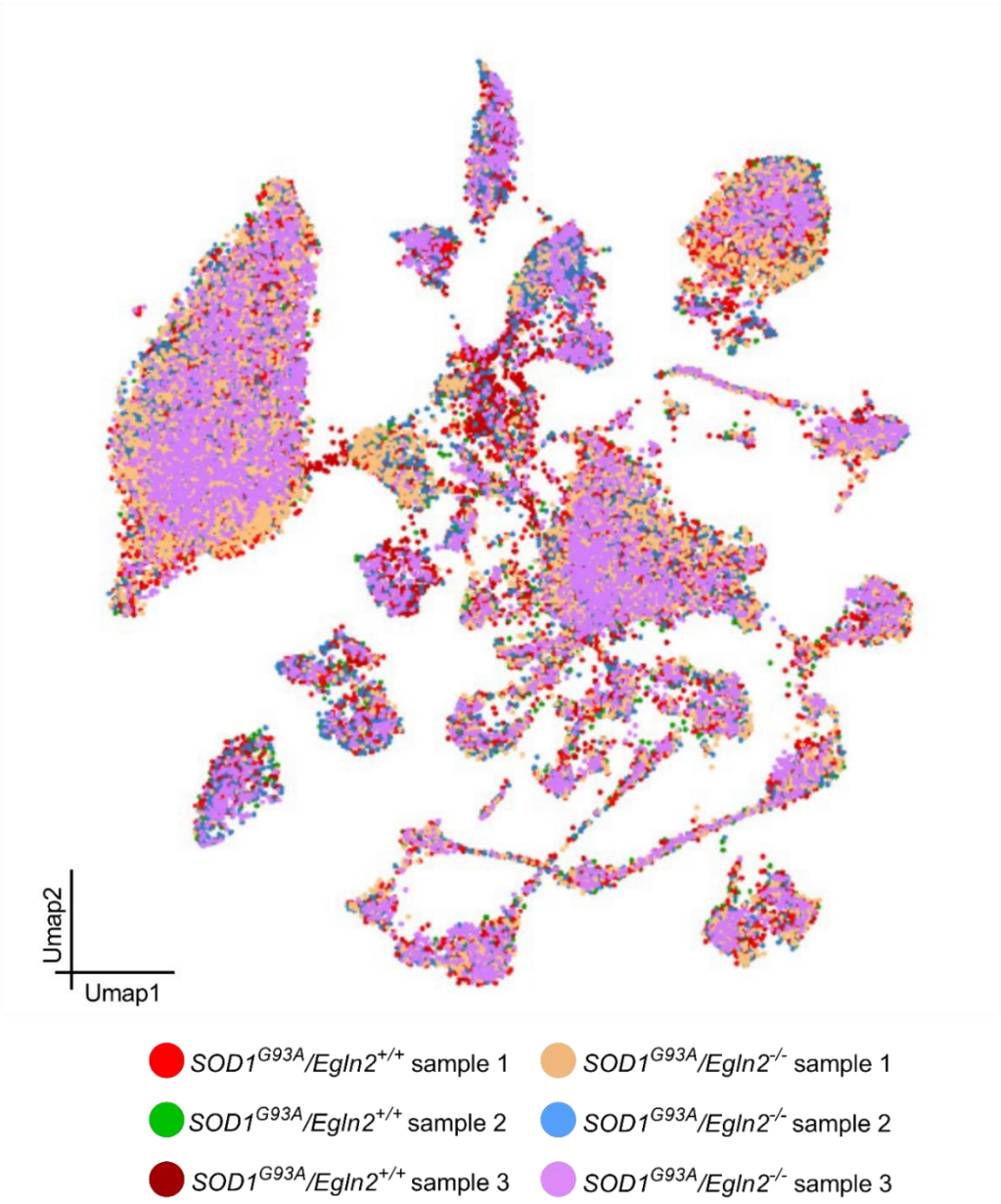


Figure 4.10. All snRNA-seq clusters contain nuclei from all six samples. UMAP showing overlap between different snRNA-seq samples.

4.3.2 *Egln2* deletion induces transcriptomic changes in neuronal and non-neuronal cells from SOD1^{G93A} spinal cord

Differentially expressed gene (DEG) analysis on all 35 clusters, revealed an overall total of 724 upregulated DEGs and 1653 downregulated DEGs in *SOD1^{G93A}/Egln2$^{-/-}$ versus SOD1^{G93A}/Egln2$^{+/+}$* clusters. GO enrichment analysis of the up- and downregulated DEGs revealed that deletion of *Egln2* induced a transcriptomic change in a range of biological processes in neuronal and non-neuronal cells (Table 4.1).

BIOLOGICAL PROCESS	GO TERM			CELL TYPE	TOP 5 DEGS
Upregulated					
Immune / defense response	GO:0042119; GO:0031347	GO:0036230;	GO:0031349;	Excitatory neurons	*Mmp12*, *Syk*, *Anxa1*, *Serping1*, *Ctss*
Synapse assembly	GO:0007416; GO:0050808	GO:0034329;	GO:0034330;	Perivascular macrophages	*Ctnna2*, *Nrxn3*, *Adgrl3*, *Lrrtm4*, *Nrg1*
Action potential	GO:0001508			Perivascular macrophages	*Grik2*, *Kcnc2*, *Dpp6*, *Dmd*, *Cntnap2*
Cell adhesion	GO:0098742; GO:0022610	GO:0098609;	GO:0007155;	Perivascular macrophages	*Robo2*, *Ctnna2*, *Tenm2*, *Nrxn3*, *Ninj1*
Translation	GO:0002181			Motor neurons	*Rpl30*, *Rps15*, *Rpl28*, *Rpl37a*, *Rpl22l1*
Downregulated					
Synapse assembly / transmission	GO:0048167; GO:0007268; GO:0099536	GO:0050804; GO:0098916;	GO:0099177; GO:0099537;	Myelinating oligodendrocytes	*Glra2*, *Kcnh1*, *Sv2b*, *Akap12*, *Erc2*
	GO:0099558; GO:0034330; GO:0007416; GO:0050804; GO:0098916; GO:0050807;	GO:0034331; GO:0060078; GO:0034329; GO:0099177; GO:0099537; GO:0050803;	GO:0050808; GO:0042391; GO:0051966; GO:0007268; GO:0099536; GO:1901890	Peripheral glial cells	*Arhgap6*, *Syn1*, *Rgs7*, *Fgf13*, *Slc4a4*
	GO:0051963			Lymphocytes	*Adgrb3*, *Mdga2*, *Negr1*, *Grid2*
	GO:1905606; GO:0050807; GO:0034329; GO:0051965; GO:0051960; GO:0042391	GO:0099174; GO:0050803; GO:0034330; GO:1901890; GO:0050804;	GO:1901888; GO:0007416; GO:0050808; GO:0051962; GO:0099177;	Motor neurons	*Dcc*, *Grik2*, *Nrg3*, *Nrp1*, *Fxyd1*
Ion transport	GO:0043269;	GO:0034762		Myelinating oligodendrocytes	*Kcnh1*, *Ano6*, *Kcnip4*, *Kcnc2*, *Jph3*
	GO:0032412; GO:0034762; GO:1904062	GO:0022898; GO:0034765;	GO:0032409; GO:0043269;	Peripheral glial cells	*Kcnh1*, *Ano6*, *Kcnip4*, *Kcnc2*, *Jph3*
	GO:1904062;	GO:0034765		Motor neurons	*Asic2*, *Fxyd1*, *Pde4d*, *Dpp10*, *Dmd*
Oxidative metabolism	GO:0006091; GO:0009060; GO:0009145; GO:0009205; GO:0015986; GO:0022904; GO:0042776;	GO:0006119; GO:0009141; GO:0009199; GO:0009206; GO:0019646; GO:0042773; GO:0045333;	GO:0006754; GO:0009142; GO:0009201; GO:0015980; GO:0022900; GO:0042775; GO:0046034	Neurons	*Slc1a3, Ndufa7, Hspa8, S100b, Uqcr11*

Viral response	GO:0045071; GO:0050792; GO:0009615;	GO:0045069; GO:0048525; GO:0140546	GO:1903900; GO:0051607;	Astrocytes	*Cxcl10, Oasl1, Isg15, Rsad2, Ifit1*
Cell death	GO:0042981;	GO:0043067;	GO:0010941	Astrocytes	*Cxcl10, Igfbp3, Ier3, Fcgr2b, Rac3*
	GO:1902255;	GO:1901798;	GO:0010942	Neurons	*Tac1, Unc13b, Rps15, Snca, Rpl26*
Translation	GO:0002181; GO:0043604; GO:0034645; GO:1901566	GO:0006412; GO:0006518; GO:0008016;	GO:0043043; GO:0043603; GO:0044271;	Neurons	*Vdr, Galnt5, Mlycd, Mrpl49, S100a10,*
Action potential	GO:0001508			Peripheral glial cells	*Cacna1c, Grin2b, Gria1, Kcnd2, Cntnap2*
Neurogenesis	GO:0051962; GO:0120039; GO:0048666; GO:0022008; GO:0007417; GO:0031344	GO:0051960; GO:0048858; GO:0030182; GO:0048667; GO:0010975;	GO:0048812; GO:0031175; GO:0048699; GO:0007420; GO:0120035;	Peripheral glial cells	*Hmga2, Fgf13, Cit, Grin2b, Dner*
	GO:0001764; GO:0010975;	GO:0048699; GO:0120035;	GO:0022008; GO:0031344	Motor neurons	*Tafa1, Asic2, Dcc, Nrp1, Cntnap2*
Cell adhesion	GO:0098742;	GO:0098609;	GO:0007155	Motor neurons	*Dcc, Nrp1, Cntnap2, Ctnnd2, Il1rapl1*

Table 4.1 *Egln2* deletion induces an effect on a range of pathways in neuronal and non-neuronal cells of SOD1^{G93A} spinal cord. GO analysis on DEGs from *SOD1^{G93A}/Egln2$^{-/-}$ versus SOD1^{G93A}/Egln2$^{+/+}$* lumbar spinal cord at P110. GO analysis performed using PANTHER (PANTHER GO biological process complete; *p < 0.05, Fischer's Exact with Bonferroni correction for multiple testing).

In the motor neuron cluster, genes related to synapse organization, ion transport, neurogenesis and cell adhesion were downregulated upon loss of EGLN2 (Table 4.1). While these included a number of genes that were linked to ALS before[383-388] (Table S4.2), no potential mechanism of action emerged. Interestingly, we also observed a downregulation of the neuroinflammation marker translocator protein (*Tspo*)[389] (Table S4.2), which has been proposed as biomarker for neuroinflammation[390]. Because of their central role in ALS-linked neuroinflammation[391], we next focused on the microglia and astrocytes.

While GO analysis did not detect any biological relevant effect of *Egln2$^{-/-}$* on inflammatory pathways in microglia, we did observe that GO terms linked to the cellular response to viruses were specifically downregulated in astrocytes (Figure 4.11, Table 4.1). Interestingly, the genes linked to these GO terms were all interferon-stimulated (Figure 4.12A, Table S4.3), of which some have been linked to motor neuron degeneration in ALS patients and models[96-100,392]. Because of this, we hypothesized that a

downregulation of the pro-inflammatory interferon-stimulated genes in astrocytes, induced by deletion of Egln2, could explain the observed motor neuron protection.

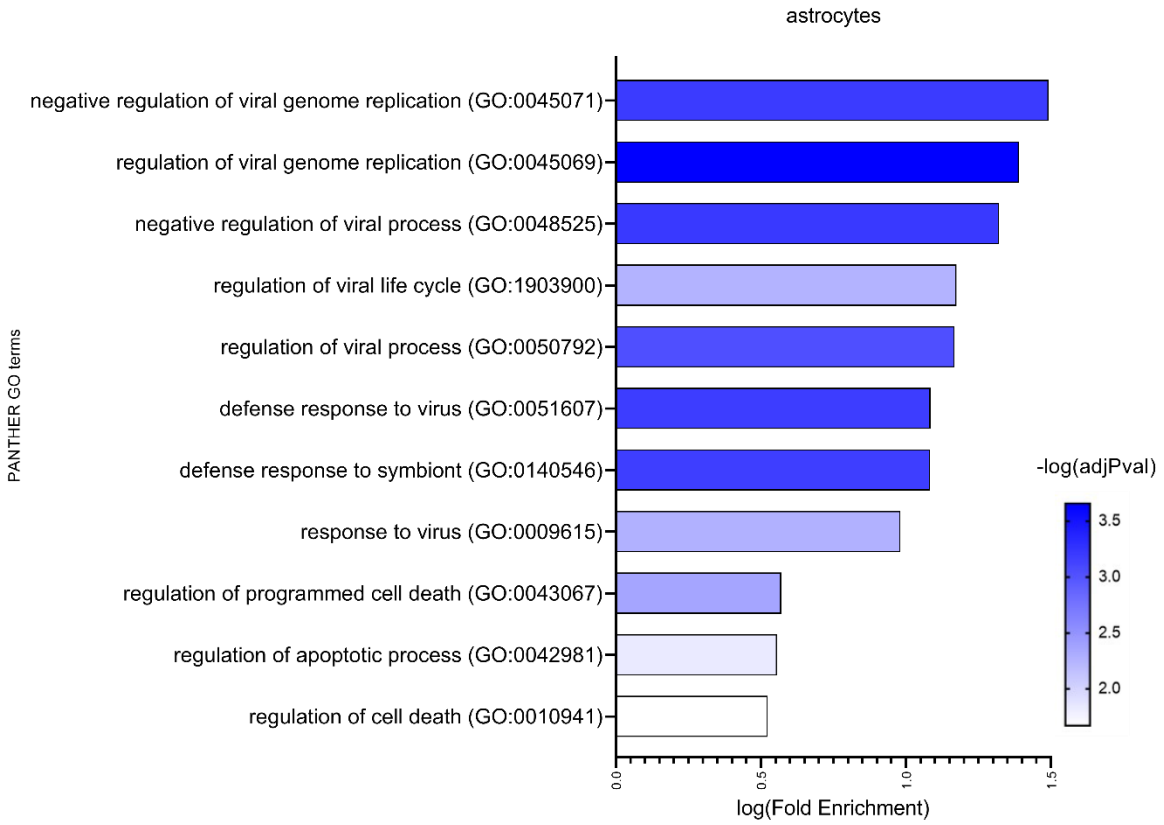


Figure 4.11 *Egln2* deletion induces downregulation of viral response and cell death pathways in astrocytes. GO analysis on DEGs from SOD1^{G93A}/Egln2$^{-/-}$ *versus* SOD1^{G93A}/Egln2$^{+/+}$ lumbar spinal cord at P110 by PANTHER. Significantly overrepresented biological processes (PANTHER GO biological process complete; *p<0.05, Fischer's Exact with Bonferroni correction for multiple testing) plotted against fold enrichment. Bar color represents -log(adjPval) of enriched GO term.

4.3.3 *Egln2* deletion downregulates the STING-induced interferon response in SOD1^{G93A} astrocytes

To explore the mechanisms through which loss of EGLN2 could affect the interferon response in astrocytes, we performed pathway analysis. Previous studies have shown that an increased interferon response in ALS motor neurons and myeloid cells can be provoked by the cGAS/STING pathway[97-100], regulating the innate immune response to cytosolic dsDNA resulting in the canonical activation through TBK1 and interferon regulatory factor 3 (IRF3) and noncanonical NFκB activation (Figure 4.12B)[95]. GSEA suggested that the expression of these genes was reduced via the canonical cGAS/STING pathway and not via a reduction of NFκB activation which even showed a trend towards

enrichment in the upregulated gene set of *SOD1*^{G93A}/*Egln2*$^{-/-}$ astrocytes (Figure 4.12C). While not reaching significance in the GSEA analysis, we observed a reduction in STING protein expression, marking decreased cGAS/STING pathway activation, in GFAP positive cells of the ventral horn of *SOD1*^{G93A}/*Egln2*$^{-/-}$ mice compared to *SOD1*^{G93A}/*Egln2*$^{+/+}$ mice (Figure 4.12D-E).

As a result, these data showed that deletion of *Egln2* reduced the expression of neuroinflammation marker *Tspo* in motor neurons while at the same time decreasing the cGAS/STING induced pro-inflammatory interferon response in astrocytes suggesting that *Egln2* deletion reduces the astrocytic interferon-dependent inflammatory axis.

4.3.4 Concluding remarks

Using a single-cell approach, we observed the cell specific effects of loss of EGLN2 on the spinal cord of SOD1^{G93A} mice. *Egln2* deletion induced transcriptomic effects on a range of pathways in neuronal and non-neuronal cells. In our search for the mechanism that could explain the beneficial effect of *Egln2*$^{-/-}$ on the motor neurons health and ALS phenotype in SOD1^{G93A} mice, we found that in motor neurons the neuroinflammation marker *Tspo* was downregulated while at the same time the pro-inflammatory interferon response was downregulated in astrocytes. Neuroinflammation marked by astrogliosis and microgliosis is a hallmark of ALS[393] and the levels of interferon-stimulated genes elevated in ALS models and patients[96-100,392]. We therefore considered this finding of particular interest and wanted to explore this further by studying the direct effect of loss of EGLN2 on patient-derived astrocytes.

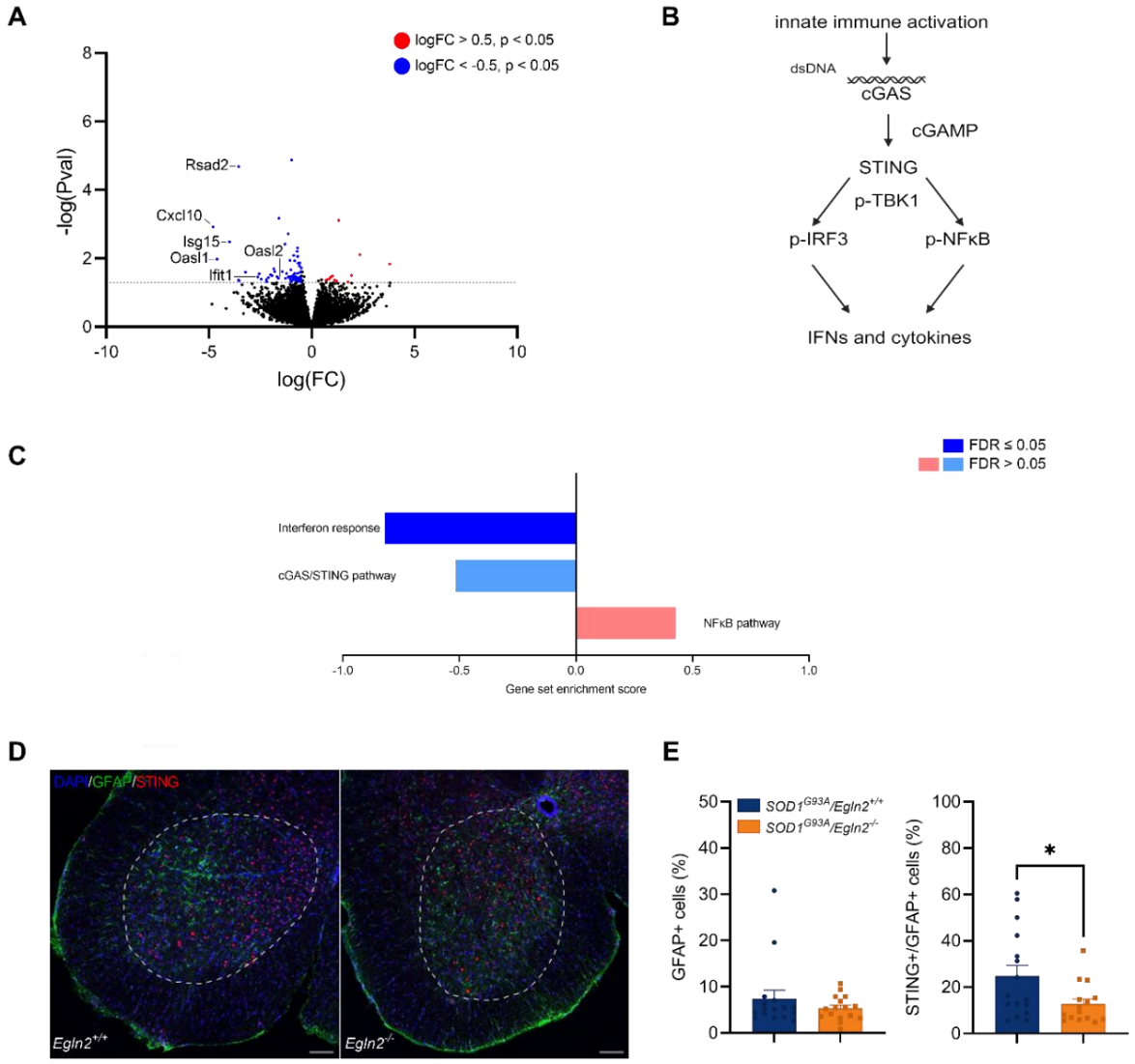


Figure 4.12 *Egln2* deletion induces astrocyte-specific downregulation of STING-induced gene expression. A, Volcano plot showing all DEGs in astrocytes from *SOD1^{G93A}/Egln2$^{-/-}$ versus SOD1^{G93A}/Egln2$^{+/+}$* lumbar spinal cord at P110. Red indicates genes with upregulated expression (Log10 (fold change) (log(FC)) > 0.5) in *SOD1^{G93A}/Egln2$^{-/-}$ versus SOD1^{G93A}/Egln2$^{+/+}$* mice, blue indicates genes with downregulated expression (log(FC) < -0.5) in *SOD1^{G93A}/Egln2$^{-/-}$ versus SOD1^{G93A}/Egln2$^{+/+}$* mice. **B**, Graphical representation of the cGAS/STING and NFκB pathway. **C**, GSEA scores for Interferon response[97], cGAS/STING pathway[394] and NFκB pathway[97] in DEGs from *SOD1^{G93A}/Egln2$^{-/-}$ versus SOD1^{G93A}/Egln2$^{+/+}$* astrocytes. **D**, Representative images of immunohistochemical analysis of 4',6-diamidino-2-phenylindole (DAPI), GFAP and STING in the lumbar spinal cord ventral horn, indicated with a white dotted line, of *SOD1^{G93A}/Egln2$^{+/+}$* and *SOD1^{G93A}/Egln2$^{-/-}$* mice at P110. Scale bar, 50 µm. **E**, Quantification of number of GFAP positive (GFAP+) cells and STING and GFAP positive (STING+/GFAP+) cells. Data represent mean ± SEM with individual values of each lumbar spinal cord section shown (N = 4 mice and n = 16 spinal cord sections per group). Statistical analyses were performed by an Unpaired T-test (*p<0.05).

4.4 Targeting EGLN2 mitigates ALS phenotypes in patient-derived astrocytes

4.4.1 *SOD1*^{A4V}-ALS patient-derived iPSCs differentiate into mature astrocytes

Before exploring the effect of loss of EGLN2 on patient-derived astrocytes, we first characterized these cells. iPSCs from an ALS patient carrying a heterozygous *SOD1*^{A4V} mutation and their isogenic control (*SOD1*^{A4A}), previously generated by genetic correction of the mutation[123], both differentiated into mature astrocytes that express Vimentin (VIM), transcription factor SOX-9 (SOX9) and odorant binding protein ASP4 (AQP4) using a previously established protocol[300] (Figure4.13A-B). Moreover, life-cell calcium recordings revealed that the astrocytes were functionally active as spontaneous fluxes of calcium were observed in the astrocyte monocultures, with no differences between the patient and the control astrocytes (Figure 4.13C-D). Finally, we also performed immunocytochemical analysis of GFAP as measurement of their activation state. No difference in GFAP expression between the patient and the control astrocytes was observed (Figure 4.14A-B). Together these data show that both mutant and isogenic control astrocytes differentiate into mature and functionally active astrocytes that do not show differences in GFAP-marked reactivity.

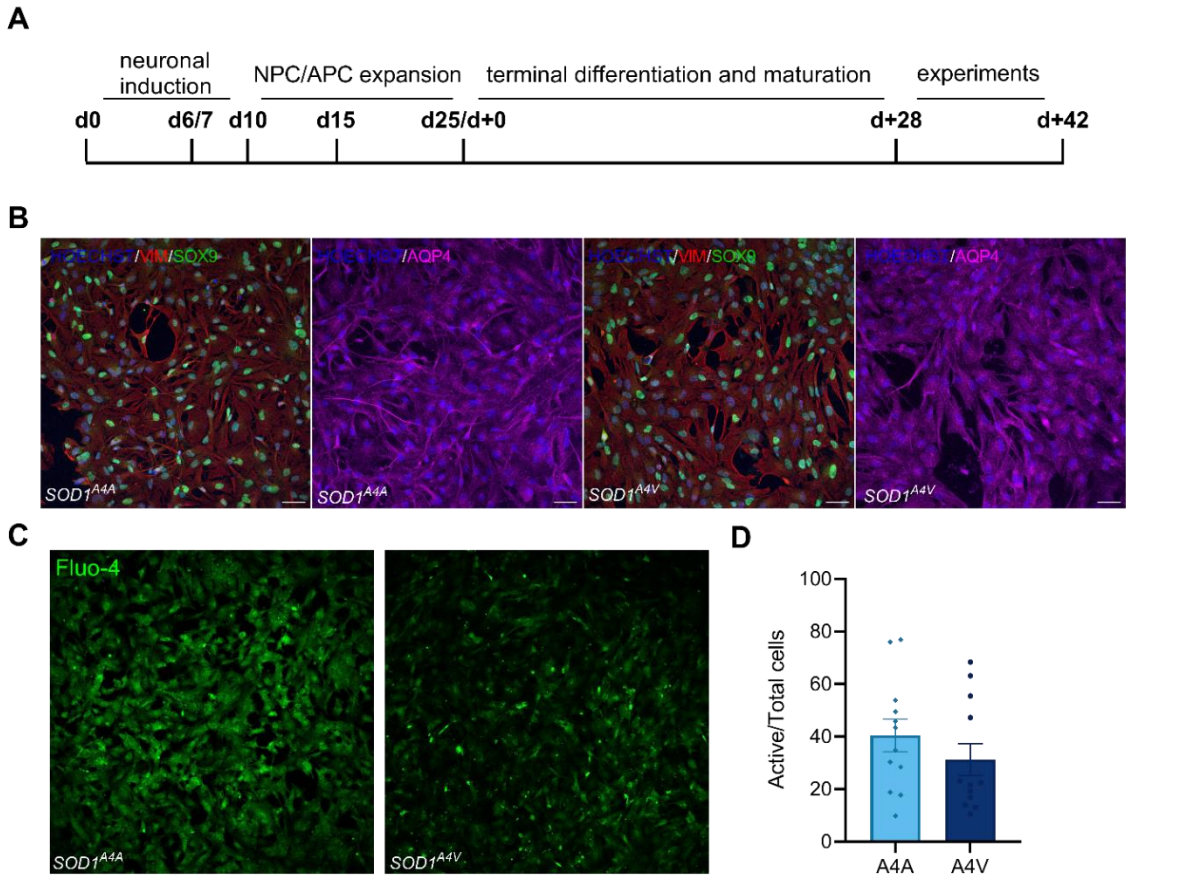


Figure 4.13. *SOD1^{A4A}* and *SOD1^{A4V}* differentiate into mature and functionally active astrocytes. A, Graphical representation of astrocyte protocol. **B**, Representative images of immunocytochemical analysis of astrocyte markers VIM, SOX9 and AQP4 in mature astrocytes (d+41). Scalebar = 50 µm. **C**, Representative images of immunocytochemical analysis of calcium indicator Fluo-4 AM. **D**, Quantification of active cells normalized to total amount of cells. Active cell defined as cell that has a difference in Fluo-4 AM intensity of at least 10 between minimum and maximum fluorescent intensity over 60 s. Data represent mean ± SEM with individual values show (N = 3 astrocyte differentiations and n = 4 wells per group). Statistical analysis in **D** was performed by an Unpaired T-test.

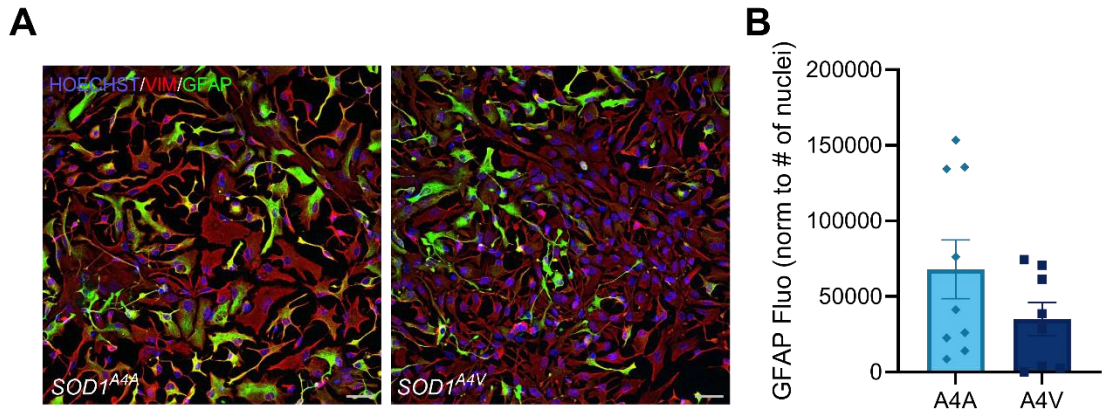


Figure 4.14. GFAP-marked astrocyte reactivity is not affected by mutant *SOD1^{A4V}* in astrocyte monocultures. **A**, Representative images of VIM (red), GFAP (green) and HOECHST (blue) staining in mature *SOD1^{A4A}* (A4A) and *SOD1^{A4V}* (A4V) astrocytes. Scale bar = 50 µm. **B**, Quantification of GFAP fluorescence, normalized to the number of HOECHST+ nuclei. Data represent mean ± SEM with individual values shown (N = 3 astrocyte differentiations and n = 3 images per group). Statistical analysis in **B** was performed by Unpaired T-test.

4.4.2 Metabolic profiling of *SOD1^{A4V}*-ALS patient-derived astrocytes

Astrocytes support motor neurons to meet their high energy demand[242]. In ALS, metabolic dysfunction has been well characterized in models and patients[154]. Therefore, we aimed to metabolically profile the *SOD1^{A4V}* patient-derived astrocytes. To map their metabolic activity, we performed metabolic flux analysis using substrate tracing experiments with radiolabeled glucose, lactate, glutamine and palmitate (Figure 4.15). This revealed that the SOD1^{A4V} mutation significantly increased the metabolic flux through both glycolysis and glucose oxidation (Figure 4.15 A-C). The increase in glucose oxidation is atypical for astrocytes as they mainly generate ATP through anaerobic glycolysis in which they catabolize glucose to lactate, which can be shuttled to motor neurons to meet their high energy demand. To investigate if the increased glucose oxidation in *SOD1^{A4V}* astrocytes is the result of compensatory effect due to mitochondrial dysfunction, we measured mitochondrial abundance and integrity. The mitochondrial abundance in astrocytes as measured by the expression of translocase of

outer mitochondrial membrane 20 (TOMM20) is not affected by mutant SOD1^{A4V} (Figure 4.16A). Moreover, also the mitochondrial integrity in astrocytes, as measured by the mitochondrial membrane potential via the uptake of TMRM dye, was also not affected by mutant SOD1^{A4V} (Figure 4.16B).

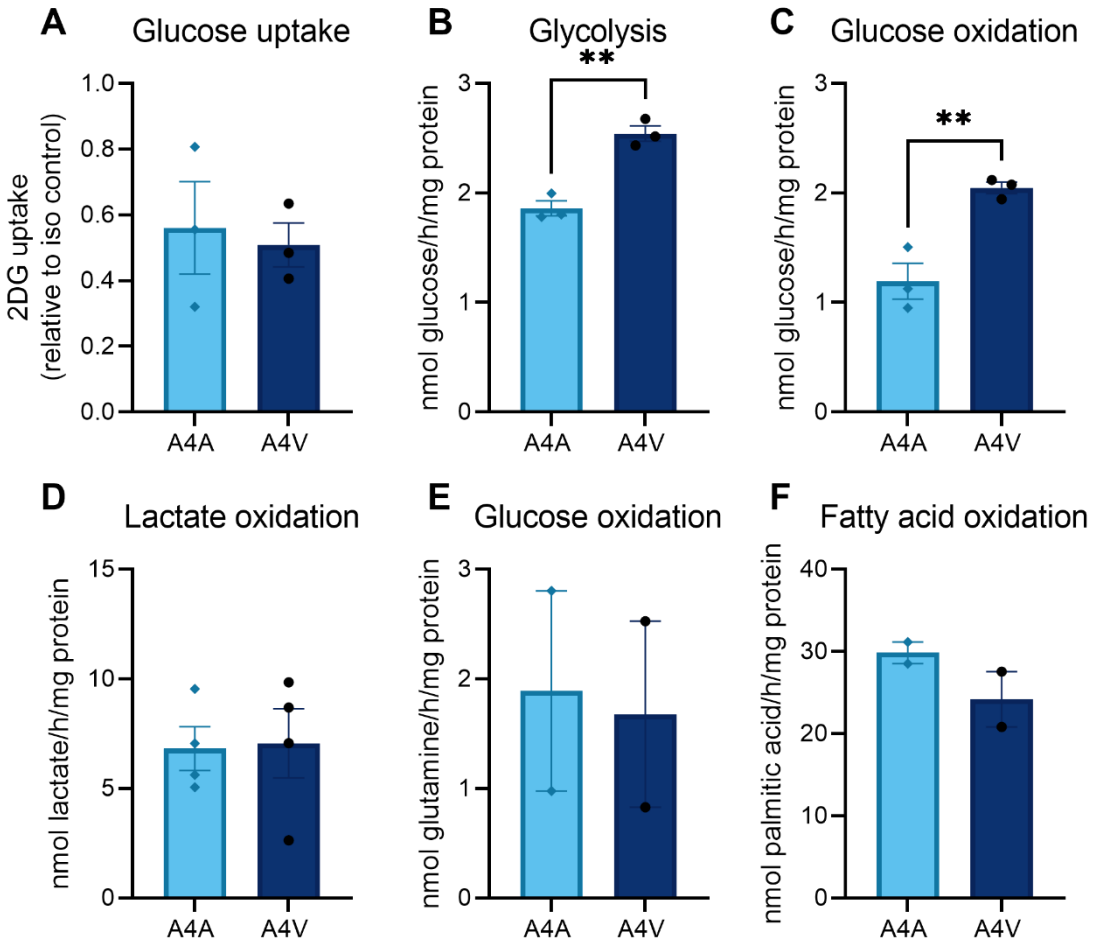


Figure 4.15. *SOD1^{A4V}* increases glucose metabolism in astrocytes. A, 2-deoxy-glucose; **B**, glycolysis; **C**, glucose oxidation, **D**, lactate oxidation; **E**, glucose oxidation and **F**, fatty acid oxidation in isogenic control (A4A) and mutant SOD1^{A4V} (A4V) astrocytes. Data represent mean ± SEM with individual values shown (N = 2-3 astrocyte differentiations). Statistical analyses were performed by an Unpaired T-test (**p<0.01).

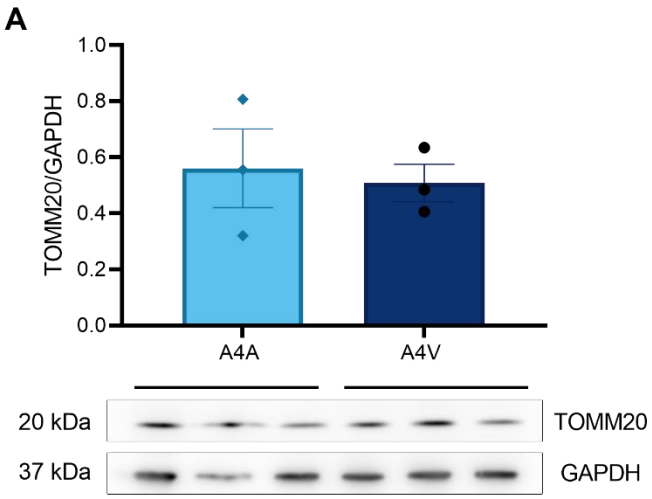


Figure 4.16 *SOD1^{A4V}* does not affect mitochondrial number and health. A, TOMM20 levels in mature *SOD1^{A4A}* (A4A) and *SOD1^{A4V}* (A4V) astrocytes normalized to GAPDH as measured by WB. **B**, TMRM mean intensity at baseline conditions in mature *SOD1^{A4A}* (A4A) and *SOD1^{A4V}* (A4V) astrocytes measured by live-cell imaging. Data represent mean ± SEM with individual values shown (N = 3 astrocyte differentiations). Statistical analyses were performed by an Unpaired T-test.

Finally, we investigated if the metabolic phenotype in *SOD1^{A4V}* astrocytes had an effect on the energy metabolism in control and mutant motor neurons. Therefore, we treated both isogenic (A4A MN) and *SOD1^{A4V}* (A4V MN) motor neurons with CAM from both isogenic (A4A CAM) and *SOD1^{A4V}* (A4V CAM) astrocytes and measured the cellular metabolism using the same substrate tracing experiments as before. This revealed no consistent changes in the glucose uptake, glycolysis, glucose oxidation, lactate oxidation, glutamine oxidation or palmitate oxidation (Figure 4.17).

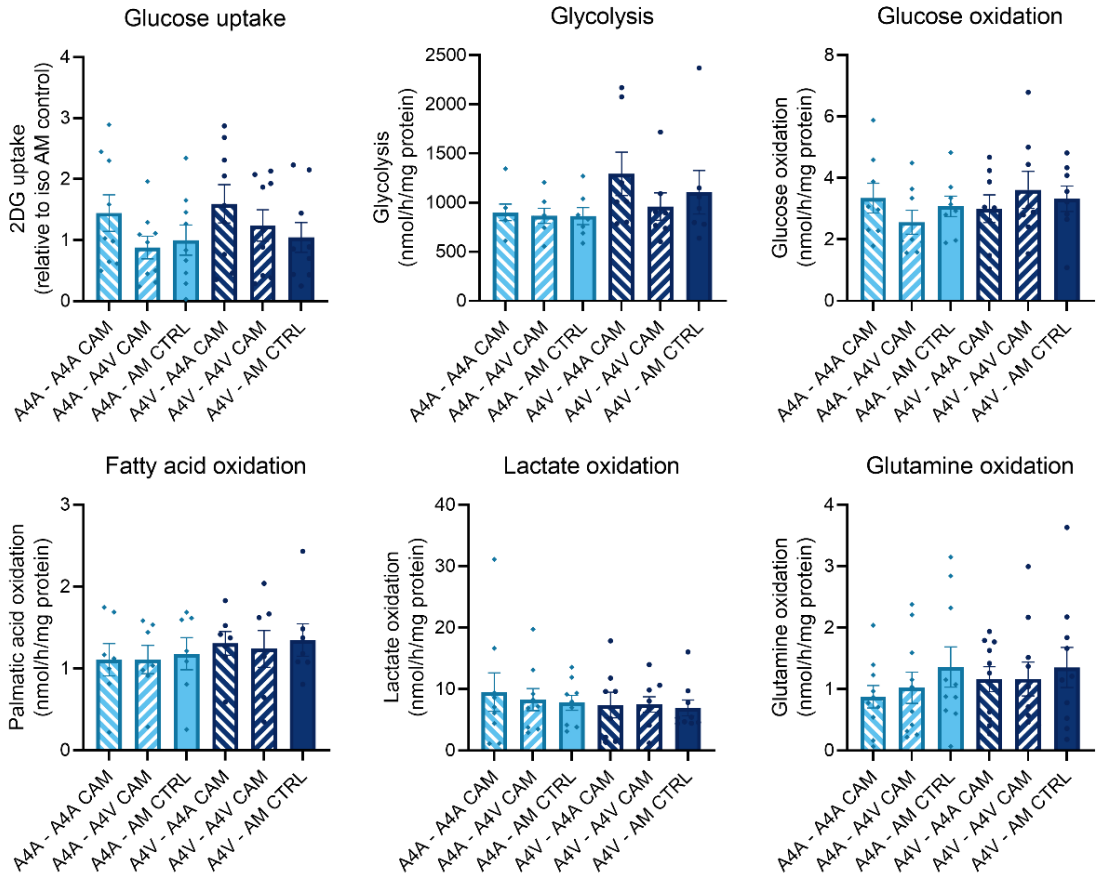


Figure 4.17. *SOD1^{A4V}* conditioned astrocyte medium does not affect motor neuron metabolic fluxes. 2-deoxy-D-glucose, glycolysis and glucose, palmitic acid, lactate and glutamine oxidation in *SOD1^{A4A}* (A4A) and *SOD1^{A4V}* (A4V) motor neurons treated for a week with 50% conditioned astrocyte medium (CAM) from *SOD1^{A4A}* (A4A CAM) or *SOD1^{A4V}* (A4V CAM) or non-conditioned astrocyte medium (AM CTRL). Data represent mean ± SEM with individual values shown (N ≥ 7 motor neuron differentiations). Statistical analysis performed by a One-way ANOVA.

4.4.3 Transcriptomic profiling of *SOD1^{A4V}*-ALS patient-derived astrocytes

Next to metabolic changes, ALS can also induce transcriptomic changes in astrocytes which can both lead to a gain-of-toxic or a loss-of-support effect[263]. To study the transcriptomic changes induced by mutant *SOD1^{A4V}* in astrocytes, we performed RNA-seq analysis on mature astrocytes. RNA-seq analysis was followed by DEG analysis which revealed that 584 genes were significantly upregulated (false discovery rate [FDR] < 0.05, logFC > 1) and 1239 genes were significantly downregulated (FDR < 0.05, logFC < -1) in *SOD1^{A4V}* versus *SOD1^{A4A}* astrocytes (Figure 4.18).

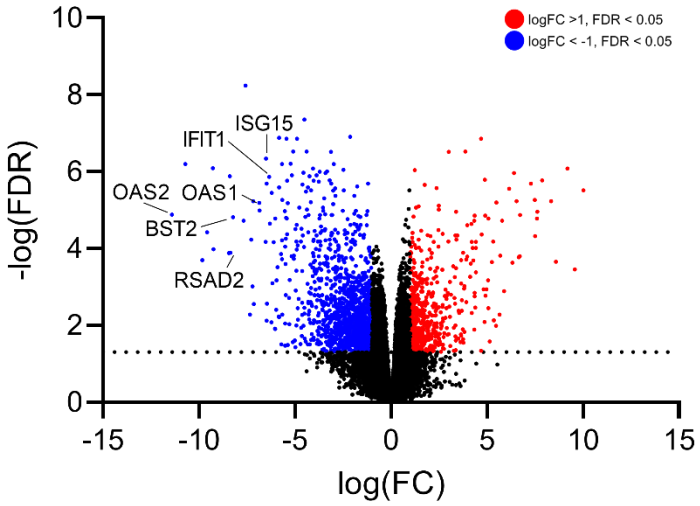


Figure 4.18. *SOD1^{A4V}* affects gene expression in patient-derived astrocytes. Volcano plot demonstrating all DEGs in *SOD1^{A4V} versus SOD1^{A4A}* astrocytes (left Volcano plot) and all significant DEGs in *SOD1^{A4V}/EGLN2$^{-/-}$ versus SOD1^{A4V}* astrocytes (right Volcano plot). Red indicates upregulated genes (Log10 (fold change) (log(FC)) > 1, false discovery rate (FDR) < 0.05), blue indicates downregulated genes (log(FC) < -1, FDR < 0.05).

Interestingly GSEA revealed a significant downregulation of genes linked the interferon response (Figure 4.19). As our snRNA-seq experiment in mice already revealed that targeting EGLN2 acts on the transcriptomic interferon response in astrocytes, we wanted to investigate if the same was true in patient-derived astrocytes in which a decreased interferon response was observed.

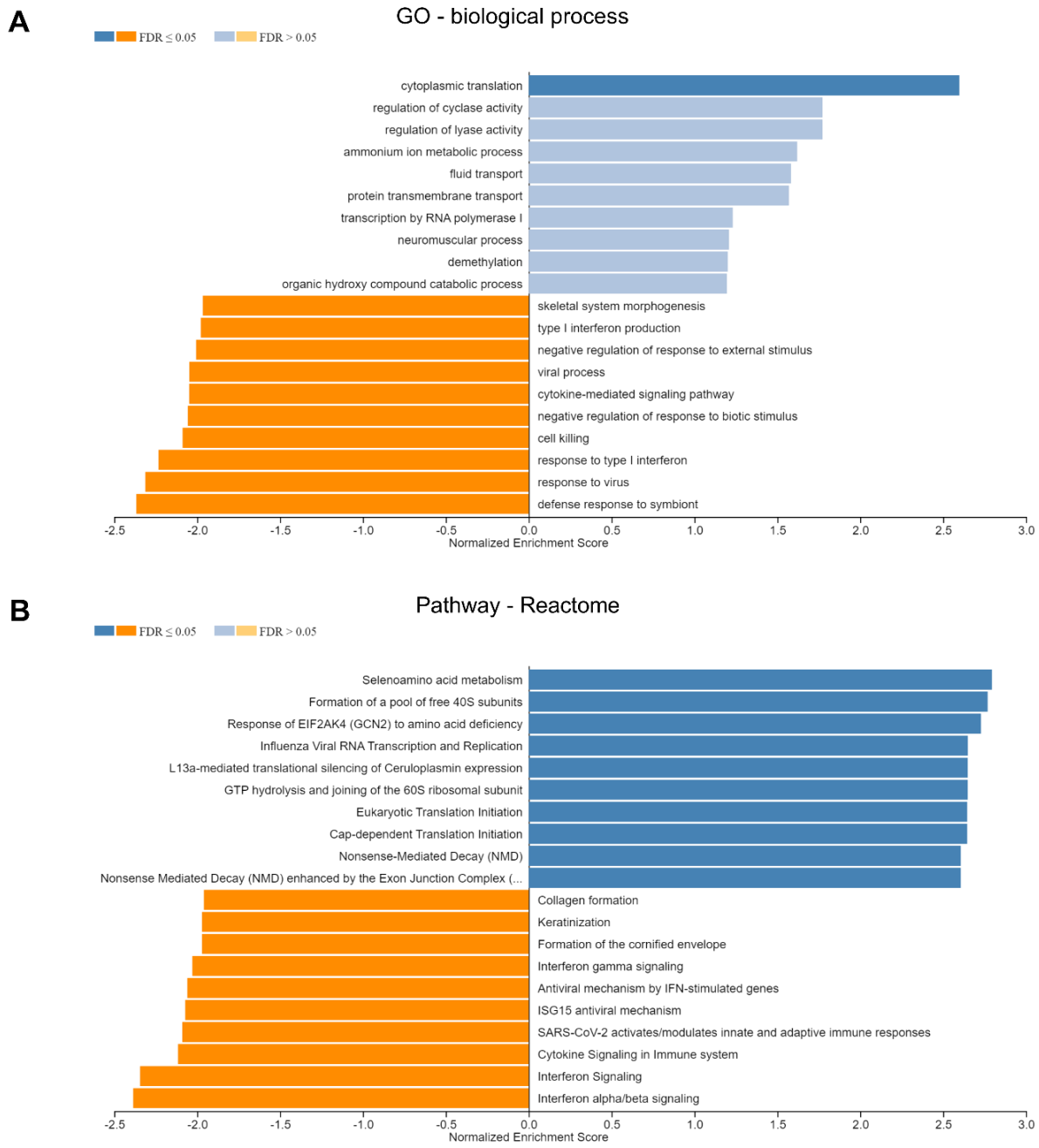


Figure 4.19. *SOD1^{A4V}* downregulates transcriptomic interferon response in patient-derived astrocytes. GSEA showing the enrichment of ranked DEGs of *SOD1^{A4V}* astrocytes versus *SOD1^{A4A}* astrocytes. **A**, Enrichment of DEGs in GO biological processes. **B**, Enrichment of DEGs in Reactome pathways.

4.4.4 Generation of *SOD1^{A4V}*-ALS patient-derived astrocytes with an *EGLN2* deletion

To investigate if knock-out of EGLN2 acted on the interferon response in patient-derived astrocytes, we first needed to generate patient-derived astrocytes with a specific *EGLN2* deletion. Using CRISPR-Cas9 with guide RNA (gRNA) that targets exon 2 of *EGLN2*, where the catalytic domain of the protein

lays, we generated a homozygous 4bp deletion in *EGLN2* in *SOD1*^{A4V} iPSCs (Figure 4.20A) without affecting the highest predicted off-target sites (Figure 4.20B, Table 4.2).

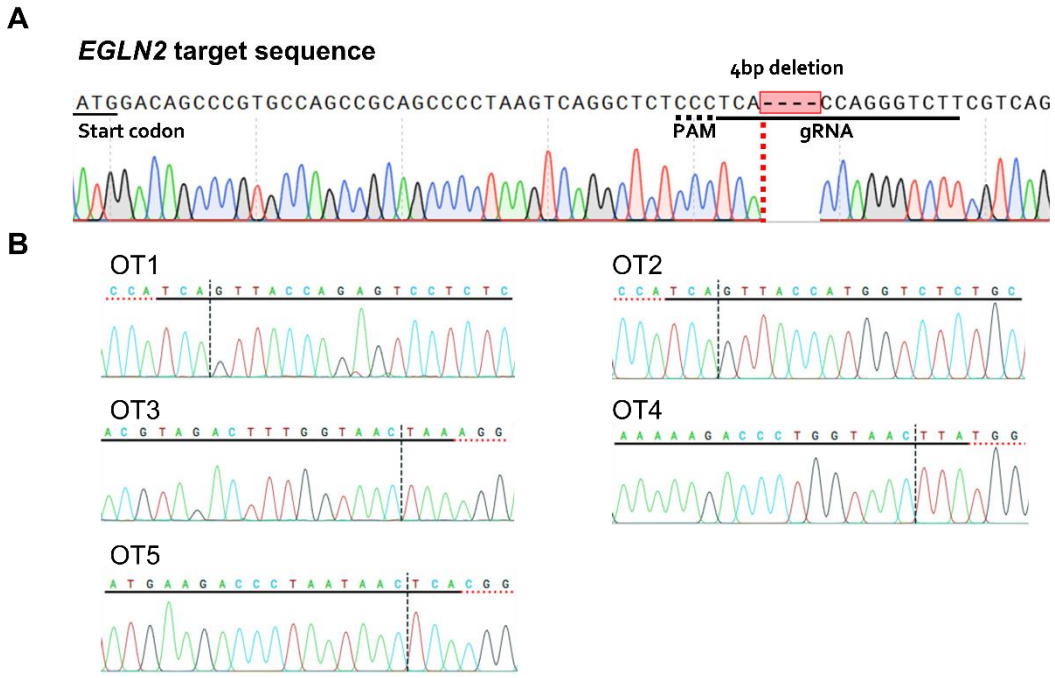


Figure 4.20. CRISPR-Cas9 induces a 4 bp deletion in *EGLN2* without affecting off-target sites. A, Target sequencing result of selected EGLN2 knock-out iPSC clone. Sanger sequencing result analyzed by Snapgene software reveals homozygous presence of 4 base pair deletion in proximity of start codon. **B**, Sanger sequencing result of the off-target (OT) sites 1-5 analyzed by Synthego ICE tool.

NAME	OFF TARGET SEQUENCE	NUMBER OF MISMATCHES	CHROMOSOME	LOCUS
OT1	GAGAGGACTCTGGTAACTGATGG	4	Chr6	intergenic
OT2	GCAGAGACCATGGTAACTGATGG	4	Chr2	intergenic
OT3	ACGTAGACTTTGGTAACTAAAGG	4	Chr3	intron: MAGI1
OT4	AAAAAGACCCTGGTAACTTATGG	3	Chr3	intron: UBE2E1
OT5	ATGAAGACCCTAATAACTCACGG	4	Chr13	Intron: DACH1

Table 4.2. Predicted off-target sites of *EGLN2* CRISPR-Cas9 gRNA. Top five identified off-target (OT) sites by CRISPOR having highest CFD scores.

Moreover, this 4bp deletion, which results in a frameshift in *EGLN2*, did not affect the pluripotency of the iPSCs as assessed by the expression of several pluripotency markers including homeobox

transcription factor NANOG (NANOG), octamer-binding transcription factor 4 (OCT4), sex determining region Y-box 2 (SOX, TRA-1-81, TRA-1-60 and stage-specific embryonic antigen-4 (SSEA4) and analysis of the EB formation (Figure 4.21).

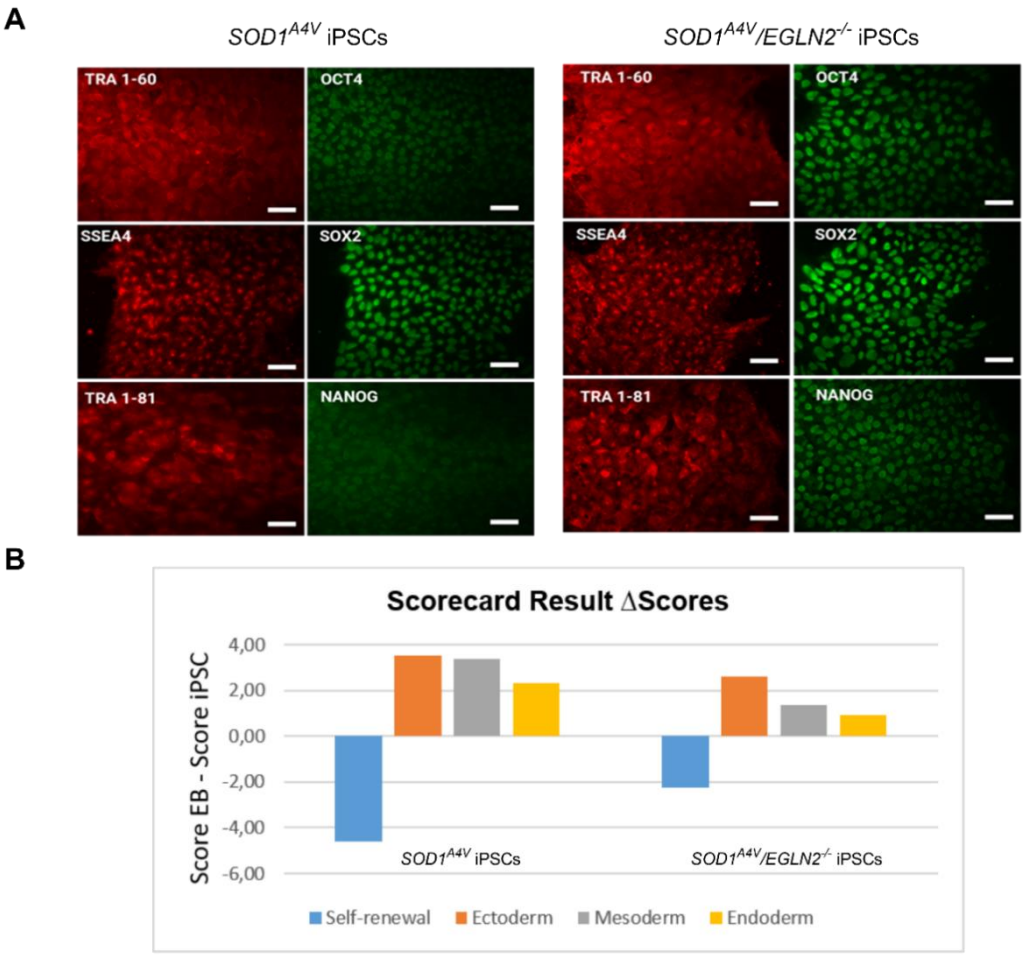


Figure 4.21. *SOD1^{A4V}/EGLN2$^{-/-}$* iPSCs are pluripotent and can form EBs. A, Immunofluorescent staining of pluripotency markers NANOG, OCT4, SOX2, TRA-1-81, TRA-1-60 and SSEA4 in *SOD1^{A4V}* and *SOD1^{A4V}/EGLN2$^{-/-}$* iPSCs. Scale bar, 50 µm. **B**, Scorecard analysis of embryoid bodies made from *SOD1^{A4V}* and *SOD1^{A4V}/EGLN2$^{-/-}$* iPSCs.

Finally, chromosomal assessment using array-CGH showed the presence of a duplication in chromosome 20 (20q.11) and chromosome 5 (5p.11, p.12) in *SOD1^{A4V}* iPSCs, with similar aberrations present in the derivative *EGLN2* knock-out clone (triplication of 20q.11 and mosaic duplication of 5p.11, p.12) (Figure S4.1-S4.3). It has to be noted that these chromosomal aberrations are amongst the most frequent aberrations observed in iPSCs[395].

4.4.5 Deletion of *EGLN2* normalizes the interferon response in *SOD1^{A4V}*-ALS patient-derived astrocytes

To explore the direct effect of loss of EGLN2 on astrocytes from ALS patients, we differentiated *SOD1^{A4V}/EGLN2$^{-/-}$* and *SOD1^{A4V}* iPSCs together with isogenic control (*SOD1^{A4A}*) iPSCs into mature astrocytes that express the astrocyte markers VIM, SOX9 and AQP4 (Figure 4.22, Figure 4.24A).

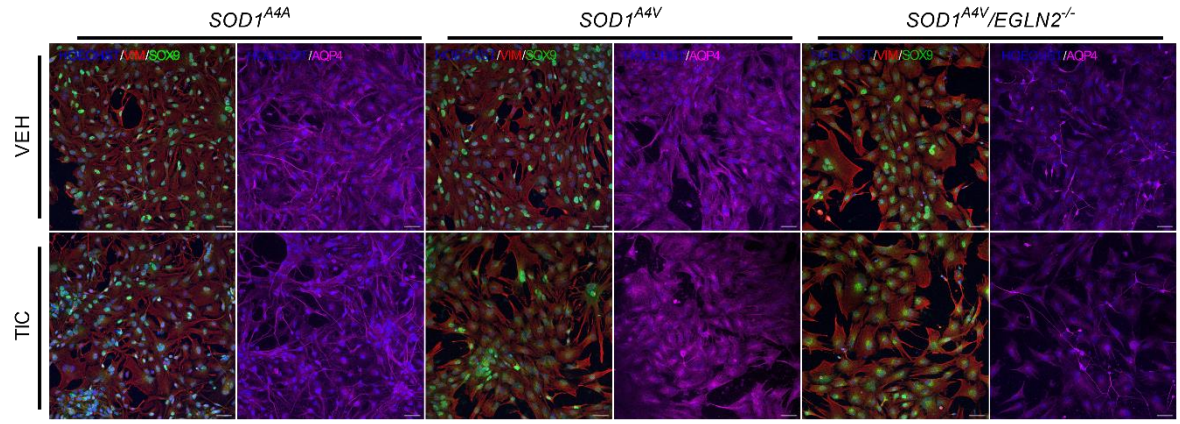


Figure 4.22. *SOD1^{A4A}*, *SOD1^{A4V}* and *SOD1^{A4V}/EGLN2$^{-/-}$* iPSCs differentiate into mature astrocytes. Representative images of immunocytochemical analysis of astrocyte markers VIM, SOX9 and AQP4 in mature astrocytes (d+41) used for RNA-seq analysis. Scalebar = 50 µm.

RNA-seq analysis revealed that the transcriptome of *SOD1^{A4V}/EGLN2$^{-/-}$* astrocytes was more similar to the transcriptome of isogenic *SOD1^{A4A}* astrocytes compared to *SOD1^{A4V}* astrocytes (Figure 4.23), indicating that *EGLN2* deletion rescued ALS-induced defects in these cells.

To identify the pathways that are rescued upon loss of *EGLN2* in astrocytes, DEG analyses between the different astrocyte lines were performed. 676 genes were both differentially expressed in *SOD1^{A4V} versus SOD1^{A4A}* astrocytes and *SOD1^{A4V}/EGLN2$^{-/-}$ versus SOD1^{A4V}* astrocytes (Figure 4.24B). From these 676 overlapping DEGs, 511 DEGs were downregulated in *SOD1^{A4V} versus SOD1^{A4A}* astrocytes and upregulated in *SOD1^{A4V}/EGLN2$^{-/-}$ versus SOD1^{A4V}* astrocytes (Figure 4.24C), indicating that the expression of these genes was rescued upon loss of EGLN2. This gene set mainly included genes linked to the interferon response, including the ones that were found to be downregulated in the snRNA-seq analysis (Figure 4.24D). As a result, this showed that in monocultured patient astrocytes, *EGLN2* deletion increased the expression of interferon-stimulated genes while these were downregulated in astrocytes from *SOD1^{G93A}/Egln2$^{-/-}$* mice. Moreover, GSEA suggested that the effect of *EGLN2* knock-out on the interferon response could be driven by an activation of the canonical cGAS/STING-TBK1-IRF3 and noncanonical NFκB pathway (Figure 4.24E).

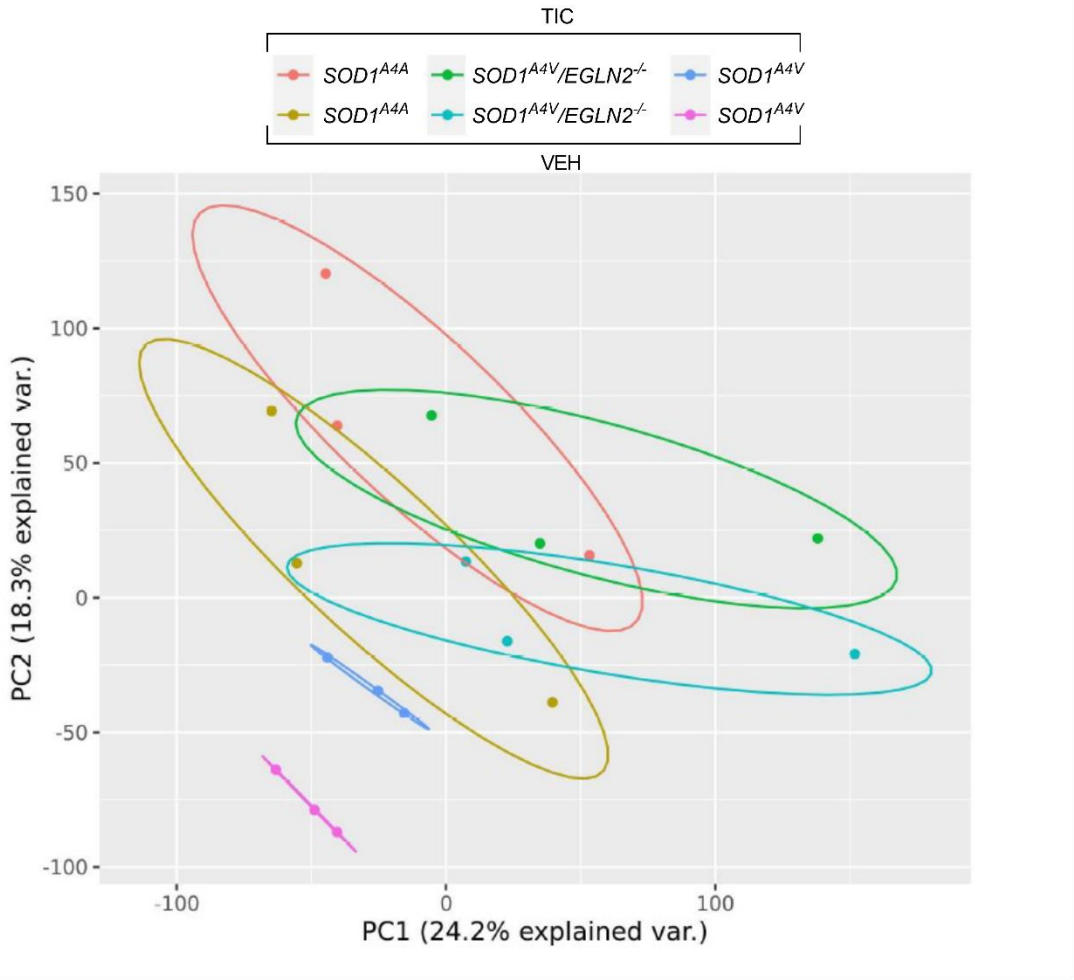


Figure 4.23. The transcriptome of *SOD1^{A4V}/EGLN2$^{-/-}$* astrocytes is more similar to *SOD1^{A4A}* astrocytes than to *SOD1^{A4V}* astrocytes. Two-dimensional graph plotting the two first principal components, determined by a principal component analysis, that explain the biological variation between the samples the best.

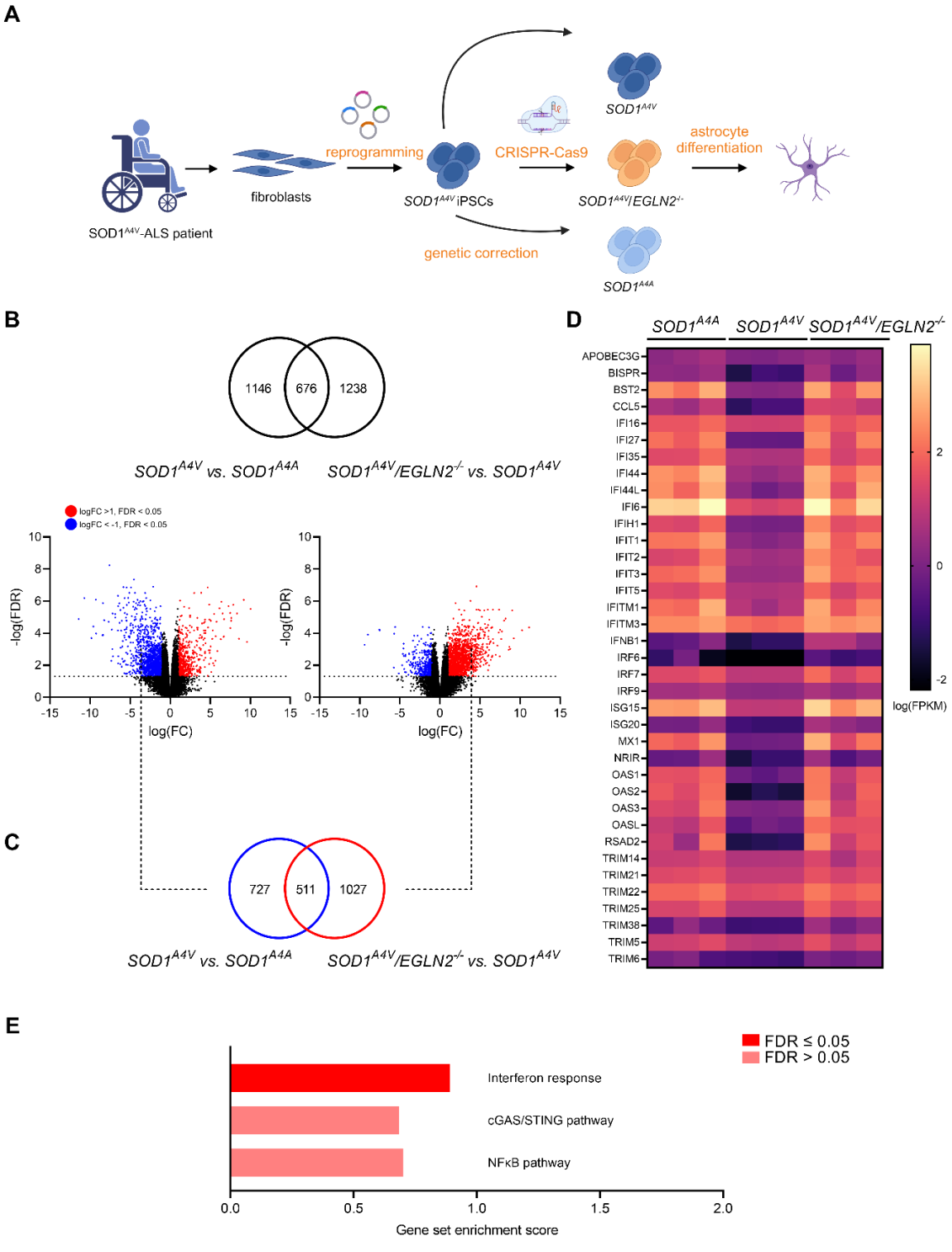

A
SOD1A4V-ALS patient
fibroblasts
reprogramming
SOD1A4V iPSCs
CRISPR-Cas9
SOD1A4V
SOD1A4V/EGLN2-/-
SOD1A4A
genetic correction
astrocyte differentiation
B
1146
676
1238
SOD1A4V vs. SOD1A4A
SOD1A4V/EGLN2-/- vs. SOD1A4V
logFC >1, FDR < 0.05
logFC < -1, FDR < 0.05
-log(FDR)
log(FC)
C
727
511
1027
SOD1A4V vs. SOD1A4A
SOD1A4V/EGLN2-/- vs. SOD1A4V
D
SOD1A4A
SOD1A4V
SOD1A4V/EGLN2-/-
APOBEC3G
BISPR
BST2
CCL5
IFI16
IFI27
IFI35
IFI44
IFI44L
IFI6
IFIH1
IFIT1
IFIT2
IFIT3
IFIT5
IFITM1
IFITM3
IFNB1
IRF6
IRF7
IRF9
ISG15
ISG20
MX1
NRIR
OAS1
OAS2
OAS3
OASL
RSAD2
TRIM14
TRIM21
TRIM22
TRIM25
TRIM38
TRIM5
TRIM6
log(FPKM)
E
FDR ≤ 0.05
FDR > 0.05
Interferon response
cGAS/STING pathway
NFκB pathway
Gene set enrichment score

Figure 4.24. *EGLN2* deletion restores the level of interferon-stimulated genes in *SOD1^{A4V}* patient-derived astrocytes. A, Schematic representation of the experimental set-up. **B**, Venn diagram demonstrating the overlap between all significant DEGs in *SOD1^{A4V} versus SOD1^{A4A}* astrocytes (left Volcano plot) and all significant DEGs in *SOD1^{A4V}/EGLN2$^{-/-}$ versus SOD1^{A4V}* astrocytes (right Volcano plot). Red indicates upregulated genes (Log10 (fold change) (log(FC)) > 1), blue indicates downregulated genes (log(FC) < -1). **C**, Venn diagram showing the overlap between the significantly downregulated genes in *SOD1^{A4V} versus SOD1^{A4A}* astrocytes (log(FC) < -1) and significantly upregulated genes in *SOD1^{A4V}/EGLN2$^{-/-}$ versus SOD1^{A4V}* astrocytes (log(FC)> 1). **D**, Heatmap showing the expression levels (fragments per kilobase million [FPKM]) of interferon-stimulated genes in *SOD1^{A4A}*, *SOD1^{A4V}* and *SOD1^{A4V}/EGLN2$^{-/-}$* astrocytes. **E**, GSEA scores for interferon response[97], cGAS/STING pathway[394] and NFκB pathway[97] in DEGs from in *SOD1^{A4V}/EGLN2$^{-/-}$ versus SOD1^{A4V}* astrocytes. N = 3 astrocyte differentiations.

The interferon response plays a crucial role in pro-inflammatory signaling and while astrogliosis and microgliosis are present in SOD1^{G93A} mice at P110[396], this is not the case in these human astrocyte monocultures (Figure 4.14A-B and Figure 4.25A). To investigate whether the lack of neuroinflammatory stimuli could explain the difference in the effect on the interferon genes, we provoked an inflammatory response, marked by the previously described markers[397], in our iPSC-derived astrocytes by treatment with a pro-inflammatory microglia-derived cocktail of TNFα, IL-1α and C1q (TIC)[261] (Figure 4.25A). *SOD1^{A4V}* astrocytes showed a greater transcriptional response to the treatment compared to their isogenic controls (Figure 4.25B) and *SOD1^{A4V}/EGLN2$^{-/-}$* astrocytes (Figure 4.25C), that responded remarkably similar (Figure 4.25D). Following the same approach as described above to identify the pathways that are rescued by *EGLN2* knock-out (Figure 4.25E-F), we found that *SOD1^{A4V}* astrocytes still expressed lower levels of interferon-stimulated genes after treatment with TIC which could again be rescued by loss of EGLN2 (Figure 4.25G). Finally, we also compared the differences in expression levels of interferon stimulated genes between *SOD1^{A4V}* and *SOD1^{A4A}* astrocytes to publicly available ALS patient-derived astrocyte RNA-seq data sets[255,263,285,398,399], however did not find a clear overlap between the expression patterns (Table S4.4).

In conclusion, we showed that, *SOD1^{A4V}*ALS patient-derived astrocytes present an altered interferon-dependent inflammatory response and that this response could be rescued by the deletion of *EGLN2*, supporting the novel link between EGLN2 and the astrocytic interferon response.

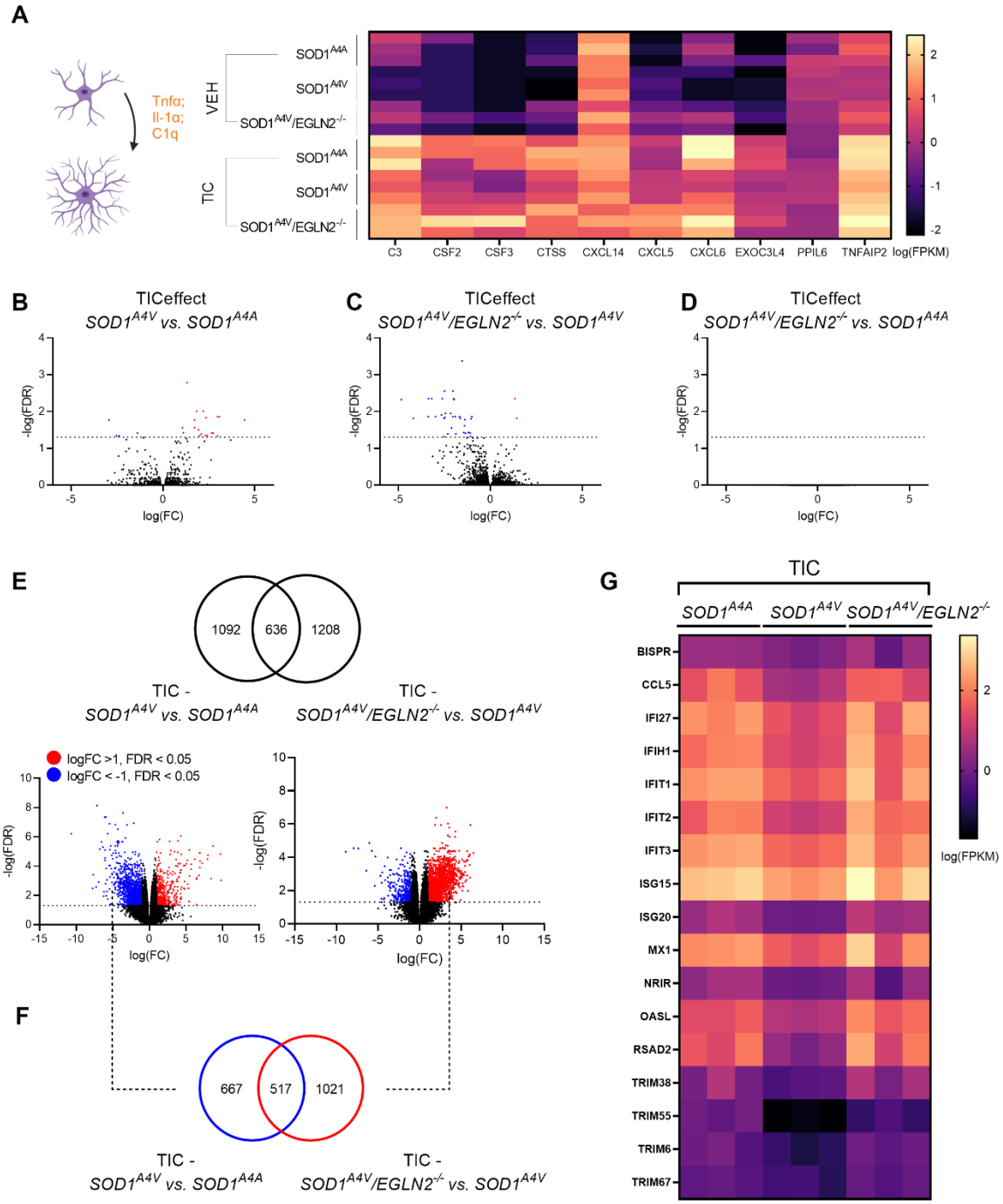

A
Tnfα;
Il-1α;
C1q
VEH
TIC
SOD1A4A
SOD1A4V
SOD1A4V/EGLN2-/-
C3
CSF2
CSF3
CTSS
CXCL14
CXCL5
CXCL6
EXOC3L4
PPIL6
TNFAIP2
log(FPKM)
B
TICeffect
SOD1A4V vs. SOD1A4A
C
TICeffect
SOD1A4V/EGLN2-/- vs. SOD1A4V
D
TICeffect
SOD1A4V/EGLN2-/- vs. SOD1A4A
-log(FDR)
log(FC)
E
1092
636
1208
TIC -
SOD1A4V vs. SOD1A4A
TIC -
SOD1A4V/EGLN2-/- vs. SOD1A4V
logFC >1, FDR < 0.05
logFC < -1, FDR < 0.05
F
667
517
1021
TIC -
SOD1A4V vs. SOD1A4A
TIC -
SOD1A4V/EGLN2-/- vs. SOD1A4V
G
TIC
SOD1A4A
SOD1A4V
SOD1A4V/EGLN2-/-
BISPR
CCL5
IFI27
IFIH1
IFIT1
IFIT2
IFIT3
ISG15
ISG20
MX1
NRIR
OASL
RSAD2
TRIM38
TRIM55
TRIM6
TRIM67
log(FPKM)

Figure 4.25. *EGLN2* deletion restores the levels of interferon-stimulated genes in reactive *SOD1^{A4V}* patient-derived astrocytes. A, Heatmap showing the expression levels (fragments per kilobase million, [FPKM]) of reactive astrocyte marker genes in *SOD1^{A4A}*, *SOD1^{A4V}* and *SOD1^{A4V}/EGLN2$^{-/-}$* astrocytes treated with vehicle (VEH) or TNFα, IL-1α and C1q (TIC). **B-D**, Volcano plot showing all genes that respond differently to the TIC treatment in **B**, *SOD1^{A4V} versus SOD1^{A4A}* astrocytes, **C**, *SOD1^{A4V}/EGLN2$^{-/-}$ versus SOD1^{A4V}* astrocytes and **D**, *SOD1^{A4V}/EGLN2$^{-/-}$ versus SOD1^{A4A}* astrocytes. Red indicates upregulated genes (Log10 (fold change) (log(FC)) > 1), blue indicates downregulated genes (log(FC) < -1). **E**, Venn diagram showing the overlap between all significant DEGs in *SOD1^{A4V} versus SOD1^{A4A}* TIC-treated astrocytes (left Volcano plot) and all significant DEGs in *SOD1^{A4V}/EGLN2$^{-/-}$ versus SOD1^{A4V}* TIC-treated astrocytes (right Volcano plot). **F**, Venn diagram showing the overlap between the significantly downregulated genes in *SOD1^{A4V} versus SOD1^{A4A}* TIC-treated astrocytes (Log(FC) < -1) and significantly upregulated genes in *SOD1^{A4V}/EGLN2$^{-/-}$ versus SOD1^{A4V}* TIC-treated astrocytes (Log(FC) > 1). **G**, Heatmap showing the expression levels (FPKM) of interferon-stimulated genes in *SOD1^{A4A}*, *SOD1^{A4V}* and *SOD1^{A4V}/EGLN2$^{-/-}$* TIC-treated astrocytes. N = 3 astrocyte differentiations.

4.4.6 Deletion of *Egln2* in SOD1^{A4V} astrocytes does not affect motor neurite outgrowth via CAM treatment

Finally, to investigate the effect of the normalized interferon response in astrocytes, mediated by *EGLN2* deletion, on motor neuron health, we studied the effect on motor neurite outgrowth. We observed an increase in neurite outgrowth in mutant SOD1^{A4V} motor neurons compared to their isogenic control (Figure 4.25A), in line with the increased axonal regrowth which has been reported before[400]. This neurite outgrowth phenotype was not rescued by deletion of *EGLN2* (Figure 4.26A). Moreover, when we treated SOD1^{A4V} motor neurons with from CAM *SOD1^{A4V}/EGLN2$^{-/-}$* astrocytes this also did not affect motor neurite outgrowth nor did treatment with *SOD1^{A4A}* CAM (Figure 4.26B), while it was reported before that the addition of healthy astrocytes to ALS motor neurons offers protection[255].

4.4.7 Concluding remarks

To conclude we observed an increased anaerobic and aerobic glucose metabolism in SOD1^{A4V} ALS patient-derived astrocytes, that was not the result of increased mitochondrial abundance nor related to a disturbed mitochondrial integrity as assessed with TMRM. In addition, at the transcriptomic level, the STING-induced interferon response was decreased in mutant *versus* isogenic astrocytes. This aberrant interferon response was normalized by knocking-out *EGLN2*, confirming its effect on the interferon response which was found to be present in SOD1^{G93A} mice when *Egln2* was deleted and which was linked to a motor neuron protective effect. However, treatment with SOD1^{A4V}/EGLN2$^{-/-}$ astrocytes CAM did not rescue the increased neurite length in SOD1^{A4V} motor neurons. In line, the metabolic phenotype observed in SOD1^{A4V} astrocytes did not affect the motor neuron metabolism when treated with CAM. This suggests the importance of the reciprocal interaction between motor

neurons and astrocytes, or could mean, especially for the metabolic phenotype, that a loss of secreted metabolites induces the in literature described motor neuron toxicity. Nevertheless, we showed that EGLN2, which protected motor neurons in three different *in vivo* models for ALS, rescued this dysregulated response in SOD1^{A4V} astrocytes.

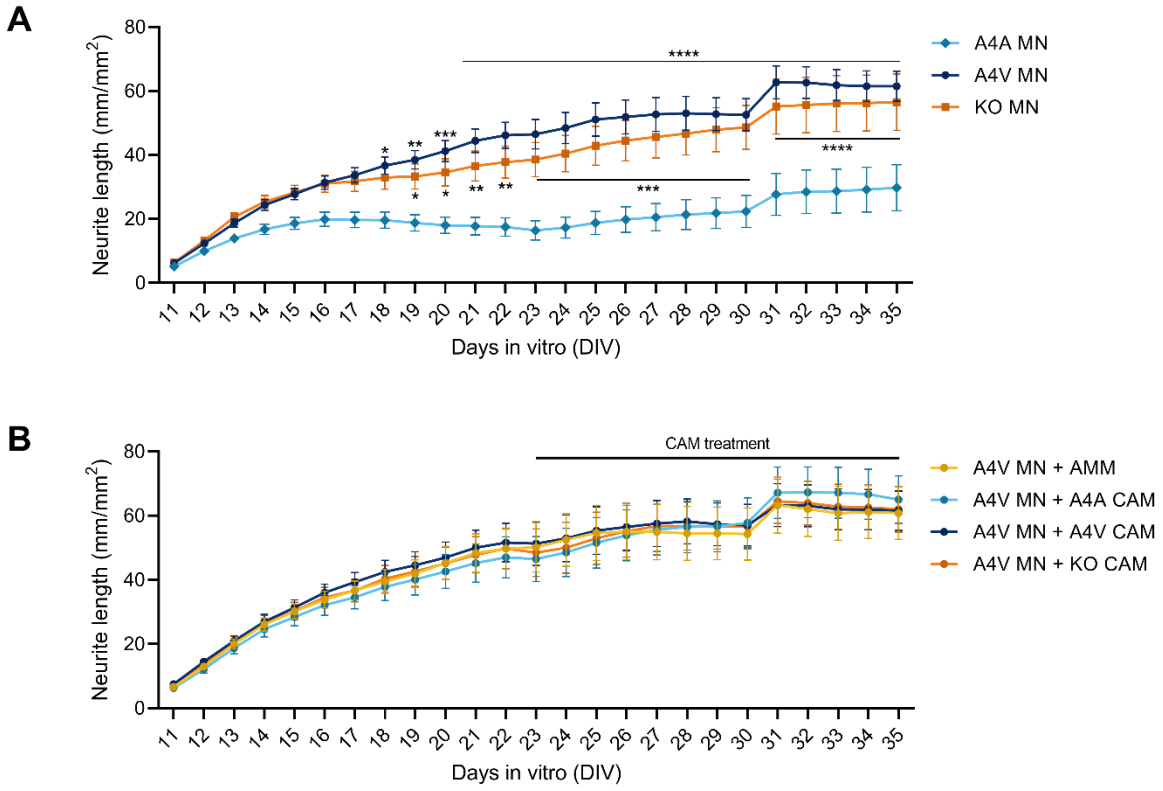


Figure 4.26. SOD1^{A4V} CAM does not affect SOD1^{A4A} motor neurite outgrowth. A, Length of neurites from SOD1^{A4A}, SOD1^{A4V} and SOD1^{A4V}/EGLN2$^{-/-}$ motor neurons measured over 25 days of their differentiation and maturation. **B,** Length of neurites from SOD1^{A4V} motor neurons treated with 50% mature astrocyte medium (AMM), or conditioned astrocyte medium (CAM) from SOD1^{A4A}, SOD1^{A4V} and SOD1^{A4V}/EGLN2$^{-/-}$ astrocytes from 23 till 35 days in vitro (DIV) measured over 25 days of their differentiation and maturation. Data represent mean ± SEM from three independent experiments. Statistical analyses were performed by Two-way ANOVA with Tukey's multiple comparison (*p< 0.05, **p<0.01, ***p<0.001, ****p<0.0001).

CHAPTER 5 GENERAL CONCLUSION AND DISCUSSION

Parts of this chapter appeared in:

Germeys, C.*, Vandoorne, T.*, Davie, K., Poovathingal, S., Heeren, K., Vermeire, W., Nami, F., Moisse, M., Quaegebeur, A., Sierksma, A., et al. (2024). Targeting EGLN2/PHD1 protects motor neurons and normalizes the astrocytic interferon response. Cell Rep *43*, 114719. 10.1016/j.celrep.2024.114719

*These authors contributed equally

CHAPTER 5 GENERAL CONCLUSION AND DISCUSSION

ALS is a neurodegenerative disorder characterized by progressive loss of upper and lower motor neurons that relentlessly leads to paralysis and death of the patient. Despite the poor prognosis, ALS remains an incurable disorder. In the last decade, significant advances have been made regarding the models to study the disease and our knowledge about the disease pathology and the involvement of cell-specific pathways beyond the motor neurons. The goal of this thesis was to use these newly gained models and knowledge together with state-of-the-art techniques to study EGLN2 as potential therapeutic target for ALS.

5.1 EGLN2 downregulation offers motor neuron protection in multiple *in vivo* ALS models

While EGLN2 is not commonly linked with ALS, neither mechanistically nor genetically, it formed a promising target as it plays a role in multiple pathways that are involved in ALS, is ubiquitously expressed and induces cell- and context specific effects via a range of potential targets. Therefore, we aimed to study the effect of EGLN2 inhibition in ALS using a multi-model approach to provide evidence across different species and ALS mutations.

To explore the effect of targeting EGLN2 in ALS, we used two different zebrafish models. Zebrafish offer a valuable tool for the search for ALS modifiers because they are fast and present a motor neuron phenotype that is robust and reproducible. By using an AMO that splices out the catalytic domain of *egln2*, we found that Egln2 inhibition rescued the motor axonopathy induced by mutant SOD1 and *C9ORF72* RNA toxicity.

Furthermore, we found, that genetic deletion of *Egln2* in $SOD1^{G93A}$ mice protected their motor neurons, increasing the total motor neuron count, neuromuscular junction innervation and survival. This increase in survival was the result of a delay in disease progression and not onset, which was unaffected by loss of EGLN2 as determined by weight and rotarod performance. As further investigation suggested a role of the astrocytes in the observed beneficial effect this strengthens the findings that targeting astrocytes in ALS affects their disease progression and not their onset[66]. While deletion of *Egln2* mitigated the ALS phenotype in $SOD1^{G93A}$ mice, it had no effect on the phenotype in $FUS^{+/+}$ mice. $FUS^{+/+}$ mice present a severe form of ALS with premature death around 90 days postnatal. To note, while metabolic alterations are already present at P30 in these mice[401], astrogliosis and microgliosis are only present at the end stage[72], in contrast with the early signs of neuroinflammation in $SOD1^{G93A}$ mice. Further investigation of the role and effect of EGLN2 downregulation in FUS-ALS, using different models, is needed to draw any conclusions.

Nevertheless, as EGLN2 downregulation was beneficial cross-species, in two SOD1-ALS models and a C9ORF72-ALS model, we hypothesized that it acts via a common mechanism in ALS

5.2 SnRNA-seq as tool to investigate ALS targets

To identify this mechanism, we used snRNA-seq as EGLN2 is known to act on multiple cell-specific pathways that could explain its beneficial effect. ALS is characterized by motor neuron death and patient-derived motor neurons recapitulate several disease phenotypes[87]. On the other hand, also non-cell-autonomous mechanisms contribute to ALS pathology[304,402,403]. Single-cell technology provides the opportunity to study the contribution of both motor neuron intrinsic and extrinsic pathways to the disease.

As a result, several studies used this technology to investigate the transcriptional changes that mark the disease at a single-cell level[404-407]. In $SOD1^{G93A}$ mice, snRNA-seq of the spinal cord identified that motor neurons and astrocytes underwent the most pronounced transcriptional changes at P90 including changes linked to an increased ROS production in motor neurons and to an increased inflammatory response in astrocytes[405]. Moreover, also in *postmortem* motor and frontal cortices of C9ORF72 ALS patients, excitatory neurons and astrocytes showed the largest transcriptomic alterations[407].

While single-cell RNA-seq is valuable to unravel the cell-specific transcriptomic signature of the disease, it can also be used to investigate potential therapeutic strategies to identify their underlying transcriptomic alterations at single-cell resolution. Indeed, non-cell-autonomous mechanisms have been shown numerous times to modify early and late ALS progression. Therefore, we applied snRNA-seq to investigate the cell-specific pathways that underlie EGLN2-mediated motor neuron protection in ALS. This revealed that loss of EGLN2 induced transcriptomic changes in neuronal and non-neuronal cells related to a range of pathways including cellular energy metabolism and neuroinflammation. While snRNA-seq is valuable to explore the cell-specific transcriptomic changes underlying an ALS mitigating strategy, we should note that further investigation of these snRNA-seq findings is crucial due to several reasons. First, changes at the RNA level do not necessarily translate into changes at the protein level. Second, no causal conclusions can be drawn based on these results as the observed transcriptomic changes could be a consequence or just a mere side effect of the genetic deletion. Third, snRNA-seq requires disruption of the tissue which results in a loss of spatial and cellular interaction information. While the different cell types are seen as separate identities with their own transcriptomic profiles in snRNA-seq, the observed transcriptomic changes could be the effect of EGLN2-induced changes in other cell types. Finally, motor neurons only make up a minor percentage of all cells in the

spinal cord, especially in an ALS model with motor neuron degeneration. The total number of extracted motor neuron nuclei and as a result the statistical power is therefore considerably low. Nevertheless, taking its limitations into account, snRNA-seq remains a powerful tool and a great starting point to explore the mechanism-of-action of any potential therapeutic ALS target, including EGLN2, providing unbiased and cell-specific information.

5.3 EGLN2 and metabolic dysfunction in ALS at single-cell resolution

Metabolic dysfunction has been extensively linked to ALS with mitochondrial dysfunction, impaired lipid and carbohydrate metabolism[154,408]. Studies measuring the carbohydrate metabolism in ALS are often based on FDG-PET and whole brain analyses. However, we must not underestimate the glial contribution to the brain's glucose consumption, especially because of their glycolytic profile. Therefore, they could very well be the source of the disturbed glucose metabolism observed in whole brain analyses. This is supported by the finding in our lab that FUS-ALS motor neuron monocultures did not show metabolic alteration[138]. In this thesis, we found that both anaerobic and aerobic glucose metabolism are upregulated in astrocytes. Especially the latter is remarkable as astrocytes mainly depend on glycolysis to generate ATP after which the generated lactate can be shuttled to motor neurons to be further metabolized in the aerobic TCA cycle. Studies have reported that the lactate shuttle is dysfunctional in ALS leading to a loss of metabolic support of the motor neurons[288]. Our study further explains how increased glucose oxidation could contribute to the dysfunctional lactate shuttle. Following this hypothesis, motor neurons would be affected by this astrocytic phenotype due to a loss of secreted lactate which would explain why we did not observe an effect of the CAM treatment on the motor neurons as in this experimental set-up physiological lactate levels were present in the medium. In addition to the lack of effect of CAM, we also found no significant differences in the metabolic glucose, fatty acid, glutamate and lactate fluxes between $SOD1^{A4A}$ and $SOD1^{A4V}$ motor neurons. This contrasts with findings by Kiskinis *et al.* who reported alterations in mitochondrial gene expression, morphology (as assessed by electron microscopy) and motility (measured using live cell imaging with MitoTracker-Green) between $SOD1^{A4A}$ and $SOD1^{A4V}$ motor neurons[123]. However, these contrasting results may be explained by differences in differentiation and culture protocols, with the most significant factor being the co-culture of motor neurons with glial cells in the aforementioned study.

The canonical target of EGLN2 is HIFα affecting a range of pathways including rewired cellular metabolism[321]. As a result, *Egln2* deletion did decrease the expression of genes linked to oxidative metabolism in neurons. However, the observed decreased expression of oxidative metabolism genes was suggested to be independent of HIF activation as we did not observe any changes in the expression

of HIF target genes in mice or zebrafish. A number of HIF- and hydroxylation-independent EGLN2 targets have been described and can give rise to a large variety of cell- and context-specific effects of EGLN2[317]. This was demonstrated by the HIF-independent protection of cortical neurons in stroke models[324]. In addition, we did not observe a downregulation of nuclear genes involved in the energy metabolism of motor neurons. This finding suggests that *Egln2*$^{-/-}$ induced motor neuron protection is not driven through metabolic rewiring.

5.4 EGLN2 and interferon signaling in ALS at single-cell resolution

SnRNA-seq revealed that loss of EGLN2 in SOD1^{G93A} spinal cord induced an astrocyte-specific downregulation of pro-inflammatory interferon-stimulated genes. We considered this to be of particular interest because interferon-stimulated genes have been found to be upregulated in SOD1^{G93A} mice spinal cord astrocytes[96] and in neuronal and myeloid cells from ALS patients and models[95,97-100]. Moreover, this increased interferon response was shown to be induced via cytoplasmic dsDNA-mediated cGAS/STING activation[97-100]. Our study provides insight on how astrocytes contribute to the increased cGAS/STING induced interferon signaling in ALS[95-100,392], underlining the contribution of non-cell autonomous mechanisms[304,402,403] and demonstrate that targeting EGLN2 can restore this response. Moreover, the effect of loss of EGLN2 on the levels of interferon-stimulated genes in astrocytes was strengthened by the finding that knocking-out *EGLN2* in patient iPSC-derived astrocytes normalized the levels of interferon-stimulated genes compared to *SOD1*^{A4V} astrocytes. In these *SOD1*^{A4V} patient-derived astrocytes, we observed a downregulation of interferon-stimulated genes and found that loss of EGLN2 increased these levels, contrary to our findings in SOD1^{G93A} mouse astrocytes. The difference in the levels of interferon-stimulated genes could be explained, by the cell type, the stage of the disease, the involvement of other cell types or the difference in the mutation. Astrocytes have been reported numerous times to play a unique role in ALS and neurodegeneration[409]. The reactive astrogliosis that occurs during neurodegeneration is not one fixed state but rather a dynamic process of multiple cellular states that can evolve over the disease course[247]. In agreement, RNA-seq analysis of SOD1^{G93A} *versus* WT astrocyte monocultures from P5 mice did not show differences in the transcriptomic interferon response[260], while this was described to be present in astrocytes from P60 SOD1^{G93A} mice and onwards[96]. P110 in SOD1^{G93A} mice, most likely, models a later disease stage compared to the patient iPSC-derived astrocytes. As a result, different disease states and the presence of different stimuli due to the presence or absence of other cell types[410], can explain the differences in interferon response. While we did mimic neuroinflammation *in vitro* by treatment with pro-inflammatory TIC cocktail that provokes astrocyte reactivity[261], this still differs from the prolonged presence of a pro-inflammatory environment in the spinal cord of SOD1^{G93A} mice. Finally, we must also consider that different (*SOD1*) mutations, while all resulting in ALS, could give rise to pathological

differences[411]. Nevertheless, independent from the increased interferon response in SOD1^{G93A} mice, as reported by Wang *et al*.[96], or decreased interferon response in *SOD1^{A4V}* patient astrocytes that we observed, deletion of *EGLN2* was able to normalize these levels.

The ability of EGLN2 as target to provoke different disease-stage dependent effects, could be attributed to its sensor function, enabling the enzyme to perceive the cellular state, via the presence of oxygen, Fe^{2+}, ascorbic acid or other metabolic intermediates[314-316]. The EGLN enzymes have been shown to act on the activator of the NFκB pathway and inducer of the inflammatory response, IKKβ[331,412-414]. GSEA on both *SOD1^{G93A}/Egln2$^{-/-}$* mouse astrocytes and *SOD1^{A4V}/EGLN2$^{-/-}$* iPSC-derived astrocytes showed an enrichment of the NFκB pathway in the upregulated gene set, even when the interferon response was downregulated in *SOD1^{G93A}/Egln2$^{-/-}$* astrocytes. However, the effect of loss of EGLN2 on the cGAS/STING pathway was in line with the downstream effect on the interferon response, namely enriched in the downregulated genes in *SOD1^{G93A}/Egln2$^{-/-}$* mouse astrocytes and enriched in the upregulated genes in *SOD1^{A4V}/EGLN2$^{-/-}$* human astrocytes. As a result, it seems likely that EGLN2 acts on the cGAS/STING pathway. In agreement, we observed a downregulation of STING protein expression in GFAP positive cells in the spinal cord of *SOD1^{G93A}/Egln2$^{-/-}$* mice. Together, this revealed that EGLN2 can directly or indirectly, for example via a decrease in ROS induced mitochondrial DNA release[100,322], modulate cGAS/STING pathway activity. As a result, our findings propose EGLN2 as a target that normalizes the cGAS/STING induced interferon-driven neuroinflammatory response that characterizes the motor neuron degeneration in ALS. This is supported by our observation that the neuroinflammation marker *Tspo*[389] was downregulated in *SOD1^{G93A}/Egln2$^{-/-}$* motor neurons.

5.5 Limitations of the study

This study indicates that targeting EGLN2 might have therapeutic potential in different forms of ALS. However, the therapeutic potential should be further confirmed using additional approaches such as ASO knockdown *in vivo*. Moreover, an ALS mouse model with an astrocyte-specific *Egln2* knock-out would provide insight to which extend the motor neuron protection *in vivo* is driven by astrocytes. However, this would require the combination of three transgenic lines (homozygous floxed *Egln2*, astrocyte specific Cre expression and *SOD1^{G93A}* overexpression) with as extra complication that female *SOD1^{G93A}* mice are sterile, that the birth rate of transgenic mice is approximately half of what can be expected and that the use of littermate controls is crucial given that a reduction of *hSOD1^{G93A}* copy-number also affects survival[78]. Therefore, we used iPSC-derived astrocytes to confirm the direct effect of *EGLN2* deletion on astrocyte monocultures, with the additional advantage that these cells are human and patient derived. While these experiments, using one patient-isogenic control iPSC pair, confirmed that EGLN2 acts on the STING-induced interferon response in patient astrocytes, the

confirmation of these findings in other familial and sporadic cell lines and other cell types such as motor neurons would be a valuable addition to this study.

5.6 Future directions and therapeutic implications

This thesis highlights EGLN2 as potential target for ALS that normalizes the STING-induced interferon response in astrocytes. Future work should focus on both the mechanistic and therapeutic aspect to further unravel the true therapeutic potential of EGLN2.

In this thesis we found evidence for a link between EGLN2, that mitigates ALS in multiple models when inhibited, and the astrocytic cGAS/STING pathway. However, cracking the complete mechanistic code is challenging as one answer is often followed by numerous new questions. At the end of this thesis the outstanding questions are '*Is the effect of EGLN2 on the astrocytic STING-induced interferon response directly responsible for the ALS mitigation*?' and '*How does loss of EGLN2 act on the cGAS/STING pathway?*'. To answer the first question, cGAS/STING pathway inhibitors and activators should be used to study if these could enhance the beneficial effects of EGLN2 inhibition in the *in vitro* and *in vivo* models. Moreover, to investigate if the effect is completely driven by astrocytes, $SOD1^{G93A}$ mice with an astrocyte-specific *Egln2* knock-out could be generated. However, as explained above this would be rather difficult and time- and money-consuming. An alternative approach would be to use the $SOD1^{A4V}/EGLN2^{-/-}$ iPSCs with the additional advantage that they are patient-derived. Astrocytes derived from these iPSCs could be co-cultured with patient-derived motor neurons in microfluidic devices with myotubes to determine their effect on neuromuscular junctions, which has been shown be affected by mutant FUS astrocytes[255]. For the second question, different approaches could be taken. EGLN2 interacts with their targets through hydroxylation or binding. To identify potential new targets that are responsible for the effect on the cGAS/STING pathway, we could use proteomics as an unbiased approach. Mass spectrometry-based proteomics could be performed on $EGLN2^{-/-}$ versus $EGLN2^{+/+}$ astrocytes to identify targets that are hydroxylated by EGLN2 in astrocytes. To identify astrocytic binding targets a pull-down could be followed by WB for a targeted or proteomics for an un-targeted approach. Finally, loss of EGLN2 could also act on the cGAS/STING activity via its role in the oxidative stress response. Increased levels of oxidative stress lead to DNA damage and activation of the cGAS/STING pathway. To investigate this possibility, metabolic flux experiments and ROS detection should be performed on $EGLN2^{-/-}$ astrocytes.

In the future, we should focus on the therapeutic implications of our findings. EGLN2 is a promising ALS target that mitigated ALS cross-species *in vivo* and in patient-derived cells and acts on a pathway that is known to be involved in fALS and sALS. Pan-EGLN inhibitors are available and are being used in clinic for anemia in chronic kidney disease[415]. However, EGLN1 and 3 have been shown to be

detrimental *in vivo*[322] and concerns are being raised about the side-effects of these drug[416]. As a result, EGLN2 has a more favorable safety profile for a chronic disorder such as ALS that likely requires long-term treatment. As a result, it is of interest to design and test ASOs against murine *Egln2* and human *EGLN2*. Murine ASOs should be tested in SOD1^{G93A} mice to investigate if they are able to sufficiently downregulate *Egln2 in vivo* and if they are able to reproduce the beneficial effects observed by deleting *Egln2*. Human ASOs should be used to verify if these are able to downregulate *EGLN2* in patient iPSC-derived cells and if this downregulation rescues the interferon response in astrocytes. However, we should note that in both the mice and patient-derived astrocytes, *EGLN2* was completely knocked-out and that only homozygous but not heterozygous deletion was beneficial in mice. While ASOs are becoming increasingly better due to optimized chemical modifications, they are not able to fully knock-out its target. However, Quaegebeur *et al.* did reveal that ASOs against murine *Egln2*, reaching 87% downregulation *in vitro*, were able to mimic the protective effect of *Egln2* deletion in an *in vivo* and *in vitro* model for stroke. As a result, testing ASOs against EGLN2 could be therapeutically valuable. Moreover, by gaining more knowledge about the mechanism of action, downstream targets of EGLN2 could also form interesting therapeutic targets.

Something else to consider, based on our findings, is the idea of astrocyte-targeted therapies. Besides the strategies that target astrocyte-mediated pathological mechanisms such as astrocyte reactivity or excitotoxicity, cell-based therapies for astrocyte replacement have been suggested[409]. However here the issue arose that even healthy astrocytes could become neurotoxic again due to the disease environment. Another promising therapeutic opportunity, stemming from the cancer field, is provided by antibody-conjugated drugs that could provide astrocyte-specific delivery of EGLN2 inhibitors. However, before considering such an approach further research on the involvement of the different cell types in the beneficial effects of EGLN2 is necessary. Especially because and increased STING-induced interferon response has been shown to present in motor neurons from ALS models and patients as well[95], raising the question if EGLN2 could also rescue this pathway in motor neurons.

Finally, we should discuss the use of SOD1^{G93A} mice for translational research. While justified critique has been provided on the model, and especially its failure into providing therapeutic strategies that resulted in therapies for patients, we believe that we should redefine how to use them as a model rather than discarding them completely. Especially because they remain one of the few *in vivo* models that closely resemble the disease as it occurs in patients. Nevertheless, we should not ignore the significant differences between this mouse model and ALS patients that have probably led to a failure of the translation of promising therapeutic strategies found in SOD1^{G93A} mice to patients. Therefore, it is crucial to not only find targets that mitigate the ALS phenotype in these mice but to also understand their mechanism of action using different models and approaches. A perfect example of how this

approach can be successful is the story of Tofersen. Extensive research has established that mutant *SOD1* induces motor neuron degeneration via gain-of-toxic events. Following this knowledge about its mechanism-of-action, SOD1 ASOs that reduce the SOD1 protein levels were created. These ASOs reduced the levels of SOD1 protein and increased the survival of $SOD1^{G93A}$ mice[417] and subsequently translated well into clinic, resulting into the FDA- and EMA-approval of the SOD1 ASO Tofersen earlier this year. We therefore strongly believe in the importance of understanding the pathological mechanisms and the mechanisms underlying therapeutic strategies for ALS, such as EGLN2 inhibition, before moving towards clinical trials.

With this in mind, this thesis, showing that inhibition of EGLN2 mitigates ALS in three *in vivo* models, including the $SOD1^{G93A}$ mouse model, and that targeting EGLN2 normalizes a pathway that is dysregulated in fALS and sALS patients, forms a strong base for further translational research.

5.7 General conclusion

In this thesis, we identified EGLN2 as motor neuron protective target using several *in vivo* ALS models, snRNA-seq and patient-derived iPSCs. We showed that targeting *egln2* using an AMO in both SOD1- and C9ORF72-ALS zebrafish, protected the motor neurons leading to a rescue of the ALS RNA induced motor axonopathy. Moreover, also in a more complex model of ALS, the $SOD1^{G93A}$ mouse model, genetic deletion of *Egln2* mitigated the ALS phenotype by protecting motor neurons and prolonging survival. SnRNA-seq revealed that loss of EGLN2 induced an astrocytic downregulation of interferon-stimulated genes in the spinal cord of these mice which was suggested to be the result of a decreased cGAS/STING pathway activity. In agreement, we observed a reduced expression of STING in GFAP positive cells. Moreover, the link between *EGLN2* downregulation and the astrocytic interferon response was confirmed in patient-derived astrocytes. Hence, our study highlights the potential of EGLN2 as ALS target mitigating motor neuron degeneration and normalizing the astrocytic pro-inflammatory interferon response *in vivo* and in patient-derived astrocytes (Figure 5.1).

5.8 Graphical abstract

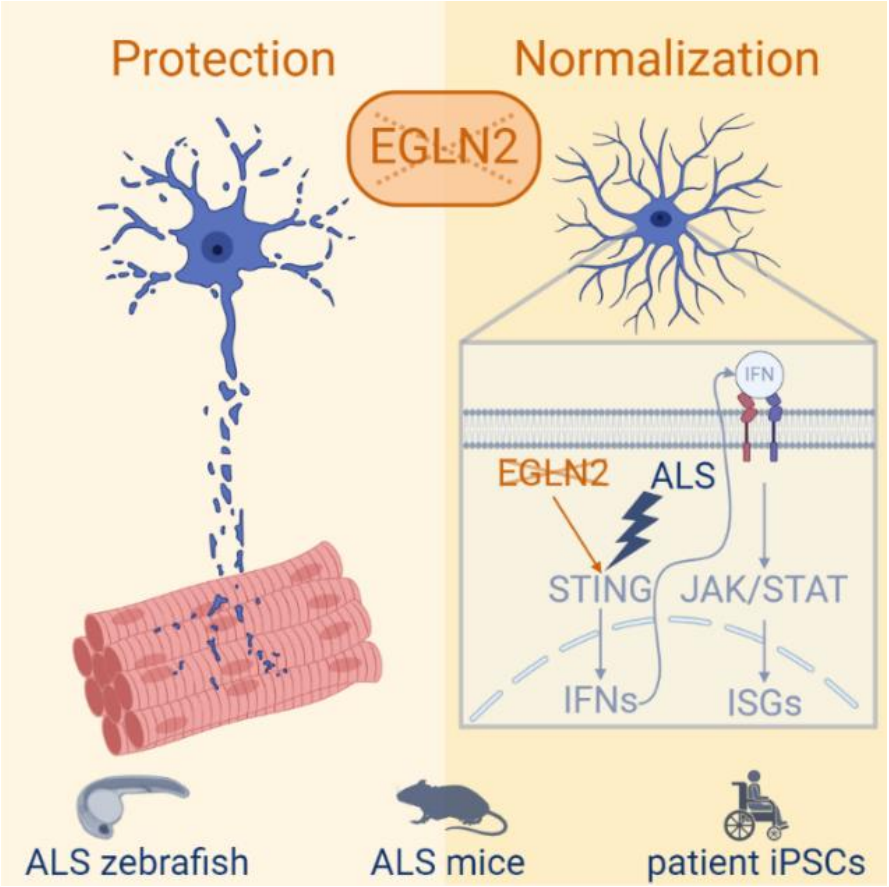


Figure 5.1. Targeting EGLN2/PHD1 protects motor neurons and normalizes the astrocytic interferon response. The egl-9 family hypoxia-inducible factor (EGLN) enzymes, also known as prolyl hydroxylase domain (PHD) enzymes, are metabolic sensors regulating cellular inflammation and metabolism. Using an oligonucleotide-based and a genetic approach, we showed that downregulation of *Egln2* protected motor neurons and mitigated the ALS phenotype in two zebrafish models and a mouse model of ALS. Single-nuclei RNA sequencing of murine spinal cord revealed that loss of EGLN2 induced an astrocyte-specific downregulation of interferon (IFN)-stimulated genes (ISGs), mediated via activation of the stimulator of interferon genes (STING) protein leading to IFN transcription and janus kinase/signal transducer and activator of transcription (JAK/STAT) activation. In addition, we found that genetic deletion of *EGLN2* restored this interferon response in patient iPSC-derived astrocytes, confirming the link between EGLN2 and astrocytic interferon signaling. In conclusion, we identified EGLN2 as a motor neuron protective target normalizing the astrocytic interferon-dependent inflammatory axis *in vivo* as well as in patient-derived cells.

Summary

Amyotrophic lateral sclerosis (ALS) is a neurodegenerative disorder characterized by progressive loss of upper and lower motor neurons in the motor cortex, the brainstem and the spinal cord. Motor neuron loss results in muscle wasting and paralysis leading to the death of the patient due to failure of the respiratory muscles, typically within three to five years after diagnosis. Nevertheless, no cure is available for ALS and this while the cumulative lifetime risk to get ALS is 1 in 400. In the last decades significant advances were made regarding the models to perform fundamental and translational research, the knowledge about the pathology and the role of both motor neuron-autonomous and non-cell-autonomous mechanisms and the available research technologies. In this thesis we aimed to apply these advances to study the role and therapeutic potential of egl-9 family hypoxia-inducible factor 2 (EGLN2) enzyme. EGLN2, also known as prolyl hydroxylase domain 1 (PHD1) enzyme, is a unique target that plays a central role in cellular energy metabolism, oxidative stress response and inflammation which are three of the main hallmarks of ALS. Given the urgent need for new therapeutic strategies for ALS, we used different ALS models, patient-derived cells and single-cell technology to study if and how inhibition of EGLN2 could be beneficial in ALS.

First, we explored the effect of targeting EGLN2 in two zebrafish model for ALS. Zebrafish expressing two of the most common genetic defects in ALS, namely a mutation in human superoxide dismutase ($SOD1^{G93A}$) and human chromosome 9 open reading frame 72 (*C9ORF72)* hexanucleotide repeat RNA, display motor axon abnormalities with a decreased axonal length and increased abnormal branching. This motor axonopathy was almost completely rescued when *egln2* was downregulated using an antisense oligonucleotide morpholino (AMO). Hence, these data indicated that targeting Egln2 mitigates the ALS phenotype in zebrafish by acting on one or more mechanism that are involved in the motor neuron toxicity mediated by mutant SOD1 and *C9ORF72* RNA toxicity.

Second, we aimed to confirm this beneficial effect by genetically targeting *Egln2* in two mouse models that closely resemble the ALS phenotype as seen in patients. Mice overexpressing human mutant SOD1 ($SOD1^{G93A}$) and human wildtype fused in sarcoma ($FUS^{+/+}$) both present an ALS phenotype with motor neuron degeneration, paralysis and premature death. Deletion of *Egln2* mitigated the ALS phenotype in $SOD1^{G93A}$ mice, increasing the total motor neuron count, neuromuscular junction innervation and survival. However, deletion of *Egln2* did not have the same motor neuron protective effect in $FUS^{+/+}$ mice. This difference might be explained by the model or the mechanism, as these SOD1- and FUS-mice show differences in the presence and timing of pathological hallmarks of ALS.

Third, to identify the cell-specific pathways that underly the beneficial effect of *Egln2* deletion in SOD1^{G93A} mice, we performed single-nuclei RNA sequencing (snRNA-seq) on the spinal cord of early symptomatic SOD1^{G93A} mice with and without *Egln2*. This revealed that loss of EGLN2 induced transcriptomic changes in neuronal and non-neuronal cells. Notably, deletion of *Egln2* downregulated the expression of translocator protein (*Tspo*) which is a proposed biomarker for neuroinflammation of ALS. In agreement, we found that the pro-inflammatory interferon response was specifically downregulated in astrocytes. This decreased interferon response was suggested to be the result of reduced stimulator of interferon genes (STING) activity, as its protein level was reduced in *SOD1^{G93A}/Egln2$^{-/-}$* spinal cord astrocytes. Together, this single-cell approach revealed that the motor neuron protective effect of EGLN2 ablation was linked to a decrease of the astrocytic interferon-dependent inflammatory axis.

Finally, we aimed to investigate the direct effect of loss of EGLN2 on patient-derived astrocyte. For this, we used induced pluripotent stem cells (iPSCs) from an ALS patient carrying a SOD1^{A4V} mutation. As till recently, SOD1^{A4V} iPSC-derived astrocytes were not characterized, we started by investigating the effect of this SOD1 mutation on astrocyte homeostasis. Metabolic and transcriptomic analysis of these astrocytes revealed that they showed an increased glucose metabolism and a decreased interferon response. Especially the latter was of interest given the previously established link between the STING-induced astrocytic interferon response and EGLN2 in ALS mice. To investigate if targeting EGLN2 could rescue this aberrant response, we generated SOD1^{A4V} iPSCs with an *EGLN2* knock-out using CRISPR-cas9. Deletion of *EGLN2* in SOD1^{A4V} astrocytes restored the levels of interferon-stimulated genes back to isogenic control levels. As a result, these findings suggest that the astrocytic interferon response is subject to disease stage and environmental stimuli while strengthening the novel link between EGLN2 and the astrocytic interferon response.

In conclusion, this thesis demonstrated how targeting EGLN2 mitigates motor neuron degeneration in three different *in vivo* ALS models. Moreover, a link between EGLN2 and the astrocytic STING-induced interferon response was established, using cell-specific tools such as snRNA-seq and patient-derived astrocytes. As a result, our data highlight EGLN2 as target that protects motor neurons and restores the interferon signaling pathway in astrocytes.

Samenvatting

Amyotrofische laterale sclerose (ALS) is een neurodegeneratieve aandoening die wordt gekenmerkt door progressief verlies van de bovenste en onderste motor neuronen in de motor cortex, de hersenstam en het ruggenmerg. Verlies van motor neuronen resulteert in spierverlies en verlamming, waardoor patiënten sterven aan de gevolgen van het falen van de ademhalingsspieren, gemiddeld drie tot vijf jaar na diagnose. Desalniettemin is er geen geneesmiddel beschikbaar voor deze verschrikkelijke ziekte en dit terwijl het levenslange cumulatieve risico om ALS te krijgen 1 op 400 bedraagt. De laatste decennia zijn er aanzienlijke vorderingen gemaakt met betrekking tot de modellen om fundamenteel en translationeel onderzoek uit te voeren, de kennis over de pathologie en de rol van zowel autonome als niet-cel-autonome mechanismen en de beschikbare onderzoeksmethoden. In deze thesis, wilden we deze nieuwe methoden en kennis toepassen om de rol en het therapeutisch potentieel van het egl-9 family hypoxia-inducible factor 2 (EGLN2) enzym te bestuderen. EGLN2, ook gekend als het prolyl hydroxylase domain 1 (PHD1) enzym, is een uniek doelwit dat een centrale rol speelt in het cellulaire energie metabolisme, de cellulaire reactie op oxidatieve stress en de cellulaire ontstekingsrespons, drie van de belangrijkste kenmerken van ALS. Gezien de dringende nood aan nieuwe therapeutische strategieën voor ALS, hebben we verschillende ALS-modellen, patiënt-afgeleide cellen en single-cell technologie gebruikt om te onderzoeken of en hoe de remming van EGLN2 gunstig zou kunnen zijn voor ALS.

Allereerst onderzochten we het effect van EGLN2 inhibitie in twee zebravismodellen voor ALS. Zebravissen die twee van de meest voorkomende genetische defecten bij ALS tot expressie brengen, namelijk een mutatie in menselijk superoxide-dismutase ($SOD1^{G93A}$) en menselijk chromosoom 9 open reading frame 72 (*C9ORF72*) hexanucleotide repeat RNA, vertonen afwijkingen in hun motor axonen waaronder een verlaagde axonale lengte en verhoogde abnormale vertakking. Deze motor axonopathie werd bijna volledig hersteld toen *egln2* werd gedownreguleerd met behulp van een antisense oligonucleotide morfolino (AMO). Deze bevindingen wezen erop dat Egln2 inhibitie het ALS-fenotype bij de zebravis verminderd door in te werken op één of meer mechanismen die betrokken zijn bij de motor neuron toxiciteit geïnduceerd door mutant SOD1- en *C9ORF72*-RNA-toxiciteit.

Ten tweede wilden we dit gunstige effect bevestigen door *Egln2* genetisch te verminderen in twee muismodellen die een ALS-fenotype vertonen dat sterk lijkt op de ziekte bij patiënten. Muizen die het menselijke mutant SOD1 ($SOD1^{G93A}$) en het menselijke wildtype fused in sarcoma ($FUS^{+/+}$) tot overexpressie brengen, vertonen beide een ALS-fenotype met degeneratie van motor neuronen, verlamming en vroegtijdige dood. Deletie van *Egln2* verbeterde het ALS-fenotype in $SOD1^{G93A}$ muizen,

met een toename van het totale aantal motor neuronen, de innervatie van de neuromusculaire juncties en de overleving. Deletie van *Egln2* had echter niet hetzelfde beschermende effect op de motor neuronen bij $FUS^{+/+}$ muizen. Dit verschil zou verklaard kunnen worden door het model of het mechanisme, aangezien deze SOD1- en FUS-muizen verschillen vertonen in de aanwezigheid en timing van pathologische kenmerken van ALS.

Ten derde, hebben we single-nuclei RNA-sequencing (snRNA-seq) uitgevoerd op het ruggenmerg van vroeg symptomatische $SOD1^{G93A}$ muizen met en zonder *Egln2*, om de cel specifieke pathways te identificeren die verantwoordelijk zijn voor het gunstige effect van *Egln2* deletie bij $SOD1^{G93A}$ muizen. Hieruit bleek dat verlies van EGLN2, veranderingen induceerde in het transcriptoom van neuronale en niet-neuronale cellen. Opvallend is dat de verwijdering van *Egln2* de expressie van translocator protein (*Tspo*) verlaagde, wat voorgesteld is als biomarker voor neuro-inflammatie bij ALS patiënten. In overeenstemming, vonden we ook dat de deletie van *Egln2* een downregulatie van de pro-inflammatoire interferon response in astrocyten induceerde. Deze verminderde interferon respons kon het gevolg zijn van een verminderde activiteit van de stimulator van interferon genes (STING), wat blijkt uit het verlaagde eiwitniveau van STING in astrocyten in het ruggenmerg van $SOD1^{G93A}/Egln2^{-/-}$ muizen. Samen onthulde deze single-cell benadering dat het beschermende effect van EGLN2-ablatie op motor neuronen gelinkt werd met een afname van de interferon-afhankelijke ontstekingsmechanismen in astrocyten.

Ten slotte wilden we het directe effect van verlies van EGLN2 op patiënt-afgeleide astrocyten onderzoeken. Hiervoor gebruikten we geïnduceerde pluripotente stamcellen (iPSCs) van een ALS-patiënt die een $SOD1^{A4V}$ mutatie droeg. Omdat tot voor kort $SOD1^{A4V}$ iPSC-afgeleide astrocyten nog niet werden gekarakteriseerd, zijn we begonnen met het onderzoeken van het effect van deze SOD1-mutatie op de homeostase van de astrocyten. Metabolische en transcriptomische analyse van deze astrocyten onthulde dat ze een verhoogd glucosemetabolisme en een verminderde interferon respons vertoonden. Vooral dit laatste was interessant gezien het eerder vastgestelde verband tussen de STING-geïnduceerde interferon respons in astrocyten en EGLN2 bij ALS-muizen. Om te onderzoeken of EGLN2 ablatie deze afwijkende reactie zou kunnen herstellen, hebben we $SOD1^{A4V}$ iPSC's met een *EGLN2* knock-out gegenereerd met behulp van CRISPR-cas9. Deletie van *EGLN2* in $SOD1^{A4V}$ astrocyten herstelde de niveaus van interferon gestimuleerde genen terug naar de niveaus in de isogene controle. Als gevolg hiervan suggereren deze bevindingen dat de interferon respons in astrocyten onderhevig is aan het ziektestadium en omgevingsstimuli, terwijl de nieuwe link tussen EGLN2 en de interferon respons in astrocyten werd versterkt.

Ter conclusie, laat deze thesis zien hoe remming van EGLN2 de degeneratie van motor neuronen vermindert in drie verschillende *in vivo* ALS-modellen. Bovendien werd een verband gelegd tussen EGLN2 en de STING-geïnduceerde interferon respons in astrocyten, met behulp van cel-specifieke tools zoals snRNA-seq en van patiënt-afgeleide astrocyten. Als gevolg hiervan benadrukt deze thesis het potentieel van EGLN2 als doelwit om motor neuronen te beschermen en de interferon pathway in astrocyten te herstellen.

Scientific acknowledgments

We gratefully thank the VIB Nucleomics Core for the library preparation and sequencing of the snRNA-seq and bulk RNA-seq experiment and statistical data analysis of the bulk RNA-seq experiment (https://nucleomicscore.sites.vib.be/en) and Dr. Antina de Boer for her help with the RNAScope experiment. This work was supported by VIB, the KU Leuven (C1 (C14/17/107; C14/22/132) and "Opening the Future" Fund), the "Fund for Scientific Research Flanders" (FWO), ALS Liga Belgium ("A Cure for ALS") and the Agency for Innovation by Science and Technology (150031). C.G. is supported by a fundamental PhD research grant awarded by the FWO (1174523N). T.V. has been supported by a strategic basic PhD research grant awarded by the FWO (1S60116N). P.C. is supported by long-term structural Methusalem funding by the Flemish government. P.V.D. holds a clinical investigatorship of the FWO and is supported by the E. von Behring Chair for Neuromuscular and Neurodegenerative Disorders, the Fund 'Een Hart voor ALS' and the 'Laevers Fund for ALS Research'. K.D.B. is endowed by the Wilhelm Schulthess Foundation. L.V.D.B. is supported by the Generet Award for Rare Diseases. Figures were created with BioRender.com.

Personal contributions

Christine Germeys designed, performed and analyzed most experiments and wrote this dissertation. Tijs Vandoorne, Annelies Quaegebeur and Caroline Eykens provided preliminary data. Kara Heeren performed zebrafish experiments, with support from Lenja De Cock. Peter Carmeliet provided *Egln2*$^{-/-}$ mice. Begga Schevenels and Nicole Hersmus helped with colony management of mice. Suresh Poovathingal and Annerieke Sierksma provided help with nuclei extraction and Suresh Poovathingal performed 10X microfluidics. Kristofer Davie, Rekin's Janky and Matthieu Moisse performed bioinformatic analyses of the (sn)RNA-seq data. Laura Rué helped with the RNAScope experiment. Wendy Vermeire and Adria Sicart provided technical support for the iPSC experiments. Katarina Stoklund Dittlau helped with the iPSC-derived astrocyte experiments. Silke Vanderhaeghe performed the TMRM experiment. Philip Van Damme and Katrien De Bock discussed data and gave conceptual advice. Ludo Van Den Bosch and Tijs Vandoorne conceived the study, supervised the experiments, discussed the results and edited the manuscript.

Conflicts of interest

Philip Van Damme has participated as investigator to clinical trials on ALS sponsored by Biogen, Cytokinetics, Ferrer, Amylyx, Wave Life Sciences (Cambridge, UK), Corcept therapeutics (Menlo Park, US), Transposon therapeutics (Westport, US), Sanofi (Paris, France), AB Science (Paris, France), IONIS Pharmaceuticals (Carlsbad, US), Apellis Pharmaceuticals (Waltham, US), Alexion Pharmaceuticals, Orphazyme (Copenhagen, Denmark), Orion Pharma (Espoo, Finland), AL-S Pharma (Schlieren, Switzerland). Philip Van Damme is supported by the E. von Behring Chair for Neuromuscular and Neurodegenerative Disorders (from CSL Behring, paid to institution). Tijs Vandoorne is an employee of Bristol-Myers Squibb (Princeton, US). Ludo Van Den Bosch is head of the Scientific Advisory Board of Augustine Therapeutics and is part of the Investment Advisory Board of Droia Ventures (Meise, Belgium).

References

1. Leigh, P.N., and Ray-Chaudhuri, K. (1994). Motor neuron disease. J Neurol Neurosurg Psychiatry *57*, 886-896. 10.1136/jnnp.57.8.886.
2. Brown, R.H., and Al-Chalabi, A. (2017). Amyotrophic Lateral Sclerosis. N Engl J Med *377*, 162-172. 10.1056/NEJMra1603471.
3. Johnston, C.A., Stanton, B.R., Turner, M.R., Gray, R., Blunt, A.H., Butt, D., Ampong, M.A., Shaw, C.E., Leigh, P.N., and Al-Chalabi, A. (2006). Amyotrophic lateral sclerosis in an urban setting: a population based study of inner city London. J Neurol *253*, 1642-1643. 10.1007/s00415-006-0195-y.
4. Alonso, A., Logroscino, G., Jick, S.S., and Hernán, M.A. (2009). Incidence and lifetime risk of motor neuron disease in the United Kingdom: a population-based study. Eur J Neurol *16*, 745-751. 10.1111/j.1468-1331.2009.02586.x.
5. Arthur, K.C., Calvo, A., Price, T.R., Geiger, J.T., Chiò, A., and Traynor, B.J. (2016). Projected increase in amyotrophic lateral sclerosis from 2015 to 2040. Nat Commun *7*, 12408. 10.1038/ncomms12408.
6. Swinnen, B., and Robberecht, W. (2014). The phenotypic variability of amyotrophic lateral sclerosis. Nat Rev Neurol *10*, 661-670. 10.1038/nrneurol.2014.184.
7. Chiò, A., Calvo, A., Moglia, C., Mazzini, L., Mora, G., and group, P.s. (2011). Phenotypic heterogeneity of amyotrophic lateral sclerosis: a population based study. J Neurol Neurosurg Psychiatry *82*, 740-746. 10.1136/jnnp.2010.235952.
8. Van Langenhove, T., van der Zee, J., and Van Broeckhoven, C. (2012). The molecular basis of the frontotemporal lobar degeneration-amyotrophic lateral sclerosis spectrum. Ann Med *44*, 817-828. 10.3109/07853890.2012.665471.
9. Bang, J., Spina, S., and Miller, B.L. (2015). Frontotemporal dementia. Lancet *386*, 1672-1682. 10.1016/S0140-6736(15)00461-4.
10. Ringholz, G.M., Appel, S.H., Bradshaw, M., Cooke, N.A., Mosnik, D.M., and Schulz, P.E. (2005). Prevalence and patterns of cognitive impairment in sporadic ALS. Neurology *65*, 586-590. 10.1212/01.wnl.0000172911.39167.b6.
11. Lomen-Hoerth, C., Murphy, J., Langmore, S., Kramer, J.H., Olney, R.K., and Miller, B. (2003). Are amyotrophic lateral sclerosis patients cognitively normal? Neurology *60*, 1094-1097. 10.1212/01.wnl.0000055861.95202.8d.
12. Masrori, P., and Van Damme, P. (2020). Amyotrophic lateral sclerosis: a clinical review. Eur J Neurol *27*, 1918-1929. 10.1111/ene.14393.
13. Taylor, J.P., Brown, R.H., and Cleveland, D.W. (2016). Decoding ALS: from genes to mechanism. Nature *539*, 197-206. 10.1038/nature20413.
14. Goutman, S.A., Hardiman, O., Al-Chalabi, A., Chió, A., Savelieff, M.G., Kiernan, M.C., and Feldman, E.L. (2022). Emerging insights into the complex genetics and pathophysiology of amyotrophic lateral sclerosis. Lancet Neurol *21*, 465-479. 10.1016/S1474-4422(21)00414-2.
15. Garcia-Santibanez, R., Burford, M., and Bucelli, R.C. (2018). Hereditary Motor Neuropathies and Amyotrophic Lateral Sclerosis: a Molecular and Clinical Update. Curr Neurol Neurosci Rep *18*, 93. 10.1007/s11910-018-0901-z.
16. Al-Chalabi, A., Calvo, A., Chio, A., Colville, S., Ellis, C.M., Hardiman, O., Heverin, M., Howard, R.S., Huisman, M.H.B., Keren, N., et al. (2014). Analysis of amyotrophic lateral sclerosis as a multistep process: a population-based modelling study. Lancet Neurol *13*, 1108-1113. 10.1016/S1474-4422(14)70219-4.
17. Chiò, A., Mazzini, L., D'Alfonso, S., Corrado, L., Canosa, A., Moglia, C., Manera, U., Bersano, E., Brunetti, M., Barberis, M., et al. (2018). The multistep hypothesis of ALS revisited: The role of genetic mutations. Neurology *91*, e635-e642. 10.1212/WNL.0000000000005996.
18. Rosen, D.R. (1993). Mutations in Cu/Zn superoxide dismutase gene are associated with familial amyotrophic lateral sclerosis. Nature *364*, 362. 10.1038/364362c0.

19. Bunton-Stasyshyn, R.K., Saccon, R.A., Fratta, P., and Fisher, E.M. (2015). SOD1 Function and Its Implications for Amyotrophic Lateral Sclerosis Pathology: New and Renascent Themes. Neuroscientist *21*, 519-529. 10.1177/1073858414561795.
20. Cleveland, D.W., Laing, N., Hurse, P.V., and Brown, R.H. (1995). Toxic mutants in Charcot's sclerosis. Nature *378*, 342-343. 10.1038/378342a0.
21. Bruijn, L.I., Becher, M.W., Lee, M.K., Anderson, K.L., Jenkins, N.A., Copeland, N.G., Sisodia, S.S., Rothstein, J.D., Borchelt, D.R., Price, D.L., and Cleveland, D.W. (1997). ALS-linked SOD1 mutant G85R mediates damage to astrocytes and promotes rapidly progressive disease with SOD1-containing inclusions. Neuron *18*, 327-338. 10.1016/s0896-6273(00)80272-x.
22. Zou, Z.Y., Zhou, Z.R., Che, C.H., Liu, C.Y., He, R.L., and Huang, H.P. (2017). Genetic epidemiology of amyotrophic lateral sclerosis: a systematic review and meta-analysis. J Neurol Neurosurg Psychiatry *88*, 540-549. 10.1136/jnnp-2016-315018.
23. Jiang, L.L., Xue, W., Hong, J.Y., Zhang, J.T., Li, M.J., Yu, S.N., He, J.H., and Hu, H.Y. (2017). The N-terminal dimerization is required for TDP-43 splicing activity. Sci Rep *7*, 6196. 10.1038/s41598-017-06263-3.
24. Suk, T.R., and Rousseaux, M.W.C. (2020). The role of TDP-43 mislocalization in amyotrophic lateral sclerosis. Mol Neurodegener *15*, 45. 10.1186/s13024-020-00397-1.
25. Neumann, M., Sampathu, D.M., Kwong, L.K., Truax, A.C., Micsenyi, M.C., Chou, T.T., Bruce, J., Schuck, T., Grossman, M., Clark, C.M., et al. (2006). Ubiquitinated TDP-43 in frontotemporal lobar degeneration and amyotrophic lateral sclerosis. Science *314*, 130-133. 10.1126/science.1134108.
26. de Boer, E.M.J., Orie, V.K., Williams, T., Baker, M.R., De Oliveira, H.M., Polvikoski, T., Silsby, M., Menon, P., van den Bos, M., Halliday, G.M., et al. (2020). TDP-43 proteinopathies: a new wave of neurodegenerative diseases. J Neurol Neurosurg Psychiatry *92*, 86-95. 10.1136/jnnp-2020-322983.
27. Kwiatkowski, T.J., Bosco, D.A., Leclerc, A.L., Tamrazian, E., Vanderburg, C.R., Russ, C., Davis, A., Gilchrist, J., Kasarskis, E.J., Munsat, T., et al. (2009). Mutations in the FUS/TLS gene on chromosome 16 cause familial amyotrophic lateral sclerosis. Science *323*, 1205-1208. 10.1126/science.1166066.
28. Vance, C., Rogelj, B., Hortobágyi, T., De Vos, K.J., Nishimura, A.L., Sreedharan, J., Hu, X., Smith, B., Ruddy, D., Wright, P., et al. (2009). Mutations in FUS, an RNA processing protein, cause familial amyotrophic lateral sclerosis type 6. Science *323*, 1208-1211. 10.1126/science.1165942.
29. Renton, A.E., Majounie, E., Waite, A., Simón-Sánchez, J., Rollinson, S., Gibbs, J.R., Schymick, J.C., Laaksovirta, H., van Swieten, J.C., Myllykangas, L., et al. (2011). A hexanucleotide repeat expansion in C9ORF72 is the cause of chromosome 9p21-linked ALS-FTD. Neuron *72*, 257-268. 10.1016/j.neuron.2011.09.010.
30. DeJesus-Hernandez, M., Mackenzie, I.R., Boeve, B.F., Boxer, A.L., Baker, M., Rutherford, N.J., Nicholson, A.M., Finch, N.A., Flynn, H., Adamson, J., et al. (2011). Expanded GGGGCC hexanucleotide repeat in noncoding region of C9ORF72 causes chromosome 9p-linked FTD and ALS. Neuron *72*, 245-256. 10.1016/j.neuron.2011.09.011.
31. van Blitterswijk, M., DeJesus-Hernandez, M., Niemantsverdriet, E., Murray, M.E., Heckman, M.G., Diehl, N.N., Brown, P.H., Baker, M.C., Finch, N.A., Bauer, P.O., et al. (2013). Association between repeat sizes and clinical and pathological characteristics in carriers of C9ORF72 repeat expansions (Xpansize-72): a cross-sectional cohort study. Lancet Neurol *12*, 978-988. 10.1016/S1474-4422(13)70210-2.
32. Braems, E., Bercier, V., Van Schoor, E., Heeren, K., Beckers, J., Fumagalli, L., Dedeene, L., Moisse, M., Geudens, I., Hersmus, N., et al. (2022). HNRNPK alleviates RNA toxicity by counteracting DNA damage in C9orf72 ALS. Acta Neuropathol *144*, 465-488. 10.1007/s00401-022-02471-y.
33. Morita, M., Al-Chalabi, A., Andersen, P.M., Hosler, B., Sapp, P., Englund, E., Mitchell, J.E., Habgood, J.J., de Belleroche, J., Xi, J., et al. (2006). A locus on chromosome 9p confers

susceptibility to ALS and frontotemporal dementia. Neurology *66*, 839-844. 10.1212/01.wnl.0000200048.53766.b4.

34. Turner, M.R., Al-Chalabi, A., Chio, A., Hardiman, O., Kiernan, M.C., Rohrer, J.D., Rowe, J., Seeley, W., and Talbot, K. (2017). Genetic screening in sporadic ALS and FTD. J Neurol Neurosurg Psychiatry *88*, 1042-1044. 10.1136/jnnp-2017-315995.
35. Williams, K.L., Topp, S., Yang, S., Smith, B., Fifita, J.A., Warraich, S.T., Zhang, K.Y., Farrawell, N., Vance, C., Hu, X., et al. (2016). CCNF mutations in amyotrophic lateral sclerosis and frontotemporal dementia. Nat Commun *7*, 11253. 10.1038/ncomms11253.
36. Kenna, K.P., van Doormaal, P.T., Dekker, A.M., Ticozzi, N., Kenna, B.J., Diekstra, F.P., van Rheenen, W., van Eijk, K.R., Jones, A.R., Keagle, P., et al. (2016). NEK1 variants confer susceptibility to amyotrophic lateral sclerosis. Nat Genet *48*, 1037-1042. 10.1038/ng.3626.
37. Brenner, D., Müller, K., Wieland, T., Weydt, P., Böhm, S., Lulé, D., Hübers, A., Neuwirth, C., Weber, M., Borck, G., et al. (2016). NEK1 mutations in familial amyotrophic lateral sclerosis. Brain *139*, e28. 10.1093/brain/aww033.
38. Johnson, J.O., Mandrioli, J., Benatar, M., Abramzon, Y., Van Deerlin, V.M., Trojanowski, J.Q., Gibbs, J.R., Brunetti, M., Gronka, S., Wuu, J., et al. (2010). Exome sequencing reveals VCP mutations as a cause of familial ALS. Neuron *68*, 857-864. 10.1016/j.neuron.2010.11.036.
39. Fecto, F., Yan, J., Vemula, S.P., Liu, E., Yang, Y., Chen, W., Zheng, J.G., Shi, Y., Siddique, N., Arrat, H., et al. (2011). SQSTM1 mutations in familial and sporadic amyotrophic lateral sclerosis. Arch Neurol *68*, 1440-1446. 10.1001/archneurol.2011.250.
40. Morgan, S., Shatunov, A., Sproviero, W., Jones, A.R., Shoai, M., Hughes, D., Al Khleifat, A., Malaspina, A., Morrison, K.E., Shaw, P.J., et al. (2017). A comprehensive analysis of rare genetic variation in amyotrophic lateral sclerosis in the UK. Brain *140*, 1611-1618. 10.1093/brain/awx082.
41. Freischmidt, A., Wieland, T., Richter, B., Ruf, W., Schaeffer, V., Müller, K., Marroquin, N., Nordin, F., Hübers, A., Weydt, P., et al. (2015). Haploinsufficiency of TBK1 causes familial ALS and fronto-temporal dementia. Nat Neurosci *18*, 631-636. 10.1038/nn.4000.
42. Diekstra, F.P., van Vught, P.W., van Rheenen, W., Koppers, M., Pasterkamp, R.J., van Es, M.A., Schelhaas, H.J., de Visser, M., Robberecht, W., Van Damme, P., et al. (2012). UNC13A is a modifier of survival in amyotrophic lateral sclerosis. Neurobiol Aging *33*, 630.e633-638. 10.1016/j.neurobiolaging.2011.10.029.
43. Sproviero, W., Shatunov, A., Stahl, D., Shoai, M., van Rheenen, W., Jones, A.R., Al-Sarraj, S., Andersen, P.M., Bonini, N.M., Conforti, F.L., et al. (2017). ATXN2 trinucleotide repeat length correlates with risk of ALS. Neurobiol Aging *51*, 178.e171-178.e179. 10.1016/j.neurobiolaging.2016.11.010.
44. Lattante, S., Pomponi, M.G., Conte, A., Marangi, G., Bisogni, G., Patanella, A.K., Meleo, E., Lunetta, C., Riva, N., Mosca, L., et al. (2018). ATXN1 intermediate-length polyglutamine expansions are associated with amyotrophic lateral sclerosis. Neurobiol Aging *64*, 157.e151-157.e155. 10.1016/j.neurobiolaging.2017.11.011.
45. Roggenbuck, J., Quick, A., and Kolb, S.J. (2017). Genetic testing and genetic counseling for amyotrophic lateral sclerosis: an update for clinicians. Genet Med *19*, 267-274. 10.1038/gim.2016.107.
46. Goutman, S.A., Savelieff, M.G., Jang, D.G., Hur, J., and Feldman, E.L. (2023). The amyotrophic lateral sclerosis exposome: recent advances and future directions. Nat Rev Neurol *19*, 617-634. 10.1038/s41582-023-00867-2.
47. Molliex, A., Temirov, J., Lee, J., Coughlin, M., Kanagaraj, A.P., Kim, H.J., Mittag, T., and Taylor, J.P. (2015). Phase separation by low complexity domains promotes stress granule assembly and drives pathological fibrillization. Cell *163*, 123-133. 10.1016/j.cell.2015.09.015.
48. Wen, X., Tan, W., Westergard, T., Krishnamurthy, K., Markandaiah, S.S., Shi, Y., Lin, S., Shneider, N.A., Monaghan, J., Pandey, U.B., et al. (2014). Antisense proline-arginine RAN dipeptides linked to C9ORF72-ALS/FTD form toxic nuclear aggregates that initiate in vitro and in vivo neuronal death. Neuron *84*, 1213-1225. 10.1016/j.neuron.2014.12.010.

49. Nagai, M., Re, D.B., Nagata, T., Chalazonitis, A., Jessell, T.M., Wichterle, H., and Przedborski, S. (2007). Astrocytes expressing ALS-linked mutated SOD1 release factors selectively toxic to motor neurons. Nat Neurosci *10*, 615-622. 10.1038/nn1876.
50. Braems, E., Tziortzouda, P., and Van Den Bosch, L. (2021). Exploring the alternative: Fish, flies and worms as preclinical models for ALS. Neurosci Lett *759*, 136041. 10.1016/j.neulet.2021.136041.
51. Murakami, T., Qamar, S., Lin, J.Q., Schierle, G.S., Rees, E., Miyashita, A., Costa, A.R., Dodd, R.B., Chan, F.T., Michel, C.H., et al. (2015). ALS/FTD Mutation-Induced Phase Transition of FUS Liquid Droplets and Reversible Hydrogels into Irreversible Hydrogels Impairs RNP Granule Function. Neuron *88*, 678-690. 10.1016/j.neuron.2015.10.030.
52. Watson, M.R., Lagow, R.D., Xu, K., Zhang, B., and Bonini, N.M. (2008). A drosophila model for amyotrophic lateral sclerosis reveals motor neuron damage by human SOD1. J Biol Chem *283*, 24972-24981. 10.1074/jbc.M804817200.
53. Estes, P.S., Boehringer, A., Zwick, R., Tang, J.E., Grigsby, B., and Zarnescu, D.C. (2011). Wild-type and A315T mutant TDP-43 exert differential neurotoxicity in a Drosophila model of ALS. Hum Mol Genet *20*, 2308-2321. 10.1093/hmg/ddr124.
54. Baldwin, K.R., Godena, V.K., Hewitt, V.L., and Whitworth, A.J. (2016). Axonal transport defects are a common phenotype in Drosophila models of ALS. Hum Mol Genet *25*, 2378-2392. 10.1093/hmg/ddw105.
55. Solomon, D.A., Stepto, A., Au, W.H., Adachi, Y., Diaper, D.C., Hall, R., Rekhi, A., Boudi, A., Tziortzouda, P., Lee, Y.B., et al. (2018). A feedback loop between dipeptide-repeat protein, TDP-43 and karyopherin-α mediates C9orf72-related neurodegeneration. Brain *141*, 2908-2924. 10.1093/brain/awy241.
56. Mizielinska, S., Grönke, S., Niccoli, T., Ridler, C.E., Clayton, E.L., Devoy, A., Moens, T., Norona, F.E., Woollacott, I.O.C., Pietrzyk, J., et al. (2014). C9orf72 repeat expansions cause neurodegeneration in Drosophila through arginine-rich proteins. Science *345*, 1192-1194. 10.1126/science.1256800.
57. Li, M., Zhao, L., Page-McCaw, P.S., and Chen, W. (2016). Zebrafish Genome Engineering Using the CRISPR-Cas9 System. Trends Genet *32*, 815-827. 10.1016/j.tig.2016.10.005.
58. Sakowski, S.A., Lunn, J.S., Busta, A.S., Oh, S.S., Zamora-Berridi, G., Palmer, M., Rosenberg, A.A., Philip, S.G., Dowling, J.J., and Feldman, E.L. (2012). Neuromuscular effects of G93A-SOD1 expression in zebrafish. Mol Neurodegener *7*, 44. 10.1186/1750-1326-7-44.
59. Hewamadduma, C.A., Grierson, A.J., Ma, T.P., Pan, L., Moens, C.B., Ingham, P.W., Ramesh, T., and Shaw, P.J. (2013). Tardbpl splicing rescues motor neuron and axonal development in a mutant tardbp zebrafish. Hum Mol Genet *22*, 2376-2386. 10.1093/hmg/ddt082.
60. Armstrong, G.A., and Drapeau, P. (2013). Loss and gain of FUS function impair neuromuscular synaptic transmission in a genetic model of ALS. Hum Mol Genet *22*, 4282-4292. 10.1093/hmg/ddt278.
61. Ciura, S., Lattante, S., Le Ber, I., Latouche, M., Tostivint, H., Brice, A., and Kabashi, E. (2013). Loss of function of C9orf72 causes motor deficits in a zebrafish model of amyotrophic lateral sclerosis. Ann Neurol *74*, 180-187. 10.1002/ana.23946.
62. Lee, Y.B., Chen, H.J., Peres, J.N., Gomez-Deza, J., Attig, J., Stalekar, M., Troakes, C., Nishimura, A.L., Scotter, E.L., Vance, C., et al. (2013). Hexanucleotide repeats in ALS/FTD form length-dependent RNA foci, sequester RNA binding proteins, and are neurotoxic. Cell Rep *5*, 1178-1186. 10.1016/j.celrep.2013.10.049.
63. Gurney, M.E., Pu, H., Chiu, A.Y., Dal Canto, M.C., Polchow, C.Y., Alexander, D.D., Caliendo, J., Hentati, A., Kwon, Y.W., and Deng, H.X. (1994). Motor neuron degeneration in mice that express a human Cu,Zn superoxide dismutase mutation. Science *264*, 1772-1775. 10.1126/science.8209258.
64. Philips, T., and Rothstein, J.D. (2015). Rodent Models of Amyotrophic Lateral Sclerosis. Curr Protoc Pharmacol *69*, 5.67.61-65.67.21. 10.1002/0471141755.ph0567s69.

65. Boillée, S., Yamanaka, K., Lobsiger, C.S., Copeland, N.G., Jenkins, N.A., Kassiotis, G., Kollias, G., and Cleveland, D.W. (2006). Onset and progression in inherited ALS determined by motor neurons and microglia. Science *312*, 1389-1392. 10.1126/science.1123511.
66. Yamanaka, K., Chun, S.J., Boillee, S., Fujimori-Tonou, N., Yamashita, H., Gutmann, D.H., Takahashi, R., Misawa, H., and Cleveland, D.W. (2008). Astrocytes as determinants of disease progression in inherited amyotrophic lateral sclerosis. Nat Neurosci *11*, 251-253. 10.1038/nn2047.
67. Kang, S.H., Li, Y., Fukaya, M., Lorenzini, I., Cleveland, D.W., Ostrow, L.W., Rothstein, J.D., and Bergles, D.E. (2013). Degeneration and impaired regeneration of gray matter oligodendrocytes in amyotrophic lateral sclerosis. Nat Neurosci *16*, 571-579. 10.1038/nn.3357.
68. Bruijn, L.I., Beal, M.F., Becher, M.W., Schulz, J.B., Wong, P.C., Price, D.L., and Cleveland, D.W. (1997). Elevated free nitrotyrosine levels, but not protein-bound nitrotyrosine or hydroxyl radicals, throughout amyotrophic lateral sclerosis (ALS)-like disease implicate tyrosine nitration as an aberrant in vivo property of one familial ALS-linked superoxide dismutase 1 mutant. Proc Natl Acad Sci U S A *94*, 7606-7611. 10.1073/pnas.94.14.7606.
69. Wong, P.C., Pardo, C.A., Borchelt, D.R., Lee, M.K., Copeland, N.G., Jenkins, N.A., Sisodia, S.S., Cleveland, D.W., and Price, D.L. (1995). An adverse property of a familial ALS-linked SOD1 mutation causes motor neuron disease characterized by vacuolar degeneration of mitochondria. Neuron *14*, 1105-1116. 10.1016/0896-6273(95)90259-7.
70. Ripps, M.E., Huntley, G.W., Hof, P.R., Morrison, J.H., and Gordon, J.W. (1995). Transgenic mice expressing an altered murine superoxide dismutase gene provide an animal model of amyotrophic lateral sclerosis. Proc Natl Acad Sci U S A *92*, 689-693. 10.1073/pnas.92.3.689.
71. Bonifacino, T., Zerbo, R.A., Balbi, M., Torazza, C., Frumento, G., Fedele, E., Bonanno, G., and Milanese, M. (2021). Nearly 30 Years of Animal Models to Study Amyotrophic Lateral Sclerosis: A Historical Overview and Future Perspectives. Int J Mol Sci *22*. 10.3390/ijms222212236.
72. Mitchell, J.C., McGoldrick, P., Vance, C., Hortobagyi, T., Sreedharan, J., Rogelj, B., Tudor, E.L., Smith, B.N., Klasen, C., Miller, C.C., et al. (2013). Overexpression of human wild-type FUS causes progressive motor neuron degeneration in an age- and dose-dependent fashion. Acta Neuropathol *125*, 273-288. 10.1007/s00401-012-1043-z.
73. Wu, L.S., Cheng, W.C., and Shen, C.K. (2012). Targeted depletion of TDP-43 expression in the spinal cord motor neurons leads to the development of amyotrophic lateral sclerosis-like phenotypes in mice. J Biol Chem *287*, 27335-27344. 10.1074/jbc.M112.359000.
74. Kino, Y., Washizu, C., Kurosawa, M., Yamada, M., Miyazaki, H., Akagi, T., Hashikawa, T., Doi, H., Takumi, T., Hicks, G.G., et al. (2015). FUS/TLS deficiency causes behavioral and pathological abnormalities distinct from amyotrophic lateral sclerosis. Acta Neuropathol Commun *3*, 24. 10.1186/s40478-015-0202-6.
75. Hicks, G.G., Singh, N., Nashabi, A., Mai, S., Bozek, G., Klewes, L., Arapovic, D., White, E.K., Koury, M.J., Oltz, E.M., et al. (2000). Fus deficiency in mice results in defective B-lymphocyte development and activation, high levels of chromosomal instability and perinatal death. Nat Genet *24*, 175-179. 10.1038/72842.
76. Hao, Z., Liu, L., Tao, Z., Wang, R., Ren, H., Sun, H., Lin, Z., Zhang, Z., Mu, C., Zhou, J., and Wang, G. (2019). Motor dysfunction and neurodegeneration in a C9orf72 mouse line expressing poly-PR. Nat Commun *10*, 2906. 10.1038/s41467-019-10956-w.
77. Choi, S.Y., Lopez-Gonzalez, R., Krishnan, G., Phillips, H.L., Li, A.N., Seeley, W.W., Yao, W.D., Almeida, S., and Gao, F.B. (2019). C9ORF72-ALS/FTD-associated poly(GR) binds Atp5a1 and compromises mitochondrial function in vivo. Nat Neurosci *22*, 851-862. 10.1038/s41593-019-0397-0.
78. Alexander, G.M., Erwin, K.L., Byers, N., Deitch, J.S., Augelli, B.J., Blankenhorn, E.P., and Heiman-Patterson, T.D. (2004). Effect of transgene copy number on survival in the G93A SOD1 transgenic mouse model of ALS. Brain Res Mol Brain Res *130*, 7-15. 10.1016/j.molbrainres.2004.07.002.

79. Benatar, M. (2007). Lost in translation: treatment trials in the SOD1 mouse and in human ALS. Neurobiol Dis *26*, 1-13. 10.1016/j.nbd.2006.12.015.
80. Fisher, E.M.C., Greensmith, L., Malaspina, A., Fratta, P., Hanna, M.G., Schiavo, G., Isaacs, A.M., Orrell, R.W., Cunningham, T.J., and Arozena, A.A. (2023). Opinion: more mouse models and more translation needed for ALS. Mol Neurodegener *18*, 30. 10.1186/s13024-023-00619-2.
81. Devoy, A., Price, G., De Giorgio, F., Bunton-Stasyshyn, R., Thompson, D., Gasco, S., Allan, A., Codner, G.F., Nair, R.R., Tibbit, C., et al. (2021). Generation and analysis of innovative genomically humanized knockin. iScience *24*, 103463. 10.1016/j.isci.2021.103463.
82. Takahashi, K., Tanabe, K., Ohnuki, M., Narita, M., Ichisaka, T., Tomoda, K., and Yamanaka, S. (2007). Induction of pluripotent stem cells from adult human fibroblasts by defined factors. Cell *131*, 861-872. 10.1016/j.cell.2007.11.019.
83. Maury, Y., Côme, J., Piskorowski, R.A., Salah-Mohellibi, N., Chevaleyre, V., Peschanski, M., Martinat, C., and Nedelec, S. (2015). Combinatorial analysis of developmental cues efficiently converts human pluripotent stem cells into multiple neuronal subtypes. Nat Biotechnol *33*, 89-96. 10.1038/nbt.3049.
84. Fernandopulle, M.S., Prestil, R., Grunseich, C., Wang, C., Gan, L., and Ward, M.E. (2018). Transcription Factor-Mediated Differentiation of Human iPSCs into Neurons. Curr Protoc Cell Biol *79*, e51. 10.1002/cpcb.51.
85. Pantazis, C.B., Yang, A., Lara, E., McDonough, J.A., Blauwendraat, C., Peng, L., Oguro, H., Kanaujiya, J., Zou, J., Sebesta, D., et al. (2022). A reference human induced pluripotent stem cell line for large-scale collaborative studies. Cell Stem Cell *29*, 1685-1702.e1622. 10.1016/j.stem.2022.11.004.
86. Workman, M.J., Lim, R.G., Wu, J., Frank, A., Ornelas, L., Panther, L., Galvez, E., Perez, D., Meepe, I., Lei, S., et al. (2023). Large-scale differentiation of iPSC-derived motor neurons from ALS and control subjects. Neuron. 10.1016/j.neuron.2023.01.010.
87. Guo, W., Fumagalli, L., Prior, R., and Van Den Bosch, L. (2017). Current Advances and Limitations in Modeling ALS/FTD in a Dish Using Induced Pluripotent Stem Cells. Front Neurosci *11*, 671. 10.3389/fnins.2017.00671.
88. Chen, H., Qian, K., Du, Z., Cao, J., Petersen, A., Liu, H., Blackbourn, L.W., Huang, C.L., Errigo, A., Yin, Y., et al. (2014). Modeling ALS with iPSCs reveals that mutant SOD1 misregulates neurofilament balance in motor neurons. Cell Stem Cell *14*, 796-809. 10.1016/j.stem.2014.02.004.
89. Naujock, M., Stanslowsky, N., Bufler, S., Naumann, M., Reinhardt, P., Sterneckert, J., Kefalakes, E., Kassebaum, C., Bursch, F., Lojewski, X., et al. (2016). 4-Aminopyridine Induced Activity Rescues Hypoexcitable Motor Neurons from Amyotrophic Lateral Sclerosis Patient-Derived Induced Pluripotent Stem Cells. Stem Cells *34*, 1563-1575. 10.1002/stem.2354.
90. Ferraiuolo, L., and Maragakis, N.J. (2021). Mini-Review: Induced pluripotent stem cells and the search for new cell-specific ALS therapeutic targets. Neurosci Lett *755*, 135911. 10.1016/j.neulet.2021.135911.
91. McKinnon, P.J. (2013). Maintaining genome stability in the nervous system. Nat Neurosci *16*, 1523-1529. 10.1038/nn.3537.
92. Blair, I.P., Bennett, C.L., Abel, A., Rabin, B.A., Griffin, J.W., Fischbeck, K.H., Cornblath, D.R., and Chance, P.F. (2000). A gene for autosomal dominant juvenile amyotrophic lateral sclerosis (ALS4) localizes to a 500-kb interval on chromosome 9q34. Neurogenetics *3*, 1-6. 10.1007/pl00022976.
93. Konopka, A., and Atkin, J.D. (2022). DNA Damage, Defective DNA Repair, and Neurodegeneration in Amyotrophic Lateral Sclerosis. Front Aging Neurosci *14*, 786420. 10.3389/fnagi.2022.786420.
94. Chen, Q., Sun, L., and Chen, Z.J. (2016). Regulation and function of the cGAS-STING pathway of cytosolic DNA sensing. Nat Immunol *17*, 1142-1149. 10.1038/ni.3558.
95. Marques, C., Held, A., Dorfman, K., Sung, J., Song, C., Kavuturu, A.S., Aguilar, C., Russo, T., Oakley, D.H., Albers, M.W., et al. (2024). Neuronal STING activation in amyotrophic lateral

sclerosis and frontotemporal dementia. Acta Neuropathol *147*, 56. 10.1007/s00401-024-02688-z.

96. Wang, R., Yang, B., and Zhang, D. (2011). Activation of interferon signaling pathways in spinal cord astrocytes from an ALS mouse model. Glia *59*, 946-958. 10.1002/glia.21167.
97. McCauley, M.E., O'Rourke, J.G., Yáñez, A., Markman, J.L., Ho, R., Wang, X., Chen, S., Lall, D., Jin, M., Muhammad, A.K.M.G., et al. (2020). C9orf72 in myeloid cells suppresses STING-induced inflammation. Nature *585*, 96-101. 10.1038/s41586-020-2625-x.
98. Rodriguez, S., Sahin, A., Schrank, B.R., Al-Lawati, H., Costantino, I., Benz, E., Fard, D., Albers, A.D., Cao, L., Gomez, A.C., et al. (2021). Genome-encoded cytoplasmic double-stranded RNAs, found in C9ORF72 ALS-FTD brain, propagate neuronal loss. Sci Transl Med *13*. 10.1126/scitranslmed.aaz4699.
99. LaClair, K.D., Zhou, Q., Michaelsen, M., Wefers, B., Brill, M.S., Janjic, A., Rathkolb, B., Farny, D., Cygan, M., de Angelis, M.H., et al. (2020). Congenic expression of poly-GA but not poly-PR in mice triggers selective neuron loss and interferon responses found in C9orf72 ALS. Acta Neuropathol *140*, 121-142. 10.1007/s00401-020-02176-0.
100. Yu, C.H., Davidson, S., Harapas, C.R., Hilton, J.B., Mlodzianoski, M.J., Laohamonthonkul, P., Louis, C., Low, R.R.J., Moecking, J., De Nardo, D., et al. (2020). TDP-43 Triggers Mitochondrial DNA Release via mPTP to Activate cGAS/STING in ALS. Cell *183*, 636-649.e618. 10.1016/j.cell.2020.09.020.
101. Kedersha, N., Ivanov, P., and Anderson, P. (2013). Stress granules and cell signaling: more than just a passing phase? Trends Biochem Sci *38*, 494-506. 10.1016/j.tibs.2013.07.004.
102. Boeynaems, S., Bogaert, E., Kovacs, D., Konijnenberg, A., Timmerman, E., Volkov, A., Guharoy, M., De Decker, M., Jaspers, T., Ryan, V.H., et al. (2017). Phase Separation of C9orf72 Dipeptide Repeats Perturbs Stress Granule Dynamics. Mol Cell *65*, 1044-1055.e1045. 10.1016/j.molcel.2017.02.013.
103. Maharjan, N., Künzli, C., Buthey, K., and Saxena, S. (2017). C9ORF72 Regulates Stress Granule Formation and Its Deficiency Impairs Stress Granule Assembly, Hypersensitizing Cells to Stress. Mol Neurobiol *54*, 3062-3077. 10.1007/s12035-016-9850-1.
104. Ramaswami, M., Taylor, J.P., and Parker, R. (2013). Altered ribostasis: RNA-protein granules in degenerative disorders. Cell *154*, 727-736. 10.1016/j.cell.2013.07.038.
105. Polymenidou, M., Lagier-Tourenne, C., Hutt, K.R., Huelga, S.C., Moran, J., Liang, T.Y., Ling, S.C., Sun, E., Wancewicz, E., Mazur, C., et al. (2011). Long pre-mRNA depletion and RNA missplicing contribute to neuronal vulnerability from loss of TDP-43. Nat Neurosci *14*, 459-468. 10.1038/nn.2779.
106. Klim, J.R., Williams, L.A., Limone, F., Guerra San Juan, I., Davis-Dusenbery, B.N., Mordes, D.A., Burberry, A., Steinbaugh, M.J., Gamage, K.K., Kirchner, R., et al. (2019). ALS-implicated protein TDP-43 sustains levels of STMN2, a mediator of motor neuron growth and repair. Nat Neurosci *22*, 167-179. 10.1038/s41593-018-0300-4.
107. Melamed, Z., López-Erauskin, J., Baughn, M.W., Zhang, O., Drenner, K., Sun, Y., Freyermuth, F., McMahon, M.A., Beccari, M.S., Artates, J.W., et al. (2019). Premature polyadenylation-mediated loss of stathmin-2 is a hallmark of TDP-43-dependent neurodegeneration. Nat Neurosci *22*, 180-190. 10.1038/s41593-018-0293-z.
108. Ma, X.R., Prudencio, M., Koike, Y., Vatsavayai, S.C., Kim, G., Harbinski, F., Briner, A., Rodriguez, C.M., Guo, C., Akiyama, T., et al. (2022). TDP-43 represses cryptic exon inclusion in the FTD-ALS gene UNC13A. Nature *603*, 124-130. 10.1038/s41586-022-04424-7.
109. Brown, A.L., Wilkins, O.G., Keuss, M.J., Hill, S.E., Zanovello, M., Lee, W.C., Bampton, A., Lee, F.C.Y., Masino, L., Qi, Y.A., et al. (2022). TDP-43 loss and ALS-risk SNPs drive mis-splicing and depletion of UNC13A. Nature *603*, 131-137. 10.1038/s41586-022-04436-3.
110. Lagier-Tourenne, C., Polymenidou, M., and Cleveland, D.W. (2010). TDP-43 and FUS/TLS: emerging roles in RNA processing and neurodegeneration. Hum Mol Genet *19*, R46-64. 10.1093/hmg/ddq137.

111. Ziff, O.J., Harley, J., Wang, Y., Neeves, J., Tyzack, G., Ibrahim, F., Skehel, M., Chakrabarti, A.M., Kelly, G., and Patani, R. (2023). Nucleocytoplasmic mRNA redistribution accompanies RNA binding protein mislocalization in ALS motor neurons and is restored by VCP ATPase inhibition. Neuron *111*, 3011-3027.e3017. 10.1016/j.neuron.2023.06.019.
112. Valdez, G., Heyer, M.P., Feng, G., and Sanes, J.R. (2014). The role of muscle microRNAs in repairing the neuromuscular junction. PLoS One *9*, e93140. 10.1371/journal.pone.0093140.
113. Emde, A., Eitan, C., Liou, L.L., Libby, R.T., Rivkin, N., Magen, I., Reichenstein, I., Oppenheim, H., Eilam, R., Silvestroni, A., et al. (2015). Dysregulated miRNA biogenesis downstream of cellular stress and ALS-causing mutations: a new mechanism for ALS. EMBO J *34*, 2633-2651. 10.15252/embj.201490493.
114. Blokhuis, A.M., Groen, E.J., Koppers, M., van den Berg, L.H., and Pasterkamp, R.J. (2013). Protein aggregation in amyotrophic lateral sclerosis. Acta Neuropathol *125*, 777-794. 10.1007/s00401-013-1125-6.
115. Polymenidou, M., and Cleveland, D.W. (2011). The seeds of neurodegeneration: prion-like spreading in ALS. Cell *147*, 498-508. 10.1016/j.cell.2011.10.011.
116. Scotter, E.L., Vance, C., Nishimura, A.L., Lee, Y.B., Chen, H.J., Urwin, H., Sardone, V., Mitchell, J.C., Rogelj, B., Rubinsztein, D.C., and Shaw, C.E. (2014). Differential roles of the ubiquitin proteasome system and autophagy in the clearance of soluble and aggregated TDP-43 species. J Cell Sci *127*, 1263-1278. 10.1242/jcs.140087.
117. Beckers, J., Tharkeshwar, A.K., Fumagalli, L., Contardo, M., Van Schoor, E., Fazal, R., Thal, D.R., Chandran, S., Mancuso, R., Van Den Bosch, L., and Van Damme, P. (2023). A toxic gain-of-function mechanism in C9orf72 ALS impairs the autophagy-lysosome pathway in neurons. Acta Neuropathol Commun *11*, 151. 10.1186/s40478-023-01648-0.
118. Parkinson, N., Ince, P.G., Smith, M.O., Highley, R., Skibinski, G., Andersen, P.M., Morrison, K.E., Pall, H.S., Hardiman, O., Collinge, J., et al. (2006). ALS phenotypes with mutations in CHMP2B (charged multivesicular body protein 2B). Neurology *67*, 1074-1077. 10.1212/01.wnl.0000231510.89311.8b.
119. Chen, H.J., Anagnostou, G., Chai, A., Withers, J., Morris, A., Adhikaree, J., Pennetta, G., and de Belleroche, J.S. (2010). Characterization of the properties of a novel mutation in VAPB in familial amyotrophic lateral sclerosis. J Biol Chem *285*, 40266-40281. 10.1074/jbc.M110.161398.
120. Castellanos-Montiel, M.J., Chaineau, M., and Durcan, T.M. (2020). The Neglected Genes of ALS: Cytoskeletal Dynamics Impact Synaptic Degeneration in ALS. Front Cell Neurosci *14*, 594975. 10.3389/fncel.2020.594975.
121. Van Schoor, E., Strubbe, D., Braems, E., Weishaupt, J., Ludolph, A.C., Van Damme, P., Thal, D.R., Bercier, V., and Van Den Bosch, L. (2024). TUBA4A downregulation as observed in ALS post-mortem motor cortex causes ALS-related abnormalities in zebrafish. Front Cell Neurosci *18*, 1340240. 10.3389/fncel.2024.1340240.
122. Williamson, T.L., and Cleveland, D.W. (1999). Slowing of axonal transport is a very early event in the toxicity of ALS-linked SOD1 mutants to motor neurons. Nat Neurosci *2*, 50-56. 10.1038/4553.
123. Kiskinis, E., Sandoe, J., Williams, L.A., Boulting, G.L., Moccia, R., Wainger, B.J., Han, S., Peng, T., Thams, S., Mikkilineni, S., et al. (2014). Pathways disrupted in human ALS motor neurons identified through genetic correction of mutant SOD1. Cell Stem Cell *14*, 781-795. 10.1016/j.stem.2014.03.004.
124. Guo, W., Naujock, M., Fumagalli, L., Vandoorne, T., Baatsen, P., Boon, R., Ordovás, L., Patel, A., Welters, M., Vanwelden, T., et al. (2017). HDAC6 inhibition reverses axonal transport defects in motor neurons derived from FUS-ALS patients. Nat Commun *8*, 861. 10.1038/s41467-017-00911-y.
125. Fazal, R., Boeynaems, S., Swijsen, A., De Decker, M., Fumagalli, L., Moisse, M., Vanneste, J., Guo, W., Boon, R., Vercruysse, T., et al. (2021). HDAC6 inhibition restores TDP-43 pathology

and axonal transport defects in human motor neurons with TARDBP mutations. EMBO J *40*, e106177. 10.15252/embj.2020106177.

126. Fumagalli, L., Young, F.L., Boeynaems, S., De Decker, M., Mehta, A.R., Swijsen, A., Fazal, R., Guo, W., Moisse, M., Beckers, J., et al. (2021). C9orf72-derived arginine-containing dipeptide repeats associate with axonal transport machinery and impede microtubule-based motility. Sci Adv *7*. 10.1126/sciadv.abg3013.
127. Tziortzouda, P., Steyaert, J., Scheveneels, W., Sicart, A., Stoklund Dittlau, K., Barbosa Correia, A.M., Burg, T., Pal, A., Hermann, A., Van Damme, P., et al. (2024). PP2A and GSK3 act as modifiers of FUS-ALS by modulating mitochondrial transport. Acta Neuropathol *147*, 41. 10.1007/s00401-024-02689-y.
128. Ling, S.C., Polymenidou, M., and Cleveland, D.W. (2013). Converging mechanisms in ALS and FTD: disrupted RNA and protein homeostasis. Neuron *79*, 416-438. 10.1016/j.neuron.2013.07.033.
129. Nijssen, J., Aguila, J., Hoogstraaten, R., Kee, N., and Hedlund, E. (2018). Axon-Seq Decodes the Motor Axon Transcriptome and Its Modulation in Response to ALS. Stem Cell Reports *11*, 1565-1578. 10.1016/j.stemcr.2018.11.005.
130. Piol, D., Robberechts, T., and Da Cruz, S. (2023). Lost in local translation: TDP-43 and FUS in axonal/neuromuscular junction maintenance and dysregulation in amyotrophic lateral sclerosis. Neuron *111*, 1355-1380. 10.1016/j.neuron.2023.02.028.
131. Zala, D., Hinckelmann, M.V., Yu, H., Lyra da Cunha, M.M., Liot, G., Cordelières, F.P., Marco, S., and Saudou, F. (2013). Vesicular glycolysis provides on-board energy for fast axonal transport. Cell *152*, 479-491. 10.1016/j.cell.2012.12.029.
132. Hua, W., Young, E.C., Fleming, M.L., and Gelles, J. (1997). Coupling of kinesin steps to ATP hydrolysis. Nature *388*, 390-393. 10.1038/41118.
133. Schnitzer, M.J., and Block, S.M. (1997). Kinesin hydrolyses one ATP per 8-nm step. Nature *388*, 386-390. 10.1038/41111.
134. Harris, J.J., Jolivet, R., and Attwell, D. (2012). Synaptic energy use and supply. Neuron *75*, 762-777. 10.1016/j.neuron.2012.08.019.
135. Sheng, Z.H. (2017). The Interplay of Axonal Energy Homeostasis and Mitochondrial Trafficking and Anchoring. Trends Cell Biol *27*, 403-416. 10.1016/j.tcb.2017.01.005.
136. Nijssen, J., Comley, L.H., and Hedlund, E. (2017). Motor neuron vulnerability and resistance in amyotrophic lateral sclerosis. Acta Neuropathol *133*, 863-885. 10.1007/s00401-017-1708-8.
137. Magistretti, P.J., and Allaman, I. (2015). A cellular perspective on brain energy metabolism and functional imaging. Neuron *86*, 883-901. 10.1016/j.neuron.2015.03.035.
138. Vandoorne, T., Veys, K., Guo, W., Sicart, A., Vints, K., Swijsen, A., Moisse, M., Eelen, G., Gounko, N.V., Fumagalli, L., et al. (2019). Differentiation but not ALS mutations in FUS rewires motor neuron metabolism. Nat Commun *10*, 4147. 10.1038/s41467-019-12099-4.
139. Divakaruni, A.S., Wallace, M., Buren, C., Martyniuk, K., Andreyev, A.Y., Li, E., Fields, J.A., Cordes, T., Reynolds, I.J., Bloodgood, B.L., et al. (2017). Inhibition of the mitochondrial pyruvate carrier protects from excitotoxic neuronal death. J Cell Biol *216*, 1091-1105. 10.1083/jcb.201612067.
140. Fendt, S.M., and Verstreken, P. (2017). Neurons eat glutamate to stay alive. J Cell Biol *216*, 863-865. 10.1083/jcb.201702003.
141. Cotter, D.G., d'Avignon, D.A., Wentz, A.E., Weber, M.L., and Crawford, P.A. (2011). Obligate role for ketone body oxidation in neonatal metabolic homeostasis. J Biol Chem *286*, 6902-6910. 10.1074/jbc.M110.192369.
142. LaManna, J.C., Salem, N., Puchowicz, M., Erokwu, B., Koppaka, S., Flask, C., and Lee, Z. (2009). Ketones suppress brain glucose consumption. Adv Exp Med Biol *645*, 301-306. 10.1007/978-0-387-85998-9_45.
143. Ciarlone, S.L., Grieco, J.C., D'Agostino, D.P., and Weeber, E.J. (2016). Ketone ester supplementation attenuates seizure activity, and improves behavior and hippocampal synaptic plasticity in an Angelman syndrome mouse model. Neurobiol Dis *96*, 38-46. 10.1016/j.nbd.2016.08.002.

144. Bouzier-Sore, A.K., Voisin, P., Bouchaud, V., Bezancon, E., Franconi, J.M., and Pellerin, L. (2006). Competition between glucose and lactate as oxidative energy substrates in both neurons and astrocytes: a comparative NMR study. Eur J Neurosci *24*, 1687-1694. 10.1111/j.1460-9568.2006.05056.x.
145. Zhang, Y., Chen, K., Sloan, S.A., Bennett, M.L., Scholze, A.R., O'Keeffe, S., Phatnani, H.P., Guarnieri, P., Caneda, C., Ruderisch, N., et al. (2014). An RNA-sequencing transcriptome and splicing database of glia, neurons, and vascular cells of the cerebral cortex. J Neurosci *34*, 11929-11947. 10.1523/JNEUROSCI.1860-14.2014.
146. Ahmed, R.M., Irish, M., Piguet, O., Halliday, G.M., Ittner, L.M., Farooqi, S., Hodges, J.R., and Kiernan, M.C. (2016). Amyotrophic lateral sclerosis and frontotemporal dementia: distinct and overlapping changes in eating behaviour and metabolism. Lancet Neurol *15*, 332-342. 10.1016/S1474-4422(15)00380-4.
147. Bouteloup, C., Desport, J.C., Clavelou, P., Guy, N., Derumeaux-Burel, H., Ferrier, A., and Couratier, P. (2009). Hypermetabolism in ALS patients: an early and persistent phenomenon. J Neurol *256*, 1236-1242. 10.1007/s00415-009-5100-z.
148. Ngo, S.T., van Eijk, R.P.A., Chachay, V., van den Berg, L.H., McCombe, P.A., Henderson, R.D., and Steyn, F.J. (2019). Loss of appetite is associated with a loss of weight and fat mass in patients with amyotrophic lateral sclerosis. Amyotroph Lateral Scler Frontotemporal Degener *20*, 497-505. 10.1080/21678421.2019.1621346.
149. Steyn, F.J., Ioannides, Z.A., van Eijk, R.P.A., Heggie, S., Thorpe, K.A., Ceslis, A., Heshmat, S., Henders, A.K., Wray, N.R., van den Berg, L.H., et al. (2018). Hypermetabolism in ALS is associated with greater functional decline and shorter survival. J Neurol Neurosurg Psychiatry *89*, 1016-1023. 10.1136/jnnp-2017-317887.
150. Jung, C., Higgins, C.M., and Xu, Z. (2002). Mitochondrial electron transport chain complex dysfunction in a transgenic mouse model for amyotrophic lateral sclerosis. J Neurochem *83*, 535-545. 10.1046/j.1471-4159.2002.01112.x.
151. Mattiazzi, M., D'Aurelio, M., Gajewski, C.D., Martushova, K., Kiaei, M., Beal, M.F., and Manfredi, G. (2002). Mutated human SOD1 causes dysfunction of oxidative phosphorylation in mitochondria of transgenic mice. J Biol Chem *277*, 29626-29633. 10.1074/jbc.M203065200.
152. Szelechowski, M., Amoedo, N., Obre, E., Léger, C., Allard, L., Bonneu, M., Claverol, S., Lacombe, D., Oliet, S., Chevallier, S., et al. (2018). Metabolic Reprogramming in Amyotrophic Lateral Sclerosis. Sci Rep *8*, 3953. 10.1038/s41598-018-22318-5.
153. So, E., Mitchell, J.C., Memmi, C., Chennell, G., Vizcay-Barrena, G., Allison, L., Shaw, C.E., and Vance, C. (2018). Mitochondrial abnormalities and disruption of the neuromuscular junction precede the clinical phenotype and motor neuron loss in hFUSWT transgenic mice. Hum Mol Genet *27*, 463-474. 10.1093/hmg/ddx415.
154. Vandoorne, T., De Bock, K., and Van Den Bosch, L. (2018). Energy metabolism in ALS: an underappreciated opportunity? Acta Neuropathol *135*, 489-509. 10.1007/s00401-018-1835-x.
155. Xu, Y.F., Gendron, T.F., Zhang, Y.J., Lin, W.L., D'Alton, S., Sheng, H., Casey, M.C., Tong, J., Knight, J., Yu, X., et al. (2010). Wild-type human TDP-43 expression causes TDP-43 phosphorylation, mitochondrial aggregation, motor deficits, and early mortality in transgenic mice. J Neurosci *30*, 10851-10859. 10.1523/JNEUROSCI.1630-10.2010.
156. Bravo-Sagua, R., Parra, V., López-Crisosto, C., Díaz, P., Quest, A.F., and Lavandero, S. (2017). Calcium Transport and Signaling in Mitochondria. Compr Physiol *7*, 623-634. 10.1002/cphy.c160013.
157. Siklós, L., Engelhardt, J., Harati, Y., Smith, R.G., Joó, F., and Appel, S.H. (1996). Ultrastructural evidence for altered calcium in motor nerve terminals in amyotropic lateral sclerosis. Ann Neurol *39*, 203-216. 10.1002/ana.410390210.
158. Lautenschläger, J., Prell, T., Ruhmer, J., Weidemann, L., Witte, O.W., and Grosskreutz, J. (2013). Overexpression of human mutated G93A SOD1 changes dynamics of the ER mitochondria calcium cycle specifically in mouse embryonic motor neurons. Exp Neurol *247*, 91-100. 10.1016/j.expneurol.2013.03.027.

159. Sasaki, S., and Iwata, M. (1996). Ultrastructural study of the synapses of central chromatolytic anterior horn cells in motor neuron disease. J Neuropathol Exp Neurol *55*, 932-939. 10.1097/00005072-199608000-00009.
160. Wiedemann, F.R., Manfredi, G., Mawrin, C., Beal, M.F., and Schon, E.A. (2002). Mitochondrial DNA and respiratory chain function in spinal cords of ALS patients. J Neurochem *80*, 616-625. 10.1046/j.0022-3042.2001.00731.x.
161. Shan, X., Chiang, P.M., Price, D.L., and Wong, P.C. (2010). Altered distributions of Gemini of coiled bodies and mitochondria in motor neurons of TDP-43 transgenic mice. Proc Natl Acad Sci U S A *107*, 16325-16330. 10.1073/pnas.1003459107.
162. Kong, J., and Xu, Z. (1998). Massive mitochondrial degeneration in motor neurons triggers the onset of amyotrophic lateral sclerosis in mice expressing a mutant SOD1. J Neurosci *18*, 3241-3250. 10.1523/JNEUROSCI.18-09-03241.1998.
163. Borthwick, G.M., Johnson, M.A., Ince, P.G., Shaw, P.J., and Turnbull, D.M. (1999). Mitochondrial enzyme activity in amyotrophic lateral sclerosis: implications for the role of mitochondria in neuronal cell death. Ann Neurol *46*, 787-790. 10.1002/1531-8249(199911)46:5<787::aid-ana17>3.0.co;2-8.
164. Wang, T., Liu, H., Itoh, K., Oh, S., Zhao, L., Murata, D., Sesaki, H., Hartung, T., Na, C.H., and Wang, J. (2021). C9orf72 regulates energy homeostasis by stabilizing mitochondrial complex I assembly. Cell Metab *33*, 531-546.e539. 10.1016/j.cmet.2021.01.005.
165. Dalakas, M.C., Hatazawa, J., Brooks, R.A., and Di Chiro, G. (1987). Lowered cerebral glucose utilization in amyotrophic lateral sclerosis. Ann Neurol *22*, 580-586. 10.1002/ana.410220504.
166. Pagani, M., Chiò, A., Valentini, M.C., Öberg, J., Nobili, F., Calvo, A., Moglia, C., Bertuzzo, D., Morbelli, S., De Carli, F., et al. (2014). Functional pattern of brain FDG-PET in amyotrophic lateral sclerosis. Neurology *83*, 1067-1074. 10.1212/WNL.0000000000000792.
167. Marini, C., Morbelli, S., Cistaro, A., Campi, C., Caponnetto, C., Bauckneht, M., Bellini, A., Buschiazzo, A., Calamia, I., Beltrametti, M.C., et al. (2018). Interplay between spinal cord and cerebral cortex metabolism in amyotrophic lateral sclerosis. Brain *141*, 2272-2279. 10.1093/brain/awy152.
168. Van Laere, K., Vanhee, A., Verschueren, J., De Coster, L., Driesen, A., Dupont, P., Robberecht, W., and Van Damme, P. (2014). Value of 18fluorodeoxyglucose-positron-emission tomography in amyotrophic lateral sclerosis: a prospective study. JAMA Neurol *71*, 553-561. 10.1001/jamaneurol.2014.62.
169. Miyazaki, K., Masamoto, K., Morimoto, N., Kurata, T., Mimoto, T., Obata, T., Kanno, I., and Abe, K. (2012). Early and progressive impairment of spinal blood flow-glucose metabolism coupling in motor neuron degeneration of ALS model mice. J Cereb Blood Flow Metab *32*, 456-467. 10.1038/jcbfm.2011.155.
170. Raman, R., Allen, S.P., Goodall, E.F., Kramer, S., Ponger, L.L., Heath, P.R., Milo, M., Hollinger, H.C., Walsh, T., Highley, J.R., et al. (2015). Gene expression signatures in motor neurone disease fibroblasts reveal dysregulation of metabolism, hypoxia-response and RNA processing functions. Neuropathol Appl Neurobiol *41*, 201-226. 10.1111/nan.12147.
171. Wang, X.S., Simmons, Z., Liu, W., Boyer, P.J., and Connor, J.R. (2006). Differential expression of genes in amyotrophic lateral sclerosis revealed by profiling the post mortem cortex. Amyotroph Lateral Scler *7*, 201-210. 10.1080/17482960600947689.
172. Palamiuc, L., Schlagowski, A., Ngo, S.T., Vernay, A., Dirrig-Grosch, S., Henriques, A., Boutillier, A.L., Zoll, J., Echaniz-Laguna, A., Loeffler, J.P., and René, F. (2015). A metabolic switch toward lipid use in glycolytic muscle is an early pathologic event in a mouse model of amyotrophic lateral sclerosis. EMBO Mol Med *7*, 526-546. 10.15252/emmm.201404433.
173. Tohgi, H., Abe, T., Yamazaki, K., Murata, T., Ishizaki, E., and Isobe, C. (1999). Increase in oxidized NO products and reduction in oxidized glutathione in cerebrospinal fluid from patients with sporadic form of amyotrophic lateral sclerosis. Neurosci Lett *260*, 204-206. 10.1016/s0304-3940(98)00986-0.

174. Bogdanov, M., Brown, R.H., Matson, W., Smart, R., Hayden, D., O'Donnell, H., Flint Beal, M., and Cudkowicz, M. (2000). Increased oxidative damage to DNA in ALS patients. Free Radic Biol Med *29*, 652-658. 10.1016/s0891-5849(00)00349-x.
175. Simpson, E.P., Henry, Y.K., Henkel, J.S., Smith, R.G., and Appel, S.H. (2004). Increased lipid peroxidation in sera of ALS patients: a potential biomarker of disease burden. Neurology *62*, 1758-1765. 10.1212/wnl.62.10.1758.
176. Mitsumoto, H., Santella, R.M., Liu, X., Bogdanov, M., Zipprich, J., Wu, H.C., Mahata, J., Kilty, M., Bednarz, K., Bell, D., et al. (2008). Oxidative stress biomarkers in sporadic ALS. Amyotroph Lateral Scler *9*, 177-183. 10.1080/17482960801933942.
177. Fergani, A., Oudart, H., Gonzalez De Aguilar, J.L., Fricker, B., René, F., Hocquette, J.F., Meininger, V., Dupuis, L., and Loeffler, J.P. (2007). Increased peripheral lipid clearance in an animal model of amyotrophic lateral sclerosis. J Lipid Res *48*, 1571-1580. 10.1194/jlr.M700017-JLR200.
178. Dodge, J.C., Treleaven, C.M., Fidler, J.A., Tamsett, T.J., Bao, C., Searles, M., Taksir, T.V., Misra, K., Sidman, R.L., Cheng, S.H., and Shihabuddin, L.S. (2013). Metabolic signatures of amyotrophic lateral sclerosis reveal insights into disease pathogenesis. Proc Natl Acad Sci U S A *110*, 10812-10817. 10.1073/pnas.1308421110.
179. Blasco, H., Corcia, P., Moreau, C., Veau, S., Fournier, C., Vourc'h, P., Emond, P., Gordon, P., Pradat, P.F., Praline, J., et al. (2010). 1H-NMR-based metabolomic profiling of CSF in early amyotrophic lateral sclerosis. PLoS One *5*, e13223. 10.1371/journal.pone.0013223.
180. Kumar, A., Bala, L., Kalita, J., Misra, U.K., Singh, R.L., Khetrapal, C.L., and Babu, G.N. (2010). Metabolomic analysis of serum by (1) H NMR spectroscopy in amyotrophic lateral sclerosis. Clin Chim Acta *411*, 563-567. 10.1016/j.cca.2010.01.016.
181. Barroso, E., Rodríguez-Calvo, R., Serrano-Marco, L., Astudillo, A.M., Balsinde, J., Palomer, X., and Vázquez-Carrera, M. (2011). The PPARβ/δ activator GW501516 prevents the down-regulation of AMPK caused by a high-fat diet in liver and amplifies the PGC-1α-Lipin 1-PPARα pathway leading to increased fatty acid oxidation. Endocrinology *152*, 1848-1859. 10.1210/en.2010-1468.
182. Thau, N., Knippenberg, S., Körner, S., Rath, K.J., Dengler, R., and Petri, S. (2012). Decreased mRNA expression of PGC-1α and PGC-1α-regulated factors in the SOD1G93A ALS mouse model and in human sporadic ALS. J Neuropathol Exp Neurol *71*, 1064-1074. 10.1097/NEN.0b013e318275df4b.
183. Ntambi, J.M. (1999). Regulation of stearoyl-CoA desaturase by polyunsaturated fatty acids and cholesterol. J Lipid Res *40*, 1549-1558.
184. Pradat, P.F., Dubourg, O., de Tapia, M., di Scala, F., Dupuis, L., Lenglet, T., Bruneteau, G., Salachas, F., Lacomblez, L., Corvol, J.C., et al. (2012). Muscle gene expression is a marker of amyotrophic lateral sclerosis severity. Neurodegener Dis *9*, 38-52. 10.1159/000329723.
185. Hussain, G., Schmitt, F., Henriques, A., Lequeu, T., Rene, F., Bindler, F., Dirrig-Grosch, S., Oudart, H., Palamiuc, L., Metz-Boutigue, M.H., et al. (2013). Systemic down-regulation of delta-9 desaturase promotes muscle oxidative metabolism and accelerates muscle function recovery following nerve injury. PLoS One *8*, e64525. 10.1371/journal.pone.0064525.
186. Kundu, P., Blacher, E., Elinav, E., and Pettersson, S. (2017). Our Gut Microbiome: The Evolving Inner Self. Cell *171*, 1481-1493. 10.1016/j.cell.2017.11.024.
187. Wu, S., Yi, J., Zhang, Y.G., Zhou, J., and Sun, J. (2015). Leaky intestine and impaired microbiome in an amyotrophic lateral sclerosis mouse model. Physiol Rep *3*. 10.14814/phy2.12356.
188. Zhang, Y.G., Wu, S., Yi, J., Xia, Y., Jin, D., Zhou, J., and Sun, J. (2017). Target Intestinal Microbiota to Alleviate Disease Progression in Amyotrophic Lateral Sclerosis. Clin Ther *39*, 322-336. 10.1016/j.clinthera.2016.12.014.
189. Fang, X., Wang, X., Yang, S., Meng, F., Wei, H., and Chen, T. (2016). Evaluation of the Microbial Diversity in Amyotrophic Lateral Sclerosis Using High-Throughput Sequencing. Front Microbiol *7*, 1479. 10.3389/fmicb.2016.01479.

190. Blacher, E., Bashiardes, S., Shapiro, H., Rothschild, D., Mor, U., Dori-Bachash, M., Kleimeyer, C., Moresi, C., Harnik, Y., Zur, M., et al. (2019). Potential roles of gut microbiome and metabolites in modulating ALS in mice. Nature *572*, 474-480. 10.1038/s41586-019-1443-5.
191. Nimmerjahn, A., Kirchhoff, F., and Helmchen, F. (2005). Resting microglial cells are highly dynamic surveillants of brain parenchyma in vivo. Science *308*, 1314-1318. 10.1126/science.1110647.
192. Li, Q., and Barres, B.A. (2018). Microglia and macrophages in brain homeostasis and disease. Nat Rev Immunol *18*, 225-242. 10.1038/nri.2017.125.
193. Butovsky, O., and Weiner, H.L. (2018). Microglial signatures and their role in health and disease. Nat Rev Neurosci *19*, 622-635. 10.1038/s41583-018-0057-5.
194. Ransohoff, R.M. (2016). A polarizing question: do M1 and M2 microglia exist? Nat Neurosci *19*, 987-991. 10.1038/nn.4338.
195. Mantovani, A., Sica, A., and Locati, M. (2005). Macrophage polarization comes of age. Immunity *23*, 344-346. 10.1016/j.immuni.2005.10.001.
196. Hu, X., Leak, R.K., Shi, Y., Suenaga, J., Gao, Y., Zheng, P., and Chen, J. (2015). Microglial and macrophage polarization—new prospects for brain repair. Nat Rev Neurol *11*, 56-64. 10.1038/nrneurol.2014.207.
197. Colonna, M., and Butovsky, O. (2017). Microglia Function in the Central Nervous System During Health and Neurodegeneration. Annu Rev Immunol *35*, 441-468. 10.1146/annurev-immunol-051116-052358.
198. Turner, M.R., Cagnin, A., Turkheimer, F.E., Miller, C.C., Shaw, C.E., Brooks, D.J., Leigh, P.N., and Banati, R.B. (2004). Evidence of widespread cerebral microglial activation in amyotrophic lateral sclerosis: an [11C](R)-PK11195 positron emission tomography study. Neurobiol Dis *15*, 601-609. 10.1016/j.nbd.2003.12.012.
199. Zürcher, N.R., Loggia, M.L., Lawson, R., Chonde, D.B., Izquierdo-Garcia, D., Yasek, J.E., Akeju, O., Catana, C., Rosen, B.R., Cudkowicz, M.E., et al. (2015). Increased in vivo glial activation in patients with amyotrophic lateral sclerosis: assessed with [(11)C]-PBR28. Neuroimage Clin *7*, 409-414. 10.1016/j.nicl.2015.01.009.
200. Tondo, G., Iaccarino, L., Cerami, C., Vanoli, G.E., Presotto, L., Masiello, V., Coliva, A., Salvi, F., Bartolomei, I., Mosca, L., et al. (2020). C-PK11195 PET-based molecular study of microglia activation in SOD1 amyotrophic lateral sclerosis. Ann Clin Transl Neurol *7*, 1513-1523. 10.1002/acn3.51112.
201. Henkel, J.S., Engelhardt, J.I., Siklós, L., Simpson, E.P., Kim, S.H., Pan, T., Goodman, J.C., Siddique, T., Beers, D.R., and Appel, S.H. (2004). Presence of dendritic cells, MCP-1, and activated microglia/macrophages in amyotrophic lateral sclerosis spinal cord tissue. Ann Neurol *55*, 221-235. 10.1002/ana.10805.
202. Brettschneider, J., Toledo, J.B., Van Deerlin, V.M., Elman, L., McCluskey, L., Lee, V.M., and Trojanowski, J.Q. (2012). Microglial activation correlates with disease progression and upper motor neuron clinical symptoms in amyotrophic lateral sclerosis. PLoS One *7*, e39216. 10.1371/journal.pone.0039216.
203. Brettschneider, J., Libon, D.J., Toledo, J.B., Xie, S.X., McCluskey, L., Elman, L., Geser, F., Lee, V.M., Grossman, M., and Trojanowski, J.Q. (2012). Microglial activation and TDP-43 pathology correlate with executive dysfunction in amyotrophic lateral sclerosis. Acta Neuropathol *123*, 395-407. 10.1007/s00401-011-0932-x.
204. Hall, E.D., Oostveen, J.A., and Gurney, M.E. (1998). Relationship of microglial and astrocytic activation to disease onset and progression in a transgenic model of familial ALS. Glia *23*, 249-256. 10.1002/(sici)1098-1136(199807)23:3<249::aid-glia7>3.0.co;2-#.
205. Alexianu, M.E., Kozovska, M., and Appel, S.H. (2001). Immune reactivity in a mouse model of familial ALS correlates with disease progression. Neurology *57*, 1282-1289. 10.1212/wnl.57.7.1282.

206. Jara, J.H., Gautam, M., Kocak, N., Xie, E.F., Mao, Q., Bigio, E.H., and Özdinler, P.H. (2019). MCP1-CCR2 and neuroinflammation in the ALS motor cortex with TDP-43 pathology. J Neuroinflammation *16*, 196. 10.1186/s12974-019-1589-y.
207. Qiu, H., Lee, S., Shang, Y., Wang, W.Y., Au, K.F., Kamiya, S., Barmada, S.J., Finkbeiner, S., Lui, H., Carlton, C.E., et al. (2014). ALS-associated mutation FUS-R521C causes DNA damage and RNA splicing defects. J Clin Invest *124*, 981-999. 10.1172/JCI72723.
208. Beers, D.R., Henkel, J.S., Xiao, Q., Zhao, W., Wang, J., Yen, A.A., Siklos, L., McKercher, S.R., and Appel, S.H. (2006). Wild-type microglia extend survival in PU.1 knockout mice with familial amyotrophic lateral sclerosis. Proc Natl Acad Sci U S A *103*, 16021-16026. 10.1073/pnas.0607423103.
209. Berriat, F., Lobsiger, C.S., and Boillée, S. (2023). The contribution of the peripheral immune system to neurodegeneration. Nat Neurosci *26*, 942-954. 10.1038/s41593-023-01323-6.
210. Liao, B., Zhao, W., Beers, D.R., Henkel, J.S., and Appel, S.H. (2012). Transformation from a neuroprotective to a neurotoxic microglial phenotype in a mouse model of ALS. Exp Neurol *237*, 147-152. 10.1016/j.expneurol.2012.06.011.
211. Gravel, M., Béland, L.C., Soucy, G., Abdelhamid, E., Rahimian, R., Gravel, C., and Kriz, J. (2016). IL-10 Controls Early Microglial Phenotypes and Disease Onset in ALS Caused by Misfolded Superoxide Dismutase 1. J Neurosci *36*, 1031-1048. 10.1523/JNEUROSCI.0854-15.2016.
212. Xiao, Q., Zhao, W., Beers, D.R., Yen, A.A., Xie, W., Henkel, J.S., and Appel, S.H. (2007). Mutant SOD1(G93A) microglia are more neurotoxic relative to wild-type microglia. J Neurochem *102*, 2008-2019. 10.1111/j.1471-4159.2007.04677.x.
213. Zhao, W., Beers, D.R., Henkel, J.S., Zhang, W., Urushitani, M., Julien, J.P., and Appel, S.H. (2010). Extracellular mutant SOD1 induces microglial-mediated motoneuron injury. Glia *58*, 231-243. 10.1002/glia.20919.
214. Weydt, P., Yuen, E.C., Ransom, B.R., and Möller, T. (2004). Increased cytotoxic potential of microglia from ALS-transgenic mice. Glia *48*, 179-182. 10.1002/glia.20062.
215. Zhao, W., Beers, D.R., Bell, S., Wang, J., Wen, S., Baloh, R.H., and Appel, S.H. (2015). TDP-43 activates microglia through NF-κB and NLRP3 inflammasome. Exp Neurol *273*, 24-35. 10.1016/j.expneurol.2015.07.019.
216. Deora, V., Lee, J.D., Albornoz, E.A., McAlary, L., Jagaraj, C.J., Robertson, A.A.B., Atkin, J.D., Cooper, M.A., Schroder, K., Yerbury, J.J., et al. (2020). The microglial NLRP3 inflammasome is activated by amyotrophic lateral sclerosis proteins. Glia *68*, 407-421. 10.1002/glia.23728.
217. O'Rourke, J.G., Bogdanik, L., Yáñez, A., Lall, D., Wolf, A.J., Muhammad, A.K., Ho, R., Carmona, S., Vit, J.P., Zarrow, J., et al. (2016). C9orf72 is required for proper macrophage and microglial function in mice. Science *351*, 1324-1329. 10.1126/science.aaf1064.
218. Lagier-Tourenne, C., Baughn, M., Rigo, F., Sun, S., Liu, P., Li, H.R., Jiang, J., Watt, A.T., Chun, S., Katz, M., et al. (2013). Targeted degradation of sense and antisense C9orf72 RNA foci as therapy for ALS and frontotemporal degeneration. Proc Natl Acad Sci U S A *110*, E4530-4539. 10.1073/pnas.1318835110.
219. Vahsen, B.F., Nalluru, S., Morgan, G.R., Farrimond, L., Carroll, E., Xu, Y., Cramb, K.M.L., Amein, B., Scaber, J., Katsikoudi, A., et al. (2023). C9orf72-ALS human iPSC microglia are pro-inflammatory and toxic to co-cultured motor neurons via MMP9. Nat Commun *14*, 5898. 10.1038/s41467-023-41603-0.
220. Banerjee, P., Mehta, A.R., Nirujogi, R.S., Cooper, J., James, O.G., Nanda, J., Longden, J., Burr, K., McDade, K., Salzinger, A., et al. (2023). Cell-autonomous immune dysfunction driven by disrupted autophagy in. Sci Adv *9*, eabq0651. 10.1126/sciadv.abq0651.
221. Lorenzini, I., Alsop, E., Levy, J., Gittings, L.M., Lall, D., Rabichow, B.E., Moore, S., Pevey, R., Bustos, L.M., Burciu, C., et al. (2023). Moderate intrinsic phenotypic alterations in. Front Cell Neurosci *17*, 1179796. 10.3389/fncel.2023.1179796.
222. Chiot, A., Zaïdi, S., Iltis, C., Ribon, M., Berriat, F., Schiaffino, L., Jolly, A., de la Grange, P., Mallat, M., Bohl, D., et al. (2020). Modifying macrophages at the periphery has the capacity to change

microglial reactivity and to extend ALS survival. Nat Neurosci *23*, 1339-1351. 10.1038/s41593-020-00718-z.

223. Michalski, J.P., and Kothary, R. (2015). Oligodendrocytes in a Nutshell. Front Cell Neurosci *9*, 340. 10.3389/fncel.2015.00340.
224. Philips, T., and Rothstein, J.D. (2017). Oligodendroglia: metabolic supporters of neurons. J Clin Invest *127*, 3271-3280. 10.1172/JCI90610.
225. Kawamata, T., Akiyama, H., Yamada, T., and McGeer, P.L. (1992). Immunologic reactions in amyotrophic lateral sclerosis brain and spinal cord tissue. Am J Pathol *140*, 691-707.
226. Tam, O.H., Rozhkov, N.V., Shaw, R., Kim, D., Hubbard, I., Fennessey, S., Propp, N., Fagegaltier, D., Harris, B.T., Ostrow, L.W., et al. (2019). Postmortem Cortex Samples Identify Distinct Molecular Subtypes of ALS: Retrotransposon Activation, Oxidative Stress, and Activated Glia. Cell Rep *29*, 1164-1177.e1165. 10.1016/j.celrep.2019.09.066.
227. Nolan, M., Scott, C., Gamarallage, M.P., Lunn, D., Carpenter, K., McDonough, E., Meyer, D., Kaanumalle, S., Santamaria-Pang, A., Turner, M.R., et al. (2020). Quantitative patterns of motor cortex proteinopathy across ALS genotypes. Acta Neuropathol Commun *8*, 98. 10.1186/s40478-020-00961-2.
228. Philips, T., Bento-Abreu, A., Nonneman, A., Haeck, W., Staats, K., Geelen, V., Hersmus, N., Küsters, B., Van Den Bosch, L., Van Damme, P., et al. (2013). Oligodendrocyte dysfunction in the pathogenesis of amyotrophic lateral sclerosis. Brain *136*, 471-482. 10.1093/brain/aws339.
229. Ferraiuolo, L., Meyer, K., Sherwood, T.W., Vick, J., Likhite, S., Frakes, A., Miranda, C.J., Braun, L., Heath, P.R., Pineda, R., et al. (2016). Oligodendrocytes contribute to motor neuron death in ALS via SOD1-dependent mechanism. Proc Natl Acad Sci U S A *113*, E6496-E6505. 10.1073/pnas.1607496113.
230. Lee, Y., Morrison, B.M., Li, Y., Lengacher, S., Farah, M.H., Hoffman, P.N., Liu, Y., Tsingalia, A., Jin, L., Zhang, P.W., et al. (2012). Oligodendroglia metabolically support axons and contribute to neurodegeneration. Nature *487*, 443-448. 10.1038/nature11314.
231. Kim, S., Chung, A.Y., Na, J.E., Lee, S.J., Jeong, S.H., Kim, E., Sun, W., Rhyu, I.J., and Park, H.C. (2019). Myelin degeneration induced by mutant superoxide dismutase 1 accumulation promotes amyotrophic lateral sclerosis. Glia *67*, 1910-1921. 10.1002/glia.23669.
232. Zhu, Y., Burg, T., Neyrinck, K., Vervliet, T., Nami, F., Vervoort, E., Ahuja, K., Sassano, M.L., Chai, Y.C., Tharkeshwar, A.K., et al. (2024). Disruption of MAM integrity in mutant FUS oligodendroglial progenitors from hiPSCs. Acta Neuropathol *147*, 6. 10.1007/s00401-023-02666-x.
233. Heller, J.P., and Rusakov, D.A. (2015). Morphological plasticity of astroglia: Understanding synaptic microenvironment. Glia *63*, 2133-2151. 10.1002/glia.22821.
234. Henneberger, C., Bard, L., Panatier, A., Reynolds, J.P., Kopach, O., Medvedev, N.I., Minge, D., Herde, M.K., Anders, S., Kraev, I., et al. (2020). LTP Induction Boosts Glutamate Spillover by Driving Withdrawal of Perisynaptic Astroglia. Neuron *108*, 919-936.e911. 10.1016/j.neuron.2020.08.030.
235. Vainchtein, I.D., and Molofsky, A.V. (2020). Astrocytes and Microglia: In Sickness and in Health. Trends Neurosci *43*, 144-154. 10.1016/j.tins.2020.01.003.
236. Liu, X., Ying, J., Wang, X., Zheng, Q., Zhao, T., Yoon, S., Yu, W., Yang, D., Fang, Y., and Hua, F. (2021). Astrocytes in Neural Circuits: Key Factors in Synaptic Regulation and Potential Targets for Neurodevelopmental Disorders. Front Mol Neurosci *14*, 729273. 10.3389/fnmol.2021.729273.
237. Allen, N.J., and Eroglu, C. (2017). Cell Biology of Astrocyte-Synapse Interactions. Neuron *96*, 697-708. 10.1016/j.neuron.2017.09.056.
238. Sibille, J., Pannasch, U., and Rouach, N. (2014). Astroglial potassium clearance contributes to short-term plasticity of synaptically evoked currents at the tripartite synapse. J Physiol *592*, 87-102. 10.1113/jphysiol.2013.261735.
239. Verkhratsky, A., and Nedergaard, M. (2018). Physiology of Astroglia. Physiol Rev *98*, 239-389. 10.1152/physrev.00042.2016.

240. Magistretti, P.J., and Allaman, I. (2018). Lactate in the brain: from metabolic end-product to signalling molecule. Nat Rev Neurosci *19*, 235-249. 10.1038/nrn.2018.19.
241. Figley, C.R. (2011). Lactate transport and metabolism in the human brain: implications for the astrocyte-neuron lactate shuttle hypothesis. J Neurosci *31*, 4768-4770. 10.1523/JNEUROSCI.6612-10.2011.
242. Bélanger, M., Allaman, I., and Magistretti, P.J. (2011). Brain energy metabolism: focus on astrocyte-neuron metabolic cooperation. Cell Metab *14*, 724-738. 10.1016/j.cmet.2011.08.016.
243. Brown, A.M. (2004). Brain glycogen re-awakened. J Neurochem *89*, 537-552. 10.1111/j.1471-4159.2004.02421.x.
244. Zamanian, J.L., Xu, L., Foo, L.C., Nouri, N., Zhou, L., Giffard, R.G., and Barres, B.A. (2012). Genomic analysis of reactive astrogliosis. J Neurosci *32*, 6391-6410. 10.1523/JNEUROSCI.6221-11.2012.
245. Sofroniew, M.V., and Vinters, H.V. (2010). Astrocytes: biology and pathology. Acta Neuropathol *119*, 7-35. 10.1007/s00401-009-0619-8.
246. Sica, R.E., Caccuri, R., Quarracino, C., and Capani, F. (2016). Are astrocytes executive cells within the central nervous system? Arq Neuropsiquiatr *74*, 671-678. 10.1590/0004-282X20160101.
247. Escartin, C., Galea, E., Lakatos, A., O'Callaghan, J.P., Petzold, G.C., Serrano-Pozo, A., Steinhäuser, C., Volterra, A., Carmignoto, G., Agarwal, A., et al. (2021). Reactive astrocyte nomenclature, definitions, and future directions. Nat Neurosci *24*, 312-325. 10.1038/s41593-020-00783-4.
248. Wang, L., Gutmann, D.H., and Roos, R.P. (2011). Astrocyte loss of mutant SOD1 delays ALS disease onset and progression in G85R transgenic mice. Hum Mol Genet *20*, 286-293. 10.1093/hmg/ddq463.
249. Ditsworth, D., Maldonado, M., McAlonis-Downes, M., Sun, S., Seelman, A., Drenner, K., Arnold, E., Ling, S.C., Pizzo, D., Ravits, J., et al. (2017). Mutant TDP-43 within motor neurons drives disease onset but not progression in amyotrophic lateral sclerosis. Acta Neuropathol *133*, 907-922. 10.1007/s00401-017-1698-6.
250. Di Giorgio, F.P., Carrasco, M.A., Siao, M.C., Maniatis, T., and Eggan, K. (2007). Non-cell autonomous effect of glia on motor neurons in an embryonic stem cell-based ALS model. Nat Neurosci *10*, 608-614. 10.1038/nn1885.
251. Di Giorgio, F.P., Boulting, G.L., Bobrowicz, S., and Eggan, K.C. (2008). Human embryonic stem cell-derived motor neurons are sensitive to the toxic effect of glial cells carrying an ALS-causing mutation. Cell Stem Cell *3*, 637-648. 10.1016/j.stem.2008.09.017.
252. Marchetto, M.C., Muotri, A.R., Mu, Y., Smith, A.M., Cezar, G.G., and Gage, F.H. (2008). Non-cell-autonomous effect of human SOD1 G37R astrocytes on motor neurons derived from human embryonic stem cells. Cell Stem Cell *3*, 649-657. 10.1016/j.stem.2008.10.001.
253. Haidet-Phillips, A.M., Hester, M.E., Miranda, C.J., Meyer, K., Braun, L., Frakes, A., Song, S., Likhite, S., Murtha, M.J., Foust, K.D., et al. (2011). Astrocytes from familial and sporadic ALS patients are toxic to motor neurons. Nat Biotechnol *29*, 824-828. 10.1038/nbt.1957.
254. Meyer, K., Ferraiuolo, L., Miranda, C.J., Likhite, S., McElroy, S., Renusch, S., Ditsworth, D., Lagier-Tourenne, C., Smith, R.A., Ravits, J., et al. (2014). Direct conversion of patient fibroblasts demonstrates non-cell autonomous toxicity of astrocytes to motor neurons in familial and sporadic ALS. Proc Natl Acad Sci U S A *111*, 829-832. 10.1073/pnas.1314085111.
255. Stoklund Dittlau, K., Terrie, L., Baatsen, P., Kerstens, A., De Swert, L., Janky, R., Corthout, N., Masrori, P., Van Damme, P., Hyttel, P., et al. (2023). FUS-ALS hiPSC-derived astrocytes impair human motor units through both gain-of-toxicity and loss-of-support mechanisms. Mol Neurodegener *18*, 5. 10.1186/s13024-022-00591-3.
256. Haidet-Phillips, A.M., Gross, S.K., Williams, T., Tuteja, A., Sherman, A., Ko, M., Jeong, Y.H., Wong, P.C., and Maragakis, N.J. (2013). Altered astrocytic expression of TDP-43 does not influence motor neuron survival. Exp Neurol *250*, 250-259. 10.1016/j.expneurol.2013.10.004.

257. Serio, A., Bilican, B., Barmada, S.J., Ando, D.M., Zhao, C., Siller, R., Burr, K., Haghi, G., Story, D., Nishimura, A.L., et al. (2013). Astrocyte pathology and the absence of non-cell autonomy in an induced pluripotent stem cell model of TDP-43 proteinopathy. Proc Natl Acad Sci U S A *110*, 4697-4702. 10.1073/pnas.1300398110.
258. Smethurst, P., Risse, E., Tyzack, G.E., Mitchell, J.S., Taha, D.M., Chen, Y.R., Newcombe, J., Collinge, J., Sidle, K., and Patani, R. (2020). Distinct responses of neurons and astrocytes to TDP-43 proteinopathy in amyotrophic lateral sclerosis. Brain *143*, 430-440. 10.1093/brain/awz419.
259. Qian, K., Huang, H., Peterson, A., Hu, B., Maragakis, N.J., Ming, G.L., Chen, H., and Zhang, S.C. (2017). Sporadic ALS Astrocytes Induce Neuronal Degeneration In Vivo. Stem Cell Reports *8*, 843-855. 10.1016/j.stemcr.2017.03.003.
260. Guttenplan, K.A., Weigel, M.K., Adler, D.I., Couthouis, J., Liddelow, S.A., Gitler, A.D., and Barres, B.A. (2020). Knockout of reactive astrocyte activating factors slows disease progression in an ALS mouse model. Nat Commun *11*, 3753. 10.1038/s41467-020-17514-9.
261. Liddelow, S.A., Guttenplan, K.A., Clarke, L.E., Bennett, F.C., Bohlen, C.J., Schirmer, L., Bennett, M.L., Münch, A.E., Chung, W.S., Peterson, T.C., et al. (2017). Neurotoxic reactive astrocytes are induced by activated microglia. Nature *541*, 481-487. 10.1038/nature21029.
262. Papadeas, S.T., Kraig, S.E., O'Banion, C., Lepore, A.C., and Maragakis, N.J. (2011). Astrocytes carrying the superoxide dismutase 1 (SOD1G93A) mutation induce wild-type motor neuron degeneration in vivo. Proc Natl Acad Sci U S A *108*, 17803-17808. 10.1073/pnas.1103141108.
263. Ziff, O.J., Clarke, B.E., Taha, D.M., Crerar, H., Luscombe, N.M., and Patani, R. (2022). Meta-analysis of human and mouse ALS astrocytes reveals multi-omic signatures of inflammatory reactive states. Genome Res *32*, 71-84. 10.1101/gr.275939.121.
264. Taha, D.M., Clarke, B.E., Hall, C.E., Tyzack, G.E., Ziff, O.J., Greensmith, L., Kalmar, B., Ahmed, M., Alam, A., Thelin, E.P., et al. (2022). Astrocytes display cell autonomous and diverse early reactive states in familial amyotrophic lateral sclerosis. Brain *145*, 481-489. 10.1093/brain/awab328.
265. Ajmone-Cat, M.A., Onori, A., Toselli, C., Stronati, E., Morlando, M., Bozzoni, I., Monni, E., Kokaia, Z., Lupo, G., Minghetti, L., et al. (2019). Increased FUS levels in astrocytes leads to astrocyte and microglia activation and neuronal death. Sci Rep *9*, 4572. 10.1038/s41598-019-41040-4.
266. Song, S., Miranda, C.J., Braun, L., Meyer, K., Frakes, A.E., Ferraiuolo, L., Likhite, S., Bevan, A.K., Foust, K.D., McConnell, M.J., et al. (2016). Major histocompatibility complex class I molecules protect motor neurons from astrocyte-induced toxicity in amyotrophic lateral sclerosis. Nat Med *22*, 397-403. 10.1038/nm.4052.
267. Gomes, C., Cunha, C., Nascimento, F., Ribeiro, J.A., Vaz, A.R., and Brites, D. (2019). Cortical Neurotoxic Astrocytes with Early ALS Pathology and miR-146a Deficit Replicate Gliosis Markers of Symptomatic SOD1G93A Mouse Model. Mol Neurobiol *56*, 2137-2158. 10.1007/s12035-018-1220-8.
268. Ouali Alami, N., Schurr, C., Olde Heuvel, F., Tang, L., Li, Q., Tasdogan, A., Kimbara, A., Nettekoven, M., Ottaviani, G., Raposo, C., et al. (2018). NF-κB activation in astrocytes drives a stage-specific beneficial neuroimmunological response in ALS. EMBO J *37*. 10.15252/embj.201798697.
269. Crosio, C., Valle, C., Casciati, A., Iaccarino, C., and Carrì, M.T. (2011). Astroglial inhibition of NF-κB does not ameliorate disease onset and progression in a mouse model for amyotrophic lateral sclerosis (ALS). PLoS One *6*, e17187. 10.1371/journal.pone.0017187.
270. Frakes, A.E., Ferraiuolo, L., Haidet-Phillips, A.M., Schmelzer, L., Braun, L., Miranda, C.J., Ladner, K.J., Bevan, A.K., Foust, K.D., Godbout, J.P., et al. (2014). Microglia induce motor neuron death via the classical NF-κB pathway in amyotrophic lateral sclerosis. Neuron *81*, 1009-1023. 10.1016/j.neuron.2014.01.013.

271. Gerber, Y.N., Sabourin, J.C., Rabano, M., Vivanco, M., and Perrin, F.E. (2012). Early functional deficit and microglial disturbances in a mouse model of amyotrophic lateral sclerosis. PLoS One *7*, e36000. 10.1371/journal.pone.0036000.
272. Rothstein, J.D., Tsai, G., Kuncl, R.W., Clawson, L., Cornblath, D.R., Drachman, D.B., Pestronk, A., Stauch, B.L., and Coyle, J.T. (1990). Abnormal excitatory amino acid metabolism in amyotrophic lateral sclerosis. Ann Neurol *28*, 18-25. 10.1002/ana.410280106.
273. Rothstein, J.D., Van Kammen, M., Levey, A.I., Martin, L.J., and Kuncl, R.W. (1995). Selective loss of glial glutamate transporter GLT-1 in amyotrophic lateral sclerosis. Ann Neurol *38*, 73-84. 10.1002/ana.410380114.
274. Rothstein, J.D., Dykes-Hoberg, M., Pardo, C.A., Bristol, L.A., Jin, L., Kuncl, R.W., Kanai, Y., Hediger, M.A., Wang, Y., Schielke, J.P., and Welty, D.F. (1996). Knockout of glutamate transporters reveals a major role for astroglial transport in excitotoxicity and clearance of glutamate. Neuron *16*, 675-686. 10.1016/s0896-6273(00)80086-0.
275. Rothstein, J.D., Martin, L.J., and Kuncl, R.W. (1992). Decreased glutamate transport by the brain and spinal cord in amyotrophic lateral sclerosis. N Engl J Med *326*, 1464-1468. 10.1056/NEJM199205283262204.
276. Van Den Bosch, L., Van Damme, P., Bogaert, E., and Robberecht, W. (2006). The role of excitotoxicity in the pathogenesis of amyotrophic lateral sclerosis. Biochim Biophys Acta *1762*, 1068-1082. 10.1016/j.bbadis.2006.05.002.
277. Van Damme, P., Bogaert, E., Dewil, M., Hersmus, N., Kiraly, D., Scheveneels, W., Bockx, I., Braeken, D., Verpoorten, N., Verhoeven, K., et al. (2007). Astrocytes regulate GluR2 expression in motor neurons and their vulnerability to excitotoxicity. Proc Natl Acad Sci U S A *104*, 14825-14830. 10.1073/pnas.0705046104.
278. Almad, A.A., Doreswamy, A., Gross, S.K., Richard, J.P., Huo, Y., Haughey, N., and Maragakis, N.J. (2016). Connexin 43 in astrocytes contributes to motor neuron toxicity in amyotrophic lateral sclerosis. Glia *64*, 1154-1169. 10.1002/glia.22989.
279. Almad, A.A., Taga, A., Joseph, J., Gross, S.K., Welsh, C., Patankar, A., Richard, J.P., Rust, K., Pokharel, A., Plott, C., et al. (2022). Cx43 hemichannels contribute to astrocyte-mediated toxicity in sporadic and familial ALS. Proc Natl Acad Sci U S A *119*, e2107391119. 10.1073/pnas.2107391119.
280. Giaume, C., Koulakoff, A., Roux, L., Holcman, D., and Rouach, N. (2010). Astroglial networks: a step further in neuroglial and gliovascular interactions. Nat Rev Neurosci *11*, 87-99. 10.1038/nrn2757.
281. Cassina, P., Cassina, A., Pehar, M., Castellanos, R., Gandelman, M., de León, A., Robinson, K.M., Mason, R.P., Beckman, J.S., Barbeito, L., and Radi, R. (2008). Mitochondrial dysfunction in SOD1G93A-bearing astrocytes promotes motor neuron degeneration: prevention by mitochondrial-targeted antioxidants. J Neurosci *28*, 4115-4122. 10.1523/JNEUROSCI.5308-07.2008.
282. Soubannier, V., Chaineau, M., Gursu, L., Lépine, S., Kalaydjian, D., Sirois, J., Haghi, G., Rouleau, G., Durcan, T.M., and Stifani, S. (2024). Early nuclear phenotypes and reactive transformation in human iPSC-derived astrocytes from ALS patients with SOD1 mutations. Glia. 10.1002/glia.24598.
283. Rojas, F., Cortes, N., Abarzua, S., Dyrda, A., and van Zundert, B. (2014). Astrocytes expressing mutant SOD1 and TDP43 trigger motoneuron death that is mediated via sodium channels and nitroxidative stress. Front Cell Neurosci *8*, 24. 10.3389/fncel.2014.00024.
284. Moujalled, D., Grubman, A., Acevedo, K., Yang, S., Ke, Y.D., Moujalled, D.M., Duncan, C., Caragounis, A., Perera, N.D., Turner, B.J., et al. (2017). TDP-43 mutations causing amyotrophic lateral sclerosis are associated with altered expression of RNA-binding protein hnRNP K and affect the Nrf2 antioxidant pathway. Hum Mol Genet *26*, 1732-1746. 10.1093/hmg/ddx093.
285. Birger, A., Ben-Dor, I., Ottolenghi, M., Turetsky, T., Gil, Y., Sweetat, S., Perez, L., Belzer, V., Casden, N., Steiner, D., et al. (2019). Human iPSC-derived astrocytes from ALS patients with

mutated C9ORF72 show increased oxidative stress and neurotoxicity. EBioMedicine *50*, 274-289. 10.1016/j.ebiom.2019.11.026.

286. Allen, S.P., Hall, B., Woof, R., Francis, L., Gatto, N., Shaw, A.C., Myszczynska, M., Hemingway, J., Coldicott, I., Willcock, A., et al. (2019). C9orf72 expansion within astrocytes reduces metabolic flexibility in amyotrophic lateral sclerosis. Brain *142*, 3771-3790. 10.1093/brain/awz302.
287. Allen, S.P., Hall, B., Castelli, L.M., Francis, L., Woof, R., Siskos, A.P., Kouloura, E., Gray, E., Thompson, A.G., Talbot, K., et al. (2019). Astrocyte adenosine deaminase loss increases motor neuron toxicity in amyotrophic lateral sclerosis. Brain *142*, 586-605. 10.1093/brain/awy353.
288. Ferraiuolo, L., Higginbottom, A., Heath, P.R., Barber, S., Greenald, D., Kirby, J., and Shaw, P.J. (2011). Dysregulation of astrocyte-motoneuron cross-talk in mutant superoxide dismutase 1-related amyotrophic lateral sclerosis. Brain *134*, 2627-2641. 10.1093/brain/awr193.
289. Madji Hounoum, B., Mavel, S., Coque, E., Patin, F., Vourc'h, P., Marouillat, S., Nadal-Desbarats, L., Emond, P., Corcia, P., Andres, C.R., et al. (2017). Wildtype motoneurons, ALS-Linked SOD1 mutation and glutamate profoundly modify astrocyte metabolism and lactate shuttling. Glia *65*, 592-605. 10.1002/glia.23114.
290. Velebit, J., Horvat, A., Smolič, T., Prpar Mihevc, S., Rogelj, B., Zorec, R., and Vardjan, N. (2020). Astrocytes with TDP-43 inclusions exhibit reduced noradrenergic cAMP and Ca. Sci Rep *10*, 6003. 10.1038/s41598-020-62864-5.
291. Huang, C., Huang, B., Bi, F., Yan, L.H., Tong, J., Huang, J., Xia, X.G., and Zhou, H. (2014). Profiling the genes affected by pathogenic TDP-43 in astrocytes. J Neurochem *129*, 932-939. 10.1111/jnc.12660.
292. Varcianna, A., Myszczynska, M.A., Castelli, L.M., O'Neill, B., Kim, Y., Talbot, J., Nyberg, S., Nyamali, I., Heath, P.R., Stopford, M.J., et al. (2019). Micro-RNAs secreted through astrocyte-derived extracellular vesicles cause neuronal network degeneration in C9orf72 ALS. EBioMedicine *40*, 626-635. 10.1016/j.ebiom.2018.11.067.
293. Kelley, K.W., Ben Haim, L., Schirmer, L., Tyzack, G.E., Tolman, M., Miller, J.G., Tsai, H.H., Chang, S.M., Molofsky, A.V., Yang, Y., et al. (2018). Kir4.1-Dependent Astrocyte-Fast Motor Neuron Interactions Are Required for Peak Strength. Neuron *98*, 306-319.e307. 10.1016/j.neuron.2018.03.010.
294. Bi, F., Huang, C., Tong, J., Qiu, G., Huang, B., Wu, Q., Li, F., Xu, Z., Bowser, R., Xia, X.G., and Zhou, H. (2013). Reactive astrocytes secrete lcn2 to promote neuron death. Proc Natl Acad Sci U S A *110*, 4069-4074. 10.1073/pnas.1218497110.
295. Mishra, P.S., Dhull, D.K., Nalini, A., Vijayalakshmi, K., Sathyaprabha, T.N., Alladi, P.A., and Raju, T.R. (2016). Astroglia acquires a toxic neuroinflammatory role in response to the cerebrospinal fluid from amyotrophic lateral sclerosis patients. J Neuroinflammation *13*, 212. 10.1186/s12974-016-0698-0.
296. Kia, A., McAvoy, K., Krishnamurthy, K., Trotti, D., and Pasinelli, P. (2018). Astrocytes expressing ALS-linked mutant FUS induce motor neuron death through release of tumor necrosis factor-alpha. Glia *66*, 1016-1033. 10.1002/glia.23298.
297. Lee, S., Kim, S., Kang, H.Y., Lim, H.R., Kwon, Y., Jo, M., Jeon, Y.M., Kim, S.R., Kim, K., Ha, C.M., and Kim, H.J. (2020). The overexpression of TDP-43 in astrocytes causes neurodegeneration via a PTP1B-mediated inflammatory response. J Neuroinflammation *17*, 299. 10.1186/s12974-020-01963-6.
298. Arredondo, C., Cefaliello, C., Dyrda, A., Jury, N., Martinez, P., Díaz, I., Amaro, A., Tran, H., Morales, D., Pertusa, M., et al. (2022). Excessive release of inorganic polyphosphate by ALS/FTD astrocytes causes non-cell-autonomous toxicity to motoneurons. Neuron *110*, 1656-1670.e1612. 10.1016/j.neuron.2022.02.010.
299. Jensen, B.K., McAvoy, K.J., Heinsinger, N.M., Lepore, A.C., Ilieva, H., Haeusler, A.R., Trotti, D., and Pasinelli, P. (2022). Targeting TNFα produced by astrocytes expressing amyotrophic lateral sclerosis-linked mutant fused in sarcoma prevents neurodegeneration and motor dysfunction in mice. Glia *70*, 1426-1449. 10.1002/glia.24183.

300. Dittlau, K.S., Chandrasekaran, A., Freude, K., and Van Den Bosch, L. (2024). Generation of Human Induced Pluripotent Stem Cell (hiPSC)-Derived Astrocytes for Amyotrophic Lateral Sclerosis and Other Neurodegenerative Disease Studies. Bio Protoc *14*, e4936. 10.21769/BioProtoc.4936.
301. Madill, M., McDonagh, K., Ma, J., Vajda, A., McLoughlin, P., O'Brien, T., Hardiman, O., and Shen, S. (2017). Amyotrophic lateral sclerosis patient iPSC-derived astrocytes impair autophagy via non-cell autonomous mechanisms. Mol Brain *10*, 22. 10.1186/s13041-017-0300-4.
302. Tripathi, P., Rodriguez-Muela, N., Klim, J.R., de Boer, A.S., Agrawal, S., Sandoe, J., Lopes, C.S., Ogliari, K.S., Williams, L.A., Shear, M., et al. (2017). Reactive Astrocytes Promote ALS-like Degeneration and Intracellular Protein Aggregation in Human Motor Neurons by Disrupting Autophagy through TGF-β1. Stem Cell Reports *9*, 667-680. 10.1016/j.stemcr.2017.06.008.
303. Mishra, V., Re, D.B., Le Verche, V., Alvarez, M.J., Vasciaveo, A., Jacquier, A., Doulias, P.T., Greco, T.M., Nizzardo, M., Papadimitriou, D., et al. (2020). Systematic elucidation of neuron-astrocyte interaction in models of amyotrophic lateral sclerosis using multi-modal integrated bioinformatics workflow. Nat Commun *11*, 5579. 10.1038/s41467-020-19177-y.
304. Vahsen, B.F., Gray, E., Thompson, A.G., Ansorge, O., Anthony, D.C., Cowley, S.A., Talbot, K., and Turner, M.R. (2021). Non-neuronal cells in amyotrophic lateral sclerosis - from pathogenesis to biomarkers. Nat Rev Neurol *17*, 333-348. 10.1038/s41582-021-00487-8.
305. Mead, R.J., Shan, N., Reiser, H.J., Marshall, F., and Shaw, P.J. (2023). Amyotrophic lateral sclerosis: a neurodegenerative disorder poised for successful therapeutic translation. Nat Rev Drug Discov *22*, 185-212. 10.1038/s41573-022-00612-2.
306. Miller, T.M., Cudkowicz, M.E., Genge, A., Shaw, P.J., Sobue, G., Bucelli, R.C., Chiò, A., Van Damme, P., Ludolph, A.C., Glass, J.D., et al. (2022). Trial of Antisense Oligonucleotide Tofersen for SOD1 ALS. N Engl J Med *387*, 1099-1110. 10.1056/NEJMoa2204705.
307. Miller, R.G., Mitchell, J.D., and Moore, D.H. (2001). Riluzole for amyotrophic lateral sclerosis (ALS)/motor neuron disease (MND). Cochrane Database Syst Rev, CD001447. 10.1002/14651858.CD001447.
308. Group, W., and Group, E.M.-A.S. (2017). Safety and efficacy of edaravone in well defined patients with amyotrophic lateral sclerosis: a randomised, double-blind, placebo-controlled trial. Lancet Neurol *16*, 505-512. 10.1016/S1474-4422(17)30115-1.
309. Paganoni, S., Macklin, E.A., Hendrix, S., Berry, J.D., Elliott, M.A., Maiser, S., Karam, C., Caress, J.B., Owegi, M.A., Quick, A., et al. (2020). Trial of Sodium Phenylbutyrate-Taurursodiol for Amyotrophic Lateral Sclerosis. N Engl J Med *383*, 919-930. 10.1056/NEJMoa1916945.
310. Bennett, C.F., and Swayze, E.E. (2010). RNA targeting therapeutics: molecular mechanisms of antisense oligonucleotides as a therapeutic platform. Annu Rev Pharmacol Toxicol *50*, 259-293. 10.1146/annurev.pharmtox.010909.105654.
311. Van Daele, S.H., Masrori, P., Van Damme, P., and Van Den Bosch, L. (2024). The sense of antisense therapies in ALS. Trends Mol Med *30*, 252-262. 10.1016/j.molmed.2023.12.003.
312. Tran, H., Moazami, M.P., Yang, H., McKenna-Yasek, D., Douthwright, C.L., Pinto, C., Metterville, J., Shin, M., Sanil, N., Dooley, C., et al. (2022). Suppression of mutant C9orf72 expression by a potent mixed backbone antisense oligonucleotide. Nat Med *28*, 117-124. 10.1038/s41591-021-01557-6.
313. Semenza, G.L. (2011). Oxygen sensing, homeostasis, and disease. N Engl J Med *365*, 537-547. 10.1056/NEJMra1011165.
314. Selak, M.A., Armour, S.M., MacKenzie, E.D., Boulahbel, H., Watson, D.G., Mansfield, K.D., Pan, Y., Simon, M.C., Thompson, C.B., and Gottlieb, E. (2005). Succinate links TCA cycle dysfunction to oncogenesis by inhibiting HIF-alpha prolyl hydroxylase. Cancer Cell *7*, 77-85. 10.1016/j.ccr.2004.11.022.
315. Isaacs, J.S., Jung, Y.J., Mole, D.R., Lee, S., Torres-Cabala, C., Chung, Y.L., Merino, M., Trepel, J., Zbar, B., Toro, J., et al. (2005). HIF overexpression correlates with biallelic loss of fumarate hydratase in renal cancer: novel role of fumarate in regulation of HIF stability. Cancer Cell *8*, 143-153. 10.1016/j.ccr.2005.06.017.

316. Schofield, C.J., and Ratcliffe, P.J. (2004). Oxygen sensing by HIF hydroxylases. Nat Rev Mol Cell Biol *5*, 343-354. 10.1038/nrm1366.
317. Wong, B.W., Kuchnio, A., Bruning, U., and Carmeliet, P. (2013). Emerging novel functions of the oxygen-sensing prolyl hydroxylase domain enzymes. Trends Biochem Sci *38*, 3-11. 10.1016/j.tibs.2012.10.004.
318. Strocchi, S., Reggiani, F., Gobbi, G., Ciarrocchi, A., and Sancisi, V. (2022). The multifaceted role of EGLN family prolyl hydroxylases in cancer: going beyond HIF regulation. Oncogene *41*, 3665-3679. 10.1038/s41388-022-02378-8.
319. Epstein, A.C., Gleadle, J.M., McNeill, L.A., Hewitson, K.S., O'Rourke, J., Mole, D.R., Mukherji, M., Metzen, E., Wilson, M.I., Dhanda, A., et al. (2001). C. elegans EGL-9 and mammalian homologs define a family of dioxygenases that regulate HIF by prolyl hydroxylation. Cell *107*, 43-54. 10.1016/s0092-8674(01)00507-4.
320. Bruick, R.K., and McKnight, S.L. (2001). A conserved family of prolyl-4-hydroxylases that modify HIF. Science *294*, 1337-1340. 10.1126/science.1066373.
321. Ivan, M., and Kaelin, W.G. (2017). The EGLN-HIF O_2-Sensing System: Multiple Inputs and Feedbacks. Mol Cell *66*, 772-779. 10.1016/j.molcel.2017.06.002.
322. Aragonés, J., Schneider, M., Van Geyte, K., Fraisl, P., Dresselaers, T., Mazzone, M., Dirkx, R., Zacchigna, S., Lemieux, H., Jeoung, N.H., et al. (2008). Deficiency or inhibition of oxygen sensor Phd1 induces hypoxia tolerance by reprogramming basal metabolism. Nat Genet *40*, 170-180. 10.1038/ng.2007.62.
323. Schneider, M., Van Geyte, K., Fraisl, P., Kiss, J., Aragonés, J., Mazzone, M., Mairbäurl, H., De Bock, K., Jeoung, N.H., Mollenhauer, M., et al. (2010). Loss or silencing of the PHD1 prolyl hydroxylase protects livers of mice against ischemia/reperfusion injury. Gastroenterology *138*, 1143-1154. 10.1053/j.gastro.2009.09.057.
324. Quaegebeur, A., Segura, I., Schmieder, R., Verdegem, D., Decimo, I., Bifari, F., Dresselaers, T., Eelen, G., Ghosh, D., Davidson, S.M., et al. (2016). Deletion or Inhibition of the Oxygen Sensor PHD1 Protects against Ischemic Stroke via Reprogramming of Neuronal Metabolism. Cell Metab *23*, 280-291. 10.1016/j.cmet.2015.12.007.
325. Kupershmidt, L., Weinreb, O., Amit, T., Mandel, S., Carri, M.T., and Youdim, M.B. (2009). Neuroprotective and neuritogenic activities of novel multimodal iron-chelating drugs in motor-neuron-like NSC-34 cells and transgenic mouse model of amyotrophic lateral sclerosis. FASEB J *23*, 3766-3779. 10.1096/fj.09-130047.
326. Nomura, E., Ohta, Y., Tadokoro, K., Shang, J., Feng, T., Liu, X., Shi, X., Matsumoto, N., Sasaki, R., Tsunoda, K., et al. (2019). Imaging Hypoxic Stress and the Treatment of Amyotrophic Lateral Sclerosis with Dimethyloxalylglycine in a Mice Model. Neuroscience *415*, 31-43. 10.1016/j.neuroscience.2019.06.025.
327. Oosthuyse, B., Moons, L., Storkebaum, E., Beck, H., Nuyens, D., Brusselmans, K., Van Dorpe, J., Hellings, P., Gorselink, M., Heymans, S., et al. (2001). Deletion of the hypoxia-response element in the vascular endothelial growth factor promoter causes motor neuron degeneration. Nat Genet *28*, 131-138. 10.1038/88842.
328. Storkebaum, E., Lambrechts, D., Dewerchin, M., Moreno-Murciano, M.P., Appelmans, S., Oh, H., Van Damme, P., Rutten, B., Man, W.Y., De Mol, M., et al. (2005). Treatment of motoneuron degeneration by intracerebroventricular delivery of VEGF in a rat model of ALS. Nat Neurosci *8*, 85-92. 10.1038/nn1360.
329. Van Den Bosch, L., Storkebaum, E., Vleminckx, V., Moons, L., Vanopdenbosch, L., Scheveneels, W., Carmeliet, P., and Robberecht, W. (2004). Effects of vascular endothelial growth factor (VEGF) on motor neuron degeneration. Neurobiol Dis *17*, 21-28. 10.1016/j.nbd.2004.06.004.
330. Rather, M.A., Khan, A., Wang, L., Jahan, S., Rehman, M.U., Makeen, H.A., and Mohan, S. (2023). TRP channels: Role in neurodegenerative diseases and therapeutic targets. Heliyon *9*, e16910. 10.1016/j.heliyon.2023.e16910.
331. Cummins, E.P., Berra, E., Comerford, K.M., Ginouves, A., Fitzgerald, K.T., Seeballuck, F., Godson, C., Nielsen, J.E., Moynagh, P., Pouyssegur, J., and Taylor, C.T. (2006). Prolyl

hydroxylase-1 negatively regulates IkappaB kinase-beta, giving insight into hypoxia-induced NFkappaB activity. Proc Natl Acad Sci U S A *103*, 18154-18159. 10.1073/pnas.0602235103.

332. Van Welden, S., De Vos, M., Wielockx, B., Tavernier, S.J., Dullaers, M., Neyt, S., Descamps, B., Devisscher, L., Devriese, S., Van den Bossche, L., et al. (2017). Haematopoietic prolyl hydroxylase-1 deficiency promotes M2 macrophage polarization and is both necessary and sufficient to protect against experimental colitis. J Pathol *241*, 547-558. 10.1002/path.4861.
333. Mojsilovic-Petrovic, J., Nedelsky, N., Boccitto, M., Mano, I., Georgiades, S.N., Zhou, W., Liu, Y., Neve, R.L., Taylor, J.P., Driscoll, M., et al. (2009). FOXO3a is broadly neuroprotective in vitro and in vivo against insults implicated in motor neuron diseases. J Neurosci *29*, 8236-8247. 10.1523/JNEUROSCI.1805-09.2009.
334. Maor-Nof, M., Shipony, Z., Lopez-Gonzalez, R., Nakayama, L., Zhang, Y.J., Couthouis, J., Blum, J.A., Castruita, P.A., Linares, G.R., Ruan, K., et al. (2021). p53 is a central regulator driving neurodegeneration caused by C9orf72 poly(PR). Cell *184*, 689-708.e620. 10.1016/j.cell.2020.12.025.
335. Panes, J.D., Wendt, A., Ramirez-Molina, O., Castro, P.A., and Fuentealba, J. (2022). Deciphering the role of PGC-1α in neurological disorders: from mitochondrial dysfunction to synaptic failure. Neural Regen Res *17*, 237-245. 10.4103/1673-5374.317957.
336. Semenza, G.L. (2007). Hypoxia-inducible factor 1 (HIF-1) pathway. Sci STKE *2007*, cm8. 10.1126/stke.4072007cm8.
337. Mikhaylova, O., Ignacak, M.L., Barankiewicz, T.J., Harbaugh, S.V., Yi, Y., Maxwell, P.H., Schneider, M., Van Geyte, K., Carmeliet, P., Revelo, M.P., et al. (2008). The von Hippel-Lindau tumor suppressor protein and Egl-9-Type proline hydroxylases regulate the large subunit of RNA polymerase II in response to oxidative stress. Mol Cell Biol *28*, 2701-2717. 10.1128/MCB.01231-07.
338. Balamurugan, K., Luu, V.D., Kaufmann, M.R., Hofmann, V.S., Boysen, G., Barth, S., Bordoli, M.R., Stiehl, D.P., Moch, H., Schraml, P., et al. (2009). Onconeuronal cerebellar degeneration-related antigen, Cdr2, is strongly expressed in papillary renal cell carcinoma and leads to attenuated hypoxic response. Oncogene *28*, 3274-3285. 10.1038/onc.2009.186.
339. Takahashi, N., Kuwaki, T., Kiyonaka, S., Numata, T., Kozai, D., Mizuno, Y., Yamamoto, S., Naito, S., Knevels, E., Carmeliet, P., et al. (2011). TRPA1 underlies a sensing mechanism for O2. Nat Chem Biol *7*, 701-711. 10.1038/nchembio.640.
340. Hiwatashi, Y., Kanno, K., Takasaki, C., Goryo, K., Sato, T., Torii, S., Sogawa, K., and Yasumoto, K. (2011). PHD1 interacts with ATF4 and negatively regulates its transcriptional activity without prolyl hydroxylation. Exp Cell Res *317*, 2789-2799. 10.1016/j.yexcr.2011.09.005.
341. Anderson, K., Nordquist, K.A., Gao, X., Hicks, K.C., Zhai, B., Gygi, S.P., and Patel, T.B. (2011). Regulation of cellular levels of Sprouty2 protein by prolyl hydroxylase domain and von Hippel-Lindau proteins. J Biol Chem *286*, 42027-42036. 10.1074/jbc.M111.303222.
342. Moser, S.C., Bensaddek, D., Ortmann, B., Maure, J.F., Mudie, S., Blow, J.J., Lamond, A.I., Swedlow, J.R., and Rocha, S. (2013). PHD1 links cell-cycle progression to oxygen sensing through hydroxylation of the centrosomal protein Cep192. Dev Cell *26*, 381-392. 10.1016/j.devcel.2013.06.014.
343. Zheng, X., Zhai, B., Koivunen, P., Shin, S.J., Lu, G., Liu, J., Geisen, C., Chakraborty, A.A., Moslehi, J.J., Smalley, D.M., et al. (2014). Prolyl hydroxylation by EglN2 destabilizes FOXO3a by blocking its interaction with the USP9x deubiquitinase. Genes Dev *28*, 1429-1444. 10.1101/gad.242131.114.
344. Deschoemaeker, S., Di Conza, G., Lilla, S., Martín-Pérez, R., Mennerich, D., Boon, L., Hendrikx, S., Maddocks, O.D., Marx, C., Radhakrishnan, P., et al. (2015). PHD1 regulates p53-mediated colorectal cancer chemoresistance. EMBO Mol Med *7*, 1350-1365. 10.15252/emmm.201505492.
345. Zhang, J., Wang, C., Chen, X., Takada, M., Fan, C., Zheng, X., Wen, H., Liu, Y., Pestell, R.G., Aird, K.M., et al. (2015). EglN2 associates with the NRF1-PGC1α complex and controls mitochondrial function in breast cancer. EMBO J *34*, 2953-2970. 10.15252/embj.201591437.

346. Zurlo, G., Liu, X., Takada, M., Fan, C., Simon, J.M., Ptacek, T.S., Rodriguez, J., von Kriegsheim, A., Liu, J., Locasale, J.W., et al. (2019). Prolyl hydroxylase substrate adenylosuccinate lyase is an oncogenic driver in triple negative breast cancer. Nat Commun *10*, 5177. 10.1038/s41467-019-13168-4.
347. D'Hulst, G., Soro-Arnaiz, I., Masschelein, E., Veys, K., Fitzgerald, G., Smeuninx, B., Kim, S., Deldicque, L., Blaauw, B., Carmeliet, P., et al. (2020). PHD1 controls muscle mTORC1 in a hydroxylation-independent manner by stabilizing leucyl tRNA synthetase. Nat Commun *11*, 174. 10.1038/s41467-019-13889-6.
348. Lee, S.B., Ko, A., Oh, Y.T., Shi, P., D'Angelo, F., Frangaj, B., Koller, A., Chen, E.I., Cardozo, T., Iavarone, A., and Lasorella, A. (2020). Proline Hydroxylation Primes Protein Kinases for Autophosphorylation and Activation. Mol Cell *79*, 376-389.e378. 10.1016/j.molcel.2020.06.021.
349. Yu, G., Yuan, L., Li, X., Zuo, M., Wang, R., Chen, M., Liu, Y., Liu, X., and Xiao, W. (2024). Zebrafish phd1 enhances mavs-mediated antiviral responses in a hydroxylation-independent manner. J Virol, e0103824. 10.1128/jvi.01038-24.
350. Lemmens, R., Van Hoecke, A., Hersmus, N., Geelen, V., D'Hollander, I., Thijs, V., Van Den Bosch, L., Carmeliet, P., and Robberecht, W. (2007). Overexpression of mutant superoxide dismutase 1 causes a motor axonopathy in the zebrafish. Hum Mol Genet *16*, 2359-2365. 10.1093/hmg/ddm193.
351. Swinnen, B., Bento-Abreu, A., Gendron, T.F., Boeynaems, S., Bogaert, E., Nuyts, R., Timmers, M., Scheveneels, W., Hersmus, N., Wang, J., et al. (2018). A zebrafish model for C9orf72 ALS reveals RNA toxicity as a pathogenic mechanism. Acta Neuropathol *135*, 427-443. 10.1007/s00401-017-1796-5.
352. Aragones, J., Schneider, M., Van Geyte, K., Fraisl, P., Dresselaers, T., Mazzone, M., Dirkx, R., Zacchigna, S., Lemieux, H., Jeoung, N.H., et al. (2008). Deficiency or inhibition of oxygen sensor Phd1 induces hypoxia tolerance by reprogramming basal metabolism. Nat Genet *40*, 170-180. 10.1038/ng.2007.62.
353. Doench, J.G., Fusi, N., Sullender, M., Hegde, M., Vaimberg, E.W., Donovan, K.F., Smith, I., Tothova, Z., Wilen, C., Orchard, R., et al. (2016). Optimized sgRNA design to maximize activity and minimize off-target effects of CRISPR-Cas9. Nat Biotechnol *34*, 184-191. 10.1038/nbt.3437.
354. Carpenter, A.E., Jones, T.R., Lamprecht, M.R., Clarke, C., Kang, I.H., Friman, O., Guertin, D.A., Chang, J.H., Lindquist, R.A., Moffat, J., et al. (2006). CellProfiler: image analysis software for identifying and quantifying cell phenotypes. Genome Biol *7*, R100. 10.1186/gb-2006-7-10-r100.
355. Swiech, L., Heidenreich, M., Banerjee, A., Habib, N., Li, Y., Trombetta, J., Sur, M., and Zhang, F. (2015). In vivo interrogation of gene function in the mammalian brain using CRISPR-Cas9. Nat Biotechnol *33*, 102-106. 10.1038/nbt.3055.
356. Sathyamurthy, A., Johnson, K.R., Matson, K.J.E., Dobrott, C.I., Li, L., Ryba, A.R., Bergman, T.B., Kelly, M.C., Kelley, M.W., and Levine, A.J. (2018). Massively Parallel Single Nucleus Transcriptional Profiling Defines Spinal Cord Neurons and Their Activity during Behavior. Cell Rep *22*, 2216-2225. 10.1016/j.celrep.2018.02.003.
357. Rosenberg, A.B., Roco, C.M., Muscat, R.A., Kuchina, A., Sample, P., Yao, Z., Graybuck, L.T., Peeler, D.J., Mukherjee, S., Chen, W., et al. (2018). Single-cell profiling of the developing mouse brain and spinal cord with split-pool barcoding. Science *360*, 176-182. 10.1126/science.aam8999.
358. Delile, J., Rayon, T., Melchionda, M., Edwards, A., Briscoe, J., and Sagner, A. (2019). Single cell transcriptomics reveals spatial and temporal dynamics of gene expression in the developing mouse spinal cord. Development *146*. 10.1242/dev.173807.
359. Zeisel, A., Hochgerner, H., Lönnerberg, P., Johnsson, A., Memic, F., van der Zwan, J., Häring, M., Braun, E., Borm, L.E., La Manno, G., et al. (2018). Molecular Architecture of the Mouse Nervous System. Cell *174*, 999-1014.e1022. 10.1016/j.cell.2018.06.021.

360. Artegiani, B., Lyubimova, A., Muraro, M., van Es, J.H., van Oudenaarden, A., and Clevers, H. (2017). A Single-Cell RNA Sequencing Study Reveals Cellular and Molecular Dynamics of the Hippocampal Neurogenic Niche. Cell Rep *21*, 3271-3284. 10.1016/j.celrep.2017.11.050.
361. Blum, J.A., Klemm, S., Shadrach, J.L., Guttenplan, K.A., Nakayama, L., Kathiria, A., Hoang, P.T., Gautier, O., Kaltschmidt, J.A., Greenleaf, W.J., and Gitler, A.D. (2021). Single-cell transcriptomic analysis of the adult mouse spinal cord reveals molecular diversity of autonomic and skeletal motor neurons. Nat Neurosci *24*, 572-583. 10.1038/s41593-020-00795-0.
362. Alkaslasi, M.R., Piccus, Z.E., Hareendran, S., Silberberg, H., Chen, L., Zhang, Y., Petros, T.J., and Le Pichon, C.E. (2021). Single nucleus RNA-sequencing defines unexpected diversity of cholinergic neuron types in the adult mouse spinal cord. Nat Commun *12*, 2471. 10.1038/s41467-021-22691-2.
363. Russ, D.E., Cross, R.B.P., Li, L., Koch, S.C., Matson, K.J.E., Yadav, A., Alkaslasi, M.R., Lee, D.I., Le Pichon, C.E., Menon, V., and Levine, A.J. (2021). A harmonized atlas of mouse spinal cord cell types and their spatial organization. Nat Commun *12*, 5722. 10.1038/s41467-021-25125-1.
364. Batiuk, M.Y., Martirosyan, A., Wahis, J., de Vin, F., Marneffe, C., Kusserow, C., Koeppen, J., Viana, J.F., Oliveira, J.F., Voet, T., et al. (2020). Identification of region-specific astrocyte subtypes at single cell resolution. Nat Commun *11*, 1220. 10.1038/s41467-019-14198-8.
365. van Bruggen, D., Agirre, E., and Castelo-Branco, G. (2017). Single-cell transcriptomic analysis of oligodendrocyte lineage cells. Curr Opin Neurobiol *47*, 168-175. 10.1016/j.conb.2017.10.005.
366. Marques, S., Zeisel, A., Codeluppi, S., van Bruggen, D., Mendanha Falcão, A., Xiao, L., Li, H., Häring, M., Hochgerner, H., Romanov, R.A., et al. (2016). Oligodendrocyte heterogeneity in the mouse juvenile and adult central nervous system. Science *352*, 1326-1329. 10.1126/science.aaf6463.
367. Davie, K., Janssens, J., Koldere, D., De Waegeneer, M., Pech, U., Kreft, Ł., Aibar, S., Makhzami, S., Christiaens, V., Bravo González-Blas, C., et al. (2018). A Single-Cell Transcriptome Atlas of the Aging Drosophila Brain. Cell *174*, 982-998. 10.1016/j.cell.2018.05.057.
368. Love, M.I., Huber, W., and Anders, S. (2014). Moderated estimation of fold change and dispersion for RNA-seq data with DESeq2. Genome Biol *15*, 550. 10.1186/s13059-014-0550-8.
369. Mi, H., Muruganujan, A., Ebert, D., Huang, X., and Thomas, P.D. (2019). PANTHER version 14: more genomes, a new PANTHER GO-slim and improvements in enrichment analysis tools. Nucleic Acids Res *47*, D419-D426. 10.1093/nar/gky1038.
370. Elizarraras, J.M., Liao, Y., Shi, Z., Zhu, Q., Pico, A.R., and Zhang, B. (2024). WebGestalt 2024: faster gene set analysis and new support for metabolomics and multi-omics. Nucleic Acids Res. 10.1093/nar/gkae456.
371. Rué, L., Oeckl, P., Timmers, M., Lenaerts, A., van der Vos, J., Smolders, S., Poppe, L., de Boer, A., Van Den Bosch, L., Van Damme, P., et al. (2019). Reduction of ephrin-A5 aggravates disease progression in amyotrophic lateral sclerosis. Acta Neuropathol Commun *7*, 114. 10.1186/s40478-019-0759-6.
372. Martin, M. (2011). Cutadapt Removes Adapter Sequences From High-Throughput Sequencing Reads. EMBnet.journal *17*. 10.14806/ej.17.1.200.
373. Morgan, M., Lawrence, M., and Aders, S. (2009). ShortRead: Base classes and methods for high-throughput short-read sequencing data.
374. Langmead, B., and Salzberg, S.L. (2012). Fast gapped-read alignment with Bowtie 2. Nat Methods *9*, 357-359. 10.1038/nmeth.1923.
375. Dobin, A., Davis, C.A., Schlesinger, F., Drenkow, J., Zaleski, C., Jha, S., Batut, P., Chaisson, M., and Gingeras, T.R. (2013). STAR: ultrafast universal RNA-seq aligner. Bioinformatics *29*, 15-21. 10.1093/bioinformatics/bts635.
376. Li, H., Handsaker, B., Wysoker, A., Fennell, T., Ruan, J., Homer, N., Marth, G., Abecasis, G., Durbin, R., and Subgroup, G.P.D.P. (2009). The Sequence Alignment/Map format and SAMtools. Bioinformatics *25*, 2078-2079. 10.1093/bioinformatics/btp352.

377. Liao, Y., Smyth, G.K., and Shi, W. (2014). featureCounts: an efficient general purpose program for assigning sequence reads to genomic features. Bioinformatics *30*, 923-930. 10.1093/bioinformatics/btt656.
378. Risso, D., Schwartz, K., Sherlock, G., and Dudoit, S. (2011). GC-content normalization for RNA-Seq data. BMC Bioinformatics *12*, 480. 10.1186/1471-2105-12-480.
379. Robinson, M.D., and Smyth, G.K. (2007). Moderated statistical tests for assessing differences in tag abundance. Bioinformatics *23*, 2881-2887. 10.1093/bioinformatics/btm453.
380. Benjamini, Y., and Hochberg, Y. (1995). Controlling the False Discovery Rate: A Practical and Powerful Approach to Multiple Testing. Journal of the Royal Statistical Society: Series B (Methodological) *57*. 10.1111/j.2517-6161.1995.tb02031.x.
381. Gurney, M.E., Pu, H., Chiu, A.Y., Dal Canto, M.C., Polchow, C.Y., Alexander, D.D., Caliendo, J., Hentati, A., Kwon, Y.W., and Deng, H.X. (1994). Motor neuron degeneration in mice that express a human Cu,Zn superoxide dismutase mutation. Science *264*, 1772-1775. 10.1126/science.8209258.
382. Xiao, S., McLean, J., and Robertson, J. (2006). Neuronal intermediate filaments and ALS: a new look at an old question. Biochim Biophys Acta *1762*, 1001-1012. 10.1016/j.bbadis.2006.09.003.
383. Morello, G., Guarnaccia, M., Spampinato, A.G., La Cognata, V., D'Agata, V., and Cavallaro, S. (2018). Copy Number Variations in Amyotrophic Lateral Sclerosis: Piecing the Mosaic Tiles Together through a Systems Biology Approach. Mol Neurobiol *55*, 1299-1322. 10.1007/s12035-017-0393-x.
384. Lee, S., Jeon, Y.M., Cha, S.J., Kim, S., Kwon, Y., Jo, M., Jang, Y.N., Kim, J., Kim, S.R., Lee, K.J., et al. (2020). PTK2/FAK regulates UPS impairment via SQSTM1/p62 phosphorylation in TARDBP/TDP-43 proteinopathies. Autophagy *16*, 1396-1412. 10.1080/15548627.2019.1686729.
385. Mòdol-Caballero, G., García-Lareu, B., Verdés, S., Ariza, L., Sánchez-Brualla, I., Brocard, F., Bosch, A., Navarro, X., and Herrando-Grabulosa, M. (2020). Therapeutic Role of Neuregulin 1 Type III in SOD1-Linked Amyotrophic Lateral Sclerosis. Neurotherapeutics *17*, 1048-1060. 10.1007/s13311-019-00811-7.
386. Tollervey, J.R., Curk, T., Rogelj, B., Briese, M., Cereda, M., Kayikci, M., König, J., Hortobágyi, T., Nishimura, A.L., Zupunski, V., et al. (2011). Characterizing the RNA targets and position-dependent splicing regulation by TDP-43. Nat Neurosci *14*, 452-458. 10.1038/nn.2778.
387. Oeckl, P., Weydt, P., Thal, D.R., Weishaupt, J.H., Ludolph, A.C., and Otto, M. (2020). Proteomics in cerebrospinal fluid and spinal cord suggests UCHL1, MAP2 and GPNMB as biomarkers and underpins importance of transcriptional pathways in amyotrophic lateral sclerosis. Acta Neuropathol *139*, 119-134. 10.1007/s00401-019-02093-x.
388. Lee, S., Shang, Y., Redmond, S.A., Urisman, A., Tang, A.A., Li, K.H., Burlingame, A.L., Pak, R.A., Jovičić, A., Gitler, A.D., et al. (2016). Activation of HIPK2 Promotes ER Stress-Mediated Neurodegeneration in Amyotrophic Lateral Sclerosis. Neuron *91*, 41-55. 10.1016/j.neuron.2016.05.021.
389. Lee, Y., Park, Y., Nam, H., Lee, J.W., and Yu, S.W. (2020). Translocator protein (TSPO): the new story of the old protein in neuroinflammation. BMB Rep *53*, 20-27. 10.5483/BMBRep.2020.53.1.273.
390. Chew, S., and Atassi, N. (2019). Positron Emission Tomography Molecular Imaging Biomarkers for Amyotrophic Lateral Sclerosis. Front Neurol *10*, 135. 10.3389/fneur.2019.00135.
391. Liu, J., and Wang, F. (2017). Role of Neuroinflammation in Amyotrophic Lateral Sclerosis: Cellular Mechanisms and Therapeutic Implications. Front Immunol *8*, 1005. 10.3389/fimmu.2017.01005.
392. Gerbino, V., Kaunga, E., Ye, J., Canzio, D., O'Keeffe, S., Rudnick, N.D., Guarnieri, P., Lutz, C.M., and Maniatis, T. (2020). The Loss of TBK1 Kinase Activity in Motor Neurons or in All Cell Types Differentially Impacts ALS Disease Progression in SOD1 Mice. Neuron *106*, 789-805.e785. 10.1016/j.neuron.2020.03.005.

393. Wilson, D.M., Cookson, M.R., Van Den Bosch, L., Zetterberg, H., Holtzman, D.M., and Dewachter, I. (2023). Hallmarks of neurodegenerative diseases. Cell *186*, 693-714. 10.1016/j.cell.2022.12.032.
394. Paul, B.D., Snyder, S.H., and Bohr, V.A. (2021). Signaling by cGAS-STING in Neurodegeneration, Neuroinflammation, and Aging. Trends Neurosci *44*, 83-96. 10.1016/j.tins.2020.10.008.
395. Nguyen, H.T., Geens, M., Mertzanidou, A., Jacobs, K., Heirman, C., Breckpot, K., and Spits, C. (2014). Gain of 20q11.21 in human embryonic stem cells improves cell survival by increased expression of Bcl-xL. Mol Hum Reprod *20*, 168-177. 10.1093/molehr/gat077.
396. Yang, W.W., Sidman, R.L., Taksir, T.V., Treleaven, C.M., Fidler, J.A., Cheng, S.H., Dodge, J.C., and Shihabuddin, L.S. (2011). Relationship between neuropathology and disease progression in the SOD1(G93A) ALS mouse. Exp Neurol *227*, 287-295. 10.1016/j.expneurol.2010.11.019.
397. Barbar, L., Jain, T., Zimmer, M., Kruglikov, I., Sadick, J.S., Wang, M., Kalpana, K., Rose, I.V.L., Burstein, S.R., Rusielewicz, T., et al. (2020). CD49f Is a Novel Marker of Functional and Reactive Human iPSC-Derived Astrocytes. Neuron *107*, 436-453.e412. 10.1016/j.neuron.2020.05.014.
398. Tyzack, G.E., Hall, C.E., Sibley, C.R., Cymes, T., Forostyak, S., Carlino, G., Meyer, I.F., Schiavo, G., Zhang, S.C., Gibbons, G.M., et al. (2017). A neuroprotective astrocyte state is induced by neuronal signal EphB1 but fails in ALS models. Nat Commun *8*, 1164. 10.1038/s41467-017-01283-z.
399. Neyrinck, K., Van Den Daele, J., Vervliet, T., De Smedt, J., Wierda, K., Nijs, M., Vanbokhoven, T., D'hondt, A., Planque, M., Fendt, S.M., et al. (2021). SOX9-induced Generation of Functional Astrocytes Supporting Neuronal Maturation in an All-human System. Stem Cell Rev Rep *17*, 1855-1873. 10.1007/s12015-021-10179-x.
400. Marshall, K.L., Rajbhandari, L., Venkatesan, A., Maragakis, N.J., and Farah, M.H. (2023). Enhanced axonal regeneration of ALS patient iPSC-derived motor neurons harboring SOD1. Sci Rep *13*, 5597. 10.1038/s41598-023-31720-7.
401. Rossaert, E., Pollari, E., Jaspers, T., Van Helleputte, L., Jarpe, M., Van Damme, P., De Bock, K., Moisse, M., and Van Den Bosch, L. (2019). Restoration of histone acetylation ameliorates disease and metabolic abnormalities in a FUS mouse model. Acta Neuropathol Commun *7*, 107. 10.1186/s40478-019-0750-2.
402. Boillée, S., Vande Velde, C., and Cleveland, D.W. (2006). ALS: a disease of motor neurons and their nonneuronal neighbors. Neuron *52*, 39-59. 10.1016/j.neuron.2006.09.018.
403. Van Harten, A.C.M., Phatnani, H., and Przedborski, S. (2021). Non-cell-autonomous pathogenic mechanisms in amyotrophic lateral sclerosis. Trends Neurosci *44*, 658-668. 10.1016/j.tins.2021.04.008.
404. Liu, W., Venugopal, S., Majid, S., Ahn, I.S., Diamante, G., Hong, J., Yang, X., and Chandler, S.H. (2020). Single-cell RNA-seq analysis of the brainstem of mutant SOD1 mice reveals perturbed cell types and pathways of amyotrophic lateral sclerosis. Neurobiol Dis *141*, 104877. 10.1016/j.nbd.2020.104877.
405. MacLean, M., López-Díez, R., Vasquez, C., Gugger, P.F., and Schmidt, A.M. (2022). Neuronal-glial communication perturbations in murine SOD1. Commun Biol *5*, 177. 10.1038/s42003-022-03128-y.
406. Maniatis, S., Äijö, T., Vickovic, S., Braine, C., Kang, K., Mollbrink, A., Fagegaltier, D., Andrusivová, Ž., Saarenpää, S., Saiz-Castro, G., et al. (2019). Spatiotemporal dynamics of molecular pathology in amyotrophic lateral sclerosis. Science *364*, 89-93. 10.1126/science.aav9776.
407. Li, J., Jaiswal, M.K., Chien, J.F., Kozlenkov, A., Jung, J., Zhou, P., Gardashli, M., Pregent, L.J., Engelberg-Cook, E., Dickson, D.W., et al. (2023). Divergent single cell transcriptome and epigenome alterations in ALS and FTD patients with C9orf72 mutation. Nat Commun *14*, 5714. 10.1038/s41467-023-41033-y.
408. Germeys, C., Vandoorne, T., Bercier, V., and Van Den Bosch, L. (2019). Existing and Emerging Metabolomic Tools for ALS Research. Genes (Basel) *10*. 10.3390/genes10121011.

409. Izrael, M., Slutsky, S.G., and Revel, M. (2020). Rising Stars: Astrocytes as a Therapeutic Target for ALS Disease. Front Neurosci *14*, 824. 10.3389/fnins.2020.00824.
410. Patani, R., Hardingham, G.E., and Liddelow, S.A. (2023). Functional roles of reactive astrocytes in neuroinflammation and neurodegeneration. Nat Rev Neurol *19*, 395-409. 10.1038/s41582-023-00822-1.
411. Huang, M., Liu, Y.U., Yao, X., Qin, D., and Su, H. (2024). Variability in SOD1-associated amyotrophic lateral sclerosis: geographic patterns, clinical heterogeneity, molecular alterations, and therapeutic implications. Transl Neurodegener *13*, 28. 10.1186/s40035-024-00416-x.
412. Fu, J., and Taubman, M.B. (2010). Prolyl hydroxylase EGLN3 regulates skeletal myoblast differentiation through an NF-kappaB-dependent pathway. J Biol Chem *285*, 8927-8935. 10.1074/jbc.M109.078600.
413. Xue, J., Li, X., Jiao, S., Wei, Y., Wu, G., and Fang, J. (2010). Prolyl hydroxylase-3 is down-regulated in colorectal cancer cells and inhibits IKKbeta independent of hydroxylase activity. Gastroenterology *138*, 606-615. 10.1053/j.gastro.2009.09.049.
414. Klotzsche-von Ameln, A., Muschter, A., Mamlouk, S., Kalucka, J., Prade, I., Franke, K., Rezaei, M., Poitz, D.M., Breier, G., and Wielockx, B. (2011). Inhibition of HIF prolyl hydroxylase-2 blocks tumor growth in mice through the antiproliferative activity of TGFβ. Cancer Res *71*, 3306-3316. 10.1158/0008-5472.CAN-10-3838.
415. Joharapurkar, A.A., Pandya, V.B., Patel, V.J., Desai, R.C., and Jain, M.R. (2018). Prolyl Hydroxylase Inhibitors: A Breakthrough in the Therapy of Anemia Associated with Chronic Diseases. J Med Chem *61*, 6964-6982. 10.1021/acs.jmedchem.7b01686.
416. Nakanishi, T., and Kuragano, T. (2024). Growing concerns about using hypoxia-inducible factor prolyl hydroxylase inhibitors for the treatment of renal anemia. Clin Kidney J *17*, sfae051. 10.1093/ckj/sfae051.
417. McCampbell, A., Cole, T., Wegener, A.J., Tomassy, G.S., Setnicka, A., Farley, B.J., Schoch, K.M., Hoye, M.L., Shabsovich, M., Sun, L., et al. (2018). Antisense oligonucleotides extend survival and reverse decrement in muscle response in ALS models. J Clin Invest *128*, 3558-3567. 10.1172/JCI99081.

Supplementary figures and tables

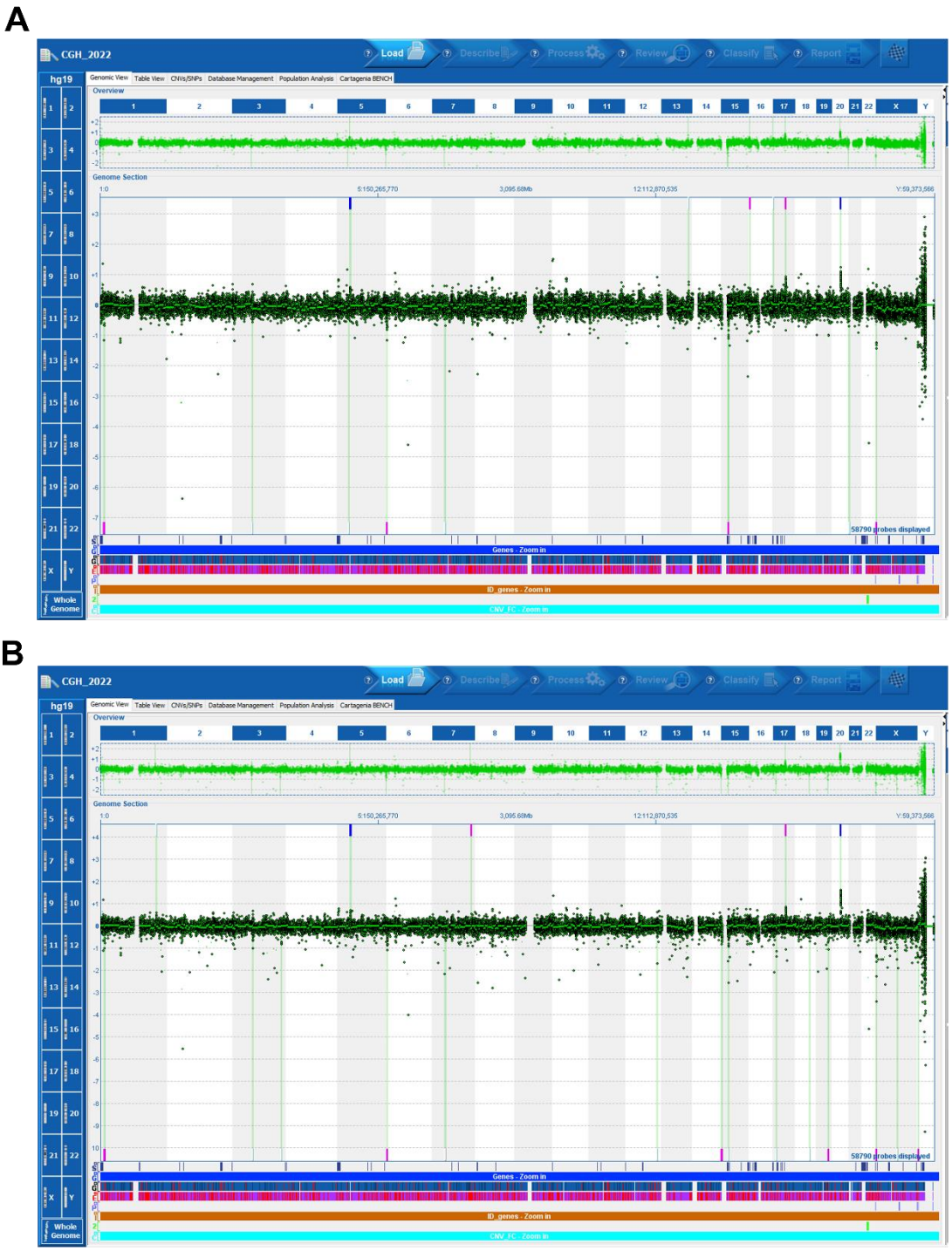
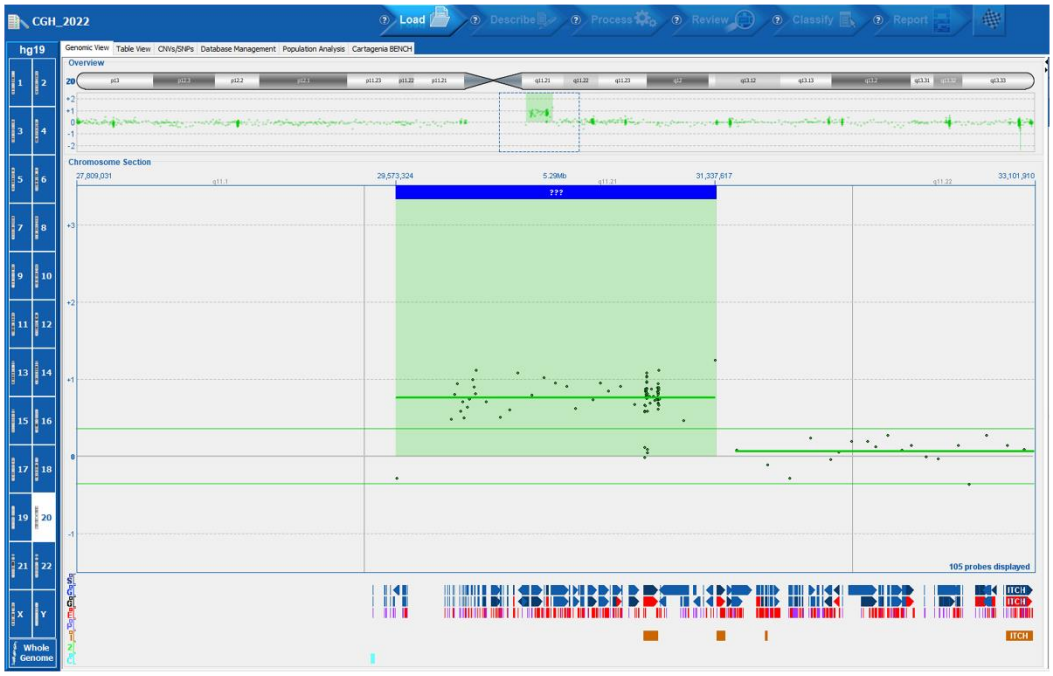


Figure S4.1. Array-CGH results of all chromosomes of *SOD1^{A4V}* and *SOD1^{A4V}/EGLN2$^{-/-}$* iPSCs. Genomic view of all chromosomes of **A,** *SOD1^{A4V}* iPSCs and **B,** *SOD1^{A4V}/EGLN2$^{-/-}$* iPSCs.

A



B

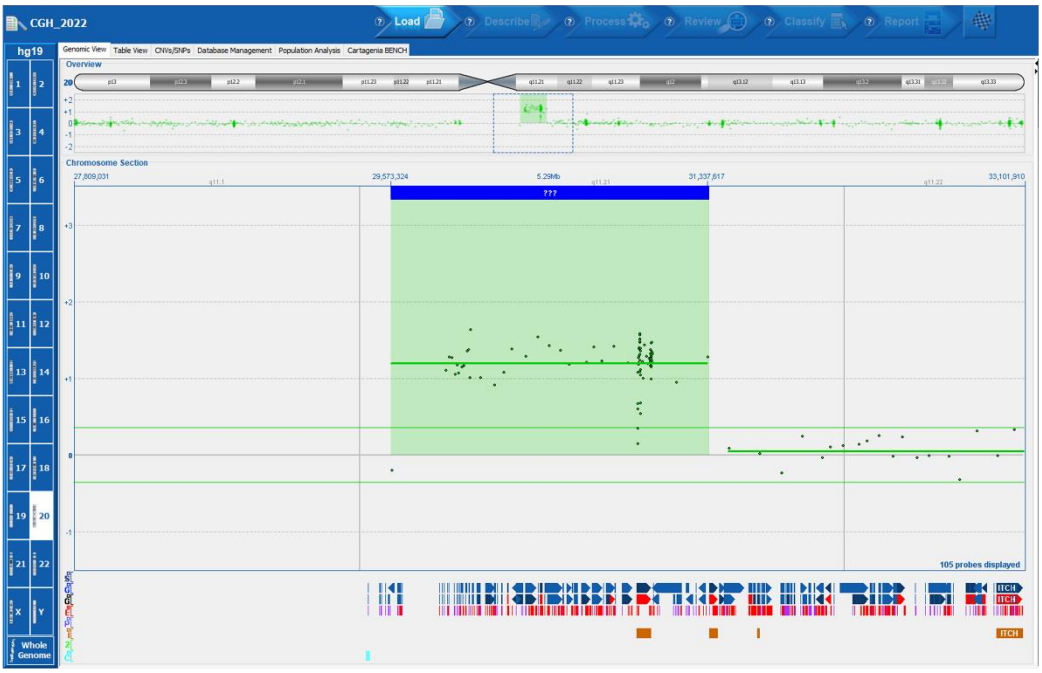


Figure S4.2. Array-CGH results of chromosome 20 of *SOD1^{A4V}* and *SOD1^{A4V}/EGLN2$^{-/-}$* iPSCs. Array-CGH result of chromosome 20 of **A,** *SOD1^{A4V}* iPSCs and **B,** *SOD1^{A4V}/EGLN2$^{-/-}$* iPSCs with 20q.11 duplication highlighted in green.

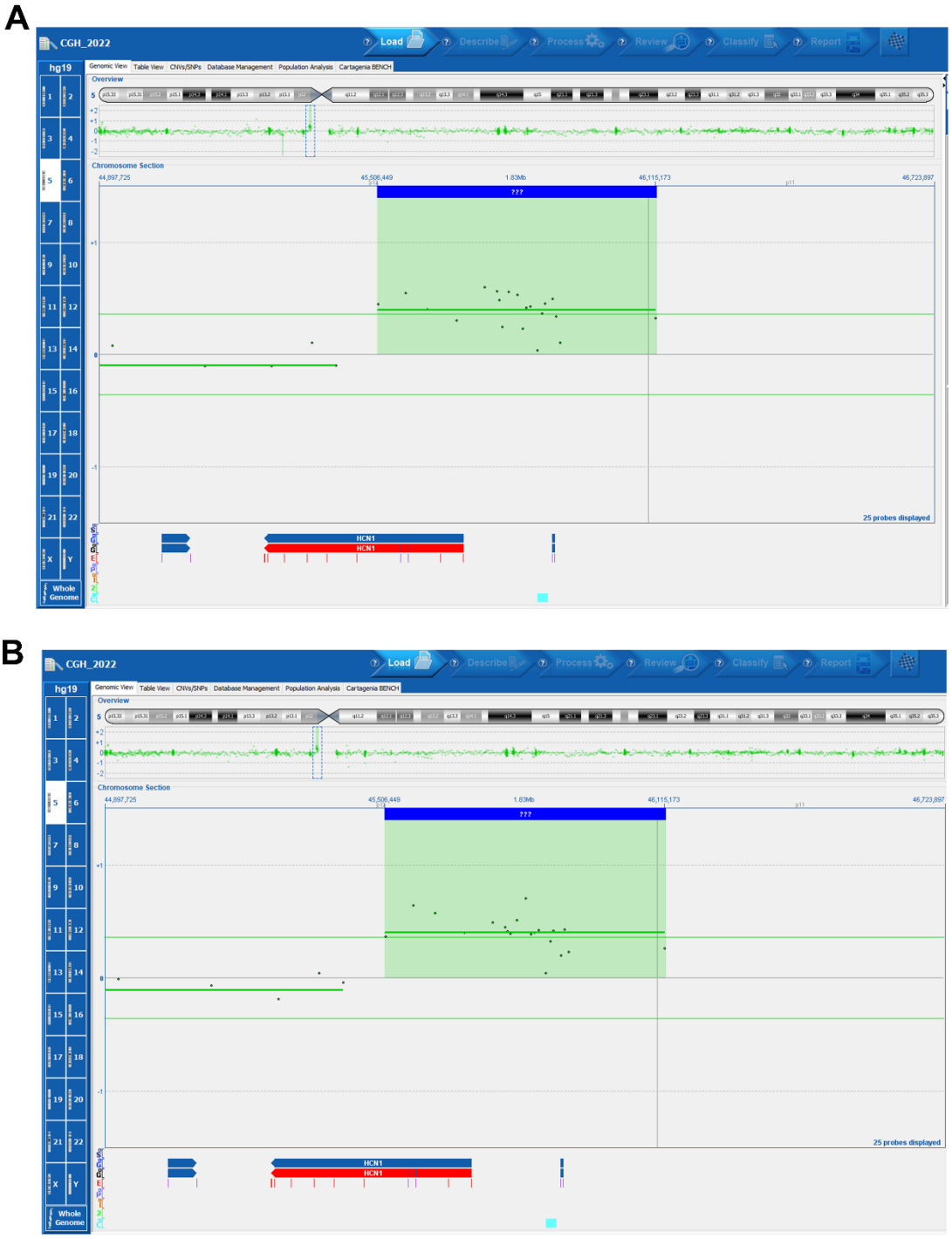


Figure S4.3. Array-CGH results of chromosome 5 of *SOD1^{A4V}* and *SOD1^{A4V}/EGLN2$^{-/-}$* iPSCs. Array-CGH result of chromosome 5 of **A,** *SOD1^{A4V}* iPSCs with 20q.11 duplication highlighted in green and **B,** *SOD1^{A4V}/EGLN2$^{-/-}$* iPSCs with 20q.11 triplication highlighted in green.

	SOD1^{G93A}/Egln2$^{+/+}$			*SOD1^{G93A}/Egln2$^{-/-}$*		
	Sample 1	Sample 2	Sample 3	Sample 1	Sample 2	Sample 3
QC NUCLEI PREPARATION						
Concentration of nuclei (nuclei/ml)	2.1 x 10^6	1.64 x 10^6	2.37 x 10^6	2.39 x 10^6	2.24 x 10^6	1.69 x 10^6
Average nuclei size (micron)	6.4	4.4	6.7	5.4	6.5	5.8
QC NUCLEI						
Fraction reads in nuclei	51.3%	76.2%	64.5%	51.2%	72.4%	70.7%
Total genes detected	21582	25490	24753	21354	25333	25134
Median UMI-counts per nucleus	2476	2360	2966	2511	2726	2799
QC MAPPING						
Reads mapped to genome	89.5%	93.8%	94.1%	87.7%	94.3%	93.9%
Reads mapped confidently to genome	87.6%	91.8%	92.3%	85.7%	92.4%	92.1%
Reads mapped confidently to intergenic regions	4.2%	5.4%	4.9%	4.3%	5.2%	5.1%
Reads mapped confidently to intronic regions	40.2%	55.5%	49.3%	43.6%	52.8%	51.6%
Reads mapped confidently to exonic regions	43.2%	30.9%	38.1%	37.8%	34.4%	35.4%
Reads mapped confidently to transcriptome	56.0%	55.5%	61.8%	51.4%	60.3%	62.4%
Reads mapped antisense to gene	27.2%	31.1%	25.3%	29.7%	26.6%	24.2%

Table S4.1. Quality control (QC) parameters snRNA-seq.

Cluster 35								
UP			DOWN					
Genes	logfoldchange	pval	Genes	logfoldchange	pval	Genes	logfoldchange	pval
Vip	5,61037701	0,018688061	Csmd1	-5,370775988	1,95261E-05	Taldo1	-2,75435665	0,029628283
Sharpin	2,862127559	0,03979774	Tafa1	-5,245302587	0,001329838	Psme4	-2,7367087	0,045390303
Nrsn2	2,487186631	0,010670689	Ccser1	-5,016056624	0,001204328	Lrrtm4	-2,73589736	0,005469941
Nol12	2,469607993	0,01204733	Sgcz	-4,96374379	0,000194902	Nrxn3	-2,72060957	0,000712692
Gm32432	2,40528186	0,035013369	Asic2	-4,649360323	0,002236816	Mrps12	-2,71605587	0,038399754
Abracl	2,128741621	0,04606203	B3galt1	-4,482104293	0,007388939	Abca3	-2,71559039	0,04228583
Ubxn2a	1,999423862	0,017329108	Arpp21	-4,390438167	0,012399446	Robo2	-2,66726821	0,044006435
Serp2	1,724473116	0,003874021	Dcc	-4,369855204	0,002231748	Prkg1	-2,66301969	0,032788427
Tango2	1,578598505	0,01535225	Rtl4	-4,115974881	0,01941963	Ctla2a	-2,61897366	0,041038902
Snrpf	1,481661976	0,035443196	Ednrb	-4,114646425	0,017532835	Ncam2	-2,57918268	0,046568285
Trappc6b	1,254554926	0,039255278	Zcchc7	-4,092093238	0,011221355	Car10	-2,46419393	0,041050696
Gap43	1,157010764	0,043697409	Grik2	-4,09064643	0,00431555	Kcnip4	-2,46065141	0,012269298
Vti1b	1,071431629	0,04566731	Adk	-3,976150191	0,013036806	Cacna2d1	-2,44906533	0,007310163
Morf4l1	1,04679153	0,017995427	Ubn2	-3,855124241	0,022617187	Rgs7	-2,4317974	0,047762387
Rpl30	0,980419202	0,027727375	Hs3st5	-3,752702803	0,011832584	Xkr4	-2,39756343	0,033506723
Tpt1	0,965699491	0,036529359	Pde10a	-3,747484086	0,033996935	Rims2	-2,39584703	0,031044812
Fth1	0,950775936	0,047883628	Nrg3	-3,737325468	3,17117E-05	Ptprd	-2,35561246	0,00432522
Rps15	0,870674909	0,049583681	Itsn2	-3,735126957	0,031115157	Snhg11	-2,33639394	0,000141892
Rpl28	0,86567275	0,041562108	Nrp1	-3,719403152	0,031370439	Fus	-2,33209568	0,045969361
Rpl37a	0,837283301	0,023169513	Fxyd1	-3,712765366	0,019863193	Csmd3	-2,28518563	0,035563301
Rpl22l1	0,830351596	0,033714214	Cntnap2	-3,709347765	1,13436E-07	Mdga2	-2,24127541	0,019347982
			Adarb2	-3,683389125	0,017873073	Tanc2	-2,22121497	0,048303428
			Tspo	-3,661379752	0,040420878	Hcn1	-2,19062481	0,024675205
			Ptk2	-3,61566773	0,038365131	Lrrc4c	-2,16540592	0,04440173
			Ust	-3,602311562	0,04173603	Lrp1b	-2,10604284	0,021779127
			Mbd5	-3,594465146	0,042764646	Msi2	-2,08589713	0,045434772
			Hipk2	-3,569108614	0,045062958	Fam155a	-2,08425235	0,009997206
			Zfp804b	-3,553810187	0,02724777	Opcml	-2,06748454	0,043976932
			Prdx6	-3,53412406	0,005436567	Son	-2,05902365	0,03145798
			Synpr	-3,529204083	0,034591118	Auts2	-2,05139909	0,042783061
			Pde4d	-3,52580806	0,00429737	Tsc22d1	-2,04950122	0,032469991
			Dpp10	-3,521675697	0,001213535	Qk	-2,03670561	0,030397986
			Cntn5	-3,491214934	0,026180549	Rora	-1,9477703	0,016269008
			Nav2	-3,482570239	0,049398871	Fgf14	-1,90942806	0,031568091
			Sorcs1	-3,445083033	0,030931123	Tubb2b	-1,89208232	0,039541535
			Ctnnd2	-3,367539993	0,009974004	Rbms3	-1,86570533	0,033353406
			Dgkh	-3,355728735	0,015530029	Cct7	-1,80604738	0,034502441
			Igfbp2	-3,303979207	0,042534675	Fstl1	-1,75808148	0,021170563
			Rasal2	-3,269800964	0,031649045	Nrg1	-1,75404329	0,022308344
			Lxn	-3,258366079	0,026500034	Sorl1	-1,74252526	0,017335685
			Il1rapl1	-3,239166489	0,00597366	Lsamp	-1,72168264	0,001172653
			Magi2	-3,219020912	0,000439437	Adgrl3	-1,65421357	0,03871169
			Slc9a9	-3,200171738	0,0386394	Serpinb6a	-1,64799024	0,028209933
			Lingo2	-3,198462723	0,005364446	Ntm	-1,63287993	0,040918142
			Cd44	-3,103529809	0,046218801	Mt3	-1,62597615	0,023203208
			Adgrb3	-3,092234007	0,003912461	Pcdh7	-1,56733476	0,018486843
			Tagln2	-3,044011111	0,042454147	Ube3a	-1,55744638	0,043012206
			Tsc22d4	-3,043739263	0,010110335	Dbi	-1,51187542	0,019537883
			Rbm25	-3,025654197	0,04558228	Rbfox1	-1,43173978	0,023123428
			Dmd	-3,024789103	0,028606548	Tppp3	-1,39845177	0,03044747
			Kcnd2	-3,004958656	0,007707104	Tubb5	-1,3383278	0,013298196
			R3hdm1	-2,99240246	0,02746423	Scd2	-1,30953179	0,022110645
			Cd9	-2,929050836	0,005054192	Pcdh9	-1,30097697	0,037713891
			Slc7a1	-2,919927639	0,042373921	Nrxn1	-1,21869326	0,04962697
			Grid2	-2,841284261	0,016769333	Kif1b	-1,11173202	0,01721771
			Nupr1	-2,809616907	0,007079238	Dync1h1	-1,08155417	0,041873872
			Meg3	-2,778391609	3,47869E-06	Uchl1	-0,808978	0,038770007

Table S4.2. DEGS in SOD1^{G93A}/Egln2$^{-/-}$ versus SOD1^{G93A}/Egln2$^{+/+}$ motor neurons.

Cluster 5								
UP			DOWN					
Genes	logFC	pval	Genes	logFC	pval	Genes	logFC	pval
Med22	3,809828195	0,014473149	Cxcl10	-4,799940047	0,001217199	Selenom	-0,90144065	0,041454288
Grik1	2,348707463	0,007762765	Oasl1	-4,601381405	0,010608093	Tubb5	-0,89735948	0,035979334
Kctd16	1,93593121	0,031480535	Isg15	-3,991118775	0,003269005	Tuba4a	-0,89580226	0,031896139
Zfp804a	1,772762259	0,049139206	Ggt1	-3,562299612	0,042609533	Nefl	-0,87600582	0,008200137
Xist	1,312782597	0,000770477	Rsad2	-3,54558345	2,06852E-05	Tubb2a	-0,83266852	0,011818016
Gan	1,217136001	0,046301696	Gm11681	-3,535025038	0,044411281	S100a6	-0,82731715	0,02792333
Ift140	1,116184869	0,042571939	Kank3	-3,215631565	0,025464232	Psmb1	-0,78172407	0,043812976
Xkr4	1,01240698	0,033091465	Ifit1	-2,621963002	0,034848411	Mdh2	-0,78071197	0,039175016
Ppp4r1	0,911671718	0,035242973	Igfbp3	-2,550307654	0,028354578	Rps17	-0,77512812	0,033699547
Arpp21	0,850599024	0,040249664	Gbp5	-2,455163817	0,040657783	Tuba1b	-0,72142553	0,047431405
Tafa1	0,751123077	0,042084459	Ier3	-2,210031753	0,041795715	Srebf1	-0,71689071	0,040448687
Prkdc	0,69399121	0,043871142	Fcgr2b	-2,18656726	0,048297799	Actg1	-0,70251428	0,006248352
			Rac3	-2,105617037	0,03682501	Rpl23a	-0,70243302	0,036966431
			Pitpnm3	-1,994316681	0,029933377	Aldoa	-0,68527876	0,008913589
			Ifngr2	-1,931989283	0,032075876	Ctsd	-0,68480496	0,004955326
			Bst2	-1,837841322	0,020195937	Calm1	-0,67344282	0,008585964
			Egln2	-1,79875826	0,024387444	Hsp90ab1	-0,67104844	0,027509176
			Eif3l	-1,682972184	0,034278885	Ndufa4	-0,66140375	0,013722871
			Oasl2	-1,614091048	0,038152856	Adgrg1	-0,65303323	0,041978576
			Hspb1	-1,594470183	0,000670139	Rplp1	-0,61663891	0,042121976
			Pfdn6	-1,422550446	0,024387858	Rpl26	-0,61385909	0,039164676
			Igfbp2	-1,290401768	0,003817149	Dbi	-0,59714401	0,016347944
			Tor3a	-1,272897209	0,038358129	Atp5j2	-0,59204898	0,047045097
			Cebpd	-1,221371431	0,027603388	Tmsb4x	-0,58782493	0,013546503
			Myoc	-1,143617853	0,001923749	Tuba1a	-0,58417028	0,04182443
			Ifitm3	-1,122229455	0,034997984	Ubc	-0,58361974	0,035381589
			Tppp3	-1,080081338	0,035039211	Cox8a	-0,57307507	0,035466624
			Cnbd2	-1,058607077	0,033777874	Snap25	-0,5569129	0,037038728
			Snrpn	-1,046743763	0,0114412	Atp6v0c	-0,55155506	0,042172539
			Mrpl23	-1,027517823	0,040871655	Ppia	-0,54087629	0,039817104
			Psma7	-1,010450771	0,021680883	Hspa8	-0,53968327	0,025442345
			Stx1b	-1,006672866	0,046729636	Ubb	-0,52594668	0,024489835
			Pfn1	-0,984266574	0,048329	Mt1	-0,52461216	0,038023126
			Uqcc2	-0,977146058	0,034275882	Itih3	-0,52164901	0,04703331
			Gm42418	-0,971263737	1,3246E-05	Prnp	-0,503713	0,018850068
			Zbtb16	-0,9043112	0,031229389			

Table S4.3. DEGS in SOD1^{G93A}/Egln2$^{-/-}$ versus SOD1^{G93A}/Egln2$^{+/+}$ astrocytes.

		Germeys and Vandoorne et al.				Tyzack et al.		Dittlau et al.				Neyrinck et al.		Birger et al.		Ziff et al.	
		SOD1A4VvsA4A		SOD1.EGLN2KOvsA4V		SOD1vsCTRL		FUS.R521HvsR521R		FUS.P525LvsP525P		FUSvsCTRL		C9orf72vsCTRL		VCPvsCTRL	
Gene Name	**Gene ID**	logFC	FDR	logFC	FDR	LogFC	FDR	logFC	FDR	logFC	FDR	LogFC	FDR	LogFC	FDR	LogFC	FDR
APOBEC3G	ENSG00000239713	-1,34	0,01	1,14	0,04	1,22	0,44	NA	NA	NA	NA	-0,24	0,82	-0,80	0,57	0,06	1,00
BISPR	ENSG00000282851	-6,11	0,00	6,03	0,00	0,32	0,90	NA	NA	NA	NA	0,45	NA	1,27	0,70	-0,17	1,00
BST2	ENSG00000130303	-8,22	0,00	7,72	0,00	0,97	0,15	0,62	0,56	-2,54	0,00	0,60	0,61	0,40	0,94	-1,13	1,00
CCL5	ENSG00000271503	-6,23	0,01	8,78	0,00	1,91	NA	NA	NA	NA	NA	1,00	NA	-0,36	0,95	-0,70	1,00
IFI16	ENSG00000163565	-1,40	0,00	1,71	0,00	0,32	0,51	1,28	0,00	-0,84	0,04	-0,50	0,00	-0,11	0,97	0,32	1,00
IFI27	ENSG00000165949	-9,28	0,00	9,01	0,00	0,03	0,98	-1,47	0,00	-0,73	0,16	0,21	0,91	-0,83	0,68	0,19	1,00
IFI35	ENSG00000068079	-3,24	0,00	3,24	0,00	-0,38	0,80	0,81	0,14	-0,94	0,05	0,91	0,12	-0,45	0,90	-0,16	1,00
IFI44	ENSG00000137965	-5,23	0,00	5,00	0,00	-0,20	0,84	-0,65	0,05	-0,21	0,56	0,99	0,07	-0,32	0,91	-0,85	1,00
IFI44L	ENSG00000137959	-5,83	0,00	5,61	0,00	-2,35	0,00	-0,89	0,03	1,12	0,00	2,05	0,00	-1,58	0,36	-1,90	0,92
IFI6	ENSG00000126709	-7,17	0,00	5,61	0,00	0,08	0,96	-0,14	0,61	-0,38	0,09	-0,36	0,53	0,37	0,88	-1,06	1,00
IFIH1	ENSG00000115267	-4,43	0,00	5,22	0,00	-1,31	0,21	0,71	0,16	0,28	0,60	1,59	0,04	0,58	0,82	-1,03	1,00
IFIT1	ENSG00000185745	-6,35	0,00	6,15	0,00	-1,17	0,00	0,71	0,02	0,23	0,49	-0,83	0,00	-0,45	0,86	-1,09	1,00
IFIT2	ENSG00000119922	-2,91	0,00	3,87	0,00	-0,19	0,82	0,93	0,00	-0,17	0,65	-1,04	0,00	0,14	0,95	0,05	1,00
IFIT3	ENSG00000119917	-5,67	0,00	5,53	0,00	-1,62	0,18	1,21	0,00	-0,75	0,06	-0,49	0,37	0,60	0,74	-0,66	1,00
IFIT5	ENSG00000152778	-1,91	0,00	2,29	0,00	0,21	0,70	0,95	0,00	-0,05	0,89	-0,43	0,01	0,05	0,98	-0,12	1,00
IFITM1	ENSG00000185885	-5,46	0,00	5,40	0,00	2,36	0,00	-0,09	0,92	-2,75	0,00	-2,60	0,00	-1,54	0,65	-2,07	0,00
IFITM3	ENSG00000142089	-1,97	0,00	2,08	0,00	2,38	0,00	1,56	0,00	-1,36	0,00	-0,66	0,00	-1,14	0,62	-0,88	1,00
IFNB1	ENSG00000171855	-2,52	0,03	6,39	0,00	NA	NA	NA	NA	NA	NA	NA	NA	-2,07	NA	-2,53	NA
IRF6	ENSG00000117595	-4,50	0,01	3,97	0,02	-0,37	NA	-0,32	0,89	-2,15	0,05	1,26	0,54	2,11	0,64	1,44	1,00
IRF7	ENSG00000185507	-2,23	0,00	2,43	0,00	-0,15	0,92	-0,17	0,67	-0,27	0,42	0,30	0,61	-0,25	0,86	0,51	1,00
IRF9	ENSG00000213928	-1,76	0,00	1,56	0,00	-0,25	0,75	-0,79	0,08	0,82	0,06	0,14	0,76	-0,41	0,64	-0,30	1,00
ISG15	ENSG00000187608	-6,51	0,00	6,62	0,00	-1,76	0,10	-0,46	0,20	-0,31	0,38	-0,09	0,85	-0,33	0,93	-0,16	1,00
ISG20	ENSG00000172183	-3,05	0,01	4,92	0,00	0,36	0,88	-1,84	0,02	-0,77	0,37	-0,42	0,83	0,81	0,59	0,03	1,00
MX1	ENSG00000157601	-8,40	0,00	8,19	0,00	-1,74	0,14	0,11	0,84	-0,53	0,19	-0,41	0,70	0,29	0,96	-1,64	1,00
NRIR	ENSG00000225964	-4,04	0,01	4,76	0,00	-1,69	NA	NA	NA	NA	NA	-0,44	NA	2,59	NA	-1,14	NA
OAS1	ENSG00000089127	-6,86	0,00	6,52	0,00	-1,43	0,65	1,30	0,15	-0,64	0,40	-0,77	0,76	-0,54	0,88	-1,00	1,00
OAS2	ENSG00000111335	-11,41	0,00	11,13	0,00	4,60	NA	NA	NA	NA	NA	-1,52	0,44	1,14	0,69	-0,99	1,00
OAS3	ENSG00000111331	-5,66	0,00	6,01	0,00	2,79	0,15	1,19	0,09	0,53	0,56	-1,70	0,01	-0,88	0,74	-0,67	1,00
OASL	ENSG00000135114	-5,37	0,00	7,37	0,00	NA	NA	NA	NA	NA	NA	2,18	0,14	-0,79	0,85	-0,04	1,00
RSAD2	ENSG00000134321	-8,36	0,00	10,25	0,00	-3,44	0,06	NA	NA	NA	NA	-1,24	0,62	-0,07	0,99	-0,08	1,00
TRIM14	ENSG00000106785	-1,63	0,01	1,43	0,04	-1,06	0,44	-0,04	0,98	-1,46	0,06	2,26	0,00	0,03	1,00	-0,23	1,00
TRIM21	ENSG00000132109	-1,88	0,00	1,76	0,00	-0,40	0,60	0,35	0,34	-0,14	0,72	0,11	0,79	0,03	0,99	0,20	1,00
TRIM22	ENSG00000132274	-1,35	0,00	1,33	0,00	1,69	0,00	0,20	0,57	-0,58	0,04	0,19	0,58	0,72	0,35	-0,22	1,00
TRIM25	ENSG00000121060	-2,15	0,00	2,39	0,00	0,36	0,68	0,84	0,01	-0,12	0,75	-0,04	0,93	-0,01	1,00	0,21	1,00
TRIM38	ENSG00000112343	-3,15	0,01	3,67	0,00	1,78	NA	1,91	0,01	-2,20	0,00	-0,20	0,77	0,51	0,86	0,98	1,00
TRIM5	ENSG00000132256	-1,26	0,00	1,13	0,02	0,03	0,97	0,31	0,19	0,06	0,81	-0,62	0,00	-0,33	0,78	-0,44	1,00
TRIM6	ENSG00000121236	-2,79	0,00	2,78	0,00	0,42	0,82	0,44	0,63	-1,55	0,01	-0,21	0,90	2,84	0,08	0,49	1,00

Table S4.4. Comparison between interferon-stimulated genes normalized upon loss of EGLN2 and their levels in ALS patient versus control astrocytes in literature.

Curriculum vitae



Christine Germeys
Biomedical scientist

Personal information

05/10/1996, Genk
+32496398741
christine.germeys@gmail.com
@christinegermeys
Lobbensestraat 89,
3271 Zichem

Interests

- Playing the piano/guitar
- Reading
- Hiking/running

Languages

- Dutch — Native
- English — Advanced
- French — Basic

Work experience

2019 – Present: Doctoral researcher
VIB-KULeuven Center for Brain and Disease

Thesis title: The role and therapeutic potential of EGLN2/PHD1 in amyotrophic lateral sclerosis (ALS).

Key qualifications and responsibilities:
Fundamental research in neuroscience focusing on ALS
- Developing, validating, performing and managing experiments in *in vivo* and *in vitro* models
- Data analysis and interpretation
- Cross-disciplinary collaborations
- Training and supervision of technicians and students
- Oral and written science communication to experts and general public

Key achievements:
- FWO Fundamental research fellowship
- Publications in peer-reviewed journals
- Presentation at national and international conferences

2018 – 2019: Master thesis
VIB-KULeuven Center for Brain and Disease

Thesis title: Using iPSCs to investigate the effect of HDAC inhibition on human FUS-ALS motor neurons.

Key qualifications and responsibilities:
Fundamental research in neuroscience focusing on ALS
- Designing, performing and managing experiments in stem cell models
- Data analysis and interpretation

Key achievements:
- Best master thesis Biomedical Sciences 2019 – third place (KUL)
- Publication in peer-reviewed journal

2017 – 2018: Student Researcher
VIB-KULeuven Center for Brain and Disease

Key qualifications and responsibilities:
Fundamental research in neuroscience focusing on epilepsy
- Performing experiments in fruit flies
- Data analysis and interpretation

Education

2019 – Present: PhD in Biomedical Sciences
KU Leuven

2017 – 2019: Master of Science in Biomedical Sciences
KU Leuven, *Magna cum laude*

2014 – 2017: Bachelor of Science in Biomedical Sciences
KU Leuven, *Cum laude*

2008 – 2014: Secondary School degree in Science and Mathematics
Sint-Michiel Leopoldsburg

Certificates

FELASA B (KUL)
Radiation Protection Training (KUL)
Driver's License B

Skills

Technical Skills

- (iPSC) Cell culture
- iPSC differentiation in neuronal and glial cells
- (Transgenic) mouse models e.g. breeding, behavioral studies, dissections
- Fruit fly models e.g. crossing, behavioral studies
- Omics e.g. metabolomics, bulk and single-cell transcriptomics
- *In vitro* tracer (radio-active and heavy isotope) studies
- Immunofluorescence and confocal microscopy + ICC, IHC, FISH
- Molecular biology e.g. RNA/protein extraction, PCR, qPCR, Western Blot

Soft skills

- Pro-active
- Problem solver
- Critical thinker
- Self-driven
- Team player
- Communicative
- Flexible
- Detail-oriented
- Creative

IT skills

- Microsoft office
- Graphpad Prism
- ImageJ
- SnapGene
- Inkscape
- R studio (basics)

Extracurricular activities

2023 – Present: EOS blogger – Eos Wetenschap
https://www.eoswetenschap.eu/christine-germeys

2022 – Present: Science on the go – VIB-KUL
Organizer of science workshops for primary school students.

2020 – 2023: Ecoteam member – KUL Green impact
Member of the lab's ecoteam focused on sustainability and environmental impact by implementing structural changes, providing information and organizing activities.

2019 – Present: Courses during PhD training

- 2023: Active Bystander (VIB)
- 2023: Communication Skills: Establishing Connective Clarity (VIB)
- 2022: Research Integrity part II (KUL)
- 2022: Tracer Metabolomics Course (KUL)
- 2021: CURE-ND Neurotechnology workshop (VIB)
- 2020: Somersault18:24 Essentials of Image Editing (KUL)
- 2020: Basic Statistics in R (VIB)
- 2019: Networking for Researchers (KUL)
- 2019: Writing skills for Biomedical Researchers (ILT)
- 2019: Metabolomics Data Interpretation (VIB)

2012 -2014: Summer camp leader – JOETZ vzw
Supervisor and organizer of group activities for children with ages ranging from 7 to 15.

2010 – 2014: Conflict mediator – Sint-Michiel
Trained as conflict mediator as part of a secondary school initiative.

Publications and Conferences

Publications

Germeys C., Vandoorne T., Davie K., Poovathingal S., Heeren K., Vermeire W., Nami F., Moisse M., Quaegebeur A., Sierksma S., Rué L., Sicart A., Eykens C., De Strooper B., Carmeliet P., Van Damme P., De Bock K. and Van Den Bosch L. (2024). Targeting EGLN2/PHD1 protects motor neurons and normalizes the astrocytic interferon response. *Cell Reprts.*

Thevissen K., Ny A., Kamata K., Copmans D., Tits J., Gielis E., Kevin Longin K., Sourbron J., Thergarajan P., Huey-Lin Tan T., Ali I., Jones N.C., O'Brien T.J., Monif M., Semple B.D., **Germeys C.**, Frizzi B., Van Den Bosch L., Cammue B.P.A., Voet A., Lagae L., de Witte P. (2024). Compound X improves catalytic activity of PHGDH and shows antiseizure efficacy in patients. *In preparation.*

Germeys, C., Vandoorne, T., Bercier, V., and Van Den Bosch, L. (2019). Existing and Emerging Metabolomic Tools for ALS Research. *Genes (Basel).*

Vandoorne, T., Veys, K., Guo, W., Sicart, A., Vints, K., Swijsen, A., Moisse, M., Eelen, G., Gounko, N.V., Fumagalli, L., Fazal R. **Germeys C.**, Quaegebeur A., Fendt S.-M., Carmeliet P., Verfaillie C., Van Damme P., Ghesquière B., De Bock K., Van Den Bosch L. (2019). Differentiation but not ALS mutations in FUS rewires motor neuron metabolism. *Nat Commun.*

Academic Conference attendance

- Oral presentation at ENCALS Meeting 2024, Stockholm, Sweden
- Oral presentation at LEUCALS Meeting 2024, Leuven, Belgium
- Oral presentation at VIB-NERF PhD Symposium 2023, Leuven, Belgium
- Poster presentation at Periphery-brain Interplay and CNS Disease Conference 2023, Leuven, Belgium
- Poster presentation at ALS Gordon Research Conference and Seminar 2023, Les Diablerets, Switzerland
- Poster presentation at Packard meeting 2023, Baltimore, US
- Poster presentation at CBD Science day 2022 and 2023, Genk, Belgium
- Poster presentation at ENCALS Meeting 2022, Edinburgh, UK
- Virtual poster presentation at ALS/MND symposium 2021 and 2022, Online
- Poster presentation at VIB-NERF PhD Symposium 2021 and 2022 Leuven, Belgium
- Poster presentation at The Brain Mosaic: Cellular heterogeneity in the CNS Conference 2019, Leuven, Belgium